R/V *Mirai* Cruise Report

MR19-04

GO-SHIP Observation
–heat and material transports by the ocean circulation and
their variability–

Indian & Southern Oceans

Dec. 5, 2019 — Feb. 21, 2020

Japan Agency for Marine-Earth Science and Technology
(JAMSTEC)

Contents

1. Cruise Information

2. Science Party

3. (To be added)

4. Hydrographic Measurement

5. Float, Drifter and Mooring

1. Cruise Information

Cruise ID	MR19-04
Name of vessel	R/V *Mirai*
Title of cruise	GO-SHIP Observation –heat and material transports by the ocean circulation and their variability–
Chief Scientist	Leg 2: Akihiko Murata Leg 3: Katsuro Katsumata, Physical and Chemical Oceanography Research Group, Global Ocean Observation Research Center, Research Institute for Global Change (RIGC), Japan Agency for Marine-Earth Science and Technology (JAMSTEC)
Cruise period	Leg 1: 15th November, 2019 – 4th December, 2019 Leg 2: 5th December, 2019 – 27th December, 2019 Leg 3: 29th December, 2019 – 10th February, 2020 Leg 4: 13th February, 2020 – 21st February, 2020
Ports of departure / call / arrival	Leg 1: Hachinohe/Singapore/Colombo Leg 2: Colombo//Port Louis Leg 3: Port Louis//Singapore Leg 4: Singapore//Koror
Research area	Leg 2: Indian Ocean Leg 3: Southern Ocean

Research map
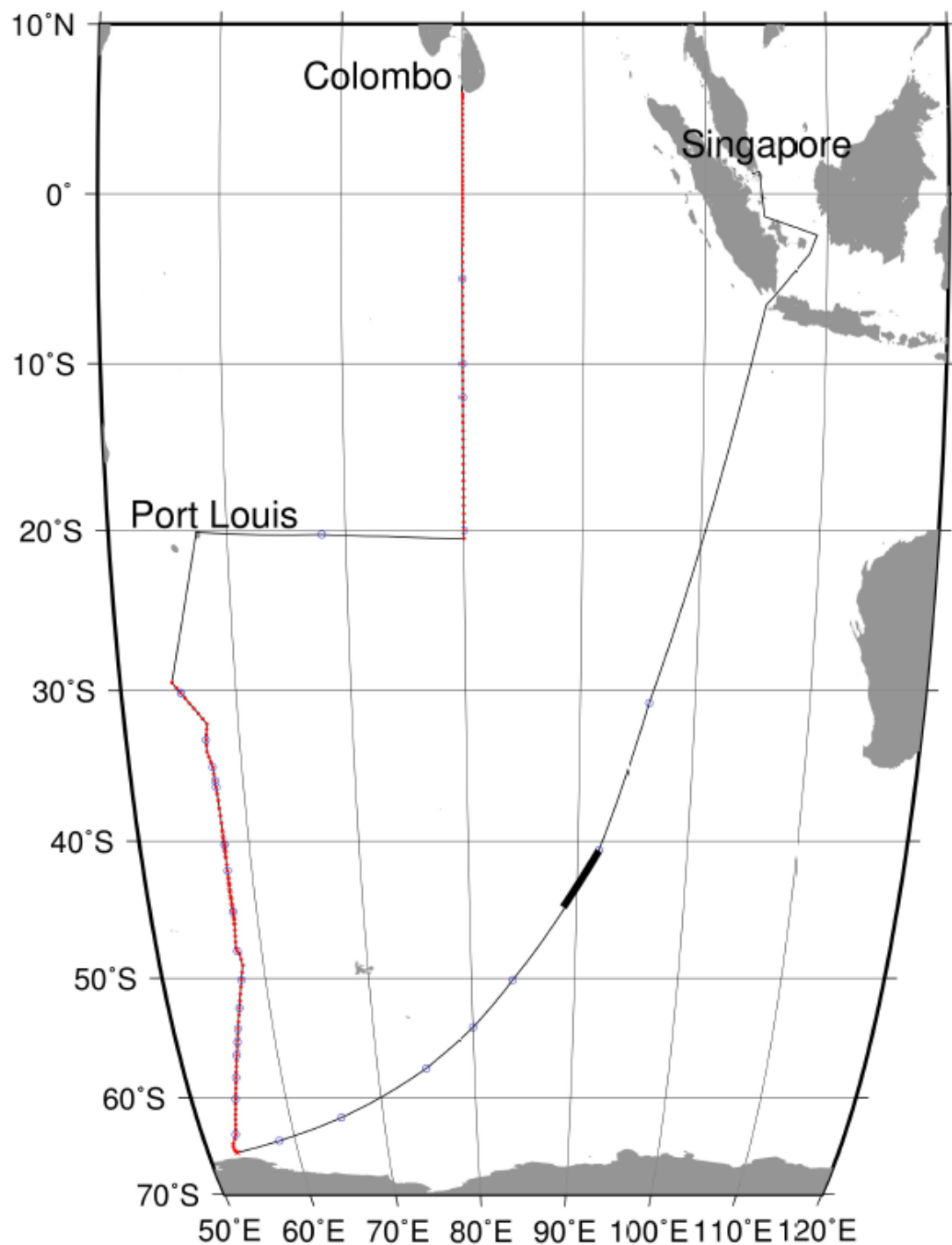
Fig. 1.1 Cruise map of MR19-04. No research activity was performed on Legs 1 and 4 hence not shown. The red dots show CTD and/or Niskin sampling stations. Blue circles show float deployments. Thick black segment shows geophysical survey. See Sections 3.18&3.19 for detail.
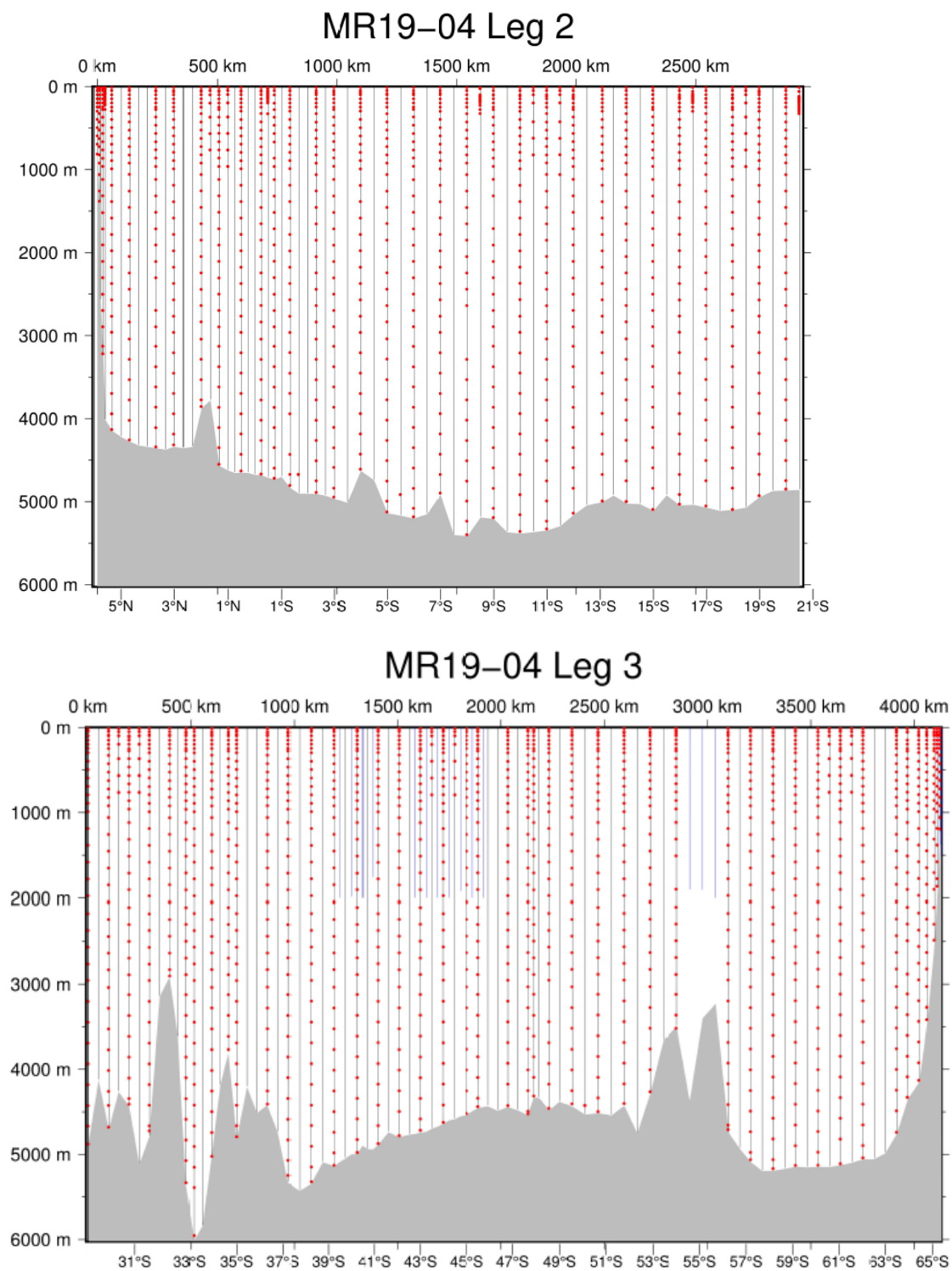
Samplng positions

Fig. 1.2. Cross sections showing data sampling positions. Blue line shows CTD trace and red dots show Niskin sampling. Gray is ocean bottom bathymetry..

Narrative for Leg 2 (A. Murata)

3rd Dec: Water sampling training sessions, which were made during a call at the port of Columbo, Sri Lanka.

4th Dec: Meeting on-board the R/V *Mirai* with people from authorities of Sri Lank for the observation within the EEZ of Sri Lank.

5th Dec: Departed from Columbo at 10:00 local time. We prayed to the Konpira Shrine, known as a guardian of sailing in Japan, for the cruise safety at the bridge. Arrived at the first CTD station.

8th Dec: The last CTD station (CTD #15) within the EEZ of Sri Lanka. Since the departure from Columbo, good weather and no big wave conditions continued.

10th Dec: Crossed the equator. A certificate for crossing the equator was issued.

13th Dec: Suspended CTD observations for 24 hours. This is for maintenance of hardware of the CTD observation system, not because of malfunction of it.

14th Dec: Re-start of CTD observation from CTD #39.

18th Dec: At one time, CTD observations were suspended, because of on-board medical crisis. A few hours later, re-started.

20th Dec: Slightly bumpy conditions.

22nd Dec: The last CTD station. After that, sailed to Port Louis.

27th Dec: Arrival at a port of Port Louis.

Narrative for Leg 3 (K. Katsumata)

29th Dec: an approaching cyclone kicked us out of Port Louis some 17 hours earlier than scheduled. As soon as we turn to head south, waves get as high as 5 m under a 15 m/s gust.

30th Dec: Emergency evacuation drill completed after water sampling training sessions.

31st Dec: is last day of the year and first CTD day of the leg. The cast started at 7:30pm, ship time. With four less water sampling personnel, due to last-minute cancellation and medical conditions, sampling took much longer than those during the previous leg

1st Jan: blessed by a nice breeze of about 7 m/s, later even milder of 5 m/s, with a bit of swell (4 m) from the cyclone far east that had chased us out of Port Louis.

2nd Jan: Station 81, the deepest cast. Although it has been occupied in 2009, we were not 100 % sure about its depth. After a discussion, we decided to proceed with all sensors on, whose pressure limits are 6000 "m" (not "dbar"). It is on a slope such that we can always escape to the shallow side... and we did — 0.5 miles westward, then it was safe.

4th Jan: oil leaked from Dynacon winch. Suspended upcast 83 for 30 minutes at about 2500 dbar. One of the two CFC analyser still under maintenance. All CFC bottles from cast 83 went to the fridge. Sea state is excellent. During downcast of 85, communication between the CTD and the deck unit was lost. The cast was cancelled and the whole set was brought back to deck. During a thorough check, the connection between the CTD and armored cable showed low resistance. Re-terminated the armored cable. Cast 2 of Station 85 began after 11 hours.

5th Jan: was instead a peaceful day.

6th Jan: at about 0200GMT, we crossed 39°01.26'S where SST dropped 17→16.1°C and SSS 35.3→34.8 (or lower). This must be a front— probably Agulhas Return Current. Indeed, surface current is towards NE, > 1.5 kt. At 0935GMT, we saw a yellow/mud patch to the Port Side of the ship . Krill? *Photo: courtesy of H.Hiroshi (MWJ).*

7th & 8th Jan: oddly enough the upper water masses returned to that of the subtropical gyre.

9th Jan: now we are nearing the *real* front at 42°54.67'S. SST 15.5°C →<11°C, SSS 35.07 →< 34. Surface current into 10° true at 3 knots!

10th Jan: a fat jelly fish leg got stucked into the CTD secondary system. The primary was clear and healty (good agreement with SBE-35) — no need for Cast 2. Now into a pressure valley and took 9 hours off. Almost halfway.

11th & 12th Jan: slow but steady. Our nitrate samples do not duplicate well. The nutrient team suspected the gloves and performed several experiments. It is certainly one of the causes. But the problem persists after we changed our gloves.

13th Jan: at last we got caught by a low pressure system; > 6.5 m significant wave height and > 20 m/s wind. Stand by for 24 hours.

14th Jan: back to work. The first cast through the well-devloped mixed layer was however terminated by more than 80 Modulo errors from CTD at around 400dbar down. After putting the CTD set back on deck and regular checkups and cleaning of connections, we did not see any Modulo error again. All is well that ends well?

15th Jan: into furious fifties where wind > 10m/s and wave height > 3 m/s. Expecting a low system approaching from W (see picture), we stretched our station spacing from 30 miles to 34 miles.
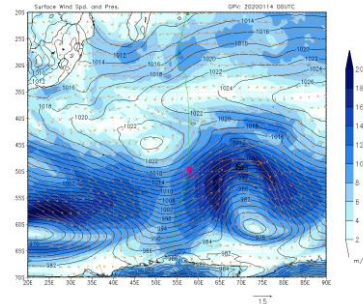
16th Jan: caught by another low pressure system. During Station 126 upcast (around 2800 dbar), wind picked up > 20 m/s and Captain decided to recover the CTD without stopping (fire-as-we-go). Reordering sampling bottle numbers was a chaos but we managed. Substituted Station 127 with an XCTD down to 2000 m. Wind > 20 m/s and wave > 5 m.

17th Jan:, we ended up deploying 3 XCTD's in places of CTD observation in a row. Once we sailed into the eye of the low pressure, the wind almost stopped but with a huge swell > 6 m from W. Resumed casts from Station 132.

18th Jan: still strong wind > 10 m/s and swell > 3.5 m in the right angle such that the ship rolled and rolled during CTD casts.

19th Jan: Finally much nicer sea, but freezing. It snows here with sub-zero air temperature.

20th Jan: Icebergs!

21st Jan: extremely calm. Almost zero wind and < 1 m wave height. It is sub-zero temperature but comfortable on the deck. Sporadic icebergs, maybe less frequent than whale breathing.

22nd Jan: the southernmost Station, 154, was covered by ice. We deployed the final CTD 2 miles north of Station 153 and farewelled Antarctica (visible!) at 0.2 miles north of Station 153 with an XCTD. Back home after 3 week transit.

2. Science Party

Table 2.1 List of participants for MR19-04 leg 2

Name	Responsibility	Affiliation
Akihiko Murata	DIC/TA/pCO_2/Water sampling	RIGC/JAMSTEC
Katsuro Katsumata	CTD/LADCP/Water sampling	RIGC/JAMSTEC
Yuichiro Kumamoto	DO/Cs/Ra/^{14}C/^{13}C/Water sampling	RIGC/JAMSTEC
Hiroshi Uchida	Salinity/Density/Microplastic/Water sampling	RIGC/JAMSTEC
Shinya Kouketsu	CTD/LADCP/Water sampling	RIGC/JAMSTEC
Sayaka Yasunaka	Water sampling	RIGC/JAMSTEC
Masahito Shigemitsu	CFCs/FDOM/DOC	RIGC/JAMSTEC
Kosei Sasaoka	Chl-a/CDOM/Water sampling	RIGC/JAMSTEC
Minoru Hamana	Water sampling	RIGC/JAMSTEC
Taichi Yokokawa	CH_4/N_2O/Bacteria/DNA/Water sampling	SUGAR/JAMSTEC
Eiji Tasumi	CH_4/N_2O/Bacteria/DNA/Water sampling	SUGAR/JAMSTEC
Akiko Makabe	CH_4/N_2O/Bacteria/DNA/Water sampling	SUGAR/JAMSTEC
Kiminori Shitashima	Radon & pH·pCO_2 sensors/Water sampling	TUMSAT
Satoko Owari	^{129}I/Water sampling	TUMSAT
Peter Leslie Croot	Iodate/Urea/Water sampling	NUIG
Li Bofeng	N_2/O_2/Ar/Water sampling	Hokkaido Univ.
Wang Chenye	N_2/O_2/Ar/Water sampling	Hokkaido Univ.
Sasaki Yusuke	Micro lidar/Water sampling	Univ. of Tokyo
S. C. W Jayasuriya	Observer	Sri Lanka Navy
K. Arulananthan	Observer/Water sampling	NARA
Adikari Appuhami lage Upul	Observer/Water sampling	NARA
Kasumi Yamauchi	FDOM	RIGC/JAMSTEC
Koki Miyakawa	DNA/Water sampling	RIGC/JAMSTEC
Soichiro Sueyoshi	Meteorology/Geophysics/ADCP	NME
Yutaro Murakami	Meteorology/Geophysics/ADCP	NME
Masanori Murakami	Meteorology/Geophysics/ADCP	NME
Yasuhiro Arii	Water sampling	MWJ
Masahiro Orui	CFCs	MWJ
Shinsuke Toyoda	CTD/Argo	MWJ
Misato Kuwahara	DO/TSG/Chl-a	MWJ
Tun Htet Aung	CTD/Argo	MWJ
Tomoyuki Tanaka	Nutrients	MWJ
Hiroki Ushiromura	Salinity	MWJ
Keisuke Takeda	CTD/Argo	MWJ
Yuta Oda	DIC/TA	MWJ
Katsunori Sagishima	CFCs	MWJ
Nagisa Fujiki	DIC/TA/pCO_2	MWJ
Hiroshi Hoshino	CFCs	MWJ
Keitaro Matsumoto	Nutrients	MWJ
Atsushi Ono	DIC/TA/pCO_2	MWJ
Tomomi Sone	Nutrients	MWJ
Erii Irie	DO/TSG/Chl-a	MWJ
Yuko Miyoshi	DO/TSG/Chl-a	MWJ

RIGC: Research Institute for Global Change, JAMSTEC: Japan Agency for Marine-Earth Science and Technology, SUGAR: Super-cutting-edge Grand and Advanced Research Program, TUMSAT: Tokyo University of Marine Science and Technology, NUIG: National University of Ireland Galway, NARA: National Aquatic Resources Research and Development Agency, NME: Nippon Marine Enterprises, MWJ: Marine Works Japan

Table 2.2 List of participants for MR19-04 leg 3

Name	Responsibility	Affiliation
Katsuro Katsumata	CTD/LADCP/Water sampling	RIGC/JAMSTEC
Yuichiro Kumamoto	DO/Cs/Ra/^{14}C/^{13}C/Water sampling	RIGC/JAMSTEC
Hiroshi Uchida	Salinity/Density/Microplastic/Water sampling	RIGC/JAMSTEC
Shinya Kouketsu	CTD/LADCP/Water sampling	RIGC/JAMSTEC
Masahito Shigemitsu	CFCs/FDOM/DOC	RIGC/JAMSTEC
Kosei Sasaoka	Chl-a/CDOM/Water sampling	RIGC/JAMSTEC
Minoru Hamana	Water sampling	RIGC/JAMSTEC
Maija I. Heller	Iodate/Urea/Water sampling	PCUV
Melissa T. Miller	SOCCOM floats/Water sampling	SIO
Sasaki Yusuke	Micro lidar/Water sampling	Univ. of Tokyo
Kasumi Yamauchi	FDOM	RIGC/JAMSTEC
Koki Miyakawa	DNA/Water sampling	RIGC/JAMSTEC
Kazuho Yoshida	Meteorology/Geophysics/ADCP	NME
WataruTokunaga	Meteorology/Geophysics/ADCP	NME
Satomi Ogawa	Meteorology/Geophysics/ADCP	NME
Yasuhiro Arii	Water sampling	MWJ
Katsunori Sagishima	CFCs	MWJ
Masanori Enoki	DIC/TA/ pCO$_2$	MWJ
Shinichiro Yokogawa	Nutrients	MWJ
Misato Kuwahara	DO/TSG/Chl-a	MWJ
Hiroshi Hoshino	CFCs	MWJ
Atsushi Ono	CFCs/ pCO$_2$	MWJ
Tomomi Sone	Nutrients	MWJ
Erii Irie	DO/TSG/Chl-a	MWJ
Yuko Miyoshi	DO/TSG/Chl-a	MWJ
Nagisa Fujiki	DIC/TA/pCO$_2$	MWJ
Hiroyuki Hayashi	CTD/Argo	MWJ
Rio Kobayashi	CTD/Argo	MWJ
Kento Fukahori	CTD/Argo	MWJ
Daiki Kawata	DIC/TA/ pCO$_2$	MWJ
Shungo Oshitani	Salinity/Argo	MWJ
Ko Morita	Nutrients	MWJ
Shuntaro Hyogo	Water sampling	MWJ
Takuma Matsumoto	Water sampling	MWJ
Mikio Hasegawa	Water sampling	MWJ
Misaki Otsuka	Water sampling	MWJ

RIGC: Research Institute for Global Change, JAMSTEC: Japan Agency for Marine-Earth Science and TechnologyPCUV: Pontifical Catholic University of Valparaiso, SIO: Scripps Institution of Oceanography, Nippon Marine Enterprises, MWJ: Marine Works Japan

4. Hydrographic Measurement

4.1 CTDO$_2$
February 9, 2020

(1) Personnel
> Hiroshi Uchida (JAMSTEC)
> Katsuro Katsumata (JAMSTEC)
> Shinya Kouketsu (JAMSTEC)
> Shinsuke Toyoda (MWJ) (leg 2)
> Keisuke Takeda (MWJ) (leg 2)
> Tun Htet Aung (MWJ) (leg 2)
> Rio Kobayashi (MWJ) (leg 3)
> Hiroyuki Hayashi (MWJ) (leg 3)
> Kento Fukahori (MWJ) (leg 3)

(2) Objective
> The CTDO$_2$/water sampling measurements were conducted to obtain vertical profiles of seawater properties by sensors and water sampling.

(3) Instruments and method
> Materials used in this cruise are as follows:

> *Winch, cable, and frame*
> Traction winch system (4.5 ton), Dynacon, Inc., Bryan, Texas, USA (Fukasawa et al., 2004)
> 8,080 m of 9.53 mm armored cable, Rochester Wire & Cable, LLC, Culpeper, Virginia, USA
> > (routinely cut 400 m after the leg 2)
> Compact underwater slip ring swivel, Hanayuu Co., Ltd., Shizuoka, Japan (Uchida et al., 2018)

> *Deck unit*
> SBE 11plus, Sea-Bird Scientific, Bellevue, Washington, USA
> > Serial no. 11P54451-0872

> *Frame, water sampler*
> 460 kg stainless steel frame for 36-position 12-L water sample bottles
> > with an aluminum rectangular fin (54 × 90 cm) to resist frame's rotation
> > (weight of the full CTD/water sampling package was about 930 kg)
> 36-position carousel water sampler, SBE 32, Sea-Bird Scientific
> > Serial no. 3254451-0826
> 12-L Niskin-X water sample bottle, model 1010X, General Oceanic, Inc., Miami, Florida, USA
> > (No TEFLON coating)
> 12-L sample bottle, model OTE 110, OceanTest Equipment, Inc., Fort Lauderdale, Florida, USA
> > (No TEFLON coating)

> *Underwater unit*
> Pressure sensor, SBE 9plus, Sea-Bird Scientific
> > Serial no. 09P54451-1027 (117457) (calibration date: April 18, 2019)
> Deep standard reference thermometer, SBE 35, Sea-Bird Scientific
> > Serial no. 0045 (calibration date: April 1, 2019)
> Temperature sensor, SBE 3F, Sea-Bird Scientific
> > Primary serial no. 031525 (calibration date: June 1, 2019)
> > Secondary serial no. 031359 (calibration date: June 27, 2019)
> Conductivity sensor, SBE 4C, Sea-Bird Scientific
> > Primary serial no. 042435 (calibration date: June 25, 2019)
> > Secondary serial no. 042854 (calibration date: June 26, 2019)
> Dissolved oxygen sensor

primary, RINKO III, JFE Advantech Co., Ltd., Osaka, Japan
    Serial no. 037, Sensing foil no. 182822 (calibration date: September 18, 2019)
Secondary, SBE 43, Sea-Bird Scientific
    Serial no. 432211 (calibration date: June 19, 2019)
Transmissometer, C-Star, WET Labs, Inc., Philomath, Oregon, USA
    Serial no. 1727DR
Chlorophyll fluorometer, Seapoint Sensors Inc., Exeter, New Hampshire, USA
    Serial no. 3618, Gain: 30X (0-5 ug/L) for stations 001 – 097,
        Gain: 10X (0-15 ug/L) for stations 098 – 153
Ultraviolet fluorometer, Seapoint Sensors Inc.
    Serial no. 6223, Gain 30X (0-50 QSU)
Turbidity meter, Seapoint Sensors Inc.
    Serial no. 14953, Gain 100X (0-25 FTU)
Photosynthetically Active Radiation (PAR) sensor, PAR-Log ICSW,
        Satlantic, LP, Halifax, Nova Scotia, Canada
    Serial no. 1025 (calibration date: July 6, 2015)
Altimeter, PSA-916T, Teledyne Benthos, Inc.
    Serial no. 1157
Pump, SBE 5T, Sea-Bird Scientific
    Primary serial no. 055816
    Secondary serial no. 054598
Other additional sensors
    Lowered acoustic Doppler current profilers (see section 4.4)
    Micro Ridar (see section 4.5)
    Refractive index density sensor (see section 4.30)
    Sound velocity profiler (see section 4.29)
    RBR TD/ODO sensors (see section 4.32)
    Radon (gamma-ray) sensor (see section 4.27)
    pH/pCO$_2$ sensors (see section 4.28)

Software
Data acquisition software, SEASAVE-Win32, version 7.23.2
Data processing software, SBEDataProcessing-Win32, version 7.23.2 and some original modules

(4) Pre-cruise calibration
(4.1) Pressure sensor
    Pre-cruise sensor calibration for linearization was performed at Sea-Bird Scientific. The time drift of the pressure sensor was adjusted by periodic recertification corrections by using electric dead-weight testers (model E-DWT-H A70M and A200M, Fluke Co., Phoenix, Arizona, USA) and a barometer (model RPM4 BA100Ks, Fluke Co.):
        Serial no. 181 (A70M) (for 10-70 MPa) (calibration date: January 19, 2019)
        Serial no. 1305 (A200M) (for 90 to 100 MPa) (calibration date: January 19, 2019)
        Serial no. 1453 (BA100Ks) (for 0 MPa) (calibration date: January 15, 2019)
These reference pressure sensors were calibrated by Ohte Giken, Inc. (Ibaraki, Japan) traceable to National Institute of Standards and Technology (NIST) pressure standards. The pre-cruise correction was performed at JAMSTEC (Kanagawa, Japan) by Marine Works Japan Ltd. (MWJ) (Kanagawa, Japan) (Fig. 4.1.1).
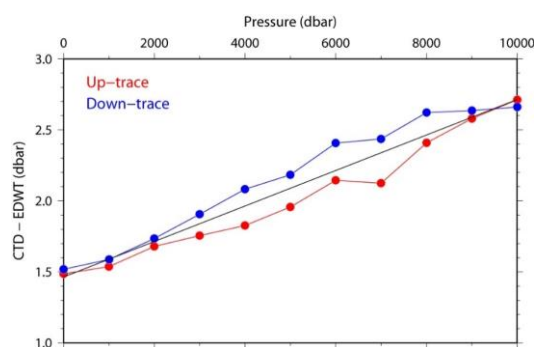
Fig. 4.1.1. Pre-cruise comparison of the CTD pressure and the reference pressure (E-DWT).

(4.2) Temperature sensors

Pre-cruise sensor calibrations of the SBE 3s were performed at Sea-Bird Scientific. Pre-cruise sensor calibration of the SBE 35 for linearization was also performed at Sea-Bird Scientific. The slow time drift of the SBE 35 was adjusted by periodic recertification corrections by measurements in thermodynamic fixed-point cells (water triple point [0.01 °C] and gallium melt point [29.7646b °C]) (Uchida et al., 2015). Since 2016, pre-cruise calibration was performed at JAMSTEC by using fixed-point cells traceable to National Metrology Institute of Japan (NMIJ) temperature standards (Fig. 4.1.2).
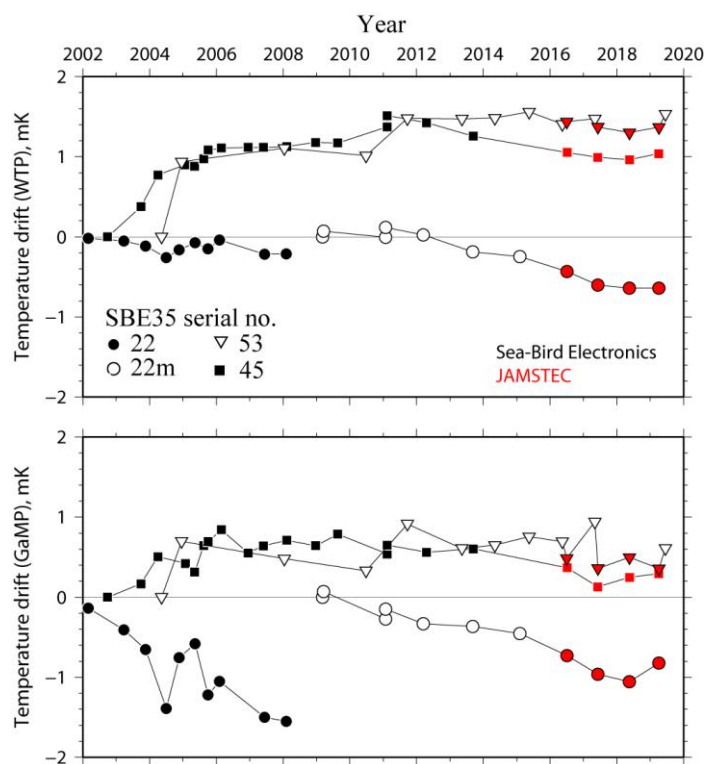

Fig. 4.1.2. Time drifts (temperature offsets relative to the first calibration) of four SBE 35s based on laboratory calibrations in fixed-point cells (water triple point: WTP, gallium melt point: GaMP).

(4.3) Conductivity sensors

Pre-cruise sensor calibrations were performed at Sea-Bird Scientific.

(4.4) Dissolved oxygen sensors

Pre-cruise sensor calibration of RINKO was performed at JAMSTEC by using O_2/N_2 standard gases (JCSS Grande 1, Taiyo Nippon Sanso Co., Japan):

3.978% of O2, chamber no. 3MK-61964 (certification date: May 29, 2018)
9.979% of O2, chamber no. 1MK-52697 (certification date: May 29, 2018)
16.97% of O2, chamber no. 3MK-35986 (certification date: May 29, 2018)
24.96% of O2, chamber no. MK-84510 (certification date: May 24, 2018)

The standard gas-saturated pure water was measured by the RINKO at temperature of 1, 10, 20 and 29 °C. Oxygen saturation was calculated from oxygen concentration of the standard gases, water temperature, and the atmospheric pressure in the calibration vessel and used to calibrate the RINKO (Fig. 4.1.3) by using the modified Stern-Volmer equation slightly modified from a method by Uchida et al. (2010). The calibration coefficients for the pressure dependency were determined from the results from the previous cruises. Details of the calibration equations are described in the sub-section of the post-cruise calibration.
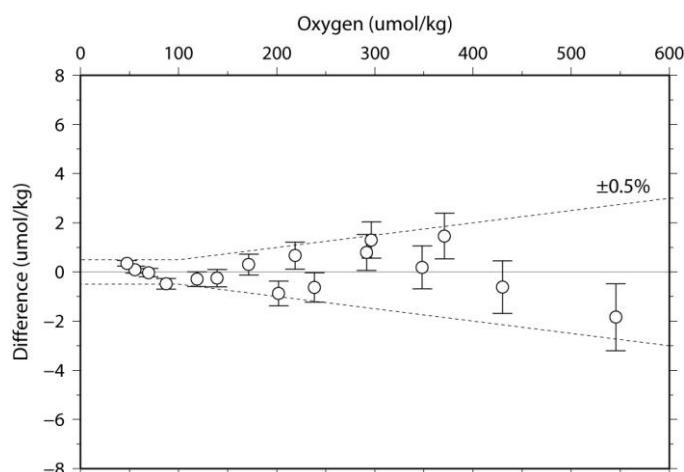

Fig. 4.1.3. Result of pre-cruise calibration of the RINKO-III (serial no. 0037). Difference between the calibrated oxygen sensor data and the reference dissolved oxygen values are shown.

Pre-cruise sensor calibration of SBE 43 was performed at Sea-Bird Scientific.

(4.5) Ultraviolet fluorometer

Periodic recertification was not performed by the manufacturer for the ultraviolet fluorometer. However, the ultra pure water and the Multi-parametric Standard Seawater (MSSW) (lot PRE18) were periodically measured at JAMSTEC (Fig. 4.1.4). The MSSW is currently under development jointly by KANSO CO., Ltd. (Osaka, Japan) (Uchida et al., 2020), and fluorescent dissolved organic matter (FDOM) will be measured after this cruise to calibrate the ultraviolet fluorometer in the laboratory.

Temperature dependency of the ultraviolet fluorometer following the method by Yamashita et al. (2015):

CTDUVFLUORcorr = CTDUVFLUOR/(1.0 + $\rho \times$ [T – T_r])
$\rho = -0.0065$
$T_r = 20$

where T is temperature (in °C), T_r is reference temperature (in °C) and ρ is the correction coefficient determined from the laboratory measurement (Fig. 4.1.4).
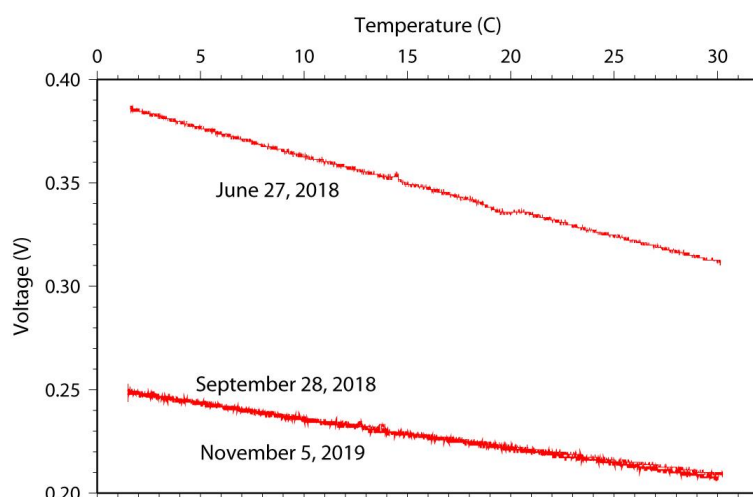
Fig. 4.1.4. Temperature dependency of the ultraviolet fluorometer for the MSSW (PRE18). The sensor output was suddenly shifted in the deep ocean during the CTD cast in July-Augast 2018 (RV Mirai cruise MR18-04).

(4.6) Transmissometer

Light transmission (T_r in %) is calibrated as

$$T_r = (V–V_d) / (V_r–V_d) \times 100$$

wehre V is the measured signal (voltage), V_d is the dark offset for the instrument, and V_r is the signal for clear water. V_d can be obtained by blocking the light path. The calibration coefficients (V_d and V_r) estimated from the previous cruise were used, because periodic recertification was not performed by the manufacturer for the transmissometer.

(4.7) Turbidity meter, chlorophyll fluorometer, PAR, altimeter

Periodic recertification was not performed by the manufacturer for these sensors.

(5) Data collection and processing

(5.1) Data collection

The CTD system was powered on at least 20 minutes in advance of the data acquisition to stabilize the pressure sensor. The data was acquired at least two minutes before and after the CTD cast to collect atmospheric pressure data on the ship's deck.

The CTD package was lowered into the water from the starboard side and held 10 m beneath the surface in order to activate the pump. After the pump was activated, the package was lifted to the surface and lowered at a rate of 1.0 m/s to 200 m (or 300 m when significant wave height was high) then the package was stopped to operate the heave compensator of the crane. The package was lowered again at a rate of 1.2 m/s to the bottom. For the up cast, the package was lifted at a rate of 1.1 m/s except for bottle firing stops. As a rule, the bottle was fired after waiting from the stop for more than 30 seconds and the package was stayed at least 5 seconds for measurement of the SBE 35 at each bottle firing stops. For depths where vertical gradient of water properties was expected to be large (from surface to thermocline), the bottle was fired after waiting from the stop for 60 seconds to enhance exchanging the water between inside and outside of the bottle. At 200 m (or 300 m) from the surface, the package was stopped to stop the heave compensator of the crane.

The water sample bottles and the stainless-steel frame of the CTD package were wiped with acetone before a cast taken water for CFCs.

(5.2) Data collection problems

There were many leaks of the water sample bottles because the top or bottom cap of the bottle did not close correctly, especially for the bottles model OTE 110 (OceanTest Equipment, Inc.).

At station 86, data quality of the primary temperature and conductivity was bad at depths deeper than 378 dbar probably due to jellyfish in the TC duct. Therefore, the secondary temperature and conductivity data were used for station 86.

15

At station 97, the chlorophyll fluorometer data were not obtained at the chlorophyll max layer (9-24 dbar in the down cast) due to low measurement range (0-5 μg/L) of the sensor.

At station 126, the water sample bottles were closed without bottle firing stops at depths shallower than 2730 dbar to finish the CTD cast urgently due to rough weather. The bottle data obtained without bottle firing stops were averaged over ±1 second of the bottle firing time.

At station 132, the RINKO data were not obtained because the cap of the sensing foil was not removed before the cast. Therefore, the SBE 43 data were used for station 132.

For the transmissometer, the sensor output was shifted at 581 dbar in the down caast of station 22. Offset correction (+0.006 V) was applied to the sensor output for depths deeper than 580 dbar. Data quality of the sensor output was bad in the down cast between 205 to 4660 dbar of station 36 and between 1135 to 4978 dbar of station 55 probably because of the effect of jellyfish, and the data quality flag was set to 4 (bad measurement) for the data.

(5.3) Data processing

The following are the data processing software (SBEDataProcessing-Win32) and original software data processing module sequence and specifications used in the reduction of CTD data in this cruise.

DATCNV converted the raw data to engineering unit data. DATCNV also extracted bottle information where scans were marked with the bottle confirm bit during acquisition. The duration was set to 4.4 seconds, and the offset was set to 0.0 second. The hysteresis correction for the SBE 43 data (voltage) was applied for both profile and bottle information data.

TCORP (original module, version 1.1) corrected the pressure sensitivity of the SBE 3 for both profile and bottle information data.

RINKOCOR (original module, version 1.0) corrected the time-dependent, pressure-induced effect (hysteresis) of the RINKO for both profile data.

RINKOCORROS (original module, version 1.0) corrected the time-dependent, pressure-induced effect (hysteresis) of the RINKO for bottle information data by using the hysteresis-corrected profile data.

BOTTLESUM created a summary of the bottle data. The data were averaged over 4.4 seconds.

ALIGNCTD converted the time-sequence of sensor outputs into the pressure sequence to ensure that all calculations were made using measurements from the same parcel of water. For a SBE 9plus CTD with the ducted temperature and conductivity sensors and a 3000-rpm pump, the typical net advance of the conductivity relative to the temperature is 0.073 seconds. So, the SBE 11plus deck unit was set to advance the primary and the secondary conductivity for 1.73 scans (1.75/24 = 0.073 seconds). Oxygen data are also systematically delayed with respect to depth mainly because of the long time constant of the oxygen sensor and of an additional delay from the transit time of water in the pumped plumbing line. This delay was compensated by 5 seconds advancing the SBE 43 oxygen sensor output (voltage) relative to the temperature data. Delay of the RINKO data was also compensated by 1 second advancing sensor output (voltage) relative to the temperature data. Delay of the transmissometer data was also compensated by 2 seconds advancing sensor output (voltage) relative to the temperature data.

WILDEDIT marked extreme outliers in the data files. The first pass of WILDEDIT obtained an accurate estimate of the true standard deviation of the data. The data were read in blocks of 1000 scans. Data greater than 10 standard deviations were flagged. The second pass computed a standard deviation over the same 1000 scans excluding the flagged values. Values greater than 20 standard deviations were marked bad. This process was applied to pressure, temperature, conductivity, and SBE 43 output.

CELLTM used a recursive filter to remove conductivity cell thermal mass effects from the measured conductivity. Typical values used were thermal anomaly amplitude alpha = 0.03 and the time constant 1/beta = 7.0.

FILTER performed a low pass filter on pressure with a time constant of 0.15 seconds. In order to produce zero phase lag (no time shift) the filter runs forward first then backwards.

WFILTER performed as a median filter to remove spikes in fluorometer, turbidity meter, transmissometer, and ultraviolet fluorometer data. A median value was determined by 49 scans of the window. For the ultraviolet fluorometer data, an additional box-car filter with a window of 361 scans was applied to remove noise.

SECTIONU (original module, version 1.1) selected a time span of data based on scan number in order to reduce a file size. The minimum number was set to be the start time when the CTD package was beneath the sea-surface after activation of the pump. The maximum number was set to be the end time when the depth of the package was 1 dbar below the surface. The minimum and maximum numbers were automatically calculated in the module.

LOOPEDIT marked scans where the CTD was moving less than the minimum velocity of 0.0 m/s (traveling backwards due to ship roll).

DESPIKE (original module, version 1.0) removed spikes of the data. A median and mean absolute deviation was calculated in 1-dbar pressure bins for both down- and up-cast, excluding the flagged values. Values greater than 4 mean absolute deviations from the median were marked bad for each bin. This process was performed 2 times for temperature, conductivity, SBE 43, and RINKO output.

DERIVE was used to compute oxygen (SBE 43).

BINAVG averaged the data into 1-dbar pressure bins. The center value of the first bin was set equal to the bin size. The bin minimum and maximum values are the center value plus and minus half the bin size. Scans with pressures greater than the minimum and less than or equal to the maximum were averaged. Scans were interpolated so that a data record exist every dbar.

BOTTOMCUT (original module, version 0.1) deleted the deepest pressure bin when the averaged scan number of the deepest bin was smaller than the average scan number of the bin just above.

DERIVE was re-used to compute salinity, potential temperature, and density

SPLIT was used to split data into the down cast and the up cast.

Remaining spikes in the CTD data were manually eliminated from the 1-dbar-averaged data. The data gaps resulting from the elimination were linearly interpolated with a quality flag of 6.

(6) Post-cruise calibration

(6.1) Pressure sensor

The CTD pressure sensor offset in the period of the cruise was estimated from the pressure readings on the ship's deck. For best results the Paroscientific sensor was powered on for at least 20 minutes before the operation. In order to get the calibration data for the pre- and post-cast pressure sensor drift, the CTD deck pressure was averaged over first and last one minute, respectively. Then the atmospheric pressure deviation from a standard atmospheric pressure (1013.25 hPa) was subtracted from the CTD deck pressure to check the pressure sensor time drift. The atmospheric pressure was measured at the captain deck (20 m high from the base line) and sub-sampled one-minute interval as a meteorological data.

Time series of the CTD deck pressure is shown in Figs. 4.1.5 and 4.1.6. The CTD pressure sensor offset was estimated from the deck pressure. Mean of the pre- and the post-casts data over the whole period gave an estimation of the pressure sensor offset (0.07 and 0.03 dbar for leg 2 and leg 3, respectively) from the pre-cruise calibration. The post-cruise correction of the pressure data is not deemed necessary for the pressure sensor.
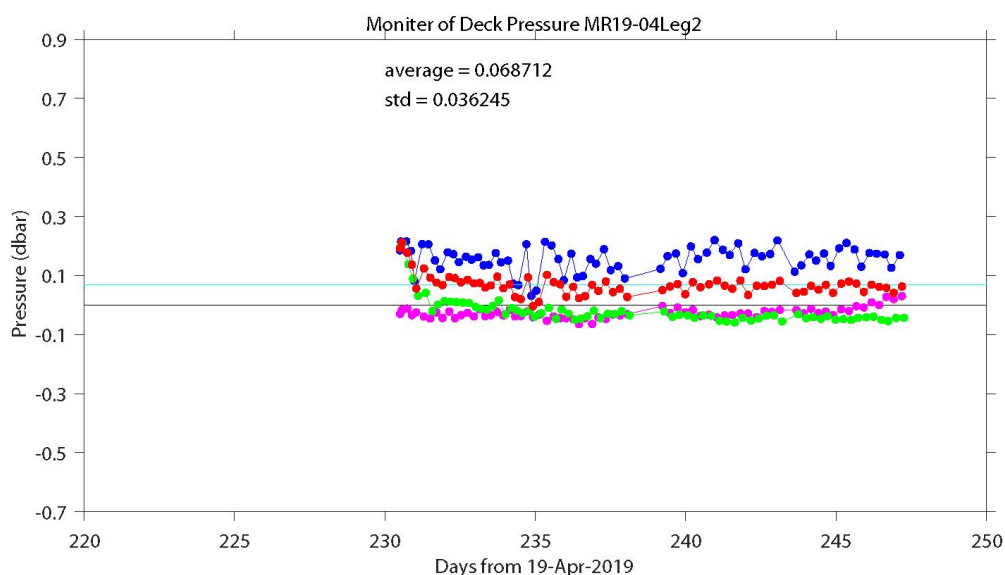

Fig. 4.1.5. Time series of the CTD deck pressure for leg 2. Atmospheric pressure deviation (magenta dots)

from a standard atmospheric pressure was subtracted from the CTD deck pressure. Blue and green dots indicate pre- and post-cast deck pressures, respectively. Red dots indicate averages of the pre- and the post-cast deck pressures.
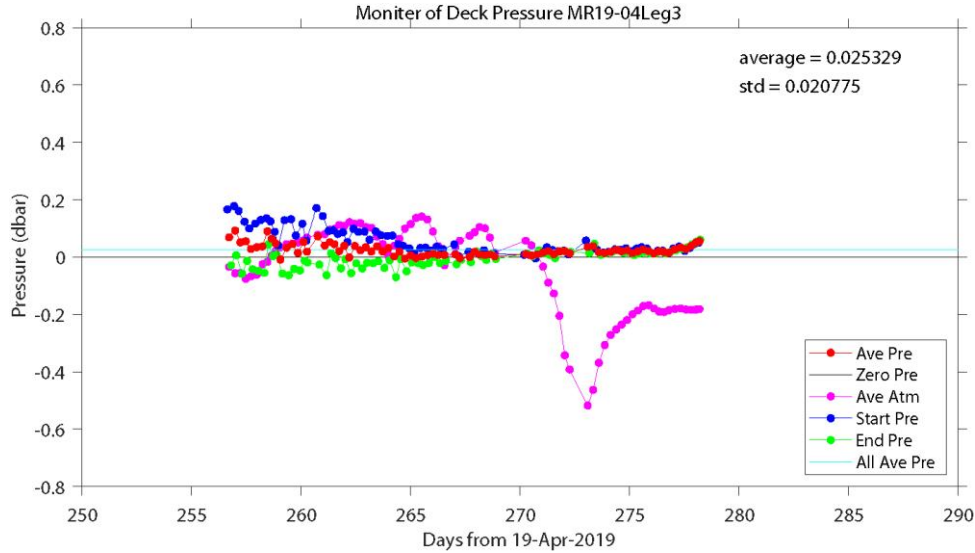

Fig. 4.1.6. Same as Fig. 4.1.5, but for leg 3.

(6.2) Temperature sensors

The CTD temperature sensors (SBE 3) were calibrated with the SBE 35 under the assumption that discrepancies between SBE 3 and SBE 35 data were due to pressure sensitivity, the viscous heating effect, and time drift of the SBE 3 (Uchida et al., 2015).

Post-cruise sensor calibration for the SBE 35 will be performed at JAMSTEC in August 2020.

The CTD temperature was calibrated as

Calibrated temperature $= T - (c_0 \times P + c_1 \times t + c_2)$

where T is CTD temperature in °C, P is pressure in dbar, t is time in days from pre-cruise calibration date of the CTD temperature and c_0, c_1, and c_2 are calibration coefficients. The coefficients were determined using the data for the depths deeper than 1950 dbar.

The primary temperature data were basically used for the post-cruise calibration. The secondary temperature sensor was also calibrated and used instead of the primary temperature data when the data quality of the primary temperature data was bad (station 86). The results of the post-cruise calibration for the CTD temperature are shown in Table 4.1.1, Figs. 4.1.7, 4.1.8, and 4.1.9, and the calibration coefficients are as follows:

c_0 = 5.19734252e-08, c_1 = 4.49880e-06, c_2 = -9.6313e-04   [for leg 2, primary]
c_0 = 1.13549796e-08, c_1 = 2.72736e-05, c_2 = -5.7034e-03   [for leg 3, primary]
c_0 = -3.56735208e-08, c_1 = 3.41359e-07, c_2 = -5.1565e-04   [for leg 3, secondary]

Table 4.1.1. Difference between the CTD temperature and the SBE 35 after the post-cruise calibration. Mean and standard deviation (Sdev) are calculated for the data below and above 1950 dbar. Number of data used is also shown.

Leg	Sensor	Pressure ≥ 1950 dbar			Pressure < 1950 dbar		
		Number	Mean (mK)	Sdev (mK)	Number	Mean (mK)	Sdev (mK)
2	Primary	450	–0.1	0.4	915	–0.6	8.4

18

| 3 | Primary | 525 | −0.0 | 0.4 | | 890 | −0.5 | 6.1 |
| 3 | Secondary | 511 | 0.0 | 0.3 | | 832 | 0.3 | 2.6 |

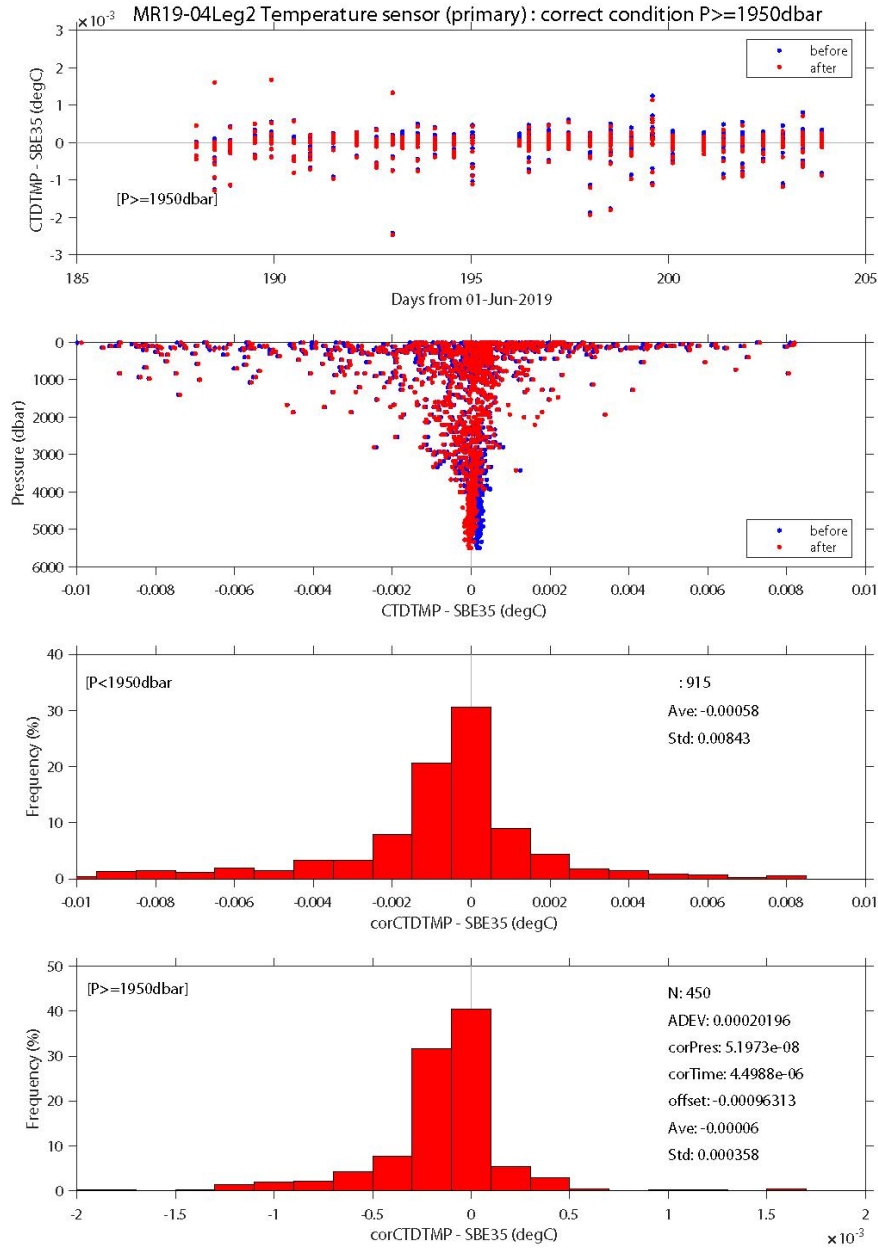

Fig. 4.1.7. Difference between the CTD temperature (primary) and the SBE 35 for leg 2. Blue and red dots indicate before and after the post-cruise calibration using the SBE 35 data, respectively. Lower two panels show histogram of the difference after the calibration.
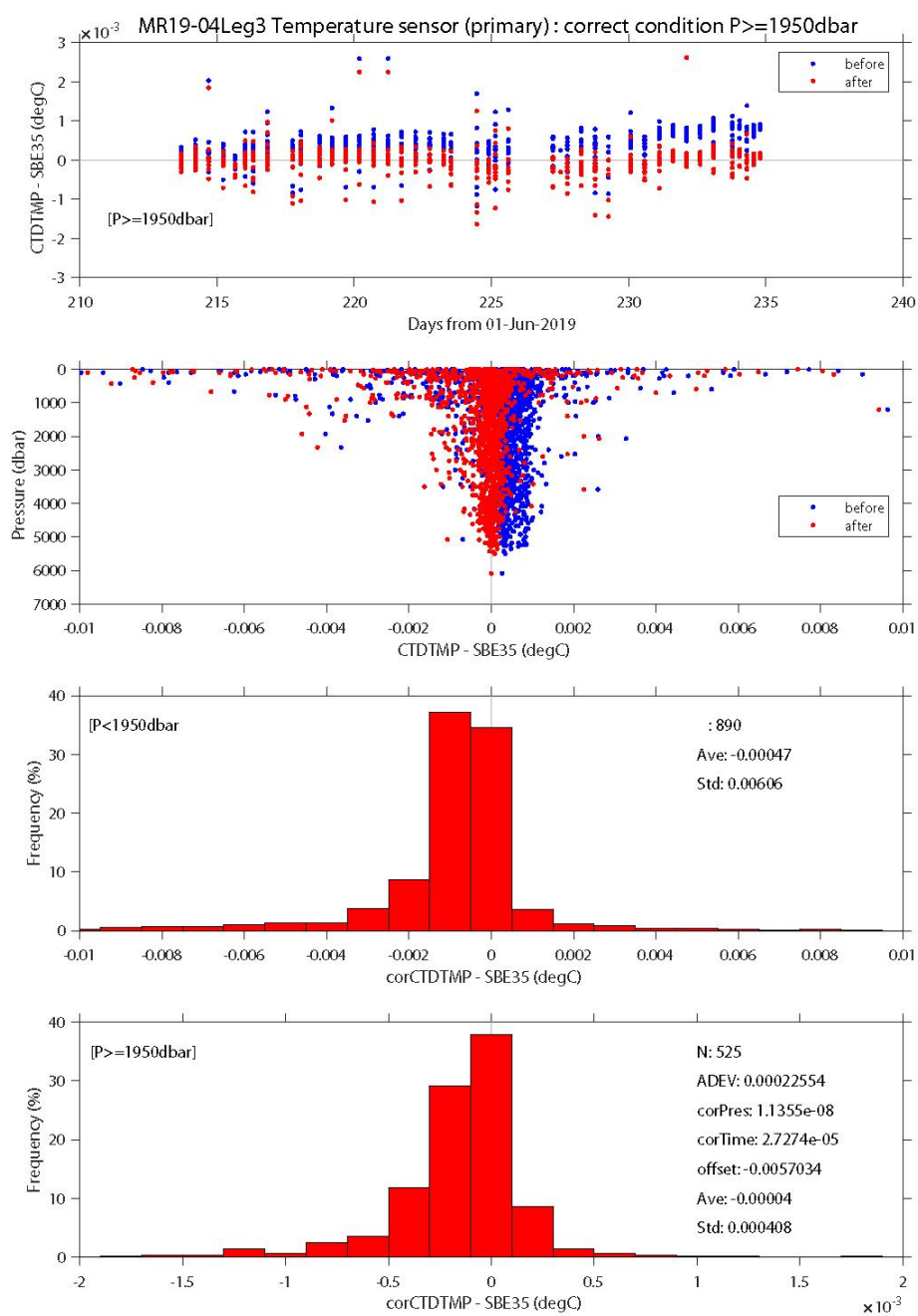
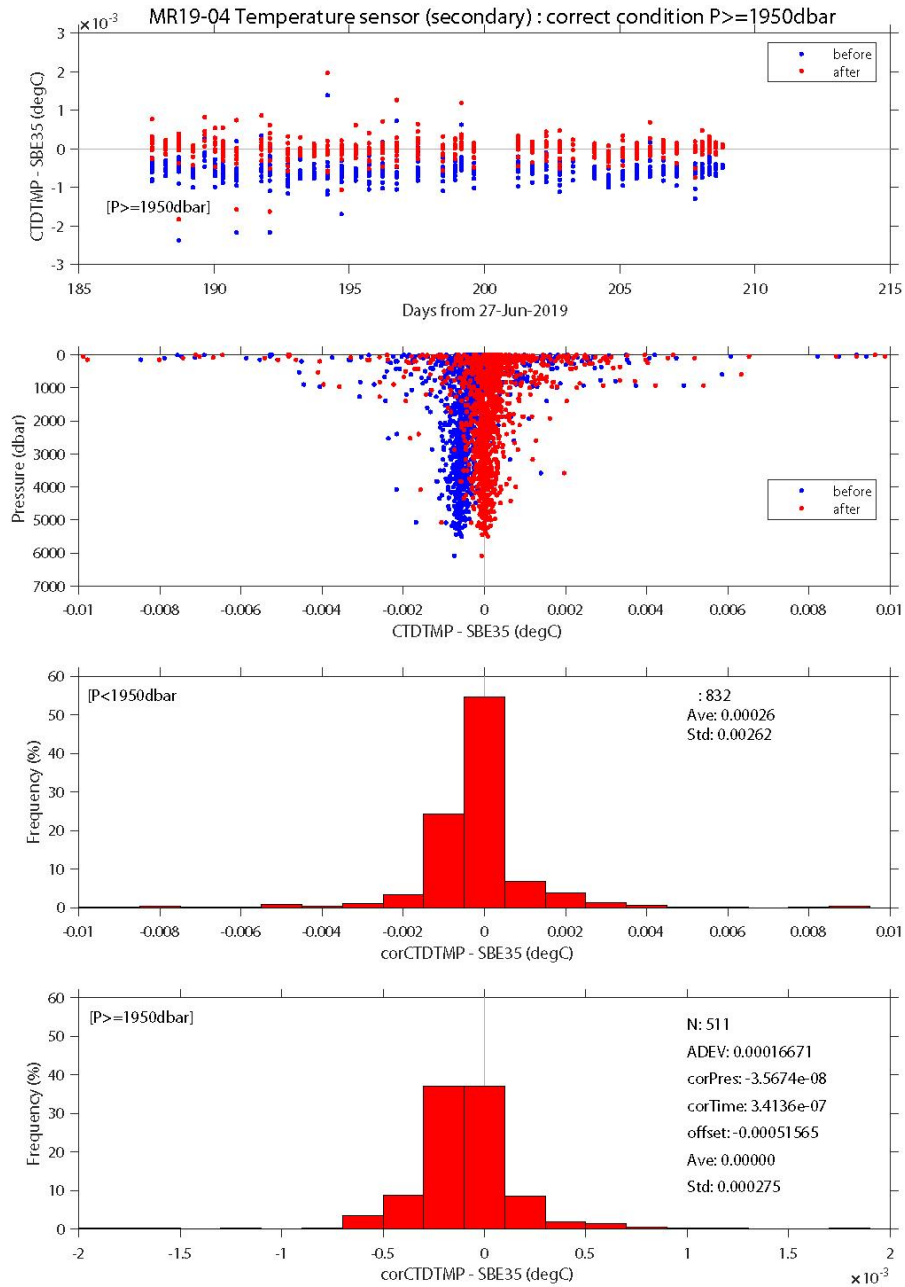Fig. 4.1.8. Same as Fig. 4.1.7, but for leg 3 (primary temperature).

Fig. 4.1.9. Same as Fig. 4.1.7, but for leg 3 (secondary temperature).

(6.3) Conductivity sensor

The discrepancy between the CTD conductivity and the conductivity calculated from the bottle salinity data with the CTD temperature and pressure data is considered to be a function of conductivity, pressure and time. The CTD conductivity was calibrated as

Calibrated conductivity =
$$C - (c_0 \times C + c_1 \times P + c_2 \times C \times P + c_3 \times P^2 + c_4 \times P^2 \times C + c_5 \times P^2 \times C^2 + c_6 \times t + c_7)$$

where C is CTD conductivity in S/m, P is pressure in dbar, t is time in days and c_0, c_1, c_2, c_3, c_4, c_5, c_6 and c_7 are calibration coefficients. The best fit sets of coefficients were determined by a least square technique to minimize the deviation from the conductivity calculated from the bottle salinity data.

The primary conductivity data created by the software module ROSSUM were used after the post-cruise calibration for the temperature data. The results of the post-cruise calibration for the CTD salinity

21

are summarized in Table 4.1.2 and shown in Figs 4.1.10, 4.1.11 and 4.1.12. The calibration coefficients are as follows:

c_0 = 5.1161481588e-05, c_1 = -2.9852469268e-07, c_2 = 8.6423667125e-08,
c_3 = -7.8216002143e-11, c_4 = 1.5213293009e-10, c_5 = -3.9207472832e-11,
c_6 = 5.5962247644e-08, c_7 = 1.8345172035e-04   [for leg 2, primary]

c_0 = 8.4059171088e-05, c_1 = 3.9805334321e-07, c_2 = -1.0817725126e-07,
c_3 = -6.6727430535e-10, c_4 = 4.3600536612e-10, c_5 = -7.1667314964e-11,
c_6 = 5.3289917898e-06, c_7 = -6.1688283232e-05   [for leg 3, primary]

c_0 = 9.2155745106e-05, c_1 = 3.2725052723e-07, c_2 = -8.7940015706e-08,
c_3 = -2.8014029332e-10, c_4 = 1.9319180823e-10, c_5 = -3.3675443715e-11,
c_6 = 4.4847233878e-06, c_7 = -2.4324855043e-04   [for leg 3, secondary]

Table 4.1.2. Difference between the CTD salinity and the bottle sampled salinity after the post-cruise calibration. Mean and standard deviation (Sdev) are calculated for the data below and above 1950 dbar. Number of data used is also shown.

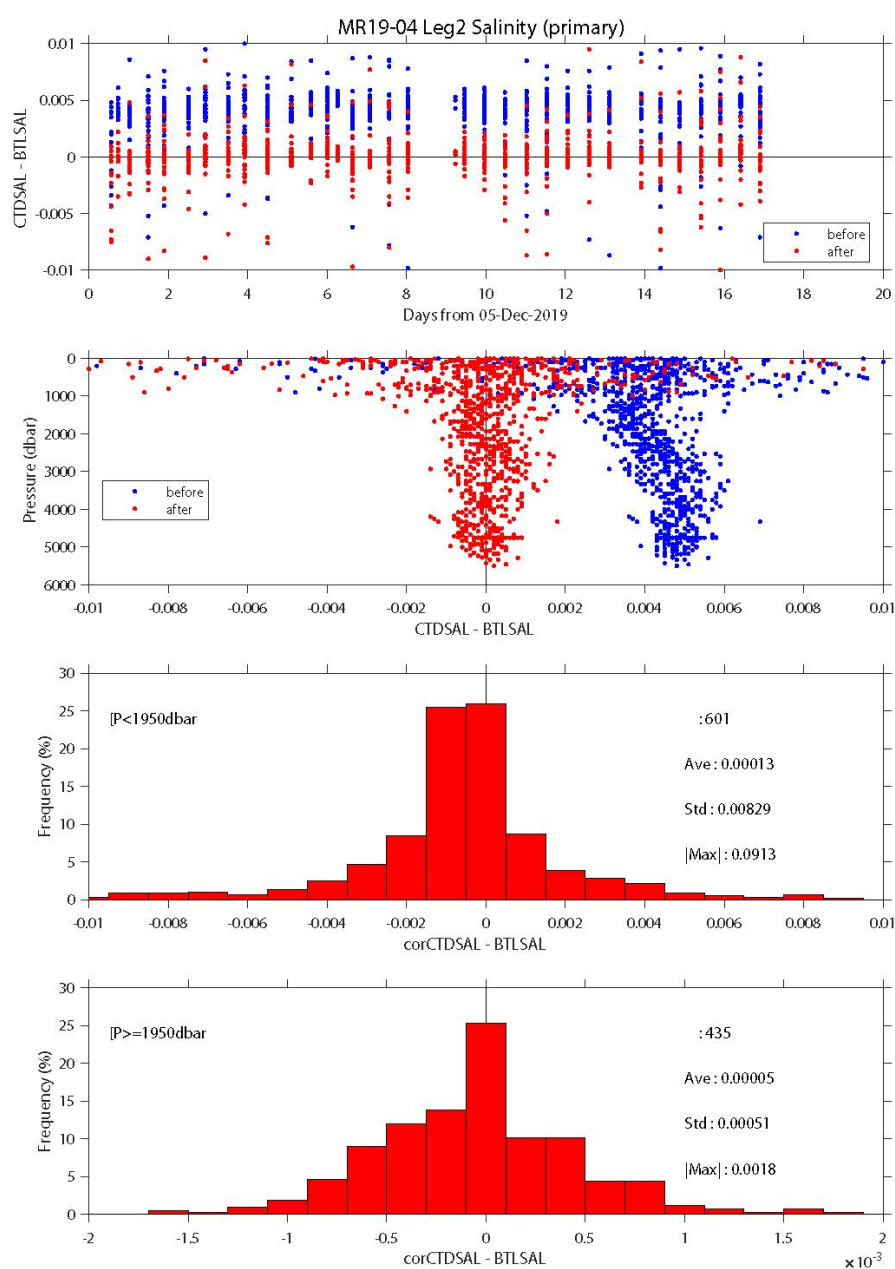| Leg	Sensor	Pressure $\geq$ 1950 dbar				Pressure < 1950 dbar		
		Number	Mean (10^{-3})	Sdev (10^{-3})		Number	Mean (10^{-3})	Sdev (10^{-3})
2	Primary	435	0.1	0.5		601	0.1	8.3
3	Primary	522	0.1	0.4		843	−0.4	4.9
3	Secondary	501	0.0	0.5		824	−0.4	4.8

Fig. 4.1.10. Difference between the CTD salinity (primary) and the bottle salinity for leg 2. Blue and red dots indicate before and after the post-cruise calibration, respectively. Lower two panels show histogram of the difference after the calibration.

Fig. 4.1.11. Same as Fig. 4.1.10, but for leg 3 (primary salinity).

Fig. 4.1.12. Same as Fig. 4.1.10, but for leg 3 (secondary salinity).

(6.4) Dissolved oxygen sensors
(6.4.1) Primary oxygen sensor, RINKO
    Data from the RINKO can be corrected for the time-dependent, pressure-induced effect by means of the same method as that developed for the SBE 43 (Edwards et al., 2010). The calibration coefficients, H1 (amplitude of hysteresis correction), H2 (curvature function for hysteresis), and H3 (time constant for hysteresis) were determined to minimize the down-cast and up-cast data.
        H1 = 0.0060, H2 = 4000.0, H3 = 2000.0   [for leg 2]
        H1 = 0.0058, H2 = 4000.0, H3 = 3000.0   [for leg 3]
    Outputs from RINKO are the raw phase shift data. The RINKO can be calibrated by the modified

Stern-Volmer equation slightly modified from a method by Uchida et al. (2010):

$$O_2 \ (\mu mol/l) = [(V_0 / V)^E - 1] / K_{sv}$$

where V is voltage, V_0 is voltage in the absence of oxygen, K_{sv} is Stern-Volmer constant. The coefficient E corrects nonlinearity of the Stern-Volmer equation. The V_0 and the K_{sv} are assumed to be functions of temperature as follows.

$$K_{sv} = c0 + c1 \times T + c2 \times T^2$$
$$V_0 = 1 + d0 \times T$$
$$V = d1 + d2 \times V_b + d3 \times t + d4 \times t \times V_b + d5 \times t^2 \times V_b$$

where T is CTD temperature (°C) and V_b is raw output (volts). V_0 and V are normalized by the output in the absence of oxygen at 0°C, and t is working time (days) integrated from the fist CTD cast for each leg. The oxygen concentration is calculated using accurate temperature data from the CTD temperature sensor instead of temperature data from the RINKO. The pressure-compensated oxygen concentration O_{2c} can be calculated as follows.

$$O_{2c} = O_2 \ (1 + cp \times P / 1000)$$

where P is CTD pressure (dbar) and cp is the compensation coefficient. Since the sensing foil of the optode is permeable only to gas and not to water, the optode oxygen must be corrected for salinity. The salinity-compensated oxygen can be calculated by multiplying the factor of the effect of salt on the oxygen solubility (Garcia and Gordon, 1992).

The post-cruise calibrated temperature and salinity data were used for the calibration. The results of the post-cruise calibration for the RINKO oxygen are summarized in Table 4.1.3 and shown in Figs. 4.1.13 and 4.1.14. The calibration coefficients are as follows:

c0 = 4.481833626824531e-03, c1 = 1.898732545208230e-04, c2 = 3.186018747588371e-06,
d0 = -4.993114971420946e-04, d1 = -8.334758478255305e-02, d2 = 0.3012446445865034,
d3 = -2.736037023481914e-04, d4 = 7.781237926511940e-04, d5 = -2.720297060792388e-05,
E = 1.2, cp = 0.025   [for leg 2]

c0 = 4.231278175431956e-03, c1 = 1.586473748345674e-04, c2 = 1.925342563039167e-06,
d0 = -3.776889529330843e-03, d1 = -8.075699587347064e-02, d2 = 0.3084927182050134,
d3 = -3.695840179696757e-04, d4 = 5.050997085259927e-04, d5 = -1.146792845027660e-05,
E = 1.2, cp = 0.024   [for leg 3]

Table 4.1.3. Difference between the CTD oxygen and the bottle sampled oxygen after the post-cruise calibration. Mean and standard deviation (Sdev) are calculated for the data below and above 1950 dbar. Number of data used is also shown.

Leg	Sensor	Pressure ≥ 1950 dbar			Pressure < 1950 dbar		
		Number	Mean (μmol/kg)	Sdev (μmol/kg)	Number	Mean (μmol/kg)	Sdev (μmol/kg)
2	Primary	421	−0.05	0.30	599	0.03	1.08
3	Primary	511	−0.04	0.30	826	0.06	0.77
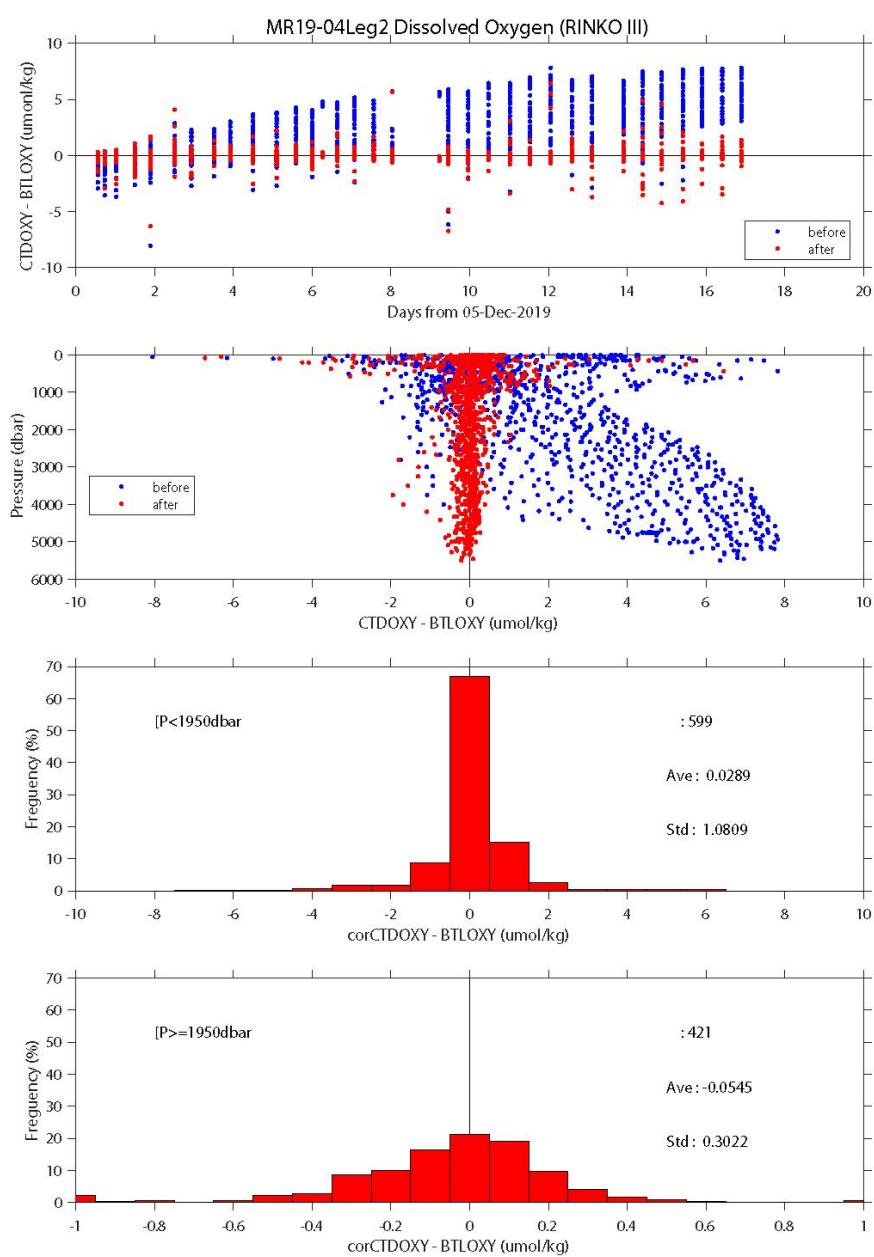
Fig. 4.1.13. Difference between the CTD oxygen and the bottle oxygen for leg 2. Blue and red dots indicate before and after the post-cruise calibration, respectively. Lower two panels show histogram of the difference after the calibration.
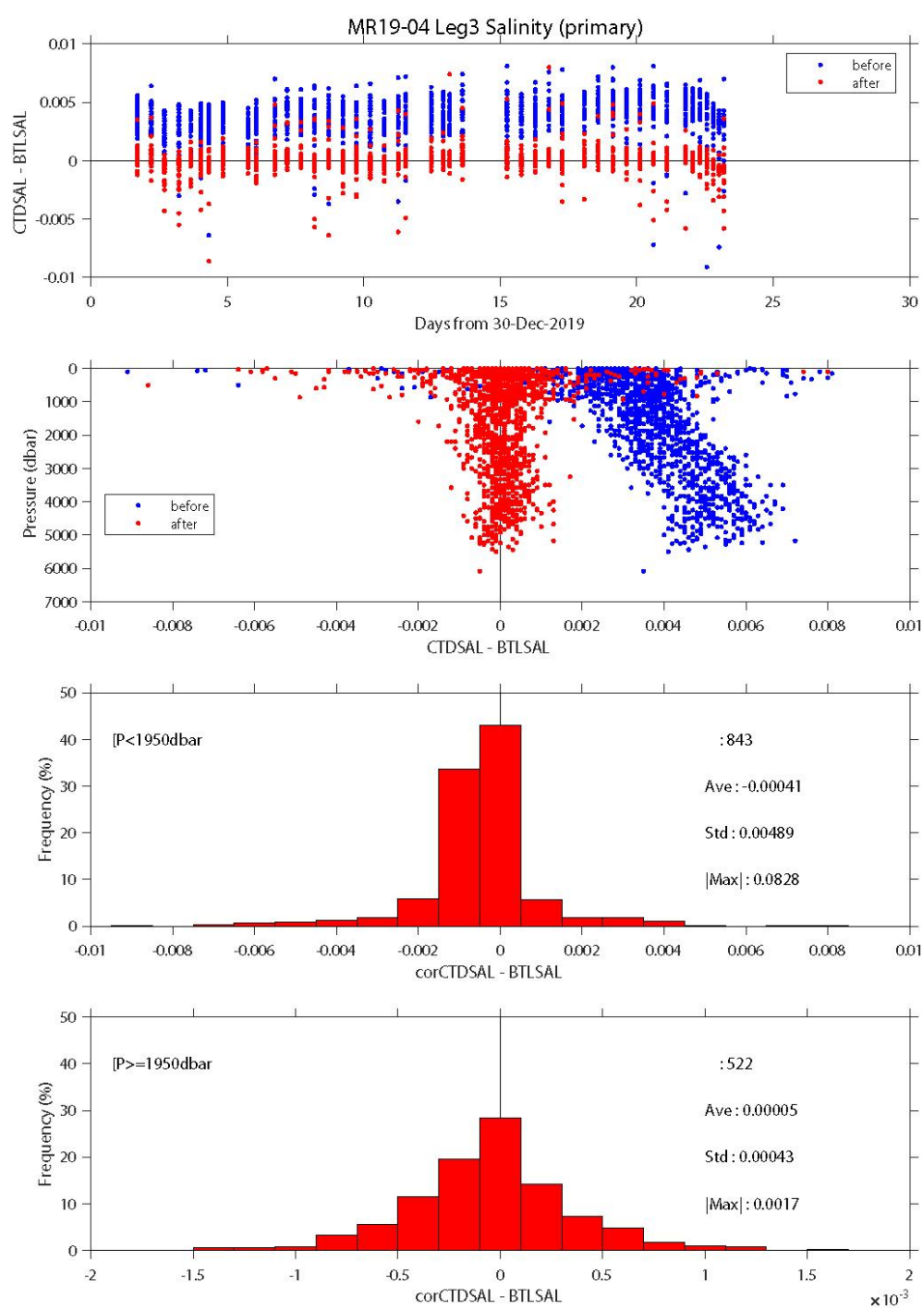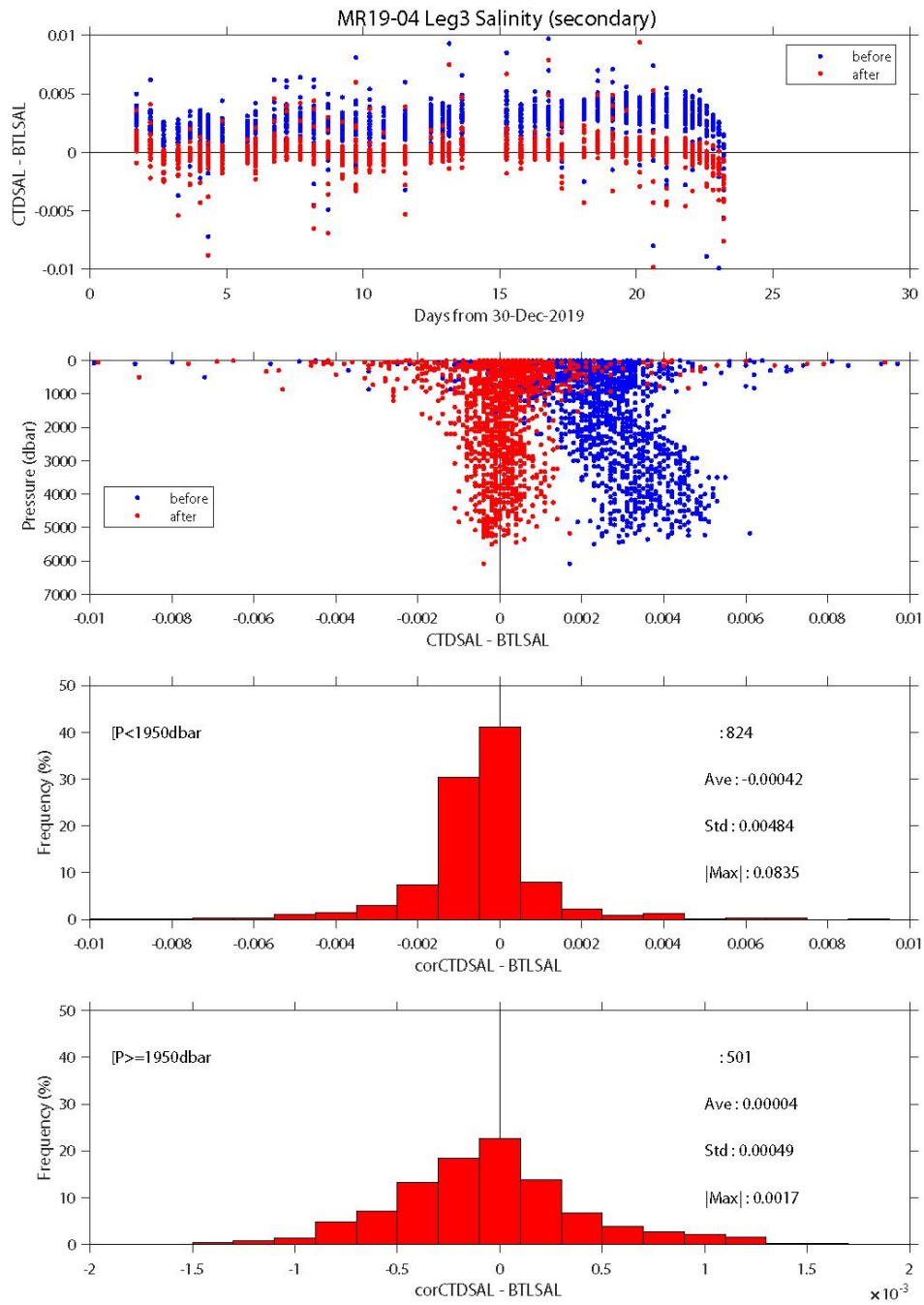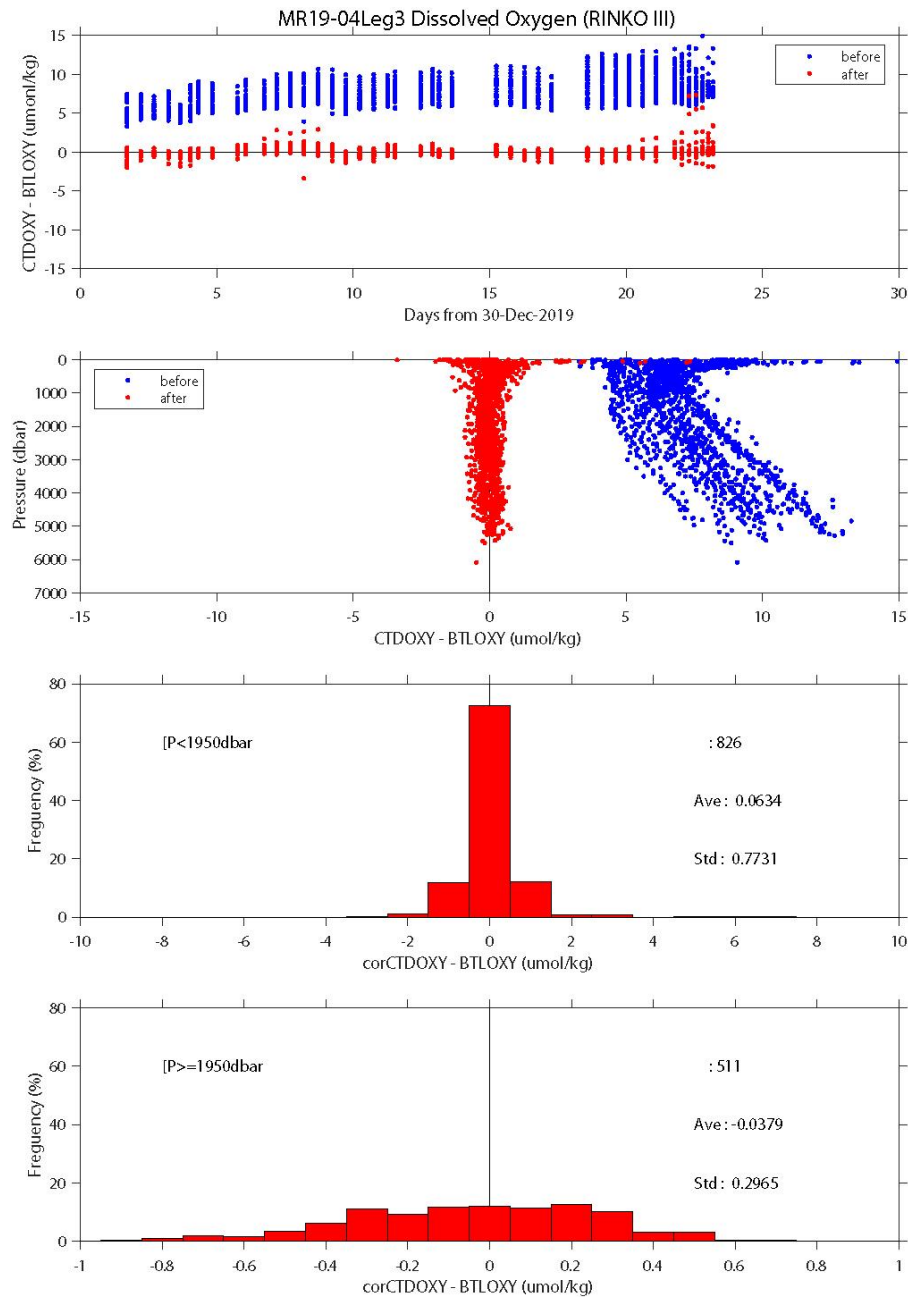
Fig. 4.1.14. Same as Fig. 4.1.13, but for leg 3.

(6.4.2) Secondary oxygen sensor, SBE 43

The primary oxygen sensor RINKO data was not available at station 132 because the cap of the sensing foil was not removed. Therefore, the secondary oxygen sensor SBE 43 was calibrated in situ for the CTD cast. The bottle sampled oxygen data were compared with the down-cast SBE 43 data extracted from the same density surfaces (Fig. 4.1.15). The SBE 43 data was calibrated by using the following equation:

$$SBE43OXY_{corr} = c0 + c1 \times SBE43OXY + c2 \times P + c3 \times T$$

$c0 = 8.776269046135372$

$c1 = 0.9875226996210535$

$c2 = 3.729733540353487e\text{-}04$

$c3 = -2.227812374383066$

where P is pressure (in dbar), T is temperature (°C) and c0-c3 are the calibration coefficients. Standard

deviation of the difference between SBE43OXY$_{corr}$ and the bottle oxygen was 0.35 (µmol/kg) for depths deeper than 950 dbar.
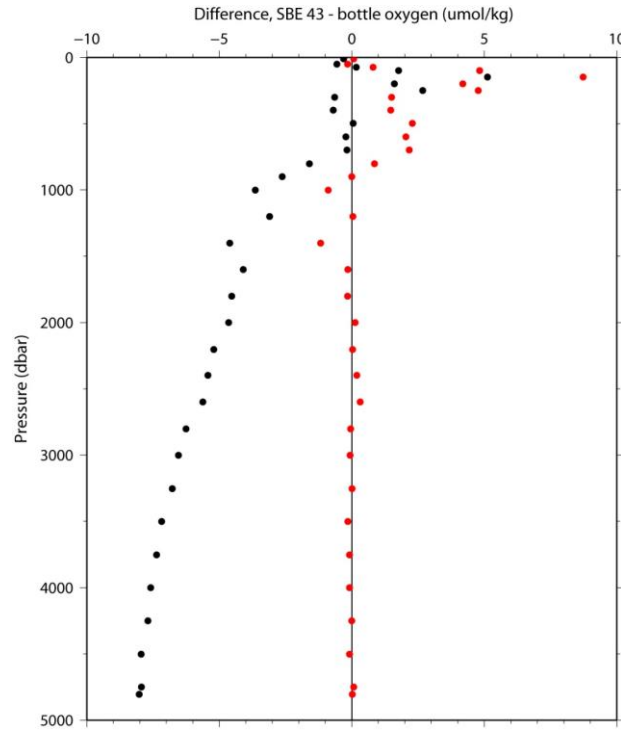
Fig. 4.1.15. Comparison of the secondary dissolved oxygen SBE 43 and the bottle sampled oxygen before the in situ calibration (black dots) and after the in situ calibration (red dots) for station 132. The down-cast oxygen sensor data were compared with the bottle sampled oxygen data.

(6.5) Transmissometer

Light transmission T_r (in %) and beam attenuation coefficient c_p are calculated from the sensor output V (in volt) as follows:

$$T_r = (V-V_d) / (V_r-V_d) \times 100$$
$$c_p = - (1 / 0.25) \ln(T_r / 100)$$

wehre V_d is the dark offset for the instrument, and V_r is the signal for clear water. V_d can be obtained by blocking the light path. V_d was measured on deck before each cast. V_r is estimated from the measured maximum signal in the deep ocean at each cast. Since the transmissometer drifted in time (Fig. 4.1.16), V_r is expressed as

$$V_r = c_0 + c_1 \times t + c_2 \times t^2$$

where t is working time (in days) of the transmissometer integrated from the first CTD cast for each leg, and c_0, c_1, and c_2 are calibration coefficients. Maximum signal was extracted for each cast. The calibration coefficients are as follows:

Leg 2, working time < 5.3169 days
c0 = 4.75484110614084, c1 = -0.00211422184747569, c2 = 0.0
V_d = 0.0012
Leg 2, working time >= 5.3169 days
c0 = 4.7436, c1 = 0.0, c2 = 0.0
V_d = 0.0012
Leg 3
c0 = 4.741726486231039, c1 = -2.045237713851287e-03, c2 = 1.050489805417849e-04
V_d = 0.0012

Also, the light transmission in air $T_{rair} = (V_{air} - V_d)/(V_{ref} - V_d)$ was estimated to be 1.03553 from the measurements after the last CTD cast of leg 3.

Fig 4.1.16. Time series of the maximum value of the transmissometer output at each cast. Red dots are not used in the calibration coefficients estimate and blue lines are the calibration equations.
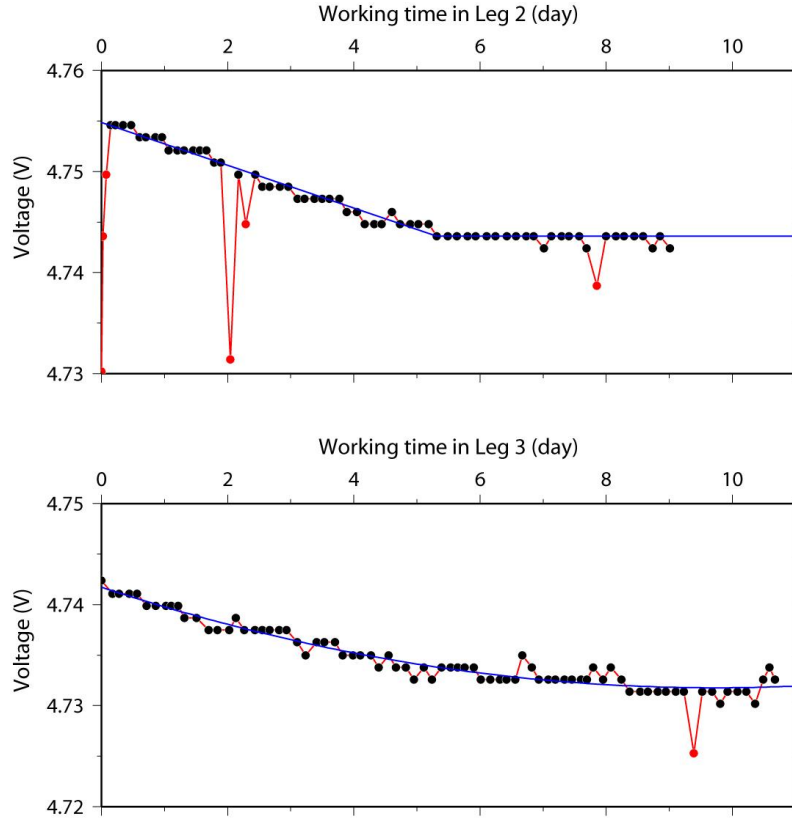
(6.6) Turbidity meter

The turbidity meter was not calibrated in situ since there was no reference data. However, the sensor offset can be easily obtained by a dark test. The optical windows were covered by a PTFE sealing tape and a black vinyl tape. The sensor offset was estimated to be zero as the data obtained in the dark condition.

(6.7) Chlorophyll fluorometer

The chlorophyll fluorometer data show positive biases in the deep ocean because of the interference by the fluorescent dissolved organic material (FDOM) (Xing et al., 2017). Therefore, the effect of the interference by FDOM was corrected by using the ultraviolet fluorometer data (Figs 4.1.17 and 4.1.18) as follows:

$$\text{CTDFLUOR}_{fdom\_corr} = \text{CTDFLUOR} - c_0 + c_1 \times \text{CTDUVFLUOR}_{corr} \times (1.0 - 0.000013 \times P)$$

$c_0 = 0.037595034491929$, $c_1 = 0.982993745243338$ [for stations 1 – 97]
$c_0 = 0.0316388799077501$, $c_1 = 0.722499476069204$ [for stations 98 – 153]

where CTDUVFLUOR_{corr} is the ultraviolet fluorometer data (see below), P is pressure (in dbar), and c_0 and c_1 are the correction coefficients.

The chlorophyll fluorometer data thus corrected was calibrated in situ by using the bottle sampled chlorophyll-a data. The chlorophyll fluorometer data was slightly noisy so that the up-cast profile data which was averaged over one decibar more agree with the bottle sampled data than the discrete chlorophyll fluorometer data obtained at bottle-firing stops. Therefore, the CTD fluorometer data at water sampling depths extracted from the up-cast profile data were compared with the bottle sampled chlorophyll-a data. The bottle sampled data obtained at dark condition [PAR (Photosynthetically Available Radiation) < 50 $\square$E/(m^2 sec)] were used for the calibration, since sensitivity of the fluorometer to chlorophyll a is different at nighttime and daytime (Figs. 4.1.19 and 4.1.20). The calibration equation is as follows:

$$\text{CTDFLUORcorr} = c_0 + c_1 \times \text{CTDFLUOR}_{fdom\_corr}$$

For $\text{CTDFLUOR}_{fdom\_corr} < 0.15$

$\quad\quad c0 = 0.0, c1 = 1.057609201250224 \quad$ [for leg 2]

$\quad\quad c0 = 0.0, c1 = 0.8095685935896424 \quad$ [for leg 3]

For $\text{CTDFLUOR}_{fdom\_corr} >= 0.15$

$\quad\quad c0 = -9.266249192486984\text{e-}3, c1 = 1.119384193144591 \quad$ [for stations $1 - 8$]

$\quad\quad c0 = 8.785619163927143\text{e-}2, c1 = 0.4719011730479180 \quad$ [for stations $9 - 69$]

$\quad\quad c0 = -5.693867583263859\text{e-}2, c1 = 1.189157837493829 \quad$ [for stations $70 - 71$]

$\quad\quad c0 = 5.686897296565606\text{e-}2, c1 = 0.4304401825407885 \quad$ [for station $72 - 102$]

$\quad\quad c0 = 8.200539268327771\text{e-}2, c1 = 0.2627010759224658 \quad$ [for stations $103 - 153$]

where c_0 and c_1 are the calibration coefficients.
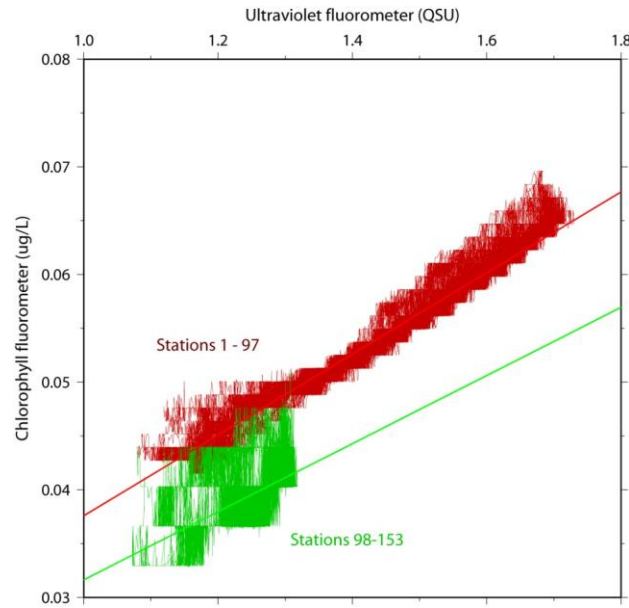
Fig. 4.1.17. Comparison between the chlorophyll fluorometer and the ultraviolet fluorometer for the deep ocean (depths deeper than 400 dbar).
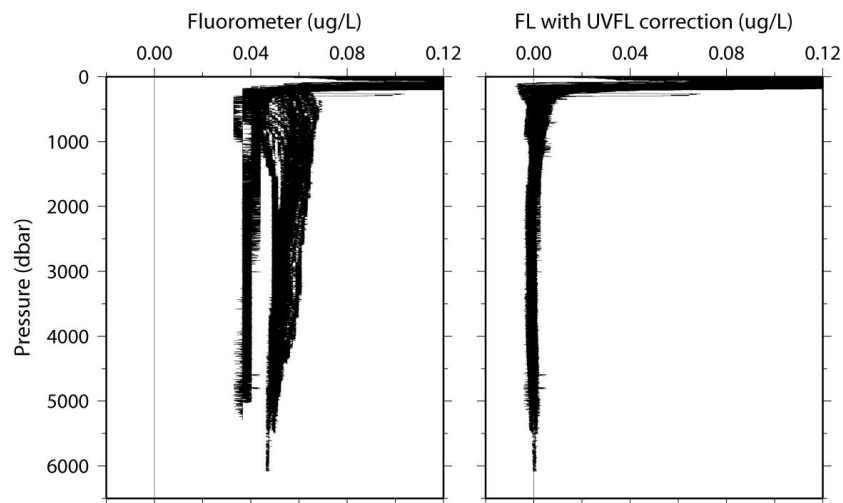
Fig. 4.1.18. Vertical profiles of the chlorophyll fluorometer before (left panel) and after (right panel) the correction for the interference by fluorescence dissolved material (FDOM).

31
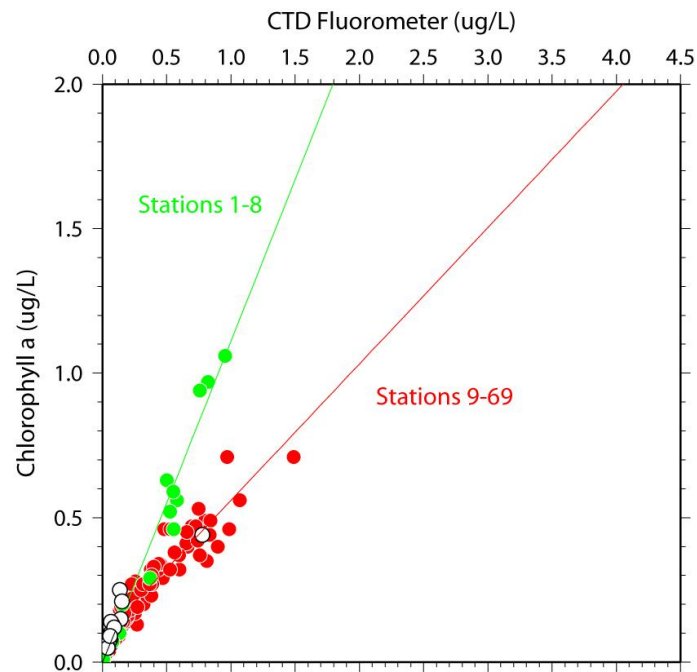
Fig. 4.1.19. Comparison of the CTD chlorophyll fluorometer and the bottle sampled chlorophyll-a for leg 2. The regression lines are also shown. Open circles were not used for the calibration because PAR was large (>= 50 μE/m^2/s).
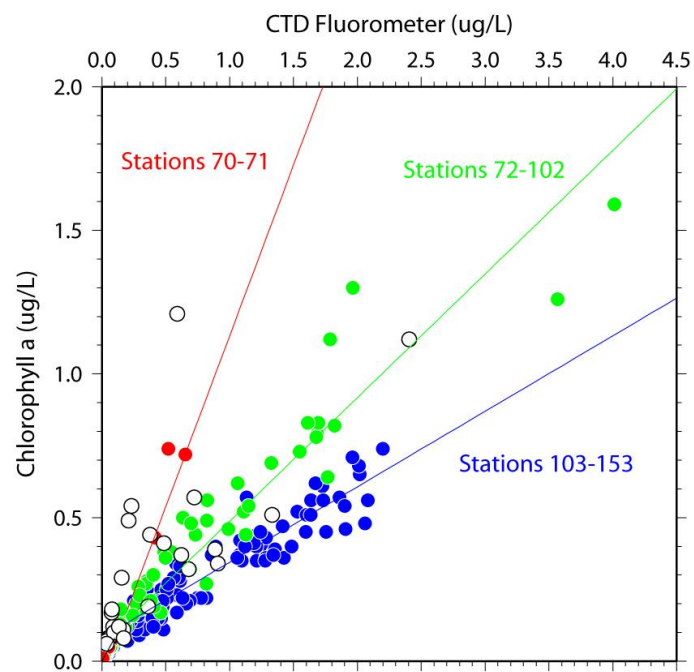
Fig. 4.1.20. Same as Fig. 4.1.19, but for leg 3.

(6.8) Ultraviolet fluorometer

The sensor output from the ultraviolet fluorometer showed difference between the down-cast and up-cast. The pressure hysteresis of the sensor output was corrected for the up-cast data by following equations:

$CTDUVFLUOR_{corr} = CTDUVFLUOR \times (1.0 + c_0 \times [P_{lim} - P])$ [for $P < P_{lim}$]

P_{lim} = 2500 dbar, c_0 = 1.5e-5   [for leg2]

P_{lim} = 2500 dbar, c_0 = 1.8e-5   [for leg 3 stations 70 – 102]

P_{lim} = 3000 dbar, c_0 = 0.4e-5   [for leg 3 stations 103 – 153]

where P is pressure (in dbar), P_{lim} is threshold value of pressure and c_0 is the correction coefficient. When the pressure P is greater than P_{lim}, c_0 was set to zero. When the maximum pressure (P_{max}) of the cast was smaller than P_{lim}, P_{lim} was set to P_{max}.

The sensor output from the ultraviolet fluorometer showed positive deviation near the surface probably because of the interference by sunlight (Fig. 4.1.21). Therefore, when the PAR data was greater than 100 $\mu E/m^2/s$, the deviated data near the surface was replaced by the surface minimum value for depths from the surface to the pressure where the minimum value was observed at each cast.

The ultraviolet fluorometer data thus corrected was calibrated in situ by using the bottle sampled fluorescence dissolved organic matter (FDOM) data (in Raman Unit [RU]) obtained at an excitation wavelength of 370 nm as follows:

$CTDUVFLUOR\text{-}370$ [RU] = $c_0 + c_1 \times CTDUVFLUOR_{corr}$ [QSU] + $c_2 \times T$

c_0 = -1.163505363380728e-02

c_1 = 1.491187270086319e-02

c_2 = -1.125715154068824e-04

where T is temperature (°C) and c_0-c_2 are the calibration coefficients. Standard deviation of the difference between CTDUVFLUOR-370 and FDOM was 0.00041 (RU) (Fig. 4.1.22).
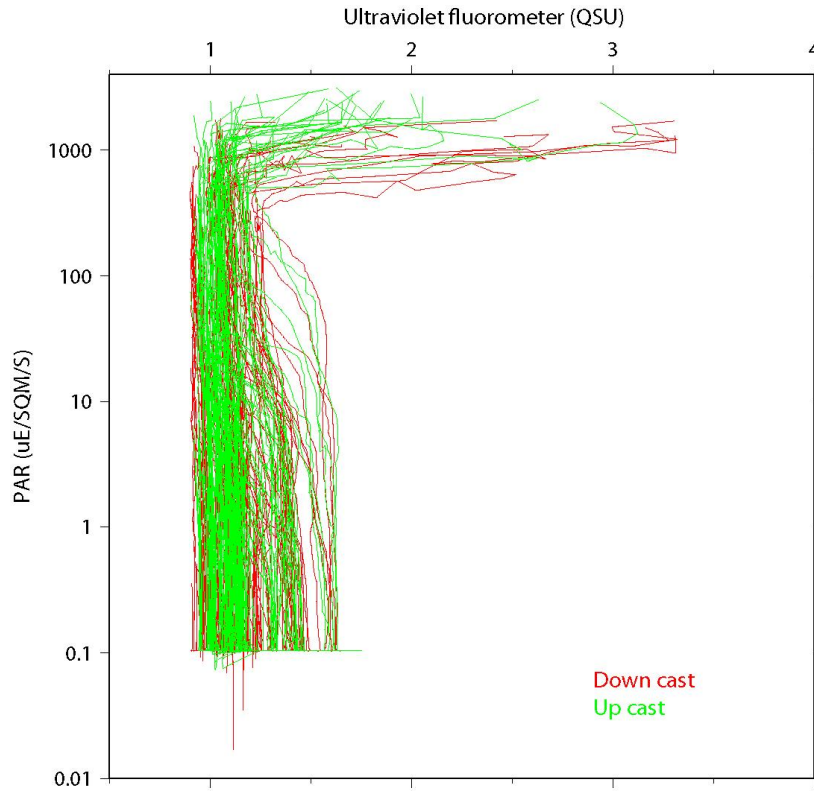
Fig. 4.1.21. Ultraviolet fluorometer data plotted against PAR data.
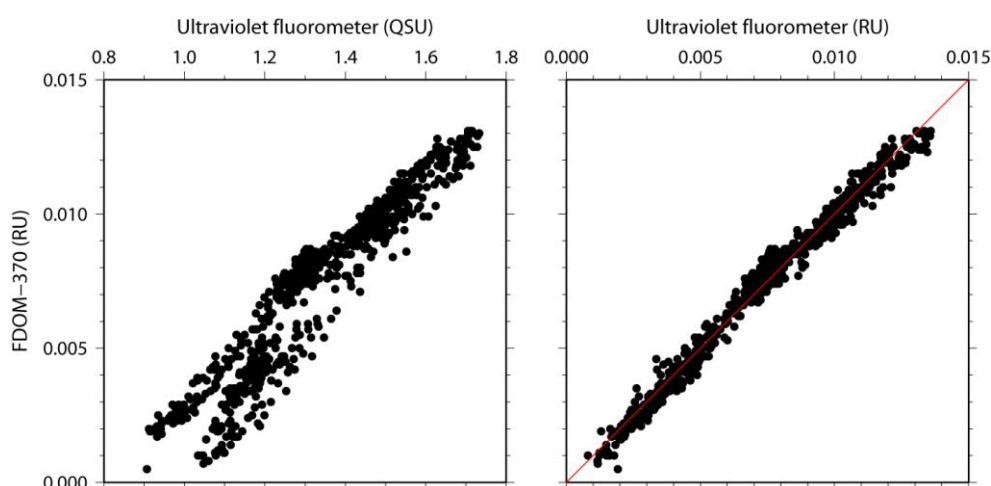
Fig. 4.1.22. Comparison of the ultraviolet fluorometer data and the fluorescent dissolved organic matter (FDOM) (left panel). The sensor data calibrated against the FDOM (Raman Unit) are also shown (right panel).

(6.9) PAR

PAR is expected to be zero in the deep ocean. Therefore, the offset measured in the deep ocean was corrected. The corrected data (PARc) is calculated from the raw data (PAR) as follows:

PARc [μE m^{-2} s^{-1}] = PAR – 0.104.

(7) References

Edwards, B., D. Murphy, C. Janzen and N. Larson (2010): Calibration, response, and hysteresis in deep-sea dissolved oxygen measurements, *J. Atmos. Oceanic Technol.*, 27, 920–931.

Fukasawa, M., T. Kawano and H. Uchida (2004): Blue Earth Global Expedition collects CTD data aboard Mirai, BEAGLE 2003 conducted using a Dynacon CTD traction winch and motion-compensated crane, *Sea Technology*, 45, 14–18.

García, H. E. and L. I. Gordon (1992): Oxygen solubility in seawater: Better fitting equations. *Limnol. Oceanogr.*, 37 (6), 1307–1312.

Uchida, H., G. C. Johnson, and K. E. McTaggart (2010): CTD oxygen sensor calibration procedures, The GO-SHIP Repeat Hydrography Manual: A collection of expert reports and guidelines, IOCCP Rep., No. 14, ICPO Pub. Ser. No. 134.

Uchida, H., T. Kawano, T. Nakano, M. Wakita, T. Tanaka and S. Tanihara (2020): An updated batch-to-batch correction for IAPSO standard seawater. submitted to J. Atmos. Oceanic Technol.

Uchida, H., Y. Maeda and S. Kawamata (2018): Compact underwater slip ring swivel: Minimizing effect of CTD package rotation on data quality, Sea Technology, 11, 30–32.

Uchida, H., T. Nakano, J. Tamba, J. V. Widiatmo, K. Yamazawa, S. Ozawa and T. Kawano (2015): Deep ocean temperature measurement with an uncertainty of 0.7 mK, J. Atmos. Oceanic Technol., 32, 2199–2210.

Xing, X., H. Claustre, E. Boss, C. Roesler, E. Organelli, A. Poteau, M. Barbieux and F. D'Ortenzio (2017): Correction of profiles of in-situ chlorophyll fluoremetry for the contribution of fluorescence originating from non-algal matter, Limnol. Oceanogr.: Methods, 15, 80–93.

Yamashita, Y., C.-J. Liu, H. Ogawa, J. Nishioka, H. Obata and H. Saito (2015): Application of an in situ fluorometer to determine the distribution of fluorescent organic matter in the open ocean, Marine Chemistry, 177, 298–305.

(8) Data archive

These obtained data will be submitted to JAMSTEC Data Management Group (DMG).

4.2 Bottle Salinity
February 5, 2020

(1) Personnel
Hiroshi Uchida (JAMSTEC)
Hiroki Ushiromura (MWJ) (leg 2)
Shungo Oshitani (MWJ) (leg 3)

(2) Objective
Bottle salinities were measured to calibrate the CTD salinity data.

(3) Instruments and method
Salinity measurement was conducted basically based on the method by Kawano (2010). Materials used in this cruise are as follows:

Standard Seawater: IAPSO Standard Seawater, Ocean Scientific International Ltd., Hampshire, UK
Batch P162
Salinometer: Autosal model 8400B; Guildline Instruments, Ltd., Ontario, Canada
Serial no. 62556
Serial no. 72874 (for spare: not used for the measurement of seawater samples)
A peristaltic-type sample intake pump, Ocean Scientific International Ltd.
Thermometers: PRT model 1502A, Fluke Co., Everett, Washington, USA
Serial no. B81550 (for monitoring the bath temperature) (calibration date: August 29, 2017)
Serial no. B78466 (for monitoring the room temperature) (calibration date: August 29, 2017)
Stabilized power supply: model PCR1000LE, Kikusui Electronics Co., Japan
Serial no. XH004198 (calibration date: February 15, 2018)
Sample bottles: 250 mL brown borosilicate glass bottles with screw caps (PTFE packing)
(A polyethylene inner plug was used for samples for the thermo-salinograph correction.)
Decade resistance substituter: model HARS-X-7-0.001-K, IET Labs., Inc., New York, USA
Serial no. E1-13514822 (calibration date: December 20, 2013)
Serial no. E1-19035551 (calibration date: January 17, 2019)

The bath temperature of the salinometer was set to 24 °C. The salinometer was standardized only at the beginning of the cruise by using the IAPSO Standard Seawater (SSW). The standardization dial was set to 621 and never changed during the cruise. The mean with standard deviation of the STANDBY and ZERO was 5144 ± 0.7 and 0.00000 ± 0.000001, respectively. The mean with standard deviation of the ambient room temperature was 23.0 ± 0.64 °C, while that of the bath temperature was 24.000 ± 0.0008 °C throughout the cruise.

The double conductivity ratios measured by the salinometer were used to calculate practical salinity using the algorithm for Practical Salinity Scale 1978 (IOC et al., 2010). A constant temperature of 24 °C was used in the calculation instead of using the measured bath temperature.

(4) Results
Ultra-pure water (Milli-Q water, Millipore, Billerica, Masachusetts, USA) and the IAPSO SSW were measured at the beginning and the end of the measurements (2~3 stations) for each day. Time-series of the measured double conductivity ratios are shown in Fig. 4.2.1. The mean value for the IAPSO SSW agreed with the certified value (1.99966) for leg 2, However, for leg 3, the salinometer was drifted in time and the linear time drift was estimated from the least squares method and corrected to match the mean value with the certified value. The measured double conductivity ratios for the water samples were corrected by using the estimated offset due to the time drift. The standard deviation of the IAPSO SSW measurements was 0.000016, which is equivalent to 0.0003 in salinity, after the time drift correction.

The results of the ultra-pure water and the IAPSO SSW measurement (Fig 4.2.1) suggest that the salinometer drifted in time by changing the span of the slope. However, the salinity range of the seawater sample was close to the salinity of SSW (about 35 g/kg) as described blow. Therefore, the offset time-drift correction is adequate for the seawater samples.

A total of 2,773 (58) samples were measured for the CTD/water sampling (thermo-salinograph) measurement. Minimum and maximum value of the measured salinity was 32.7 and 35.8, respectively

As for the data quality flag, two samples (stations 103 #14 and 118_2 #13) were set to flag 4 (bad measurement) due to mis trip of the Niskin bottle, and four samples (stations 81 #3, 89 #18, 93 #20 and 122 #15) were set to flag 3 (questionable measurement) judging from relatively large deviation from the CTD sensor value.

A total of 366 pairs of replicate samples was collected and the standard deviation of the replicate samples was 0.00024 in salinity.

At station 030, duplicate samples were collected from all Niskin bottles at 4750.3 ±0.7 dbar, except for bottles #12 and #25 which were not closed properly. Mean with standard deviation for the duplicate samples was 34.7170 ± 0.00030 in salinity. For the bottles #12 and #25, duplicate samples were collected from four bottles (#6, #12, #18 and #25) at 4999.7 ± 0.2 dbar of station 039. Mean with standard deviation for the second duplicate samples was 34.7165±0.00050 in salinity.

The linearity error of the salinometer was estimated by using decade resistance substituters (see Uchida et al. [2020] for more detail). For the salinometer (serial no. 62556) used in this cruise, the linearity error was estimated to be ± 0.0005 in salinity for salinity around 35 (Fig. 4.2.2).
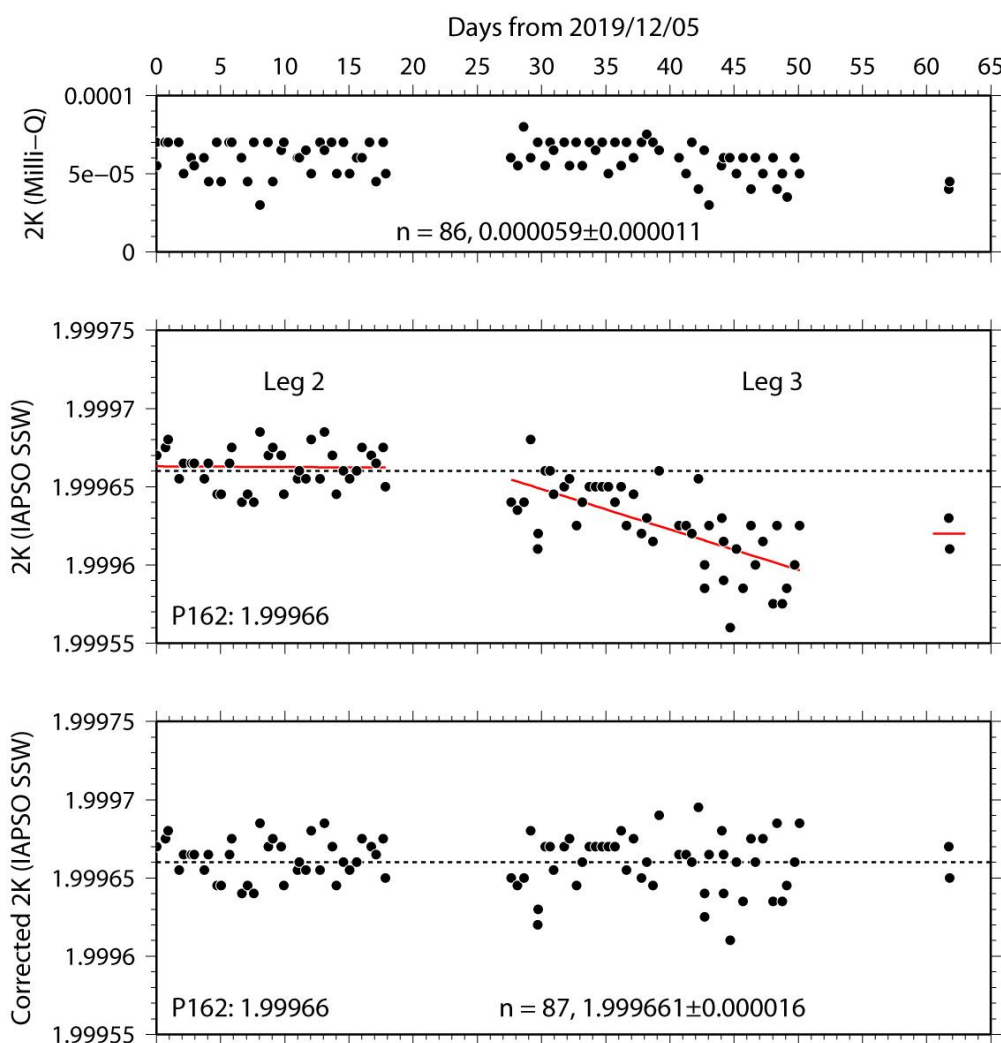
Figure 4.2.1. Time-series of the measured double conductivity ratios for the ultra-pure water (upper panel) and the IAPSO SSW (middle panel). The time-drift corrected double conductivity ratios for the IAPSO SSW were also shown (lower panel). The last two dots are the measurements only for the thermo-salinograph samples.
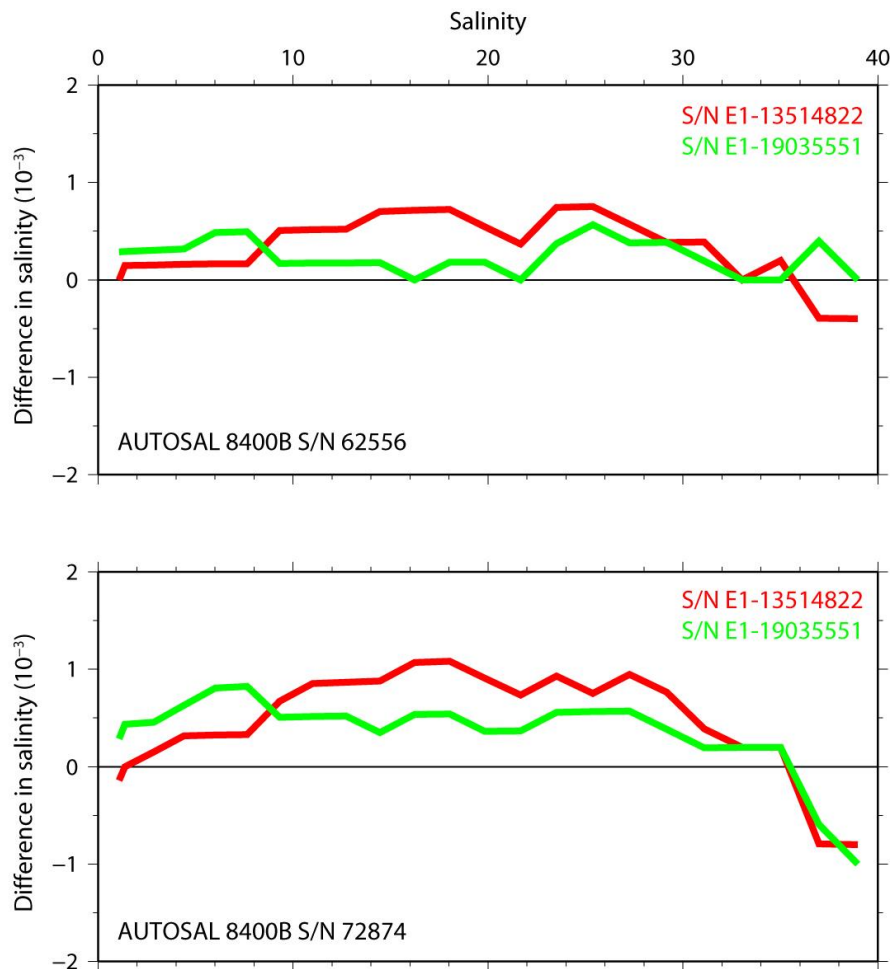
Figure 4.2.2. Linearity errors in practical salinity estimated from measurements of two decade resistance substituters for salinometers with serial numbers 62556 (upper panel) and 72874 (lower panel).

(5) References

IOC, SCOR and IAPSO (2010): The international thermodynamic equation of seawater – 2010: Calculation and use of thermodynamic properties. Intergovernmental Oceanographic Commission, Manuals and Guides No. 56, UNESCO (English), 196 pp.

Kawano, T. (2010): Salinity. The GO-SHIP Repeat Hydrography Manual: A collection of Expert Reports and Guidelines, IOCCP Report No. 14, ICPO Publication Series No. 134, Version 1.

Uchida, H., T. Kawano, T. Nakano, M. Wakita, T. Tanaka and S. Tanihara (2020): An updated batch-to-batch correction for IAPSO standard seawater. submitted to J. Atmos. Oceanic Technol.

(6) Data archive

These obtained data will be submitted to JAMSTEC Data Management Group (DMG).

4.3 Density
February 2, 2020

(1) Personnel

       Hiroshi Uchida (JAMSTEC)

(2) Objective

    The objective of this study is to collect absolute salinity (also called "density salinity") data and to evaluate the algorithm to estimate absolute salinity anomaly provided along with TEOS-10 (the International Thermodynamic Equation of Seawater 2010) (IOC et al., 2010).

(3) Instruments and method

    Seawater density for water samples were measured with a vibrating-tube density meter (DMA 5000M [serial no. 80570578], Anton-Paar GmbH, Graz, Austria) with a sample changer (Xsample 122 [serial no. 8548492], Anton-Paar GmbH). The sample changer is used to load samples automatically from up to forty-eight 12-mL glass vials.

    The water samples collected in 250 mL brown borosilicate glass bottles with screw caps (PTFE packing) for practical salinity measurement were measured by taking the water sample into two 12-mL glass vials for each bottle just before practical salinity measurement. The glass vial was sealed with Parafilm M (Pechiney Plastic Packaging, Inc., Menasha, Wisconsin, USA) immediately after filling. Densities of the samples were measured at 20 °C by the density meter two times (two vials) for each bottle and averaged to estimate the density.

    The density meter was initially calibrated by measuring air and pure water according to the instrument manual. However, measured density for the IAPSO Standard Seawater deviates from density of TEOS-10 calculated from practical salinity and composition of seawater, probably due to non-linearity of the density meter (Uchida et al., 2011). The non-linearity can be corrected by measuring a reference sample simultaneously as:

$$\rho_{\text{corr}} = \rho - (\rho_{\text{ref}} - \rho_{\text{ref\_true}}) + c\,(\rho - \rho_{\text{ref\_true}}),$$

where ρ_{corr} is the corrected density of the sample, ρ is measured density of the sample, ρ_{ref} is measured density of the reference, $\rho_{\text{ref\_true}}$ is true density of the reference, and c is non-linearity correction factor.

    The non-linearity factor is estimated to be 0.000411 for the density meter (serial no. 80570578). In this cruise, the non-linearity and time drift of the density meter was monitored and corrected by periodically measuring the density of the Multi-parametric Standard Seawater (MSSW) (lot PRE19) currently under development jointly by KANSO Co., Ltd., Osaka, Japan (Uchida et al., submitted to J. Atmos. Oceanic Technol.) or the IAPSO Standard Seawater (batch P162) as the reference. True density at 20 °C for the PRE19 and P162 is estimated to be 1024.2186 kg/m^3 and 1024.7609 kg/m^3, respectively, from practical salinity and composition of seawater using TEOS-10. The IAPSO Standard Seawater was referred for the stations 078, 081, 083, 111, 114, 138 and 149, and the MSSW was referred for the rest of the stations.

(4) Results

    Density salinity ("DNSSAL") can be back calculated from the measured density and temperature (20 °C) with TEOS-10. A total of 203 pairs of replicate samples was measured and the standard deviation of the replicate samples was 0.0014 g/kg. The measured density salinity anomalies (δS_A) are shown in Fig. 4.3.1. The measured δS_A were well agree with the δS_A estimated from Pawlowicz et al. (2011) which exploits the correlation between δS_A and nutrient concentrations and carbonate system parameters based on mathematical investigation using a model relating composition, conductivity and density of arbitrary seawaters.

(5) References

IOC, SCOR and IAPSO (2010): The international thermodynamic equation of seawater – 2010: Calculation and use of thermodynamic properties. Intergovernmental Oceanographic Commission, Manuals and Guides No. 56, UNESCO (English), 196 pp.

Pawlowicz, R., D.G. Wright and F. J. Millero (2011): The effects of biogeochemical processes on ocean conductivity/salinity/density relationships and the characterization of real seawater. Ocean Science, 7, 363-387.

Uchida, H., T. Kawano, M. Aoyama and A. Murata (2011): Absolute salinity measurements of standard seawaters for conductivity and nutrients. La mer, 49, 237-244.

Uchida, H., T. Kawano, T. Nakano, M. Wakita, T. Tanaka and S. Tanihara: An updated batch-to-batch correction for IAPSO standard seawater. submitted to J. Atmos. Oceanic Technol.

(6) Data archive

These obtained data will be submitted to JAMSTEC Data Management Group (DMG).
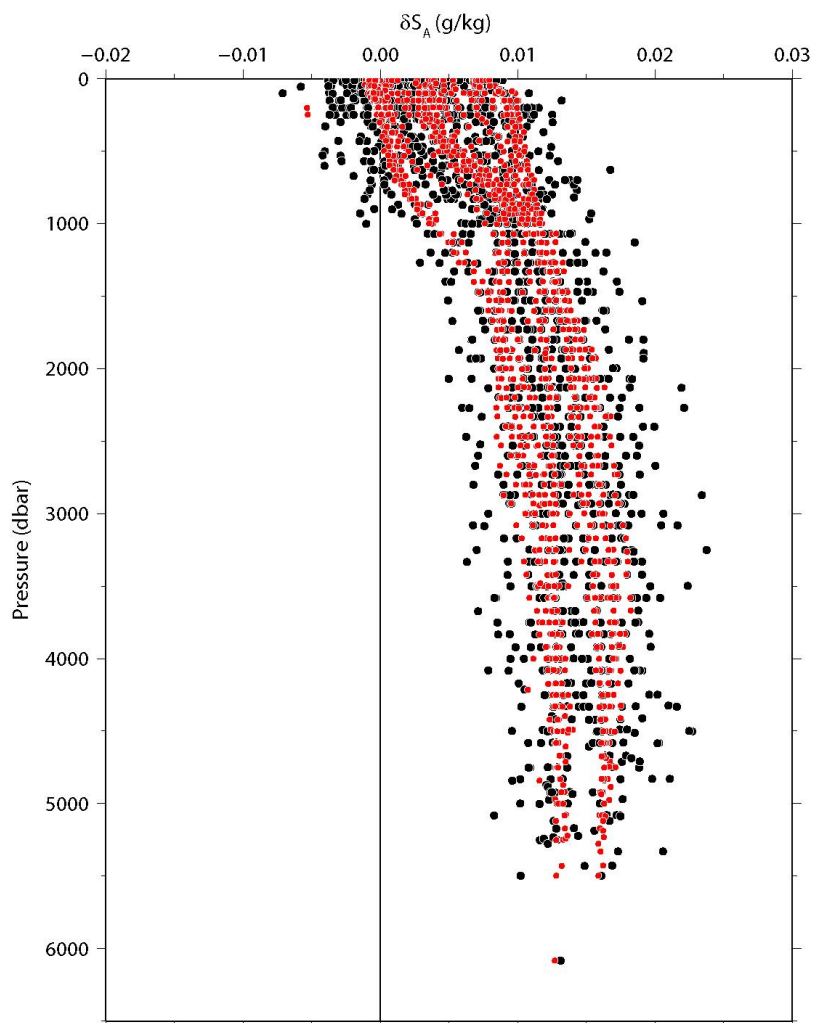
Figure 4.3.1. Vertical distribution of density salinity anomaly measured by the density meter (black dots). Absolute salinity anomaly estimated from nutrients and carbonate system parameters (Pawlowicz et al., 2011) are also shown (red dots).

4.4. Lowered Acoustic Doppler Current Profiler

(1) Personnel

      Shinya Kouketsu   (JAMSTEC) (principal investigator)
      Katsuro Katsumata (JAMSTEC)

(2) Overview of the equipment

      Two acoustic Doppler current profilers (ADCP) were integrated with the CTD/RMS package. The lowered ADCP (LADCP)s, Workhorse Monitor WHM300 (Teledyne RD Instruments, San Diego, California, USA), which has 4 downward facing transducers with 20-degree beam angles, rated to 6000 m, make direct current measurements at the depth of the CTD, thus providing a full profile of velocity. The LADCP was powered during the CTD casts by a 48 volts battery pack. The LADCP unit was set for recording internally prior to each cast. After each cast the internally stored observed data were uploaded to the computer on-board. By combining the measured velocity of the sea water and bottom with respect to the instrument, and shipboard navigation data during the CTD cast, the absolute velocity profile can be obtained (e.g. Visbeck, 2002 as implemented by A.Thunherr and available online at ftp://ftp.ldeo.columbia.edu/pub/LADCP).

      The instruments used in this cruise were as follows.
          Teledyne RD Instruments, WHM300
               S/N 24545 (downward looking), S/N 20754 (upward looking)

(3) Data collection

      In this cruise, data were collected with the following configuration.
          Bin size: 8.0 m
          Number of bins: 12
          Pings per ensemble: 1
          Ping interval: 1.0 sec

The downloaded file fragmentation occurred at the stations of 41, 42, and 148 due to cable problems. The data from upward looking at the station 2, 5 and 72 and the downward looking data at the station 46 were lost due to operation problems. A part of data during the upcast was lost at station 8 due to battery shortage.

Reference

Visbeck, M. (2002): Deep velocity profiling using Lowered Acoustic Doppler Current Profilers: Bottom track and inverse solutions. *J. Atmos. Oceanic Technol.*, **19**, 794-807.

4.5. Micro Rider

(1) Personnel

Yusuke Sasaki   (Univ. of Tokyo) (Principal investigator)
Shinya Kouketsu   (JAMSTEC)
Katsuro Katsumata (JAMSTEC)
Hiroshi Uchida   (JAMSTEC)

(2) Objective

The objective is to measure microstructure in temperature to evaluate vertical mixing.

(3) Instruments and method

Micro structure observations were carried out by micro-Rider 6000 (MR6000; Rockland Scientific International Inc.), which was mounted on the CTD rosette and was powered from SBE 9plus. We installed two FP07 thermistors to observe the high-frequency changes in temperature. We had to replace probes, as some of the probes failed during the cruise. High-frequency pressure and acceleration profiles are also obtained by the internal sensors in MR6000. Low-frequency profiles of temperature and conductivity were recorded in the MR6000 with the input from the SBE-3 sensors on the CTD system. We downloaded the raw data from the MR6000 after each cast. In a near future, we plan to examine methods for calibration and quality check of the data by comparing these micro temperature with CTD, free fall instruments, and free fall micro shear structure data.

(4) Measurement history

(4-1) Micro Temperature
- Sensor socket 1: T1813 (St. 1-70), T1604 (St. 71-80) and T1320 (St. 81-153)
- Sensor socket 2: T1817 (St. 1-69), T1818 (St. 70-77), T1510 (St. 78-86) and T1341 (St. 87-153)

(4-2) Low-frequency Temperature and conductivity

The low-frequency-temperature profiles of the first several stations (St.1-4) are corrupted, probably due to cable problems connected with SBE-3 sensor on the CTD system. The low frequency temperature for these stations were not used for analysis.

(5) Note for using data

The file included in the data 'mr6000.csv'shows the correspondence between the station number and the data file name (DAT_???.P).

4.6 Oxygen

February 3, 2020
Yuichiro Kumamoto
Japan Agency for Marine-Earth Science and Technology

(1) Personnel

Yuichiro Kumamoto [1], Erii Irie [2], Misato Kuwahara[2], Yuko Miyoshi [2]
1) Japan Agency for Marine-Earth Science and Technology
2) Marine Works Japan Co. Ltd

(2) Objectives

Dissolved oxygen is one of chemical tracers for the ocean circulation. Climate models predict a decline in dissolved oxygen concentration and a consequent expansion of oxygen minimum layer due to the global warming, which results mainly from decreased interior advection and ongoing oxygen consumption by remineralization. In order to discuss the temporal change in oxygen concentration in the water column, we measured dissolved oxygen concentration from surface to bottom layer at all the water sampling stations in the western Indian Ocean during MR19-04 Leg-2 and Leg-3 cruises.

(3) Reagents

Pickling Reagent I: Manganous chloride solution (3M), Lot: 1-19E
Pickling Reagent II: Sodium hydroxide (8M) / sodium iodide solution (4M), Lot: 2-19F
Sulfuric acid solution (5M), Lot: S-19C, -19D, -19F
Sodium thiosulfate (0.025M), Lot: T-19T, -19S, -19R, -19U, -19V, -19Q
Potassium iodate (0.001667M): National Metrology Institute of Japan (NMIJ), Certified Reference Material (CRM), 3006-a No.073, Mass fraction: 99.973 ± 0.018 % (expanded uncertainty)
   Lot: K19E01-07 (Leg-2), K19F01-09, K19G01-03 (Leg-3)
CSK standard of potassium iodate: Lot TWJ0280, Wako Pure Chemical Industries Ltd., 0.0100N

(4) Instruments

Detector: Automatic photometric titrator, DOT-15X manufactured by Kimoto Electronic Co. Ltd., Lot: DOT-09, -10
Burette: APB-620 and APB-510 manufactured by Kyoto Electronic Co. Ltd. / 10 cm^3 of titration piston, Lot: DOT-09, MB-06/MY10-06; DOT-10, MB-01/MY10-01; KIO$_3$, MB-11/MY10-11
Dispenser: FORTUNA Optifix 1 cm^3, Lot: Pickling Reagent I, MO-42; Pickling Reagent II, MO-27, -31, -33, -43

(5) Seawater sampling

Seawater samples were collected using 12-liter sample bottles attached to the CTD-system. The seawater was transferred to a volume-calibrated glass flask (ca. 100 cm^3) through a plastic tube. Three times volume of the flask of seawater was overflowed. Sample temperature was measured during the water sampling using a thermometer. Then two reagent solutions (Reagent I, II) of 1.0 cm^3 each were added immediately into the sample flask and the stopper was inserted carefully into the flask. The sample flask was then shaken to mix the contents and to disperse the precipitate finely throughout. After the precipitate has settled at least halfway down the flask, the flask was shaken again to disperse the precipitate. The sample flasks containing pickled samples were stored in an air-conditioned laboratory until they were measured.

(6) Sample measurement

At least two hours after the re-shaking, the pickled samples were measured on board. A magnetic stirrer bar and 1 cm^3 sulfuric acid solution were added into the sample flask and stirring began.   Samples were titrated by sodium thiosulfate solution whose molarity was determined by potassium iodate solution. Temperature of sodium thiosulfate during titration was recorded by a thermometer. We measured dissolved oxygen concentration using two sets of the titration apparatus system, named DOT-09 and DOT-10. Molal concentration of dissolved oxygen (μmol kg^{-1}) was calculated by the sample temperature during the water sampling, salinity, flask volume, and concentration and titrated volume of the sodium thiosulfate solution (titrant).

(7) Standardization

Concentration of sodium thiosulfate titrant (ca. 0.025M) was determined by potassium iodate standard solution. The NMIJ-CRM potassium iodate was dried in an oven at 130°C. 1.78 g potassium iodate weighed out accurately was dissolved in deionized water and diluted to final volume of 5 dm^3 in a calibrated volumetric flask (0.001667M). Then the aliquot (about 400 ml) of the solution was stored in a brown glass bottle (500 ml). 10 cm^3 of the standard potassium iodate solution was added to a flask using a volume-calibrated dispenser. Then 90 cm^3 of deionized water, 1 cm^3 of sulfuric acid solution, and 1.0 cm^3 of pickling reagent solution II and I were added into the flask in order. Amount of titrated volume of sodium thiosulfate (usually 5 times measurements average) gave the molarity of the sodium thiosulfate titrant. Table 4.6.1 show results of the standardization during the cruises. The averaged coefficient of variation (C.V.) for the standardizations was 0.014 ± 0.007 % (standard deviation, n = 44).

(8) Blank determination

The oxygen in the pickling reagents I (1.0 cm^3) and II (1.0 cm^3) was assumed to be 7.6×10^{-8} mol (Murray *et al.*, 1968). The redox species apart from oxygen in the reagents (the pickling reagents I, II, and the sulfuric acid solution) also affect the titration, which is called the reagent blank. The reagent blank was determined as follows. 1 and 2 cm^3 of the standard potassium iodate solution were added to two flasks respectively. Then 100 cm^3 of deionized water, 1 cm^3 of sulfuric acid solution, and 1.0 cm^3 of pickling reagent II and I each were added into the two flasks in order. The reagent blank was determined by difference between the two times of the first (1 cm^3 of KIO_3) titrated volume of the sodium thiosulfate and the second (2 cm^3 of KIO_3) one. The three results of the blank determination were averaged (Table 4.6.1). The averaged coefficient of variation (C.V.) for the reagent blank determination against the titration volume of the potassium iodate standard (about 4 ml) or 250 μmol kg^{-1} of dissolved oxygen concentration was 0.040 ± 0.030 % (standard deviation, n = 44). The redox species in seawater sample itself are measured as "dissolved oxygen", which is called as the seawater blank, unless they are corrected. Because we did not measure the seawater blank, the dissolved oxygen concentration reported here includes the sum of those concentrations that is less than 1 μmol kg^{-1} in the open ocean except those in suboxic and anoxic waters (Kumamoto *et al.*, 2015).

Table 4.6.1 Results of standardization (End Point, cm^3) and reagent blank determination (cm^3).

No	Date (UTC)	Leg	Lot	KIO_3 Lot	$Na_2S_2O_3$ Lot	DOT-9 E.P.	DOT-9 blank	DOT-10 E.P.	DOT-10 blank	Δ (%)*	Remarks
1	2019/Dec/02	2	1	K19E01	T-19T	3.963	-0.002	3.962	0.000	0.080	Test
2	2019/Dec/05	2	3	K19E02	T-19T	3.964	-0.001	3.963	0.003	0.136	Stn.002-014
3	2019/Dec/08	2	5	K19E03	T-19T	3.965	-0.002	3.967	0.003	0.082	Stn.017-032
4	2019/Dec/12	2	6	K19E04	T-19T	3.965	-0.002	3.966	0.004	0.120	Stn.034-046
5	2019/Dec/16	2	7	K19E05	T-19T	3.965	-0.002	3.967	0.004	0.107	$Na_2S_2O_3$ change
6	2019/Dec/16	2	8	K19E05	T-19S	3.967	-0.001	3.963	0.000	0.126	Stn.048-058
7	2019/Dec/19	2	9	K19E06	T-19S	3.966	-0.002	3.967	0.003	0.093	Stn.060-068
8	2019/Dec/22	2	10	K19E07	T-19S	3.966	-0.001	3.967	0.005	0.141	Final standardization
9	2019/Dec/31	3	1	K19F01	T-19R	3.965	-0.003	3.966	0.001	0.108	Stn.070-081
10	2020/Jan/04	3	3	K19F02	T-19R	3.970	-0.001	3.971	0.005	0.102	Stn.083-099
11	2020/Jan/08	3	4	K19F03	T-19R	3.970	0.001	3.969	0.004	0.097	$Na_2S_2O_3$ change
12	2020/Jan/08	3	6	K19F04	T-19U	3.966	0.000	3.962	0.005	0.227	Stn.101-108
13	2020/Jan/09	3	7	K19F05	T-19U	3.966	0.000	3.964	0.008	0.260	Test
14	2020/Jan/11	3	8	K19F06	T-19U	3.966	0.001	3.969	0.006	0.054	Stn.111-116
15	2020/Jan/11	3	9	K19F07	T-19U	3.967	0.001	3.969	0.006	0.099	Test
16	2020/Jan/13	3	10	K19F08	T-19U	3.966	0.000	3.968	0.005	0.074	Stn.118-124
17	2020/Jan/16	3	11	K19F09	T-19U	3.964	-0.001	3.965	0.004	0.088	$Na_2S_2O_3$ change
18	2020/Jan/16	3	12	K19F09	T-19V	3.960	-0.002	3.962	0.004	0.122	Stn.126-138

19	2020/Jan/19	3	13	K19G01	T-19V	3.966	0.000	3.967	0.005	0.107	Stn.140-147
20	2020/Jan/22	3	15	K19G02	T-19V	3.964	-0.001	3.965	0.004	0.127	Stn.148-153
21	2020/Jan/25	3	16	K19G03	T-19V	3.965	-0.001	3.962	0.001	0.103	Final standardization
22	2020/Jan/25	3	17	K19G03	T-19Q	3.963	-0.005	3.965	0.000	0.079	Test

*Difference in sodium thiosulfate concentration determined by the standardization between DOT-9 and DOT-10.

(9) Replicate sample measurement

At all the water sampling stations during Leg-2 and 3 cruises, a pair of replicate samples was collected at one or two depths. The standard deviations from the difference of pairs of replicate measurements was estimated to be 0.09 μmol kg^{-1} (n = 146), which corresponds 0.036% of the relative standard deviation against 250 μmol kg^{-1}, using the standard operating procedure 23 of Dickson *et al.* (2007). The standard deviations of the difference between the pair of replicate measurement for the samples whose oxygen concentration is higher and lower than 150 μmol kg^{-1} are 0.08 (n = 121) and 0.15 μmol kg^{-1} (n = 25), respectively (Fig. 4.6.1). The difference between the two standard deviations is significant (F-test at 95% confidence level) and is probably due to contamination of atmospheric O_2 during the water sampling.
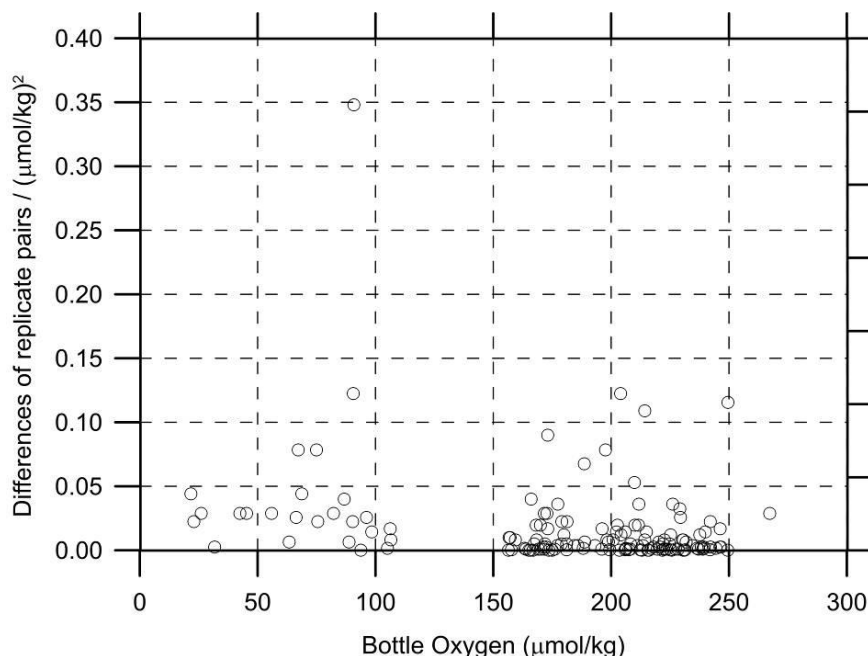
Figure 4.6.1 Oxygen difference between measurements of a replicate pair against oxygen concentration.

(10) Duplicate sample measurement

During Leg-2 the duplicate samplings were taken for all the 36 bottles at two stations (Table 4.6.2). The standard deviation of the duplicate measurements at the station 30 and 39 were calculated to be 0.09 (n = 34) and 0.13 μmol kg^{-1} (n = 4), respectively. The F-test at 95% confidence level indicates that there is no reason to believe that these standard deviations are significantly different from that of the replicate measurements (section 9). Therefore, we concluded that there is no difference among the results of the duplicate measurements, which suggests that all the bottles tripped correctly.

Table 4.6.2 Results of the duplicate sample measurements.

No.	Leg	Station	Sampling Pres.(db)	Position #	Bottle #	Dissolved oxygen (μmol/kg)
1	2	30	4750	1	X12S01	177.29
				2	X12046	177.42
				3	X12S03	177.13

44

				4	X12S04	177.36
				5	X12S05	177.41
				6	X12S06	177.26
				7	X12S07	177.40
				8	X12103	177.38
				9	X12S09	177.46
				10	X12S10	177.35
				11	X12S11	177.41
				12	X12S12	*
				13	X12S13	177.44
				14	X12S14	177.56
				15	X12S15	177.44
				16	X12S16	177.53
				17	X12S17	177.46
				18	X12S18	177.61
				19	X12S19	177.42
				20	X12S20	177.35
				21	X12S21	177.37
				22	X12S22	177.35
				23	X12S23	177.39
				24	X12S24	177.46
				25	X12S25	*
				26	X12S26	177.30
				27	X12S27	177.38
				28	X12S28	177.36
				29	X12S29	177.47
				30	X12S30	177.34
				31	X12S31	177.45
				32	X12S32	177.44
				33	X12S33	177.41
				34	X12S34	177.41
				35	X12S35	177.35
				36	X12S36	177.48
2	2	39	5000	6	X12S06	182.51
				12	X12S12	182.34
				18	X12S18	182.34
				25	X12S25	182.18

*Sample lost due to mis-trip (leaking).

(11) CSK standard measurements

The CSK standard is a commercial potassium iodate solution (0.0100 N) for analysis of dissolved oxygen. We titrated the CSK standard solution (Lot TWJ0280) against our KIO_3 standards as samples during the cruises (Table 4.6.3). The good agreement among them confirms that there was no systematic shift in our oxygen analyses on board.

Table 4.6.3 Results of the CSK standard (Lot TWJ0280) measurements.

Date (UTC)	KIO_3 ID No.	Conc. (N)	error (N)	Conc. (N)	error (N)	Remarks
		DOT-9		DOT-10		
2019/12/02	K19E01	0.01001	0.00001	0.01001	0.00001	Leg-2
2019/12/05	K19E02	0.01002	0.00001	0.01001	0.00001	Leg-2
2019/12/31	K19F01	0.01002	0.00001	0.01002	0.00002	Leg-3
2020/01/19	K19G01	0.01001	0.00001	0.01001	0.00000	Leg-3

(12) Quality control flag assignment

Quality flag values for oxygen data from sample bottles were assigned according to the code defined in Table 4.9 of WHP Office Report WHPO 90-1 Rev.2 section 4.5.2 (Joyce *et al*., 1994). Measurement flags of 2 (good), 3 (questionable), 4 (bad), and 5 (missing) have been assigned (Table 4.6.4). For the choice between 2, 3, or 4, we basically followed a flagging procedure as listed below:

    a. Bottle oxygen concentration at the sampling layer was plotted against sampling pressure. Any points not lying on a generally smooth trend were noted.

    b. Difference between bottle oxygen and oxygen sensor was then plotted against sampling pressure. If a datum deviated from a group of plots, it was flagged 3.

    c. Vertical sections against pressure and potential density were drawn. If a datum was anomalous on the section plots, datum flag was degraded from 2 to 3, or from 3 to 4.

    d. If there was problem in the measurement, the datum was flagged 4.

    e. If the bottle flag was 4 (did not trip correctly), a datum was flagged 4 (bad). In case of the bottle flag 3 (leaking) or 5 (unknown problem), a datum was flagged based on steps a, b, c, and d.

Table 4.6.4 Summary of assigned quality control flags.

Flag	Definition	Number*
2	Good	2352
3	Questionable	18
4	Bad	2
5	Not report (missing)	0
	Total	2372

*The replicate samples (n = 146) and duplicate samples (n = 38) were not included.

(13) Uncertainty

We assume that the uncertainty of dissolved oxygen determination is derived from those of concentration/titration of potassium iodate standard solution, reagent blank determination, titration of seawater sample, and volume of sample flask (Table 4.6.5). We found temporal variation in the standardization due to unknown causes in the titrators (section 14), whose uncertainty was also added. These uncertainties yielded 0.09% of the combined uncertainty and 0.18% the expanded combined uncertainty. Note that this combined uncertainty does not include that derived from temporal change in room temperature. However, that was negligible because the its variation was small (17.0-21.5°C). The uncertainty due to the seawater blank (section 8) is unknow because we did not measure it. If it is assumed that the seawater blank concentration is 0.50 ± 0.50 μmol kg^{-1} and the distribution of the possible values is uniform or rectangular, its standard uncertainty is calculated to be 0.29 μmol kg^{-1} (= 0.50/√3). This value corresponds to the standard uncertainty of 0.12% relative to 250 μmol kg^{-1} of dissolved oxygen concentration. The combined standard uncertainty, which includes the uncertainty of the seawater blank concentration, is calculated to be 0.15% (the extended combined uncertainty is 0.30%). These combined uncertainties, however, are applicable only for the dissolved oxygen concentration corrected by the seawater blank concentration (0.50 μmol kg^{-1}).

Table 4.6.5 Uncertainties of estimated items for the oxygen determination.

	Estimated items	Relative uncertainty to 250 μmol kg^{-1} (%)	References
1	Sodium thiosulfate concentration	0.052	2, 3, 4
2	Potassium iodate concentration	0.030	Kumamoto *et al.* (2015)
3	Titration of potassium iodate	0.014	Section 7
4	Reagent blank determination	0.040	Section 8
5	Titration of seawater sample	0.036	Section 9
6	Volume of sample flask	0.015	Kumamoto *et al.* (2015)
7	Stability of titrators	0.047	Section 14
	Combined uncertainty (k=1)	0.091	1, 4, 5, 6, 7
Expanded combined uncertainty (k=2)		0.182	

(14) Problem

    a. The concentrations of sodium thiosulfate solution determined using DOT-10 was higher than those

determined using DOT-09 by $0.115 \pm 0.047\%$ (standard deviation, n = 22, Table 4.6.1). The difference was cancelled in the calculation of dissolved oxygen concentration. However, we found that it changed temporally by unknown causes, which probably affected the determination of dissolved oxygen concentration. Therefore, we added the uncertainty derived from this to the combined uncertainty of our oxygen measurement (section 13).

b. We found white turbidity in the pickling reagent II solution (Lot 2-19F). Although we replaced the dispenser (MO-43, -31, -27) two times during the cruises, the turbidity did not disappear from the reagent solution, which implies that the solution of this lot (2-19F) may have defect.

c. In some measurements, the titration did not finish automatically because the final absorbance of light through the sample flask was higher than 0.15. We believe the problem is that we cannot adjust this value of the threshold limit.

d. The titration was disturbed by air bubbles in the light path in a sample measurement, which implies that the rotation speed of the stirrer (8 rpm) is faster than the optimum one.

e. During the cruises, six samples were re-measured because of problems in the titration curve, including the problems c and d. We add 1 ml of the KIO_3 standard solution into the sample flask and the total volume of sodium thiosulfate solution titrated was recorded. Eventually the result of the first titration was accepted in each sample measurement.

f. A sample flask was turned over by accident just before the measurement (titration), about six hours after the water sampling. There was, however, no problem in the concentration calculated from this titration.

(15) Data archives

The data obtained in the cruises will be submitted to the Data Management Group of JAMSTEC and will

be opened to the public via "Data Research System for Whole Cruise Information in JAMSTEC (DARWIN)"

in the JAMSTEC web site.

References
Dickson, A. G., C.L. Sabine, and J.R. Christian (Eds.) (2007) Guide to best practices for ocean CO_2 measurements, PICES Special Publication 3, 191 pp.
Joyce, T., and C. Corry, eds., C. Corry, A. Dessier, A. Dickson, T. Joyce, M. Kenny, R. Key, D. Legler, R. Millard, R. Onken, P. Saunders, M. Stalcup (1994) Requirements for WOCE Hydrographic Programme Data Reporting, WHPO Pub. 90-1 Rev. 2, May 1994 Woods Hole, Mass., USA.
Kumamoto, Y., Y. Takatani, T. Miyao, H. Sato, and K. Matsumoto (2015) Dissolved oxygen, Guideline of Ocean Observations, vol. 3, chap. 1, G301JP:001−029 (in Japanese).
Murray, C.N., J.P. Riley, and T.R.S. Wilson (1968) The solubility of oxygen in Winkler reagents used for determination of dissolved oxygen, Deep-Sea Res., 15, 237-238.

4.7. Nutrients
as of 19 November 2019 ver3.3
  as of 9 March 2020 ver3.6
  as of 17 march 2020 ver3.7
  as of 27 March 2020 ver4.0
  as of 31 March 2020 ver4.1
  as of 2 April 2020 ver4.2
  as of 3 April 2020 ver4.3, ver4.4 and ver4.5

(1) Personnel
  Michio AOYAMA (JAMSTEC/Tsukuba Univ.): Principal Investigator
  Yuichiro KUMAMOTO (JAMSTEC)
  LEG2
  Keitaro MATSUMOTO (MWJ): Operation Leader
  Tomomi SONE (MWJ)
  Tomoyuki TANAKA (MWJ)
  LEG3
  Shinichiro YOKOGAWA (MWJ): Operation Leader
  Tomomi SONE (MWJ)
  Ko Morita (MWJ)

(2) Objectives
  The objective of nutrients analyses during the R/V Mirai MR19-04 cruise in the Indian Ocean and Southern Ocean, of which EXPOCODE are 49NZ20191205 and 49NZ20191230, is as follows:
- Describe the present status of nutrients concentration with excellent comparability using certified reference material of nutrient in seawater.

(3) Parameters
  The determinants are nitrate, nitrite, silicate, phosphate and ammonia in the Indian Ocean and Southern Ocean.

(4) Instruments and methods
(4.1) Analytical detail using QuAAtro 2-HR systems (BL TEC K.K.)
  Nitrate + nitrite and nitrite are analyzed following a modification of the method of Grasshoff (1976). The sample nitrate is reduced to nitrite in a cadmium tube the inside of which is coated with metallic copper. The sample stream after reduction is treated with an acidic, sulfanilamide reagent to produce a diazonium ion. N-1-naphthylethylenediamine dihydrochloride is added to the sample stream to produce a red azo dye. With the reduction of the nitrate to nitrite, both nitrate and nitrite react and are measured. Thus, for the nitrite analysis, no reduction is performed and the alkaline buffer is not necessary. Nitrate is computed by the difference between nitrate+nitrite concentration and nitrite concnetration,.
  The silicate method is analogous to that described for phosphate. The method used is essentially that of Grasshoff et al. (1999). Silicomolybdic acid is first formed from the silicate in the sample and molybdic acid. The silicomolybdic acid is reduced to silicomolybdous acid, or "molybdenum blue," using ascorbic acid.
  The phosphate analysis is a modification of the procedure of Murphy and Riley (1962). Molybdic acid is added to the seawater sample to form phosphomolybdic acid which is in turn reduced to phosphomolybdous acid using L-ascorbic acid as the reductant.
  The ammonia in seawater is mixed with an alkaline containing EDTA, ammonia as gas state is formed from seawater. The ammonia (gas) is absorbed in sulfuric acid by way of 0.5 μm pore size membrane filter (ADVANTEC PTFE) at the dialyzer attached to the analytical system. The ammonia absorbed in sulfuric acid is determined by coupling with phenol and hypochlorite to form indophenols blue.
  The details of a modification of analytical methods for four parameters, nitrate, nitrite, silicate and phosphate, used in this cruise are also compatible with the methods described in nutrients section

in the new GO-SHIP repeat hydrography nutrients manual (Becker et al., 2019) which is a revised version of the GO-SHIP repeat hydrography nutrients manual (Hydes et al., 2019), while an analytical method of ammonium is compatible with the determination of ammonia in seawater using a vaporization membrane permeability method (Kimura, 2000). The flow diagrams and reagents for each parameter are shown in Figures 4.7-1 to 4.7-5.

(4.2) Nitrate + Nitrite Reagents
50 % Triton solution
    50 mL Triton^{TM} X-100 provided by Sigma-Ardrich Japan G. K. (CAS No. 9002-93-1) were mixed with 50 mL ethanol (99.5 %).

Imidazole (buffer), 0.06 M (0.4 % w/v)
    Dissolve 4 g imidazole (CAS No. 288-32-4), in 1000 mL ultra-pure water, add 2 mL hydrogen chloride (CAS No. 7647-01-0). After mixing, 1 mL 50 % triton solution is added.

Sulfanilamide, 0.06 M (1 % w/v) in 1.2 M HCl
    Dissolve 10 g 4-aminobenzenesulfonamide (CAS No. 63-74-1), in 900 mL of ultra-pure water, add 100 mL hydrogen chloride (CAS No. 7647-01-0). After mixing, 2 mL 50 % triton solution is added.

NED, 0.004 M (0.1 % w/v)
    Dissolve 1 g N-(1-naphthalenyl)-1,2-ethanediamine, dihydrochloride (CAS No. 1465-25-4), in 1000 mL of ultra-pure water and add 10 mL hydrogen chloride (CAS No. 7647-01-0). After mixing, 1 mL 50 % Triton solution is added. This reagent was stored in a dark bottle.

Figure 4.7-1 NO$_3$+NO$_2$ (1ch.) flow diagram.

(4.3) Nitrite Reagents
50 % Triton solution
    50 mL Triton^{TM} X-100 provided by Sigma-Ardrich Japan G. K. (CAS No. 9002-93-1) .were mixed with 50 mL ethanol (99.5 %).

Sulfanilamide, 0.06 M (1 % w/v) in 1.2 M HCl

Dissolve 10 g 4-aminobenzenesulfonamide (CAS No. 63-74-1), in 900 mL of ultra-pure water, add 100 mL hydrogen chloride (CAS No. 7647-01-0). After mixing, 2 mL 50 % triton solution is added.

NED, 0.004 M (0.1 % w/v)

Dissolve 1 g N-(1-naphthalenyl)-1,2-ethanediamine, dihydrochloride (CAS No. 1465-25-4), in 1000 mL of ultra-pure water and add 10 mL hydrogen chloride (CAS No. 7647-01-0). After mixing, 1 mL 50 % triton solution is added. This reagent was stored in a dark bottle.
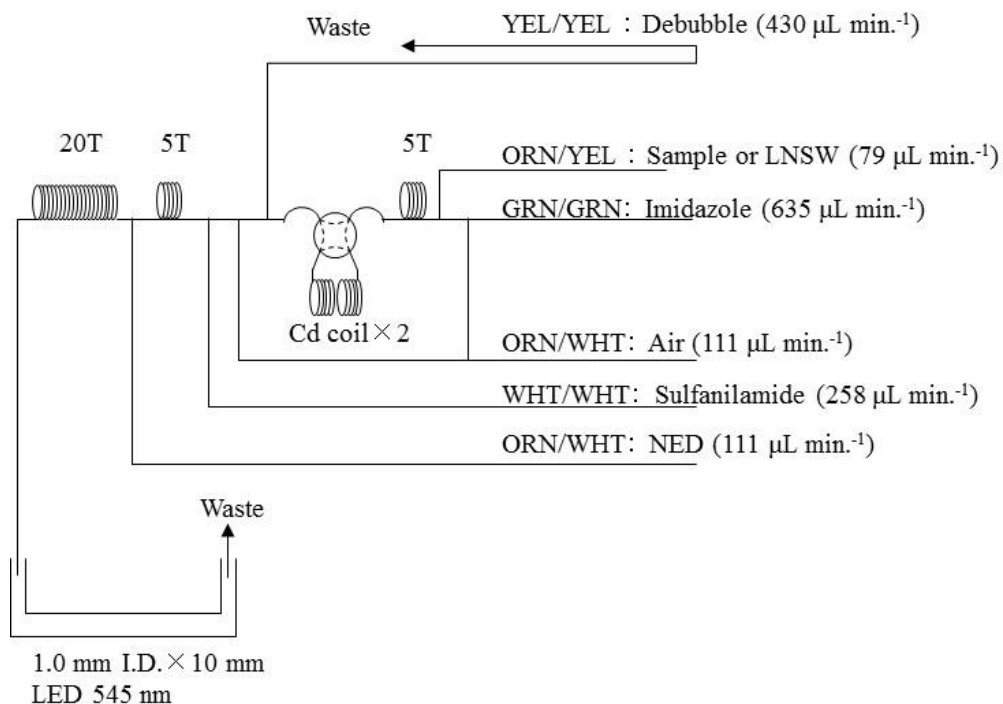

Figure 4.7-2 NO$_2$ (2ch.) flow diagram.

(4.4) Silicate Reagents

15 % Sodium dodecyl sulfate solution

75 g sodium dodecyl sulfate (CAS No. 151-21-3) was mixed with 425 mL ultra-pure water.

Molybdic acid, 0.03 M (1 % w/v)

Dissolve 7.5 g sodium molybdate dihydrate (CAS No. 10102-40-6), in 980 mL ultra-pure water, add 12 mL 4.5M sulfuric acid. After mixing, 20 mL 15 % sodium dodecyl sulfate solution is added. Note that the amount of sulfuric acid is reduced from previous reports because we readjusted to Grasshoff et al. (1999).

Oxalic acid, 0.6 M (5 % w/v)

Dissolve 50 g oxalic acid (CAS No. 144-62-7), in 950 mL of ultra-pure water.

Ascorbic acid, 0.01 M (3 % w/v)

Dissolve 2.5 g L-ascorbic acid (CAS No. 50-81-7), in 100 mL of ultra-pure water. This reagent was freshly prepared every day.

Waste ← WHT/WHT: Debubble (258 μL min.⁻¹)

5T   20T   20T   10T 5T   20T   WHT/WHT: Sample or LNSW (258 μL min.⁻¹)

BLU/BLU: Molybdic acid (530 μL min.⁻¹)

ORN/WHT: Air (111 μL min.⁻¹)

WHT/WHT: Oxalic acid (258 μL min.⁻¹)

ORN/WHT: Ascorbic acid (111 μL min.⁻¹)
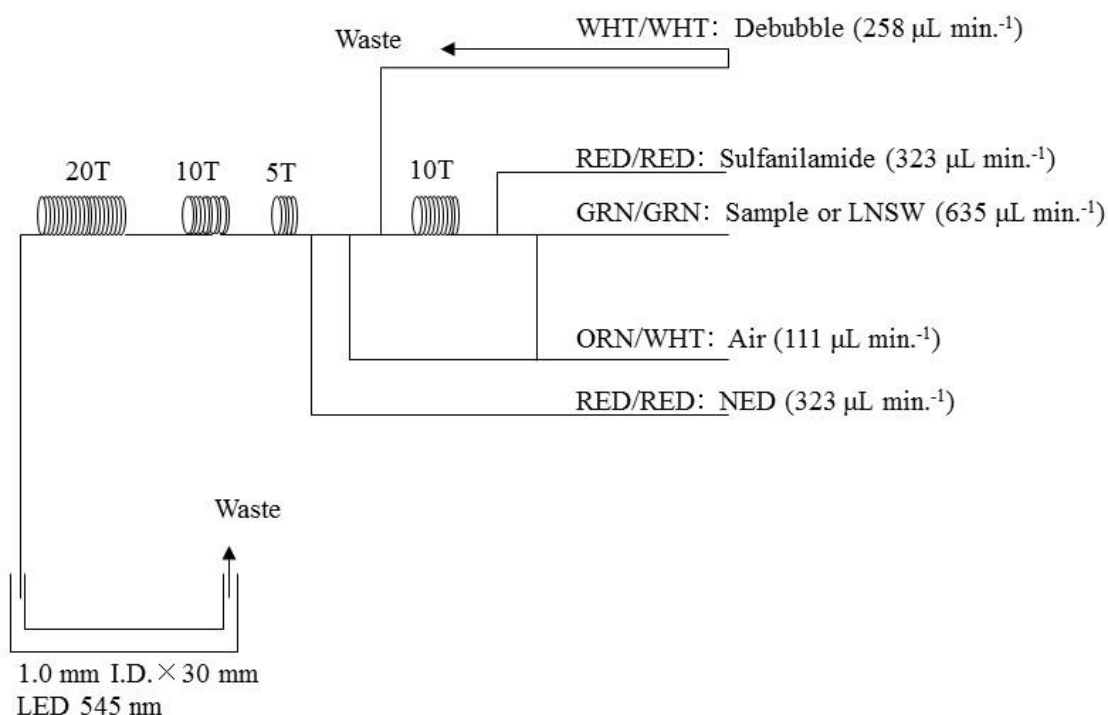
Waste

1.0 mm I.D. × 10 mm
LED 630 nm
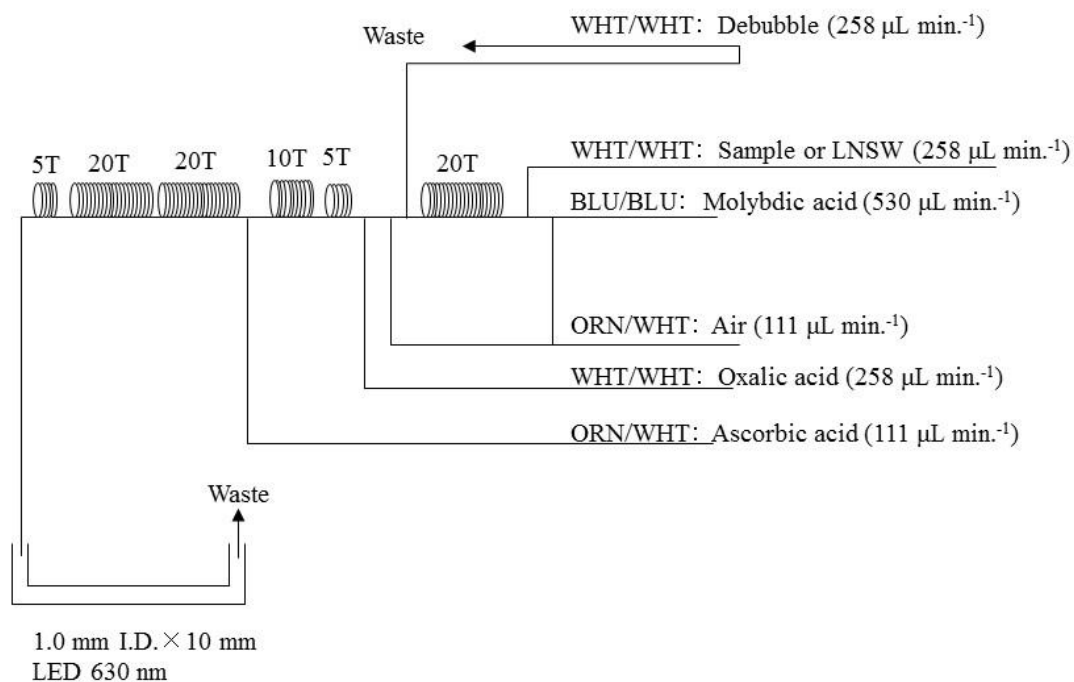
Figure 4.7-3 SiO_2 (3ch.) flow diagram.

(4.5) Phosphate Reagents
15 % Sodium dodecyl sulfate solution
    75 g sodium dodecyl sulfate (CAS No. 151-21-3) were mixed with 425 mL ultra-pure water.

Stock molybdate solution, 0.03 M (0.8 % w/v)
    Dissolve 8 g sodium molybdate dihydrate (CAS No. 10102-40-6), and 0.17 g antimony potassium tartrate trihydrate (CAS No. 28300-74-5), in 950 mL of ultra-pure water and added 50 mL sulfuric acid (CAS No. 7664-93-9).

PO_4 color reagent
    Dissolve 1.2 g L-ascorbic acid (CAS No. 50-81-7), in 150 mL of stock molybdate solution. After mixing, 3 mL 15 % sodium dodecyl sulfate solution is added. This reagent was freshly prepared before every measurement.
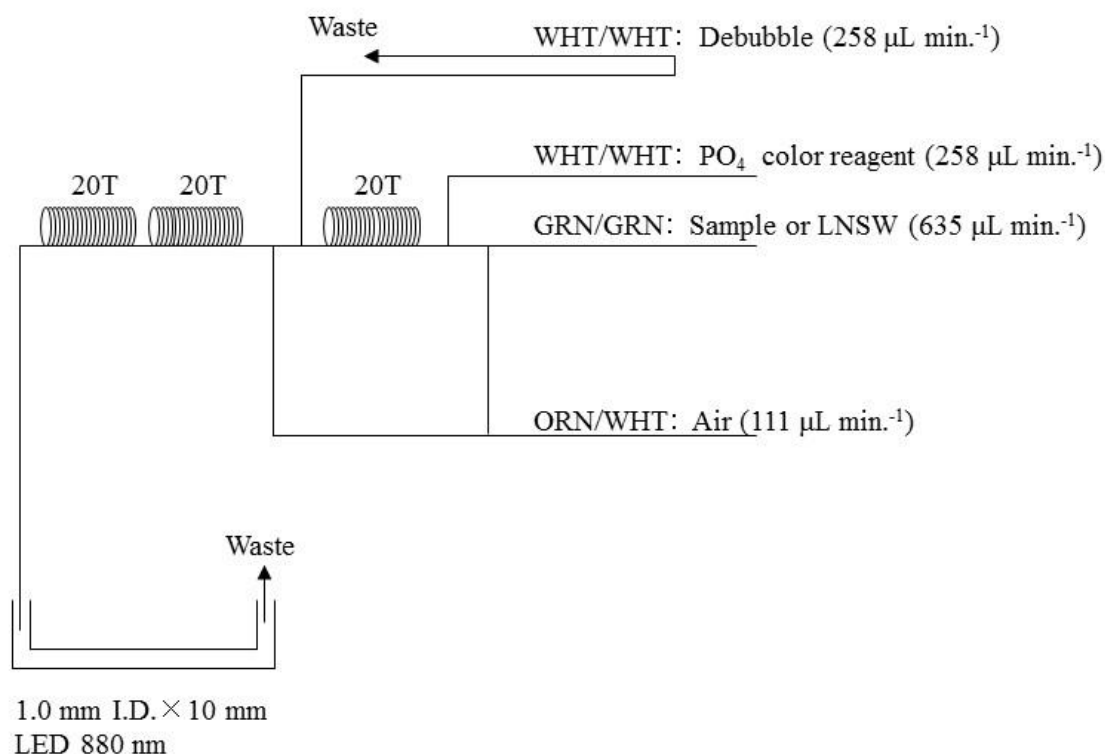
Figure 4.7-4 PO$_4$ (4ch.) flow diagram.

(4.6) Ammonia Reagents

30 % Triton solution

    30 mL Triton^{TM} X-100 provided by Sigma-Ardrich Japan G. K. (CAS No. 9002-93-1) .were mixed with 70 mL ultra-pure water.

EDTA

    Dissolve 41 g tetrasodium;2-[2-[bis(carboxylatomethyl)amino]ethyl-(carboxylatemethyl)amino]acetate;tetrahydrate (CAS No. 13235-36-4), and 2 g boric acid (CAS No. 10043-35-3), in 200 mL of ultra-pure water. After mixing, a 1 mL 30 % triton solution is added. This reagent is prepared a week approximately.

NaOH liquid

    Dissolve 1.5 g sodium hydroxide (CAS No. 1310-73-2), and 16 g tetrasodium;2-[2-[bis(carboxylatomethyl)amino]ethyl-(carboxylatemethyl)amino]acetate;tetrahydrate (CAS No. 13235-36-4) in 100 mL of ultra-pure water. This reagent is prepared a week about. Note that we reduced the amount of sodium hydroxide from 5 g to 1.5 g because pH of C standard solutions lowered 1 due to the change of recipe of B standards solution.

Stock nitroprusside

    Dissolve 0.25 g sodium nitroferricyanide dihydrate (CAS No. 13755-38-9) in 100 mL of ultra-pure water and add 0.2 mL 1M sulfuric acid. Stored in a dark bottle and prepared a month approximately.

Nitroprusside solution

    Mix 4 mL stock nitroprusside and 5 mL 1M sulfuric acid in 500 mL of ultra-pure water. After mixing, 2 mL 30 % triton solution is added. This reagent is stored in a dark bottle and prepared every 2 or 3 days.

Alkaline phenol

Dissolve 10 g phenol (CAS No. 108-95-2), 5 g sodium hydroxide (CAS No. 1310-73-2) and 2 g sodium citrate dihydrate (CAS No. 6132-04-3), in 200 mL ultra-pure water. Stored in a dark bottle and prepared a week approximately.

NaClO solution

Mix 3 mL sodium hypochlorite (CAS No. 7681-52-9) in 47 mL ultra-pure water. Stored in a dark bottle and fleshly prepared before every measurement. This reagent is prepared 0.3 % available chlorine.
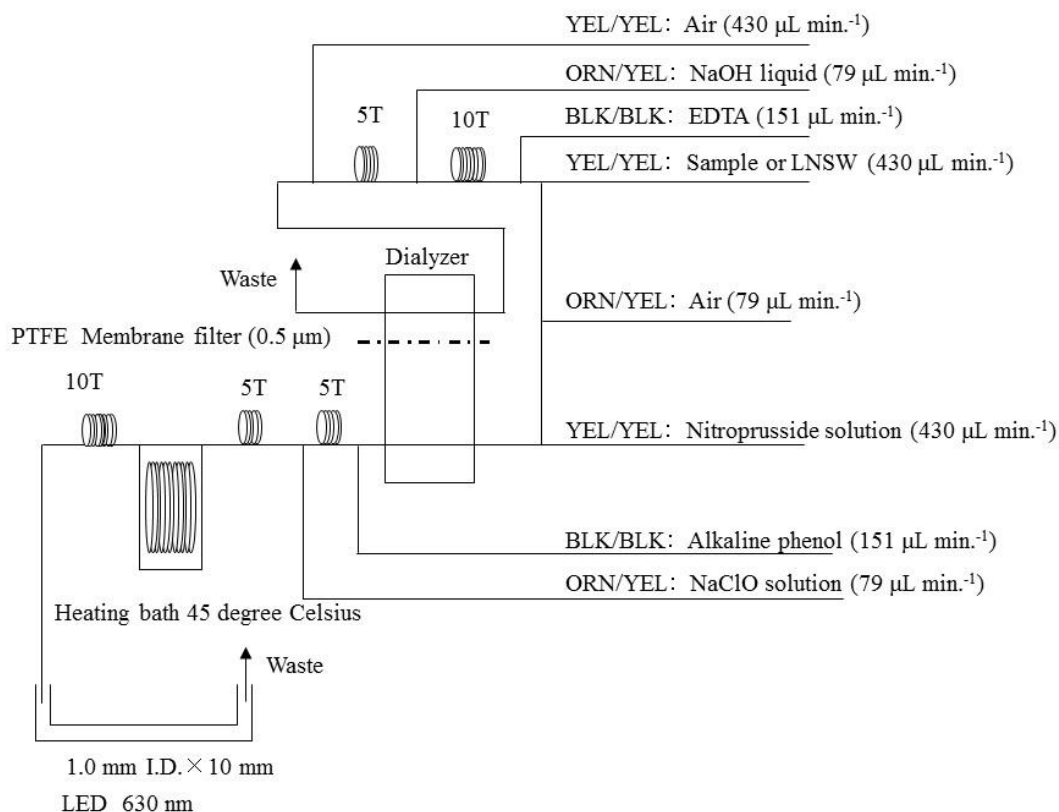
Figure 4.7-5 NH_4 (5ch.) flow diagram.

(4.7) Sampling procedures

Sampling of nutrients followed that oxygen, salinity and trace gases. Samples were drawn into a new 10 mL polyacrylates vials without sample drawing tubes. These were rinsed three times before filling and the vials were capped immediately after the drawing without headspace. The vials are put into water bath adjusted to ambient temperature, 19.9 ± 0.9 degree Celsius, in about 30 minutes before use to stabilize the temperature of samples. When we found the value of Xmiss of the sample was less than 95 % or doubtful for the particles in the sample, we carried out centrifuging (Table 4.7-12) for the samples by using a centrifuge (type: CN-820, Hsiang Tai). The conditions of centrifuging were set about 3400 rpm for 2.5 minute. We also put coolant in the centrifuge to suppress temperature increase of samples during centrifugation.

No transfer from the vial to another container was made and the vials were set an autosampler tray directly. Samples were analyzed after collection within 24 hours.

(4.8) Data processing

Raw data from QuAAtro 2-HR were treated as follows:

- Check the baseline shift.
- Check the shape of each peak and positions of peak values taken, and then change the positions of peak values taken if necessary.
- Carry-over correction and baseline drift correction were applied to peak heights of each sample followed by sensitivity correction.
- Baseline correction and sensitivity correction were done basically using linear regression.
- Load pressure and salinity from uncalibrated CTD data to calculate density of seawater tentatively. To calculate the final nutrient concentration, we used salinity data from calibrated CTD conductivity sensor data.
- Calibration curves to get nutrients concentration were assumed second order equations.

(4.9) Summary of nutrients analysis

We made 33 QuAAtro runs for the samples collected by 37 casts at 37 stations in Leg2 and 43 runs for the samples collected by 44 casts at 44 stations in Leg3 as shown in Table 4.7-1 during MR19-04. The total amount of layers of the seawater sample reached to 2096 in Leg2 and 2746 in Leg3. We made basically duplicate measurements at all the sampling layers. The station locations for nutrients measurement is shown in Figure 4.7-6.
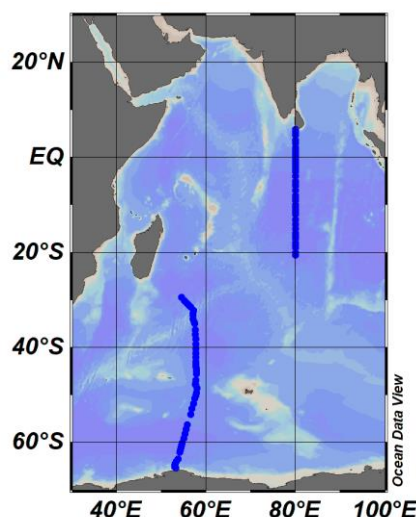
Figure 4.7-6 Sampling positions of nutrients sample.

(5) Station list

The sampling station list for nutrients is shown in Table 4.7-1.

Table 4.7-1 List of stations

Station	Cast	Date (UTC) (mmddyy)	Position* Latitude	Position* Longitude	Depth (m)
002	1	120519	5-52.31N	79-59.22E	824
003	1	120519	5-47.51N	79-59.64E	1390
005	1	120619	5-39.95N	80-00.40E	3233
006	1	120619	5-34.97N	80-00.13E	4015
007	1	120619	5-19.97N	79-59.75E	4147
009	1	120619	4-39.95N	79-59.91E	4276
012	1	120719	3-40.31N	80-00.04E	4358
014	1	120719	3-00.04N	80-00.04E	4340
017	1	120819	2-00.07N	80-00.05E	3875
019	1	120819	1-20.05N	80-00.01E	4569
022	1	120919	0-30.16N	80-00.12E	4651

025	1	121019	0-15.07S	80-00.33E	4683
026	1	121019	0-30.04S	80-00.24E	4712
027	1	121019	0-44.93S	80-00.02E	4735
029	1	121119	1-20.05S	80-00.05E	4834
032	1	121119	2-19.99S	79-59.99E	4909
034	1	121219	2-59.96S	79-59.87E	4967
036	1	121219	4-00.12S	79-59.84E	4630
038	1	121319	4-59.96S	79-59.89E	5140
040	1	121419	5-59.99S	79-59.98E	5202
042	1	121419	7-00.02S	79-59.94E	4917
044	1	121519	8-00.13S	80-00.16E	5416
045	1	121519	8-50.00S	80-00.00E	5190
046	1	121619	9-00.02S	79-59.95E	5207
048	1	121619	10-00.01S	79-59.98E	5383
050	1	121719	11-00.00S	79-59.83E	5347
052	1	121719	12-00.01S	80-00.01E	5159
054	1	121819	13-05.81S	80-00.04E	5003
056	1	121819	13-59.90S	80-00.15E	5024
058	1	121919	14-59.93S	80-00.12E	5111
060	1	121919	15-59.94S	80-00.10E	5046
061	1	122019	16-29.83S	79-59.96E	5038
062	1	122019	16-59.91S	80-00.06E	5072
064	1	122019	17-59.93S	80-00.05E	5100
066	1	122119	18-59.82S	79-59.99E	4946
068	1	122119	20-00.01S	80-00.01E	4866
069	1	122219	20-29.77S	79-59.99E	4859
070	1	123119	29-29.64S	54-2984E	4904
072	1	010120	30-09.31S	55-11.21E	4704
074	1	010120	30-49.31S	55-52.43E	4432
076	1	010220	31-29.07S	56-33.55E	4787
078	1	010220	32-08.99S	57-15.01E	2918
080	1	010320	32-51.01S	57-07.00E	5341
081	1	010320	33-12.01S	57-02.42E	6010
083	1	010320	33-58.01S	57-02.10E	5030
085	2	010420	34-39.33S	57-17.38E	3808
086	1	010520	35-00.02S	57-25.07E	4820
089	1	010520	36-20.02S	57-32.53E	4421
091	1	010620	37-13.31S	57-37.53E	5331
093	1	010620	38-15.36S	57-39.32E	5347
095	1	010720	39-14.74S	57-41.49E	5151
097	1	010720	40-14.98S	57-44.98E	4997
099	1	010820	41-09.64S	57-44.65E	4889
101	1	010820	42-04.75S	57-45.14E	4797
103	1	010920	42-59.79S	57-45.46E	4744
105	1	010920	43-59.87S	57-45.52E	4639
107	1	010920	45-00.07S	57-47.24E	4538

108	1	011020	45-30.04S	57-47.96E	4458
111	1	011120	46-48.27S	57-40.99E	4444
113	1	011120	47-40.79S	57-35.35E	4539
114	1	011220	47-55.12S	57-41.06E	4332
116	1	011220	48-33.64S	57-55.90E	4481
118	2	011420	49-33.58S	57-49.82E	4439
120	1	011420	50-40.49S	57-29.87E	4515
122	1	011520	51-47.57S	57-10.43E	4428
124	1	011520	52-54.29S	56-50.00E	4281
126	1	011620	54-01.24S	56-29.93E	3496
132	1	011720	56-15.08S	55-50.16E	4746
134	1	011720	57-12.99S	55-33.05E	5092
136	1	011820	58-11.14S	55-15.82E	5192
138	1	011820	59-09.08S	54-58.44E	5145
140	1	011920	60-07.23S	54-41.19E	5147
142	1	011920	61-05.10S	54-23.86E	5126
144	1	012020	62-03.31S	54-06.25E	5058
147	1	012020	63-30.11S	53-40.64E	4758
148	1	012120	63-58.03S	53-25.09E	4347
149	1	012120	64-26.12S	53-04.69E	4149
150	1	012120	64-46.99S	52-59.27E	3437
151	1	012120	65-06.19S	53-00.99E	2504
152	1	012220	65-13.45S	53-07.85E	1880
153	1	012220	65-20.20S	53-15.16E	1205

* Position indicates latitude and longitude where CTD reached maximum depth at the cast.

(6) Certified Reference Material of nutrients in seawater

KANSO certified reference materials (CRMs, Lot: CE, CJ, CG, CB, BZ, CF) were used to ensure the comparability and traceability of nutrient measurements during this cruise. The details of CRMs are shown below.

Production

KANSO CRMs for inorganic nutrients in seawater were produced by KANSO Co.,Ltd. This CRM has been produced using autoclaved natural seawater based on the quality control system under ISO Guide 34 (JIS Q 0034).

KANSO Co.,Ltd. has been accredited under the Accreditation System of National Institute of Technology and Evaluation (ASNITE) as a CRM producer since 2011. (Accreditation No.: ASNITE 0052 R)

Property value assignment

The certified values are arithmetic means of the results of 30 bottles from each batch (measured in duplicates) analysed by KANSO Co.,Ltd. and Japan Agency for Marine-Earth Science and Technology (JAMSTEC) using the colorimetric method (continuous flow analysis, CFA, method). The salinity of solutions of calibration standards to get a calibration curve was adjusted to close the salinity of this CRM within ± 0.5.

Metrological Traceability

Each certified value of nitrate, nitrite, and phosphate of KANSO CRMs were calibrated versus one of Japan Calibration Service System (JCSS) standard solutions for each nitrate ions, nitrite ions,

and phosphate ions. JCSS standard solutions are calibrated versus the secondary solution of JCSS for each of these ions. The secondary solution of JCSS is calibrated versus the specified primary solution produced by Chemicals Evaluation and Research Institute (CERI), Japan. CERI specified primary solutions are calibrated versus the National Metrology Institute of Japan (NMIJ) primary standards solution of nitrate ions, nitrite ions and phosphate ions, respectively.

For a certified value of silicate of KANSO CRM was determined by one of Merck KGaA silicon standard solution 1000 mg L^{-1} Si traceable to National Institute of Standards and Technology (NIST) SRM of silicon standard solution (SRM 3150).

The certified values of nitrate, nitrite, and phosphate of KASNO CRM are thus traceable to the International System of Units (SI) through the unbroken chain of calibrations, JCSS, CERI and NMIJ solutions as stated above, each having stated uncertainties. The certified values of silicate of KANSO CRM are traceable to the SI through the unbroken chain of calibrations, Merck KGaA and NIST SRM 3150 solutions, each having stated uncertainties.

As stated in the certificate of NMIJ CRMs, each certified value of dissolved silica, nitrate ions, and nitrite ions was determined by more than one method using one of NIST SRM of silicon standard solution and NMIJ primary standards solution of nitrate ions and nitrite ions. The concentration of phosphate ions as stated information value in the certificate was determined NMIJ primary standards solution of phosphate ions. Those values in the certificate of NMIJ CRMs are traceable to the SI.

One of the analytical methods used for certification of NMIJ CRM for nitrate ions, nitrite ions, phosphate ions and dissolved silica was a colorimetric method (continuous mode and batch one). The colorimetric method is the same as the analytical method (continuous mode only) used for certification of KANSO CRM. For certification of dissolved silica, exclusion chromatography/isotope dilution-inductively coupled plasma mass spectrometry and ion exclusion chromatography with post-column detection was used. For certification of nitrate ions, ion chromatography by direct analysis and ion chromatography after halogen-ion separation was used. For certification of nitrite ions, ion chromatography by direct analysis was used.

NMIJ CRMs were analyzed at the time of certification process for CRM and the results were confirmed within expanded uncertainty stated in the certificate of NMIJ CRMs.

(6.1) CRM for this cruise

60 sets of CRM lots CE, CJ, CG, CB, BZ and CF which almost cover a range of nutrients concentrations in the Indian Ocean and Southern Ocean are prepared.

These CRM assignments were done based on a random number. The CRM bottles were stored at a room in the ship, BIOCHEMICAL LABORATORY, where the temperature was maintained around 18.0 degree Celsius – 21.8 degree Celsius.

(6.2) CRM concentration

Nutrients concentrations for the CRM lots CE, CJ, CG, CB, BZ and CF are shown in Table 4.7-2.

Table 4.7-2 Certified concentration and uncertainty (k=2) of CRMs.

unit: μmol kg^{-1}

Lot	Nitrate	Nitrite	Silicate	Phosphate	Ammonia*
CE	0.01 ± 0.03	0.03 ± 0.01	0.06 ± 0.09	0.012 ± 0.006	0.69
CJ	16.20 ± 0.20	0.04 ± 0.01	38.50 ± 0.40	1.190 ± 0.020	0.77
CG	23.70 ± 0.20	0.07 ± 0.03	56.40 ± 0.50	1.700 ± 0.020	0.61
CB	35.79 ± 0.27	0.13 ± 0.01	109.20 ± 0.62	2.520 ± 0.022	0.77
BZ	43.35 ± 0.33	0.23 ± 0.01	161.00 ± 0.93	3.056 ± 0.033	0.49
CF	43.40 ± 0.40	0.09 ± 0.02	159.70 ± 1.00	3.060 ± 0.030	0.46

*For ammonia values are not certified and shown as only reference values.

(7) Nutrients standards
(7.1) Volumetric laboratory-ware of in-house standards

All volumetric glassware and polymethylpentene (PMP)-ware used were gravimetrically calibrated. Plastic volumetric flasks were gravimetrically calibrated at the temperature of use within 4 K at around 22 deg. C.

(7.1.1) Volumetric flasks

Volumetric flasks of Class quality (Class A) are used because their nominal tolerances are 0.05 % or less over the size ranges likely to be used in this work. Class A flasks are made of borosilicate glass, and the standard solutions were transferred to plastic bottles as quickly as possible after they are made up to volume and well mixed in order to prevent the excessive dissolution of silicate from the glass. PMP volumetric flasks was gravimetrically calibrated and used only within 4 K of the calibration temperature.

The computation of volume contained by glass flasks at various temperatures other than the calibration temperatures were done by using the coefficient of linear expansion of borosilicate crown glass.

Because of their larger temperature coefficients of cubical expansion and lack of tables constructed for these materials, the plastic volumetric flasks were gravimetrically calibrated over the temperature range of intended use and used at the temperature of calibration within 4 K. The weights obtained in the calibration weightings were corrected for the density of water and air buoyancy.

(7.1.2) Pipettes

All glass pipettes have nominal calibration tolerances of 0.1 % or better. These were gravimetrically calibrated to verify and improve upon this nominal tolerance.

(7.2) Reagents, general considerations
(7.2.1) Specifications

For nitrate standard, "potassium nitrate 99.995 suprapur®" provided by Merck, Batch B1452165, CAS No. 7757-79-1, was used.

For nitrite standard solution, we used "nitrite ion standard solution (NO_2^- 1000) provided by Wako, Lot APJ6212, Code. No. 140-06451.". This standard solution was certified by Wako using ion chromatography method. Calibration result is 1003 mg L^{-1} at 20 degree Celsius. Expanded uncertainty of calibration (k=2) is 0.8 % for the calibration result.

For the silicate standard, we changed from "Silicon standard solution SiO_2 in NaOH 0.5 M CertiPUR®" provided by Merck, to in-house Si standard solution exp64 which was produced by alkali fusion technique from 5N SiO_2 powder produced jointly by JAMSTEC and KANSO. The mass fraction of Si in the exp64 solution was calibrated based on NMIJ CRM 3645-a02 Si standard solution.

For phosphate standard, "potassium dihydrogen phosphate anhydrous 99.995 suprapur®" provided by Merck, Batch B1642608, CAS No.: 7778-77-0, was used.

For ammonia standard, "Ammonium Chloride (CRM 3011-a)" provided by NMIJ, CAS No. 12125-02-9. The purity of this standard was greater than 99.9 %. Expanded uncertainty of calibration (k=2) is 0.022 %.

(7.2.2) Ultra-pure water

Ultra-pure water (Milli-Q water) freshly drawn was used for preparation of reagent, standard solutions and for measurement of reagent and system blanks.

(7.2.3) Low nutrients seawater (LNSW)

Surface water having low nutrient concentration was taken and filtered using 0.20 μm pore capsule cartridge filter at MR18-04 cruise in August 2018. This water is stored in 20 L cubitainer with cardboard box.

Nutrients concentrations in LNSW were measured on February 2019.

(7.2.4) Concentrations of nutrients for A, D, B and C standards

The "A" standards for nitrate, nitrite, phosphate and ammonia are made separately as relatively high concentration stock standards. In this cruise we use lot exp.61 of certified silicon standard solution as A-3 standard, The "B" standard is next prepared by mixing five aliquots of single nitrate, nitrite, silicate, phosphate and ammonia A standard(s) and making the solution up to an accurately known volume. Finally, an aliquot of the B standard is made up to working, calibration-standard concentrations, or "C-5" standard for nitrate, nitrite, phosphate, silicate and ammonia, and C-7 and C-8 for ammonia typical, oceanic concentrations using LNSW. The D standards are prepared to measure the reduction rate from nitrate to nitrite.

Concentrations of nutrients for A, B, C and D standards are set as shown in Table 4.7-3.

We developed a new receipt to prepare the B standard without the addition of HCl to neutralize alkali Merck silicon standard solution. Pure water was used to prepare the B standard and to adjust salinity and density, we add NaCl powder as appropriately.

The C standard is prepared according to recipes as shown in Table 4.7-4. All volumetric laboratory tools were calibrated prior to the cruise as stated in chapter (6.1). Then the actual concentration of nutrients in each fresh standard was calculated based on the ambient temperature, solution temperature and determined factors of volumetric laboratory-wares.

The calibration curves for each run were obtained using 6 levels, C-1, C-2, C-3, C-4, C-5 and C-6. C-1, C-2, C-3, C-4 and C-6 were the CRM of nutrients in seawater and C-5 was in-house standard.

Table 4.7-3 Nominal concentrations of nutrients for A, D, B and C standards.

Unit: $\mu mol\ kg^{-1}$

	A	B	D	C-1	C-2	C-3	C-4	C-5	C-6	C-7	C-8
NO_3	45000	900	900	CE	CJ	CG	CB	45.6	BZ	-	-
NO_2	21800	17	870	CE	CJ	CG	CB	0.86	BZ	-	-
SiO_2	35600	2850		CE	CJ	CG	CB	143	BZ	-	-
PO_4	6000	60		CE	CJ	CG	CB	3.0	BZ	-	-
NH_4	4000	120		-	-	-	-	6.0	-	2.4	0

Table 4.7-4 Working calibration standard recipes.

C Std.	B Std.
C-5	25 mL
C-7	10mL

(7.2.5) Renewal of in-house standard solutions

In-house standard solutions as stated in paragraph (7.2.4) were renewed as shown in Table 4.7-5(a) to (c).

Table 4.7-5(a) Timing of renewal of in-house standards.

NO_3, NO_2, SiO_2, PO_4, NH_4	Renewal
A-1 Std. (NO_3)	maximum a month
A-2 Std. (NO_2)	commercial prepared solution
A-3 Std. (SiO_2)	JAMSTEC-KANSO Si standard solution
A-4 Std. (PO_4)	maximum a month
A-5 Std. (NH_4)	maximum a month
D-1 Std.	maximum 8 days
D-2 Std.	maximum 8 days

B Std. (mixture of A-1, D-2, A-3, A-4 and A-5 std.)	maximum 8 days

Table 4.7-5(b) Timing of renewal of working calibration standards.

Working standards	Renewal
C Std. (dilute B Std.)	every 24 hours

Table 4.7-5(c) Timing of renewal of in-house standards for reduction estimation.

Reduction estimation	Renewal
36 μM NO_3 (dilute D-1 Std.)	when C Std. renewed
35 μM NO_2 (dilute D-2 Std.)	when C Std. renewed

(8) Quality control

(8.1) The precision of nutrients analyses during the cruise

The precision of nutrients analyses during this cruise was evaluated based on the 6 to 10 measurements, which are measured every 8 to 13 samples, during a run at the concentration of C-5 std. Summary of precisions is shown in Table 4.7-6 and Figures 4.7-7 to 4.7-11. During this cruise, analytical precisions were 0.16 % for nitrate, 0.22 % for nitrite, 0.12 % for silicate, 0.16 % for phosphate and 0.31 % for ammonia in terms of a median of precision, respectively.

The precisions for each parameter during this cruise are generally consistent with the analytical precisions during the R/V Mirai cruises conducted in 2009 - 2018.   We also can say that time series of precision as shown in Figures 4.7-7 to 4.7-11 showed that the analytical precisions for nitrate, nitrite, silicate, phosphate and ammonia were maintained throughout this cruise except for a few runs.

Table 4.7-6 Summary of precision based on the replicate analyses.(k=1)

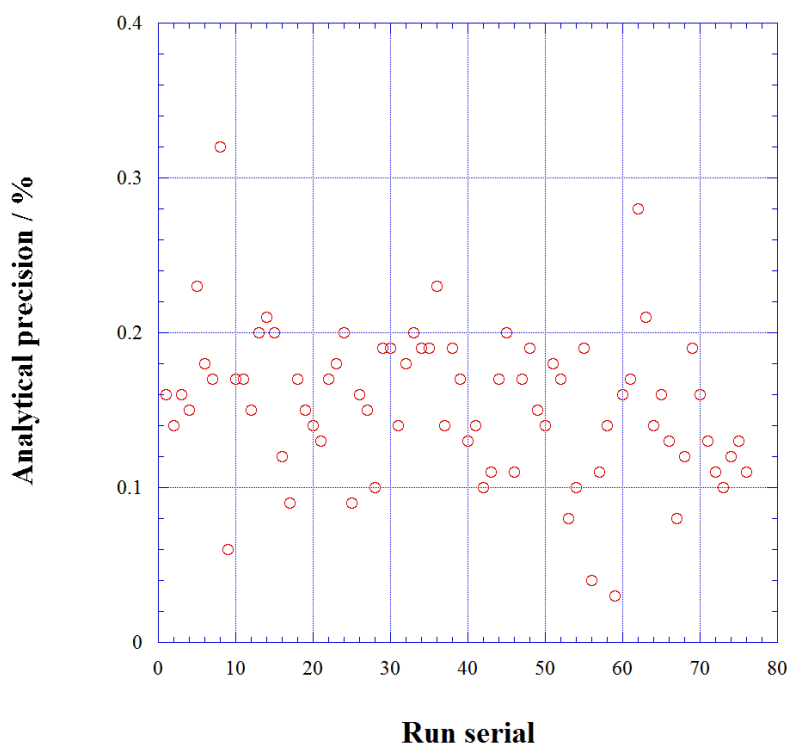|	Nitrate CV %	Nitrite CV %	Silicate CV %	Phosphate CV %	Ammonia CV %
Median	0.16	0.22	0.12	0.16	0.31
Mean	0.15	0.24	0.12	0.16	0.34
Maximum	0.32	0.60	0.24	0.69	0.69
Minimum	0.03	0.11	0.05	0.06	0.15
N	76	76	76	76	76

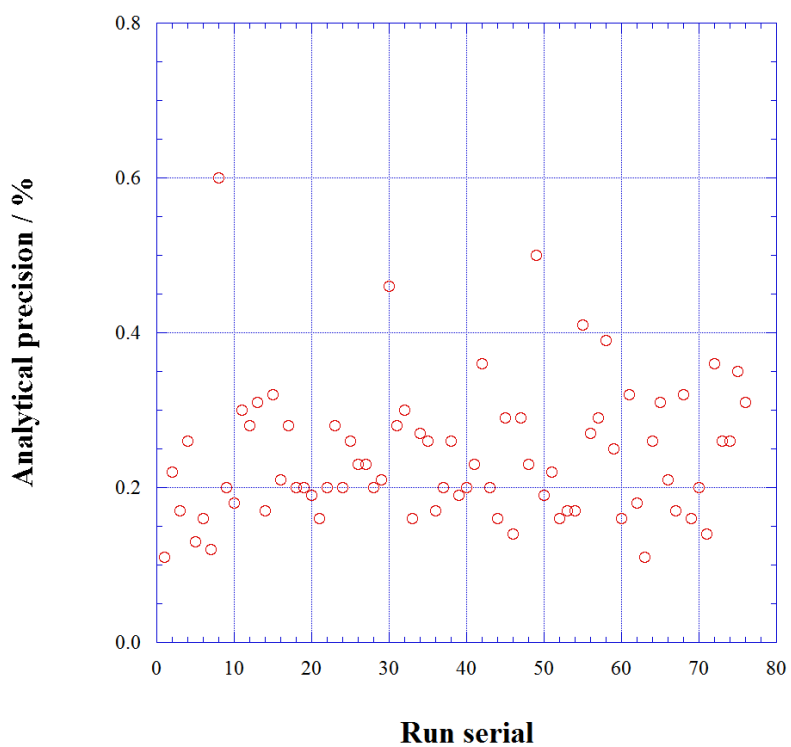Figure 4.7-7 Time series of precision of nitrate in MR19-04

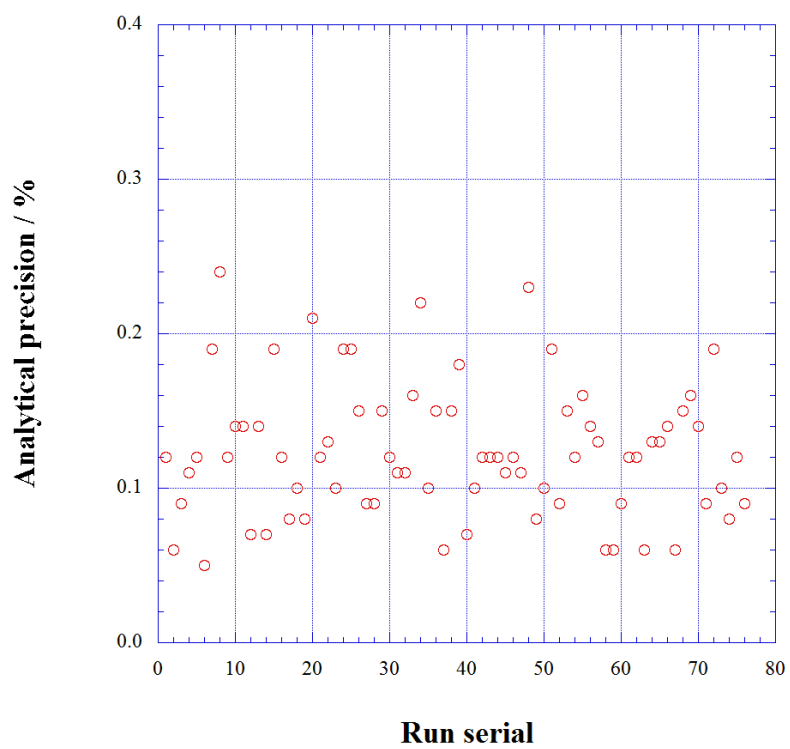Figure 4.7-8 Same as 4.7-7 but for nitrite.
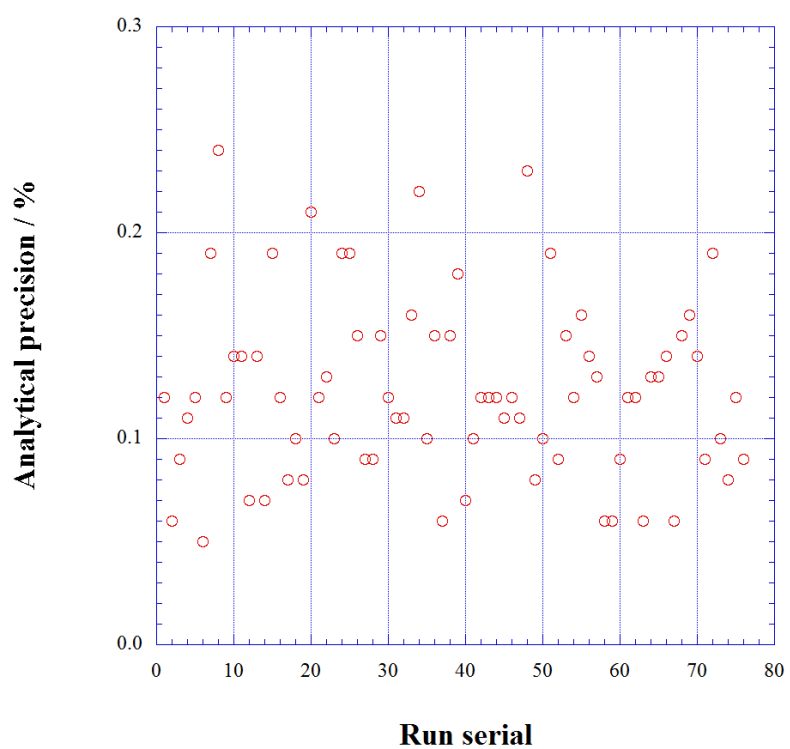
Figure 4.7-9 Same as 4.7-7 but for silicate.

Figure 4.7-10 Same as 4.7-7 but for phosphate.

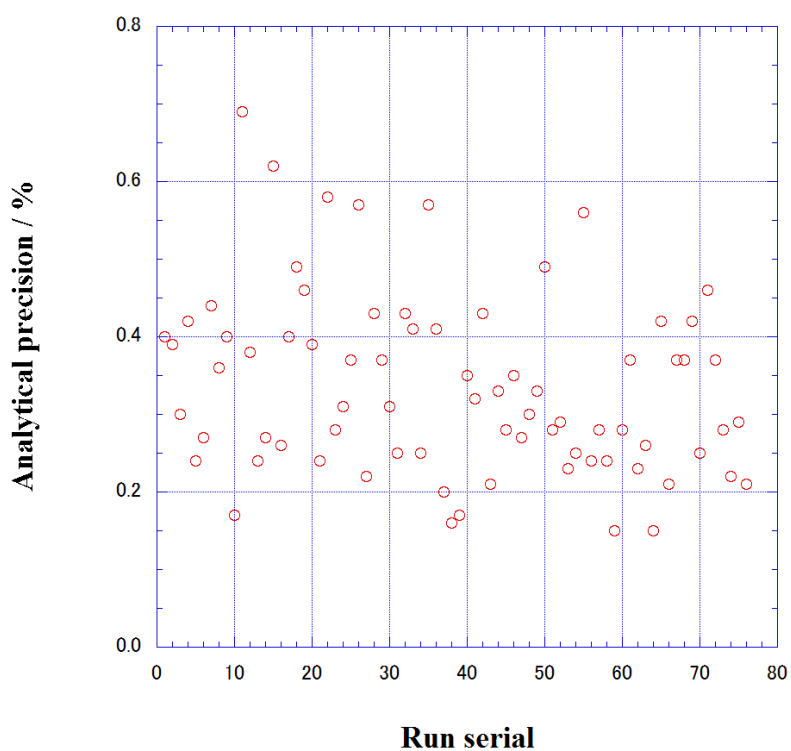Figure 4.7-11 Same as 4.7-7 but for ammonia.

(8.2) CRM lot. CF measurement during this cruise

CRM lot. CF was measured every run to evaluate the comparability tthroughout the cruise. The results of lot. CF during this cruise are shown as Figures 4.7-12 to 4.7-16. All of the measured concentrations of CRM lot. CF was within the uncertainty of certified values for nitrate, nitrite, silicate and phosphate.
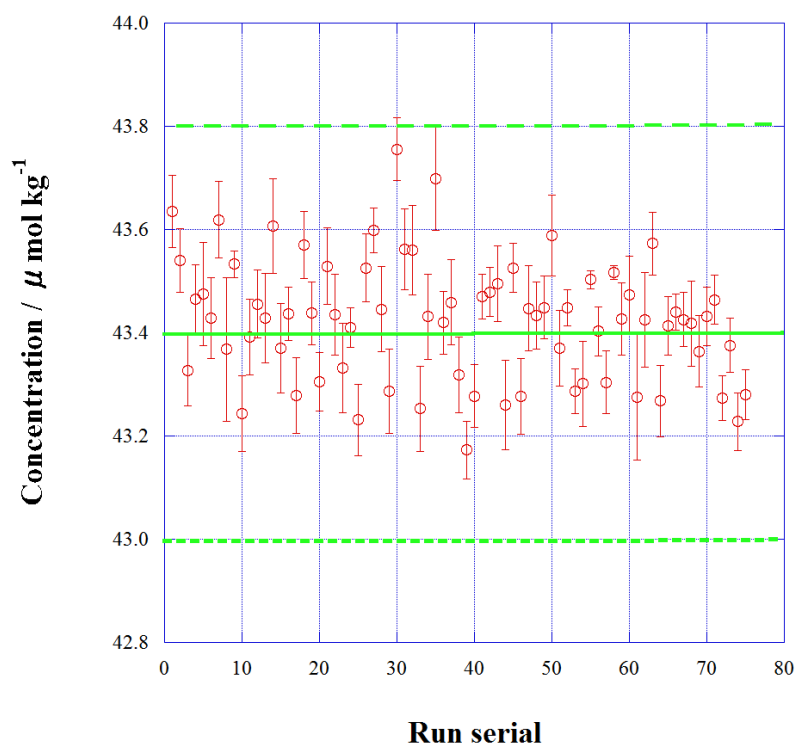
Figure 4.7-12 Time series of CRM-CF of nitrate in MR19-04. Solid green line is certified nitrate concentration of CRM and dotted green line show uncertainty of certified value at k=2.

Figure 4.7-13 Same as Figure 4.7-12, but for nitrite.

Figure 4.7-14 Same as Figure 4.7-12, but for silicate.

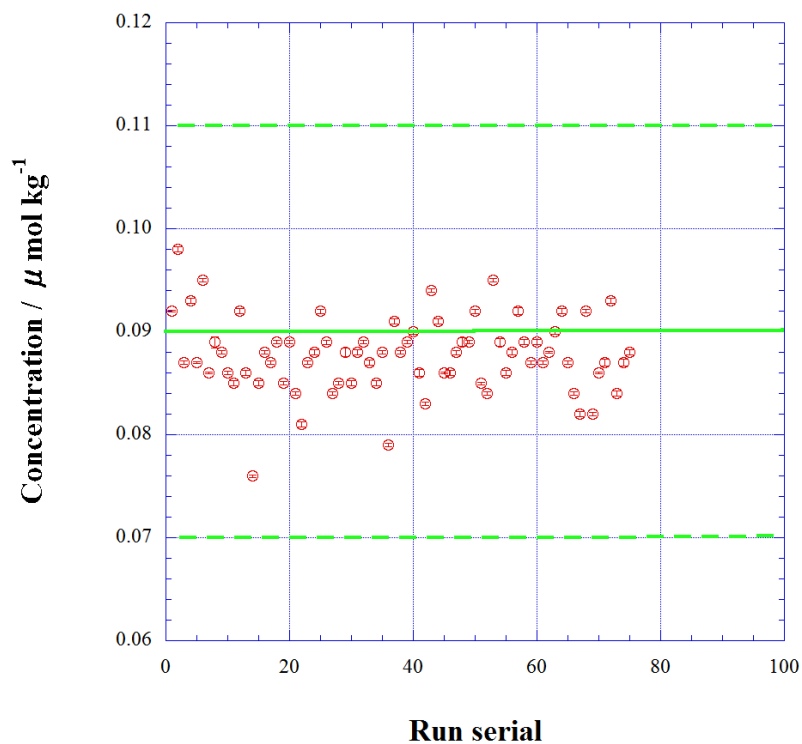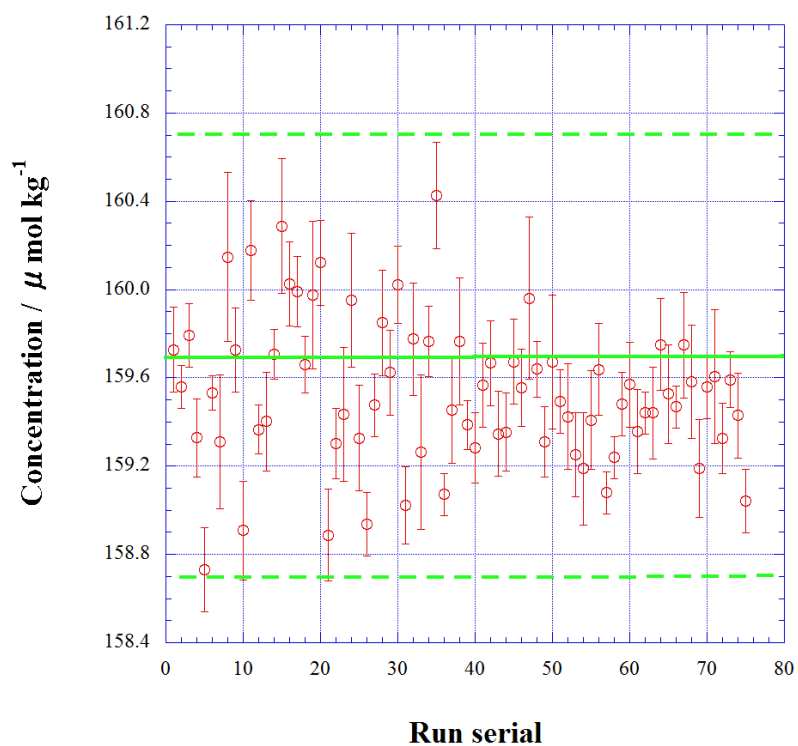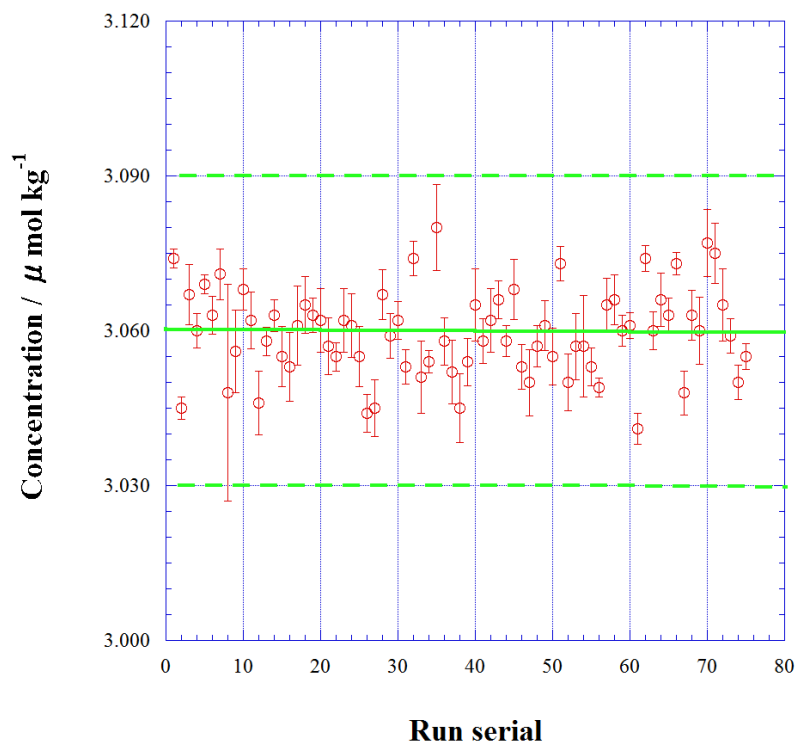

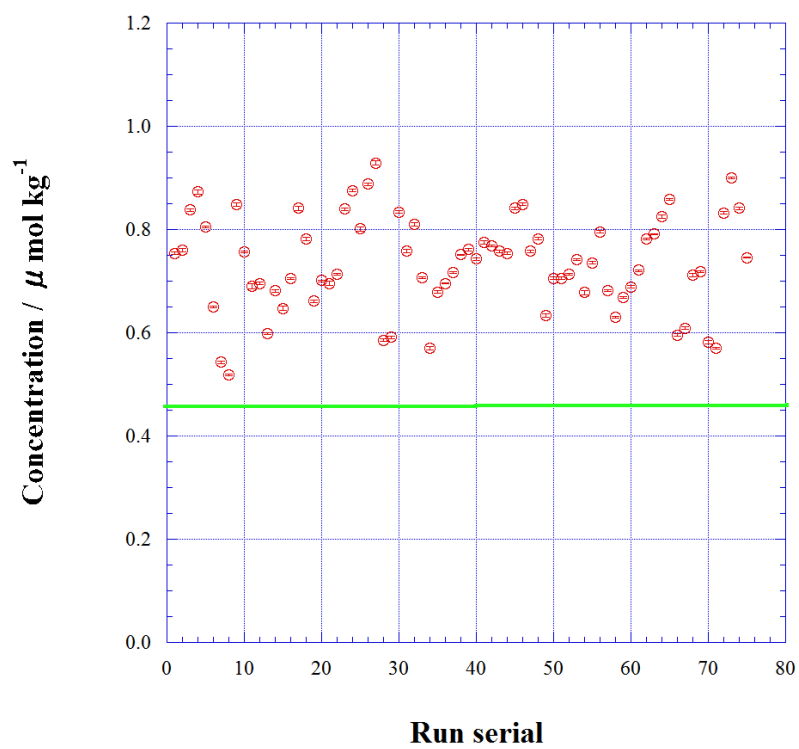Figure 4.7-15 Same as Figure 4.7-12, but for phosphate.

Figure 4.7-16 Time series of CRM-CF of ammonia in MR19-04. Green line is reference value for ammonia concentration of CRM-CF.

(8.3) Carryover
The carryover results from the finite and more or less incomplete flushing of the flow system between samples. Thus, an error is present in any given absorbance reading. The carryover signal can be approximated as linearly dependent upon the difference between the absorbance of a given sample and that of the preceding sample for a linear system. The carryover coefficient, k, is obtained for each channel by measuring the difference between the absorbances of the second and first full-scale standards following a near-zero standard or sample, all having the same, natural seawater matrix composition. It can equally well be calculated from the difference between the first two near-zero standards following a full-scale standard or sample. Measurement of the carryover is done in triplicate at the beginning of a cruise in order to obtain a statistically significant number. It must be checked carefully every time any change in the plumbing of a channel is done, including a simple pump tube or coil replacement. Carryover corrections for well-designed and maintained channels are usually less than 0.3%.

We summarize the magnitudes of carryover throughout the cruise. Although we observed that carryover increased in leg 3 probably due to overhaul of the analyzer, these are still small enough within acceptable levels of 0.3 % except ammonia as shown in Table 4.7-7 and Figure 4.7-17 to 4.7-21.

Table 4.7-7 Summary of carryover throughout MR19-04.

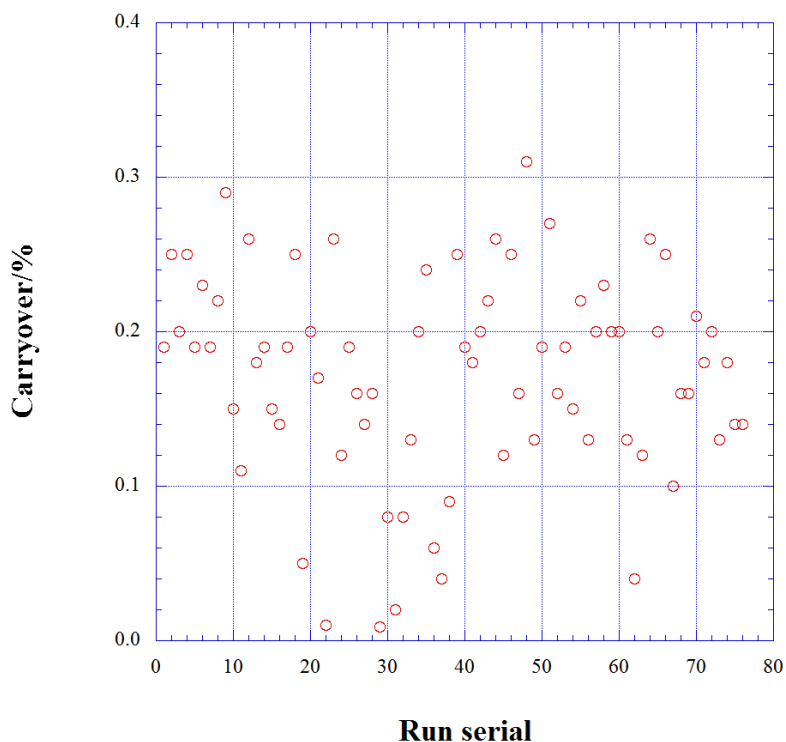|	Nitrate %	Nitrite %	Silicate %	Phosphate %	Ammonia %
Median	0.19	0.08	0.21	0.13	0.69
Mean	0.17	0.11	0.21	0.12	0.81
Maximum	0.31	0.53	0.31	0.30	2.30
Minimum	0.01	0.00	0.08	0.00	0.14
N	76	76	76	76	76

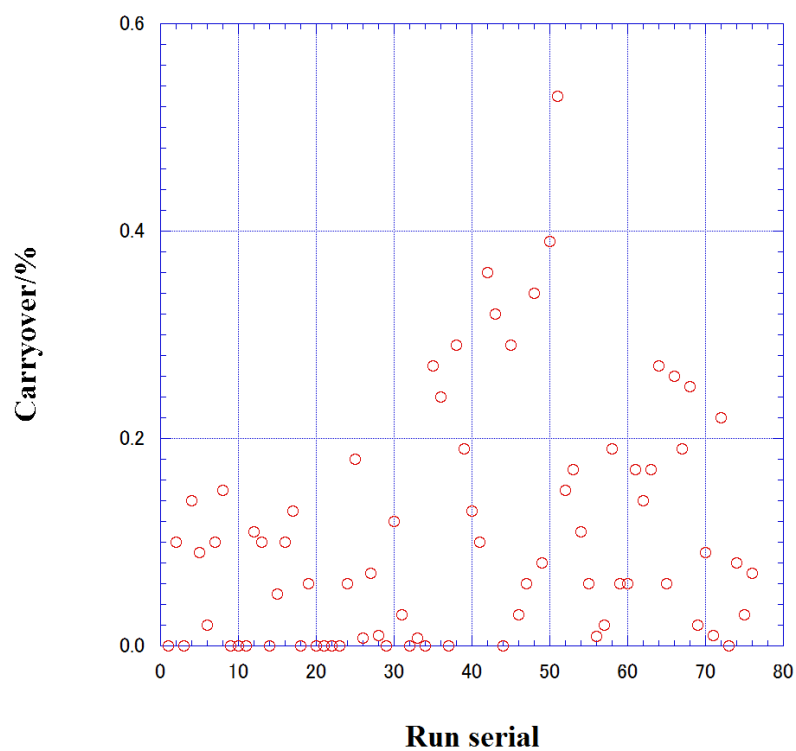Figure 4.7-17 Time series of carry over of nitrate in MR19-04.

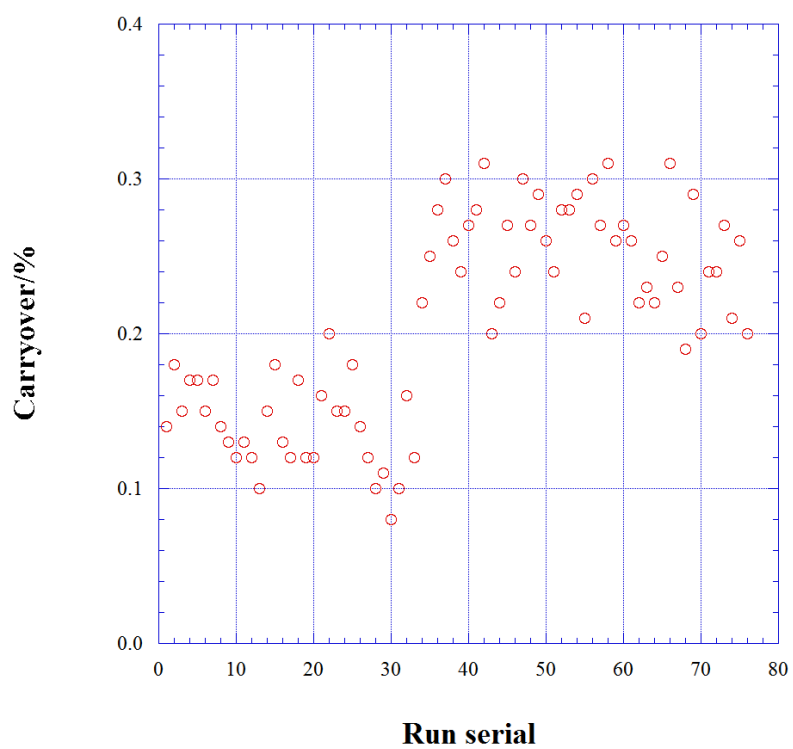Figure 4.7-18 Same as 4.7_17 but for nitrite.
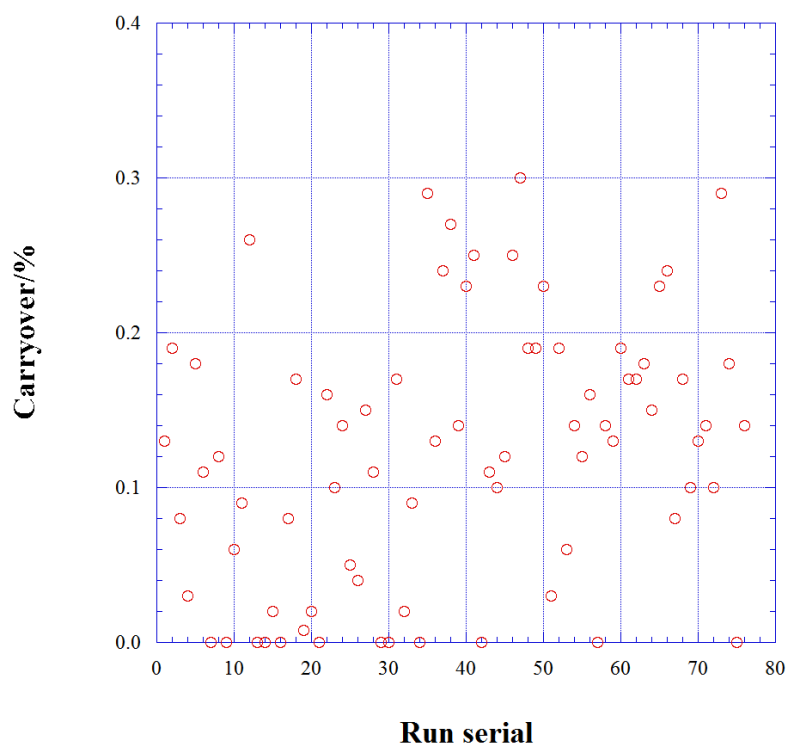

Figure 4.7-19 Same as 4.7_17 but for silicate

Figure 4.7-20 Same as 4.7_17 but for phosphate.
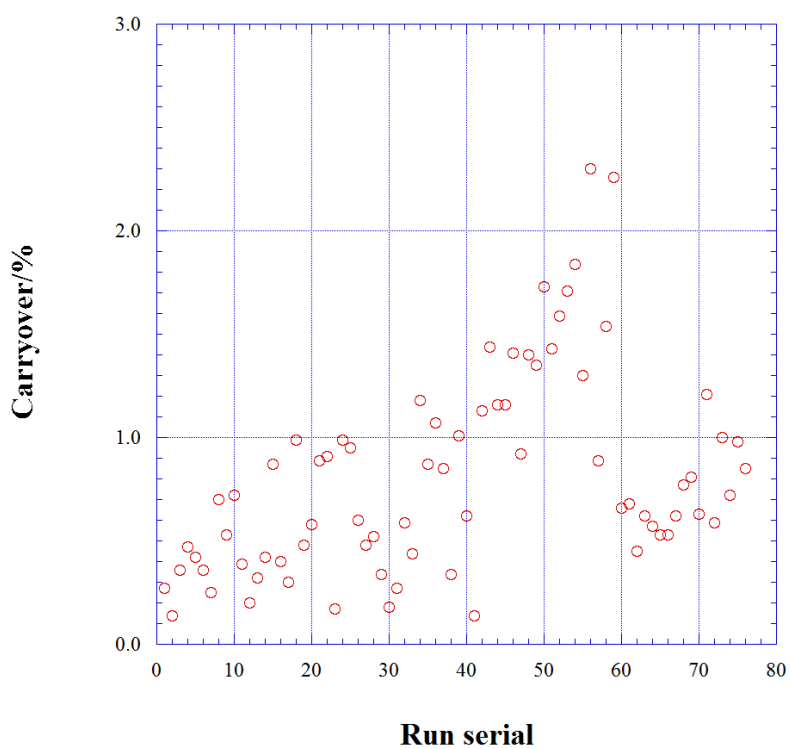
Figure 4.7-21 Same as 4.7_17 but for ammonia.

(8.4) Estimation of uncertainty of nitrate, silicate, phosphate, nitrite and ammonia concentrations

Empirical equations, eq. (1), (2) and (3) to estimate the uncertainty of measurement of nitrate, silicate and phosphate are used based on 76 measurements of 52 sets of CRMs (Table 4.7-2) to obtain calibration curve during this cruise. These empirical equations are as follows, respectively.

Nitrate Concentration C_{NO3} in μmol kg^{-1}:
Uncertainty of measurement of nitrate (%) =
$0.10303 + 7.0029 * (1 / C_{NO3}) - 0.1113 * (1 / C_{NO3}) * (1 / C_{NO3})$ --- (1)
where C_{NO3} is nitrate concentration of sample.

Silicate Concentration C_{SiO2} in μmol kg^{-1}:
Uncertainty of measurement of silicate (%) =
$0.14938 + 6.7786 * (1 / C_{SiO2}) - 0.12377 * (1 / C_{SiO2}) * (1 / C_{SiO2})$ --- (2)
where C_{SiO2} is silicate concentration of sample.

Phosphate Concentration C_{PO4} in μmol kg^{-1}:
Uncertainty of measurement of phosphate (%) =
$0.17278 + 0.28937 * (1 / C_{PO4})$ --- (3)
where C_{PO4} is phosphate concentration of sample.

Empirical equations, eq. (4) and (5) to estimate the uncertainty of measurement of nitrite and ammonia are used based on duplicate measurements of the samples.

Nitrite Concentration C_{NO2} in μmol kg^{-1}:
Uncertainty of measurement of nitrite (%) =
$- 0.027319 + 0.32334 * (1 / C_{NO2}) - 0.00019896 * (1 / C_{NO2}) * (1 / C_{NO2})$ --- (4)
where C_{NO2} is nitrite concentration of sample.

Ammonia Concentration C_{NH4} in μmol kg^{-1}:
Uncertainty of measurement of ammonia (%) =
$11.768 + 0.79428 * (1 / C_{NH4})$ --- (5)
where C_{NH4} is ammonia concentration of sample.

y = m1 + m2 * (1/m0) + m3 * (1/m0) * (1/m0)		
	Value	Error
m1	0.10303	0.01152
m2	7.0029	0.29917
m3	-0.1113	0.0059791
chi-square	0.00029428	NA
R	1	NA

Figure 4.7-22 Estimation of uncertainty for nitrate.

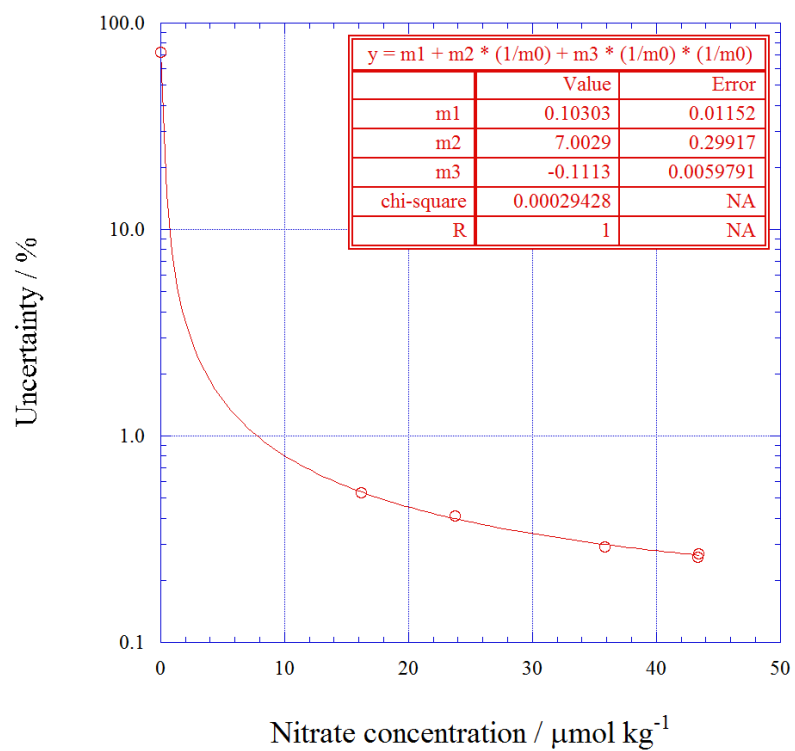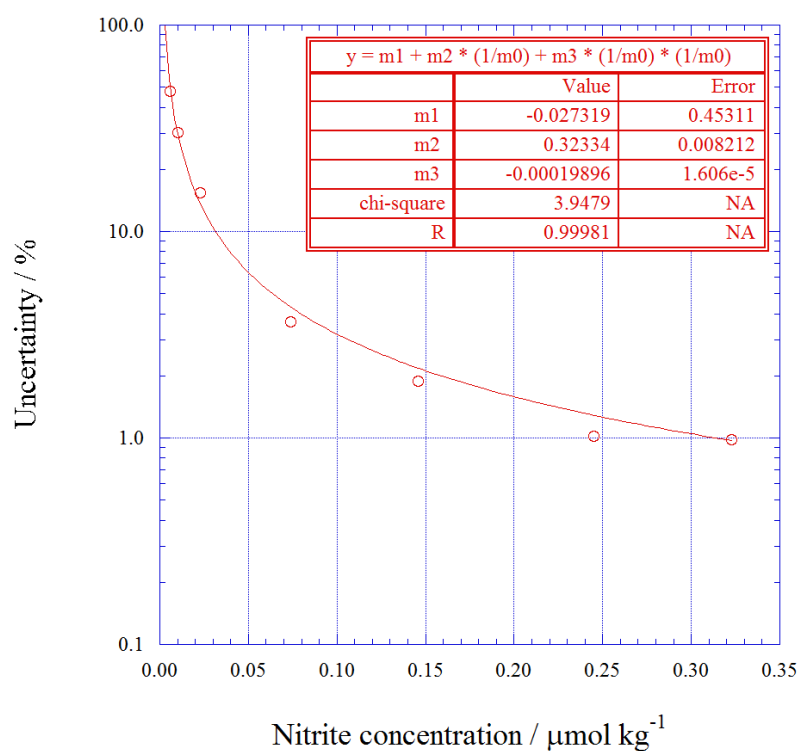| y = m1 + m2 * (1/m0) + m3 * (1/m0) * (1/m0)		
	Value	Error
m1	-0.027319	0.45311
m2	0.32334	0.008212
m3	-0.00019896	1.606e-5
chi-square	3.9479	NA
R	0.99981	NA

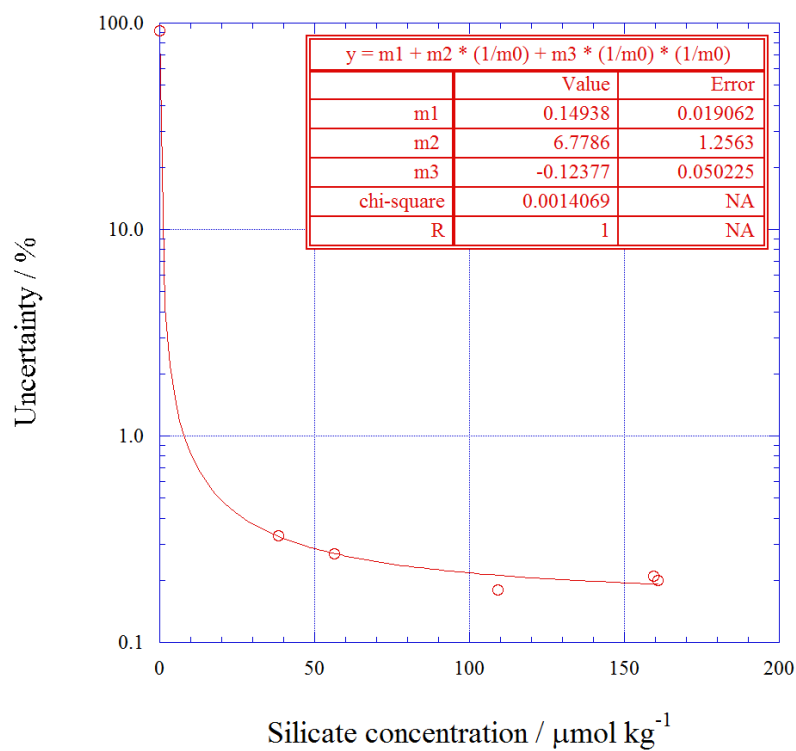Figure 4.7-23 Estimation of uncertainty for nitrite.

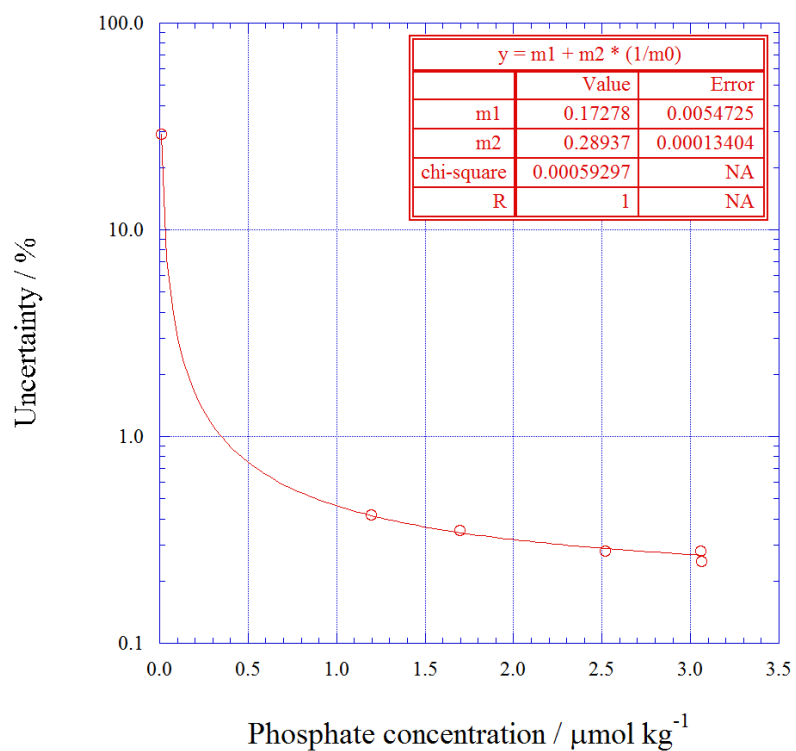Figure 4.7-24 Estimation of uncertainty for silicate.

Figure 4.7-25 Estimation of uncertainty for phosphate.
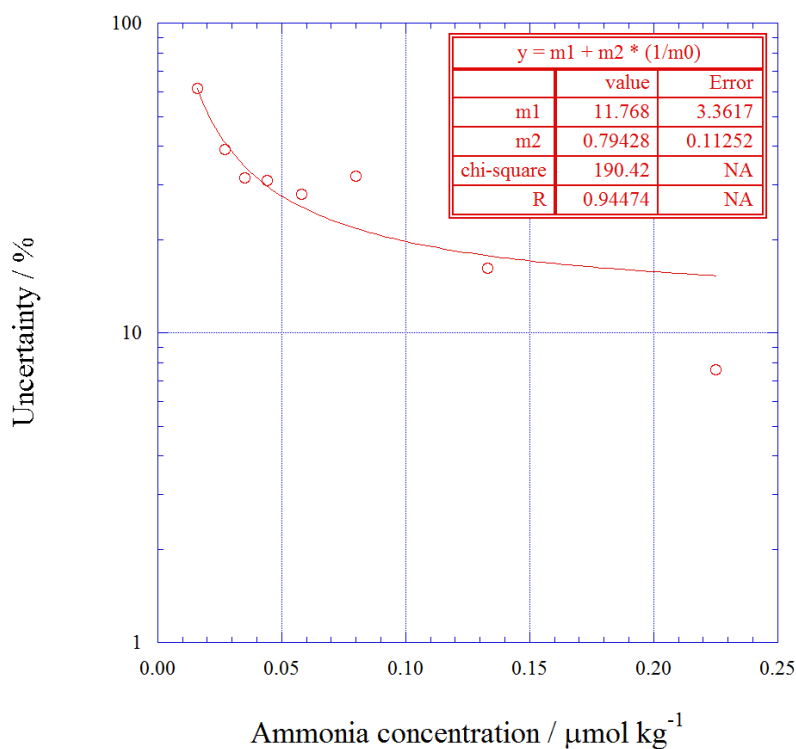
Figure 4.7-26 Estimation of uncertainty for ammonia

(9) Problems and our actions/solutions

In this section we describe what we observed and what we did to react to solve these problems.

During this cruise, we see a few problems especially in nitrate measurements as shown below.

1, Serious nitrate contamination from the environment to the seawater samples

2. Malfunction of one of the analyzers of nutrients named #1 and nitrate concentration measured by unit #1 showed larger variability which exceeds normal analytical precision about 0.2 %.

3. We needed to replace the cadmium reduction column for nitrate measurements rather than usual operation.

We faced serious nitrate contamination from the environment to the seawater samples. We observed a larger difference of nitrate concentrations of two duplicate samples collected from the same sampling bottle for several bottles of 36 bottles throughout the cruise in general. The difference of nitrate contamination of the two samples was up to 1.6 μmol kg^{-1} during the leg 2 (stations 2-69), 2.2 μmol kg^{-1} during the first half of the leg 3 (stations 70-101), and 1.4 μmol kg^{-1} during the second half of the leg 3 (stations 103-153). As shown in Figure 4.7_22, the nitrate vs. phosphate concentration ratio became high in some samples collected at stations between 30 and 50 approximately compared with the range of natural values between 13.6 and 14.7 approximately during leg 2. We also see high ratio anomalies in some samples at stations 90-100 and 110-130 approximately during leg 3.

The magnitude of the difference between duplicate samples increased in the first half of the leg 3 and frequency we see a larger difference of nitrate concentrations between duplicate samples had also increased (Figure 4.7-22). The nitrate vs. phosphate concentration ratio in the "large-difference" sample increased and showed a linear relationship (the broken line from 14.5 of Nitrate vs. phosphate ratio at nitrate concentration difference is zero to around 15.4 of nitrate vs. phosphate ratio at nitrate concentration difference is 1.5 μmol kg^{-1}) in Figure 4.7_23a, b and c. This relationship indicated that nitrate contamination occurred one of two duplicate samples without phosphate contamination. We also observed that nitrate vs. phosphate ratio did not change while nitrate concentration difference is

1.5 μmol kg-[1] eg. indicated as a horizontal line in Figure 4.7_23a. We guess that the malfunction of sampler we stated later may cause nitrate concentration change due to a change of the amount of intake of seawater sample compared with the intake of reagents. Furthermore, we also observed an increase of nitrate vs. phosphate ratio in spite of less difference of nitrate concentration as shown ellipses in Figure 4.7_23a for leg 1 and Figure 4.7_23c for the second half of leg 3. In leg 1 case, we guess that nitrate contamination may occur for both samples without phosphate contamination while in the second half of leg 3 case we guess that higher nitrate vs. phosphate ration were natural phenomena due to intrusion of Atlantic Ocean origin seawater at that region.

We did not observe nitrate contamination on samples taken from CRMs and C-5 standards solution, too. This may indicate that nitrate contamination occurred during a sample drawing from the environment and/or nitrate contamination inside the surface of the sampling bottles.
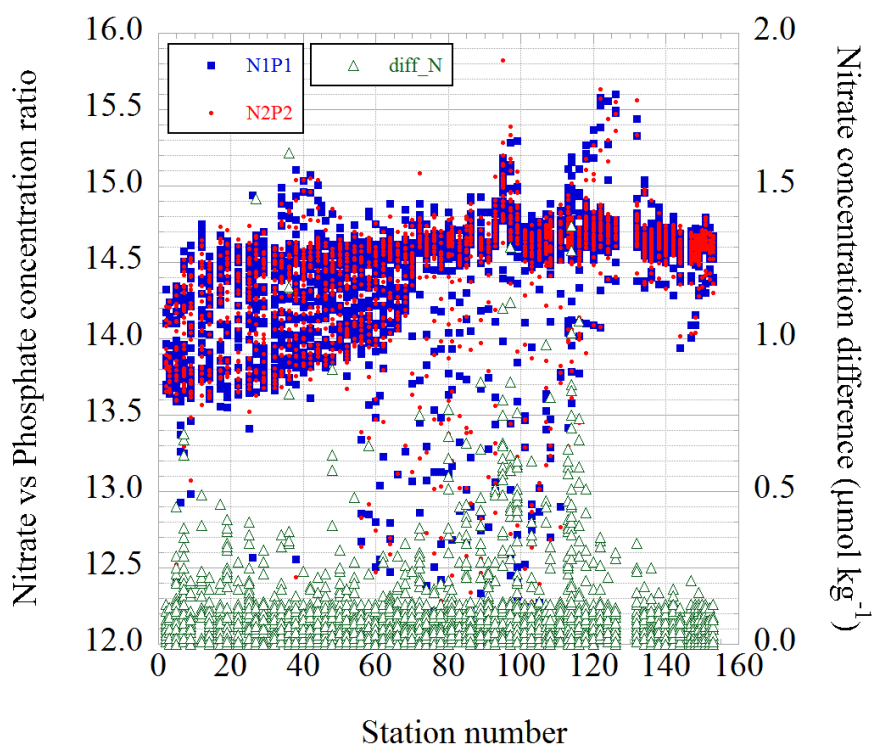
Figure 4.7-22 Nitrate/phosphate concentration ratio and difference of nitrate concentration between duplicate two samples.

Leg2 stn002-069
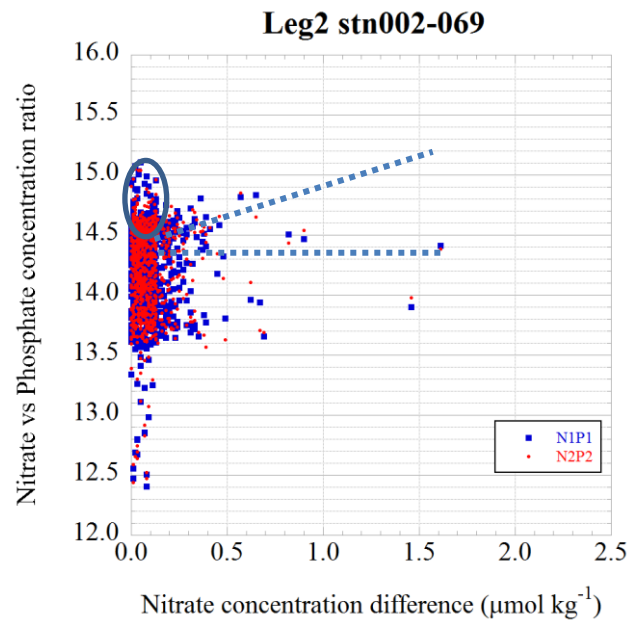
Figure 4.7_23a Relationship of nitrate concentration differences to nitrate vs. phosphate concentration ratio during the leg 2. Blue and red dots indicate the ratio in the first and second samples of duplicate pair, respectively.

Leg3 stn070-101
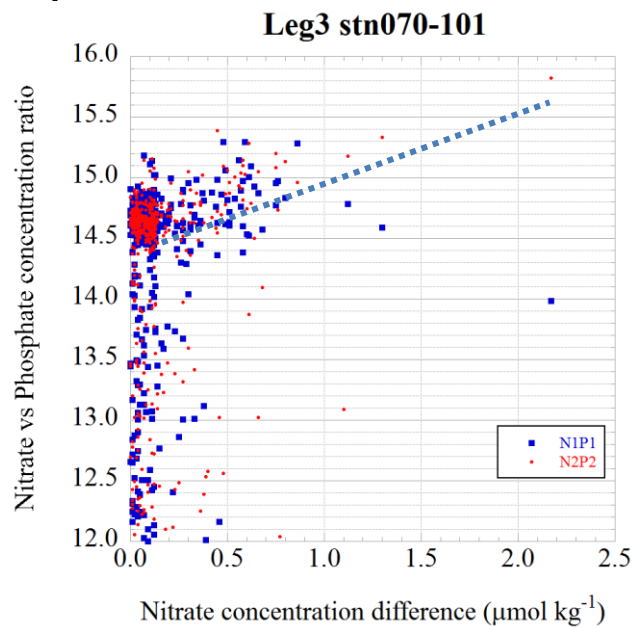
Figure 4.7_23b Same as 4.7_23a but for the data at stations 70-101 in the leg 3.
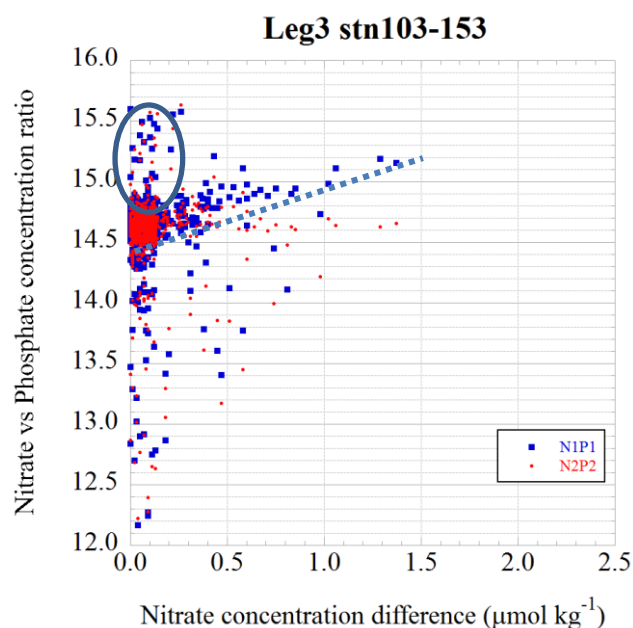
Figure 4.7_23c Same as 4.7_23a but for the data at stations 103-153 in the leg 3.

We started to seek cause(es) of this nitrate contamination. We had been using latex gloves during the water sampling because of its good performance of handling. First, we checked the possibility of nitrate contamination from latex gloves on board. We also tested other gloves made from different materials as shown in Table 4.7-8. As already stated in Becker et al. (2019), the soaking tests showed that latex gloves might be a source of nitrate especially at the beginning of the use of new gloves taken from a package. Therefore, we stopped to use latex gloves and used polyvinyl chloride gloves after station 101 on 8 January 2020. The situation, however, did not change and the nitrate contamination continued, which suggests other nitrate sources in the ship. We also checked the possibility of contamination from the atmosphere by exposing tests with LNSW at the CTD room, chemical laboratory, and a few other places in the ship and by soaking small black particles collected on the deck of in the ship. The exposing tests showed that ambient air might not be a source of nitrate contamination while the small black particles could be one of the potential sources of nitrate source (Table 4.7-9). Then we cleaned up the CTD room by freshwater at station 124. As we can see in Figure 4.7-22, the difference of two replicate samples became small gradually after that and we found a normal situation just before the end of this cruise. We believe the small particle deposited on the deck may be one of the sources of nitrate contamination.

As stated previously, we also found a linear relationship between the N/P ratio and the difference in the replicate samples in the second half of the leg 3 (Figures 4.7_23c), which is similar to that observed in the first half of the leg 3 (Figures 4.7_23b). On the other hand, we also observed the higher N/P ratio without the large difference at stations 120-130 approximately in the second half of the leg 3 (Figure 4.7-22), which was not observed in the first half of the leg 3 but in the leg 2 (Figures 4.7_23a). The high N/P ration without the large difference implies that the nitrate contamination occurred in both two replicate samples or did not occurre. The latter means that the high N/P ratios are within the natural variation. We concluded that those at station 120-130 approximately in the second half of the leg 3 are probably due to the natural variability because of Atlantic Ocean water intrusion.

Therefore, we concluded that serious nitrate contamination from the environment to the seawater samples occurred during the sample drawing although we could find the exact cause of these contaminations.

Malfunction of one of the analyzers of nutrients named #1 and nitrate concentration measured by

unit #1 resulted in larger variability, which exceeds normal analytical precision about 0.2 % for the samples collected at stations 2, 7, 12, 19, 25 and 27. We found damage on a timing disk of autosampler of #1 machine and we suspect that intake of the sample seawater during the measurement was unstable. This resulted in the large nitrate concentration difference without the high N/P ratio in the early stage of the leg 2 (Figure 4.7_23a).

.

Table 4.7-8 Results of tests for contamination from gloves.

Gloves	Methods	Measurement date	Seq.	Nitrate (µmol L^{-1})	Nitrite (µmol L^{-1})	Silicate (µmol L^{-1})	Phosphate (µmol L^{-1})	Anmonia (µmol L^{-1})	Sample name
Latex A1-1	(1)	22-Dec-19	1	2.95	0.00	0.99	0.059	0.19	sample1_1_1
			2	0.38	0.01	0.98	0.051	0.09	sample2_1_1
			3	0.11	0.01	1.02	0.051	0.06	sample3_1_1
Latex A1-2		07-Jan-20	1	4.78	0.00	0.99	0.037	0.58	kuaran_1_1
			2	0.62	0.00	1.02	0.043	0.08	kuaran_1_2
			3	0.29	0.00	0.99	0.042	0.05	kuaran_1_3
Latex A2		07-Jan-20	1	1.95	0.00	0.98	0.045	0.12	kuarao_1_1
			2	0.20	0.00	0.99	0.041	0.07	kuarao_1_2
			3	0.16	0.00	1.00	0.041	0.05	kuarao_1_3
Latex B		07-Jan-20	1	1.65	0.00	0.97	0.039	0.03	positive_1_1
			2	0.43	0.00	0.98	0.040	0.03	positive_1_2
			3	0.20	0.00	0.98	0.039	0.04	positive_1_3
Latex C		07-Jan-20	1	0.34	0.00	1.01	0.037	0.03	diamond_1_1
			2	0.17	0.00	0.98	0.037	0.03	diamond_1_2
			3	0.12	0.00	1.00	0.038	0.01	diamond_1_3
Latex D-1		08-Jan-20	1	0.29	0.00	1.12	0.039	0.00	labtex_2_1
			2	0.27	0.01	1.12	0.039	0.00	labtex_2_2
			3	0.18	0.01	1.05	0.039	0.00	labtex_2_3
Latex D-2		07-Jan-20	1	0.11	0.00	1.05	0.041	0.06	labtex_1_1
			2	0.07	0.00	0.99	0.039	0.06	labtex_1_2
			3	0.07	0.00	1.00	0.041	0.07	labtex_1_3
Latex D-3		08-Jan-20	1	0.05	0.00	1.06	0.037	0.00	labtex_3_1
			2	0.08	0.01	1.09	0.036	0.00	labtex_3_2
			3	0.04	0.01	1.05	0.040	0.00	labtex_3_3
Latex D-4	(2)	09-Jan-20	replicated	4.42	0.02	1.17	0.304	0.62	labtex_4_1
				4.90	0.03	1.17	0.263	0.40	labtex_4_2
				4.17	0.02	1.11	0.256	0.48	labtex_4_3
Nitrile rubber	(1)	07-Jan-20	1	1.20	0.00	1.01	0.040	0.07	safe_1_1
			2	0.09	0.00	0.98	0.038	0.03	safe_1_2
			3	0.07	0.00	0.98	0.037	0.04	safe_1_3
Polyethylene		07-Jan-20	1	0.06	0.00	0.97	0.039	0.03	saniment_1_1
			2	0.06	0.00	0.96	0.039	0.05	saniment_1_2
			3	0.05	0.00	0.97	0.036	0.03	saniment_1_3
Polyvinyl chloride-1		07-Jan-20	1	0.02	0.00	0.99	0.039	0.02	clean_1_1
			2	0.04	0.00	1.01	0.039	0.01	clean_1_2
			3	0.03	0.00	1.02	0.043	0.04	clean_1_3
Polyvinyl chloride-2		08-Jan-20	1	0.00	0.01	1.09	0.048	0.02	clean_2_1
			2	0.00	0.00	1.03	0.041	0.00	clean_2_2
			3	0.00	0.00	1.03	0.051	0.00	clean_2_3
Polyvinyl chloride-3		10-Jan-20	1	0.00	0.00	0.96	0.043	0.05	clean_4_1
			2	0.01	0.01	0.95	0.040	0.03	clean_4_2
			3	0.00	0.00	1.01	0.041	0.02	clean_4_3
Polyvinyl chloride-4		10-Jan-20	1	0.00	0.00	0.98	0.041	0.02	clean_5_1
			2	0.00	0.00	0.98	0.041	0.01	clean_5_2
			3	0.00	0.00	0.98	0.038	0.01	clean_5_3
Polyvinyl chloride-5	(3)	09-Jan-20	replicated	0.03	0.01	1.02	0.101	0.06	clean_3_1
				0.03	0.01	1.01	0.090	0.03	clean_3_2
				0.05	0.01	0.99	0.107	0.05	clean_3_3
Blank	(4)	11-Jan-20	replicated	0.01	0.01	0.98	0.042	0.06	cap_1_1
				0.00	0.00	0.95	0.031	0.05	cap_1_2
				0.01	0.00	1.01	0.036	0.03	cap_1_3

(1) A fingertip (1 cm) of the glove was dipped into low nutrient seawater (LNSW) in the three sample tubez (10 ml) sequentially for 5 seconds each.

(2) A fingertip (2 cm) of the glove was dipped into LNSW in the sample tube (10 ml) for 1 hour.

(3) A fingertip (2 cm) of the glove was dipped into LNSW in the sample tube (10 ml) for 10 hours.

(4) LNSW in a sample tube (10 ml) with three time rinses.

Table 4.7-9 Results of tests for contamination.

Experiments		Measurement date	Nitrate (µmol L⁻¹)	Nitrite (µmol L⁻¹)	Silicate (µmol L⁻¹)	Phosphate (µmol L⁻¹)	Anmonia (µmol L⁻¹)	Sample name
Exposure of low nutreint seawater (LNSW) in sample tube (10 ml) without lid for three hours.	CTD room	13-Jan-20	0.02	0.04	1.02	0.044	0.09	ctdroom_1_1
			0.00	0.05	1.00	0.042	0.08	ctdroom_1_2
			0.00	0.06	0.97	0.042	0.10	ctdroom_1_3
	No.1 buoy mooring room	13-Jan-20	0.00	0.03	0.94	0.038	0.05	no1mooring_1_1
			0.00	0.03	0.99	0.040	0.07	no1mooring_1_2
			0.00	0.03	0.96	0.039	0.08	no1mooring_1_3
	Chemical laboratory	13-Jan-20	0.00	0.08	0.97	0.037	0.38	chemicallab_1_1
			0.00	0.11	0.99	0.040	0.47	chemicallab_1_2
			0.00	0.10	1.02	0.038	0.45	chemicallab_1_3
	Within chamber for autosampler	13-Jan-20	0.00	0.05	1.01	0.040	0.29	autosampler_1_1
			0.00	0.05	0.98	0.040	0.31	autosampler_1_2
			0.00	0.06	1.01	0.042	0.33	autosampler_1_3
Exposure of LNSW in sample tube (10 ml) without lid for 1.5 hours.	Position A in CTD room	15-Jan-20	0.05	0.00	1.90	0.037	0.04	119_A_1
			0.04	0.00	1.81	0.038	0.02	119_A_2
			0.03	0.00	1.79	0.042	0.01	119_A_3
	Position B in CTD room	15-Jan-20	0.00	0.00	1.59	0.043	0.01	119_B_1
			0.00	0.00	1.61	0.032	0.01	119_B_2
			0.00	0.00	1.62	0.032	0.00	119_B_3
	Position C in CTD room	15-Jan-20	0.00	0.01	1.68	0.034	0.03	119_C_1
			0.01	0.00	1.62	0.034	0.00	119_C_2
			0.01	0.00	1.61	0.038	0.00	119_C_3
	Position D in CTD room	15-Jan-20	0.00	0.01	1.61	0.033	0.00	119_D_1
			0.00	0.01	1.57	0.040	0.00	119_D_2
			0.00	0.01	1.69	0.044	0.01	119_D_3
Dipping of sampling tube tip into LNSW in sample tube (10 ml) for 5 seconds.		10-Jan-20	0.01	0.00	0.98	0.040	0.00	tube_1_1
			0.01	0.00	0.97	0.041	0.00	tube_1_2
			0.03	0.00	1.02	0.045	0.00	tube_1_3
Pure water that flowed over the surface of paper towel	White paper towel	11-Jan-20	0.04	0.00	0.00	0.000	0.13	kim_1_1
			0.11	0.01	0.05	0.014	0.25	kim_1_2
	Brown paper towel	11-Jan-20	0.04	0.01	0.00	0.513	0.13	kim_2_1
			0.08	0.01	0.00	0.493	0.16	kim_2_2
Fresh water for general use		11-Jan-20	0.16	0.00	0.00	1.358	0.04	water_1_1
			0.19	0.00	0.01	1.439	0.04	water_1_2
Dipping of small black particulates collected in No.1 bouy mooring room into LNSW in sample tube (10 ml)		15-Jan-20	1.63	0.00	1.80	0.115	0.28	hachinohe_1_1
			0.97	0.03	1.83	0.231	0.26	hachinohe_1_2

During this cruise, we changed the sample drawing order as shown in Table 4.7-10 due to the trail of nitrate contamination check. It is, however, the sample drawing order was not a cause of nitrate contamination.

Table 4.7-10 Sampling order.

Station	Sampling order
002-099, 103	Oxygen, CFCs, Salinity, gas, Nutrients, NO_3-Si, others
101	Oxygen, CFCs, Nutrients, Salinity, gas, others
105-153	Oxygen, CFCs, Salinity, Nutrients, NO_3-Si, gas, others

We also need to note that replacement of cadmium reduction columns for nitrate measurements had forced more frequently rather than usual operation during the Stn 118, 122, 124, 126, 132 those were located around 50-56 deg. S (Table 4.7-11).

Table 4.7-11 The number of cadmium coil in NO_3+NO_2 flow and reactivation frequency of cadmium coil.

Station	Cast	machine	cadmium coil	new cadmium coil or reactivation
2	1	unit #1	double	
3	1			
5	1	unit #2	double	
6	1	unit #1	double	
7	1			
9	1	unit #2	double	
12	1	unit #1	double	○
14	1	unit #2	double	○
17	1	unit #2	double	
19	1	unit #1	double	○
22	1	unit #2	double	
25	1	unit #1	double	
26	1	unit #1	double	
27	1			
29	1	unit #2	double	
32	1	unit #2	double	
34	1	unit #2	double	
36	1	unit #3	double	
38	1	unit #2	double	
40	1	unit #3	double	
42	1	unit #2	double	○
44	1	unit #2	double	
45	1	unit #3	double	
46	1			
48	1	unit #3	double	
50	1	unit #2	double	
52	1	unit #3	double	
54	1	unit #3	double	
56	1	unit #2	double	○
58	1	unit #2	double	
60	1	unit #2	double	
61	1	unit #2	double	
69	1			
62	1	unit #2	double	
64	1	unit #2	double	○
66	1	unit #2	double	
68	1	unit #2	double	

Station	Cast	machine	cadmium coil	new cadmium coil or reactivation
70	1	unit #3	double	○
72	1	unit #2	double	○
74	1	unit #3	double	
76	1	unit #2	single	
78	1	unit #2	single	
80	1	unit #3	double	○
81	1	unit #2	single	
83	1	unit #2	single	○
85	2	unit #2	single	
86	1	unit #3	double	
89	1	unit #3	double	
91	1	unit #2	single	
93	1	unit #3	double	
95	1	unit #2	single	○
97	1	unit #3	double	
99	1	unit #2	single	
101	1	unit #2	single	
103	1	unit #3	double	
105	1	unit #2	single	
107	1	unit #3	double	○
108	1	unit #2	single	○
111	1	unit #3	double	
113	1	unit #2	single	
114	1	unit #3	double	
116	1	unit #2	single	
118	2	unit #2	single	
120	1	unit #2	single	○
122	1	unit #2	single	
124	1	unit #2	single	○
126	1	unit #2	single	○
132	1	unit #2	single	
134	1	unit #3	single	○
136	1	unit #2	single	○
138	1	unit #2	single	
140	1	unit #3	single	
142	1	unit #2	single	
144	1	unit #3	single	
147	1	unit #2	single	
148	1	unit #3	single	
149	1	unit #2	single	
150	1	unit #2	single	
151	1	unit #3	single	
152	1	unit #2	single	
153	1			

Table 4.7-12 Centrifuged samples in leg3.

Station	Cast	Bottle	Depth (dbar)	Trans (%)	Station	Cast	Bottle	Depth (dbar)	Trans (%)
78	1	36	10.0	98.4	97	1	36	9.5	88.1
78	1	35	50.1	98.4	97	1	2	35.9	94.9
78	1	2	88.3	97.9	97	1	35	49.8	97.2
78	1	34	101.7	97.1	97	1	34	100.9	98.6
78	1	33	151.1	99.3	97	1	33	151.2	99.0
81	1	36	10.7	98.6	99	1	36	10.7	93.8
81	1	35	50.0	98.3	99	1	2	37.5	95.4
81	1	2	95.2	98.2	99	1	35	50.0	96.3
81	1	34	101.7	98.2	99	1	34	98.1	99.3
81	1	33	150.5	98.8	99	1	33	150.7	99.3
83	1	36	9.3	97.6	101	1	36	10.5	91.8
83	1	35	50.0	98.2	101	1	2	25.2	92.2
83	1	2	76.7	98.3	101	1	35	50.8	98.2
83	1	34	101.2	98.8	101	1	34	100.6	99.0
83	1	33	150.7	99.2	101	1	33	150.5	99.2
80	1	36	10.8	98.8	103	1	36	10.1	92.2
80	1	35	49.9	98.6	103	1	35	50.1	93.7
80	1	2	70.7	98.7	103	1	34	100.3	97.0
80	1	34	100.2	99.1	103	1	33	151.3	98.6
80	1	33	150.0	99.4	105	1	36	10.3	91.7
85	2	36	10.8	96.0	105	1	2	30.8	91.7
85	2	35	50.4	94.2	105	1	35	50.2	95.9
85	2	2	77.5	97.5	105	1	34	99.8	99.4
85	2	34	100.9	98.7	105	1	33	149.5	99.6
85	2	33	149.7	99.3	107	1	36	10.4	94.2
86	1	36	9.7	96.9	107	1	2	42.8	93.9
86	1	35	50.5	97.6	107	1	35	50.4	96.0
86	1	2	85.5	97.2	107	1	34	100.9	99.5
86	1	34	100.7	98.6	107	1	33	150.9	99.6
86	1	33	150.3	99.2	108	1	36	11.0	94.5
93	1	36	10.2	92.5	108	1	2	45.0	95.1
93	1	2	24.8	89.6	108	1	35	50.6	95.8
93	1	35	50.5	95.0	108	1	34	100.8	98.8
93	1	34	100.1	98.8	108	1	33	149.9	99.6
93	1	33	150.6	99.1	111	1	36	11.2	93.6
89	1	36	10.0	93.9	111	1	35	50.8	94.1
89	1	35	49.9	93.6	111	1	2	58.2	94.2
89	1	2	73.4	95.4	111	1	34	100.2	99.0
89	1	34	100.4	98.9	111	1	33	150.3	99.5
89	1	33	151.0	99.1	113	1	36	9.8	94.9
91	1	36	10.6	95.1	113	1	2	30.1	95.0
91	1	35	50.3	94.0	113	1	35	49.6	95.2
91	1	2	65.4	96.0	113	1	34	100.5	98.7
91	1	34	100.7	99.0	113	1	33	150.6	99.4
91	1	33	150.6	99.2	114	1	36	11.6	95.3
95	1	36	10.3	86.9	114	1	2	34.7	95.3
95	1	2	23.6	91.6	114	1	35	49.2	95.4
95	1	35	50.6	98.1	114	1	34	101.0	98.5
95	1	34	100.4	99.5	114	1	33	151.8	99.4
95	1	33	152.3	99.6					

Table 4.7-12 Centrifuged samples in leg3 (continued).

Station	Cast	Bottle	Depth (dbar)	Trans (%)	Station	Cast	Bottle	Depth (dbar)	Trans (%)
116	1	36	11.3	95.2	140	1	36	9.9	97.2
116	1	2	25.6	95.2	140	1	35	49.2	97.2
116	1	35	51.1	95.4	140	1	2	55.5	97.7
116	1	34	100.6	98.5	140	1	34	99.9	99.4
116	1	33	152.4	99.5	140	1	33	150.0	99.7
118	2	36	11.1	95.7	142	1	36	10.8	97.8
118	2	35	50.2	95.8	142	1	2	40.0	97.7
118	2	2	84.8	95.1	142	1	35	50.6	97.4
118	2	34	99.9	97.0	142	1	34	100.7	99.3
118	2	33	150.5	99.4	142	1	33	150.3	99.7
120	1	36	9.3	95.4	144	1	36	10.7	98.0
120	1	35	50.2	95.3	144	1	35	50.2	97.2
120	1	2	71.8	95.4	144	1	2	60.8	98.2
120	1	34	100.2	98.2	144	1	34	100.6	99.3
120	1	33	150.2	99.2	144	1	33	150.4	99.6
122	1	36	10.2	95.2	147	1	36	10.1	98.7
122	1	35	50.8	95.1	147	1	35	50.1	98.5
122	1	2	62.3	95.1	147	1	2	58.1	98.4
122	1	34	100.5	97.9	147	1	34	100.6	99.2
122	1	33	150.8	99.1	147	1	33	150.8	99.6
124	1	36	11.2	95.8	148	1	36	10.3	98.3
124	1	35	51.1	95.5	148	1	35	50.4	98.0
124	1	2	69.5	95.4	148	1	2	56.6	98.7
124	1	34	101.0	97.8	148	1	33	150.3	99.6
124	1	33	151.0	99.4	148	1	32	199.5	99.7
126	1	35	10.3	95.5	149	1	36	10.7	98.8
126	1	33	50.2	95.2	149	1	35	51.2	98.6
126	1	32	74.5	95.0	149	1	2	84.9	99.0
126	1	31	99.0	97.2	149	1	34	100.4	99.3
126	1	30	147.5	99.3	149	1	33	150.3	99.6
132	1	36	9.9	95.7	150	1	36	10.4	98.4
132	1	35	50.4	95.6	150	1	35	50.3	97.3
132	1	2	73.1	95.7	150	1	2	80.2	98.8
132	1	34	99.9	98.6	150	1	34	100.3	99.5
132	1	33	148.5	99.5	150	1	33	150.9	99.6
134	1	36	9.1	95.2	151	1	36	10.0	98.0
134	1	2	27.8	95.2	151	1	35	50.0	97.8
134	1	35	50.3	95.3	151	1	2	69.9	97.9
134	1	34	100.6	98.7	151	1	34	99.6	99.4
134	1	33	151.7	99.5	151	1	33	149.9	99.9
138	1	36	9.4	97.0	152	1	36	10.3	98.2
138	1	2	41.1	96.9	152	1	35	50.1	97.2
138	1	35	51.0	96.9	152	1	2	80.1	98.1
138	1	34	98.9	99.3	152	1	34	100.4	99.1
138	1	33	151.8	99.6	152	1	33	150.3	99.9
136	1	36	9.4	95.7	153	1	36	9.7	97.2
136	1	35	51.2	95.9	153	1	35	50.4	97.7
136	1	2	61.4	96.0	153	1	2	87.4	98.0
136	1	34	101.4	99.2	153	1	34	100.4	99.1
136	1	33	151.8	99.6	153	1	33	150.1	99.9

(10) List of reagents
List of reagents is shown in Table 4.7-13.

Table 4.7-13 List of reagent in MR19-04.

IUPAC name	CAS Number	Formula	Compound Name	Manufacture	Grade
4-Aminobenzenesulfonamide	63-74-1	$C_6H_8N_2O_2S$	Sulfanilamide	Wako Pure Chemical Industries, Ltd.	JIS Special Grade
Antimony potassium tartrate trihydrate	28300-74-5	$K_2(SbC_4H_2O_6)_2 \cdot 3H_2O$	Bis[(+)-tartrato]diantimonate(III) Dipotassium Trihydrate	Wako Pure Chemical Industries, Ltd.	JIS Special Grade
Boric acid	10043-35-3	H_3BO_3	Boric Acid	Wako Pure Chemical Industries, Ltd.	JIS Special Grade
Hydrogen chloride	7647-01-0	HCl	Hydrochloric Acid	Wako Pure Chemical Industries, Ltd.	JIS Special Grade
Imidazole	288-32-4	$C_3H_4N_2$	Imidazole	Wako Pure Chemical Industries, Ltd.	JIS Special Grade
L-Ascorbic acid	50-81-7	$C_6H_8O_6$	L-Ascorbic Acid	Wako Pure Chemical Industries, Ltd.	JIS Special Grade
N-(1-Naphthalenyl)-1,2-ethanediamine, dihydrochloride	1465-25-4	$C_{12}H_{16}Cl_2N_2$	N-1-Naphthylethylenediamine Dihydrochloride	Wako Pure Chemical Industries, Ltd.	for Nitrogen Oxides Analysis
Oxalic acid	144-62-7	$C_2H_2O_4$	Oxalic Acid	Wako Pure Chemical Industries, Ltd.	Wako Special Grade
Phenol	108-95-2	C_6H_6O	Phenol	Wako Pure Chemical Industries, Ltd.	JIS Special Grade
Sodium citrate dihydrate	6132-04-3	$Na_3C_6H_5O_7 \cdot 2H_2O$	Trisodium Citrate Dihydrate	Wako Pure Chemical Industries, Ltd.	JIS Special Grade
Sodium dodecyl sulfate	151-21-3	$C_{12}H_{25}NaO_4S$	Sodium Dodecyl Sulfate	Wako Pure Chemical Industries, Ltd.	for Biochemistry
Sodium hydroxide	1310-73-2	NaOH	Sodium Hydroxide for Nitrogen Compounds Analysis	Wako Pure Chemical Industries, Ltd.	for Nitrogen Analysis
Sodium hypochlorite	7681-52-9	NaClO	Sodium Hypochlorite Solution	Kanto Chemical co., Inc.	Extra pure
Sodium molybdate dihydrate	10102-40-6	$Na_2MoO_4 \cdot 2H_2O$	Disodium Molybdate(VI) Dihydrate	Wako Pure Chemical Industries, Ltd.	JIS Special Grade
Sodium nitroferricyanide dihydrate	13755-38-9	$Na_2[Fe(CN)_5NO] \cdot 2H_2O$	Sodium Pentacyanonitrosylferrate(III) Dihydrate	Wako Pure Chemical Industries, Ltd.	JIS Special Grade
Sulfuric acid	7664-93-9	H_2SO_4	Sulfuric Acid	Wako Pure Chemical Industries, Ltd.	JIS Special Grade
tetrasodium;2-[2-[bis(carboxylatomethyl)amino]ethyl-(carboxylatomethyl)amino]acetate;tetrahydrate	13235-36-4	$C_{10}H_{12}N_2Na_4O_8 \cdot 4H_2O$	Ethylenediamine-N,N,N',N'-tetraacetic Acid Tetrasodium Salt Tetrahydrate (4NA)	Dojindo Molecular Technologies, Inc.	-
Synonyms: t-Octylphenoxypolyethoxyethanol 4-(1,1,3,3-Tetramethylbutyl)phenyl-polyethylene glycol Polyethylene glycol tert-octylphenyl ether	9002-93-1	$(C_2H_4O)_nC_{14}H_{22}O$	Triton™ X-100	Sigma-Aldrich Japan G.K.	-

(11) Data archives
These data obtained in this cruise will be submitted to the Data Management Group of JAMSTEC, and will be opened to the public via "Data Research System for Whole Cruise Information in JAMSTEC (DARWIN)" in JAMSTEC web site.
<http://www.godac.jamstec.go.jp/darwin/e>

(12) References

Susan Becker, Michio Aoyama E. Malcolm S. Woodward, Karel Bakker, Stephen Coverly, Claire Mahaffey, Toste Tanhua, (2019) The precise and accurate determination of dissolved inorganic nutrients in seawater, using Continuous Flow Analysis methods, n: The GO-SHIP Repeat Hydrography Manual: A Collection of Expert Reports and Guidelines. Available online at: http://www.go-ship.org/HydroMan.html. DOI: http://dx.doi.org/10.25607/OBP-555

Grasshoff, K. 1976. Automated chemical analysis (Chapter 13) in Methods of Seawater Analysis. With contribution by Almgreen T., Dawson R., Ehrhardt M., Fonselius S. H., Josefsson B., Koroleff F.,

Kremling K. Weinheim, New York: Verlag Chemie.

Grasshoff, K., Kremling K., Ehrhardt, M. et al. 1999. Methods of Seawater Analysis. Third, Completely Revised and Extended Edition. WILEY-VCH Verlag GmbH, D-69469 Weinheim (Federal Republic of Germany).

Hydes, D.J., Aoyama, M., Aminot, A., Bakker, K., Becker, S., Coverly, S., Daniel, A., Dickson, A.G., Grosso, O., Kerouel, R., Ooijen, J. van, Sato, K., Tanhua, T., Woodward, E.M.S., Zhang, J.Z., 2010. Determination of Dissolved Nutrients (N, P, Si) in Seawater with High Precision and Inter-Comparability Using Gas-Segmented Continuous Flow Analysers, In: GO-SHIP Repeat Hydrography Manual: A Collection of Expert Reports and Guidelines. IOCCP Report No. 14, ICPO Publication Series No 134.

Kimura, 2000. Determination of ammonia in seawater using a vaporization membrane permeability method. 7th auto analyzer Study Group, 39-41.

Murphy, J., and Riley, J.P. 1962. Analytica Chimica Acta 27, 31-36.

4.8 Chlorofluorocarbons and Sulfur hexafluoride

(1) Personnel
Masahito Shigemitsu, Ken'ichi Sasaki (JASMTEC), Masahiro Orui, Hiroshi Hoshino, Atsushi Ono and Katsunori Sagishima (MWJ)

(2) Introduction
Chlorofluorocarbons (CFCs) and sulfur hexafluoride (SF_6) are man-made stable gases. These atmospheric gases can slightly dissolve in the sea surface water by air-sea gas exchange and spread into the ocean interior. Thus, the dissolved gases could be used as chemical tracers for the ocean circulation/ventilation. In this cruise, we try to gain insights into the ventilation rates and pathways in the Indian Ocean. To this end, we measured the concentrations of three chemical species of CFCs, CFC-11 (CCl_3F), CFC-12 (CCl_2F_2), and CFC-113 ($C_2Cl_3F_3$), and SF_6 in the seawater on board.

(3) Instrument and method
Bottle sampling

Discrete water samples for each station were collected using 12 liter Niskin bottles mounted on a CTD system. Each sample was introduced to a glass bottle of 450 ml developed in JAMSTEC by connecting a spigot of Niskin bottle through Tygon tubing. Before water sampling, each glass bottle was filled with CFCs/SF_6-free N_2. Seawater of twice the bottle volume was overflowed for each sample. The seawater samples were stored in a thermostatic water bath kept at 7°C immediately after the water sampling, and the samples were measured as soon as possible (usually within 18 hours after sampling).

Air sampling

In order to confirm CFCs/SF_6 concentrations of the standard gases and the stabilities of the concentrations as well as to check the saturation levels in the sea surface waters, the mixing ratios in background air were periodically analyzed. Air samples were continuously led into a laboratory by an air pump. The end of 10 mm OD Dekaron tubing was put on a head of the compass deck and the other end was connected onto the air pump in the laboratory. The tubing was relayed by a T-type union which had a small stopcock. Air sample was collected from the flowing air into a 200 ml glass cylinder by attaching the cylinder to the cock.

CFCs/SF_6 measurements

The two SF_6/CFCs analyzing systems, which were based on purging and trapping gas chromatography, were used. Constant volume of water sample (approximately 200 ml) was introduced into a sample loop. The sample was first drawn into a stripping chamber and the dissolved SF_6 and CFCs were extracted by CFCs/SF_6-free N_2 gas purging for 8 minutes at 220 ml min^{-1}. The extracted gases were dried by passing them through a magnesium perchlorate desiccant tube, and concentrated in a main trap column cooled down to -80 °C. The main trap column was a 30-cm length of 1/8-in stainless steel tubing packed with 80/100 mesh Porapak Q of 5 cm and 100/120 mesh Carboxen 1000 of 5cm. Stripping efficiencies were confirmed by re-stripping of surface layer samples for every station and more than 99 % of dissolved SF_6 and CFCs were extracted on the first purge. The purging and trapping were followed by the isolation and heating to 180 °C of the main trap column. After 1 minute, the desorbed gases were transferred to a focus trap (same as the main trap, except for 1/16-in tubing) cooled down to -80 °C for 30 seconds. Then, the sample gases held in the focus trap were desorbed by the same manner as in the main trap, and were transferred into a pre-column 1 (PC 1, ~6 m of Silica Plot capillary column with i.d. of 0.53 mm and film thickness of 6 μm, held at 95 °C). The sample gases were roughly separated in the PC 1, and the SF_6 and CFCs were eluted into a pre-column 2 (PC 2, ~5 m of

Molsieve 5A Plot capillary column with i.d. of 0.53 mm and film thickness of 15 μm, held at 95 ℃). Then, the PC1 was connected to a cleaning line, and the remained gases with high boiling points were flushed by a counter flow of CFCs/SF_6-free N_2. SF_6 and CFCs were quickly eluted from the PC 2 onto a main-column 1 (MC 1, ~9 m of Pola Bond-Q capillary column with i.d. of 0.53 mm and film thickness of 6 μm which is connected to ~18 m of Silica Plot capillary column, held at 95 ℃) and N_2O was retained on the PC 2. The PC 2 was then connected to a back-flush carrier gas line and N_2O was sent onto a main-column 2 (MC 2, ~3 m of Molsieve 5A Plot connected to ~9 m of Pola Bond-Q capillary column, held at 95 ℃). SF_6 and CFCs were further separated on the MC 1 and detected by the one ECD. N_2O sent onto the MC 2 was detected by the other ECD. However, N_2O was not targeted in this cruise. The PC1, PC2, MC1 and MC2 were in a Shimadzu GC2014 gas chromatograph with the ECDs held at 300 ℃. Please note that the CFCs/SF_6-free N_2 used in the water sampling and the measurements of SF_6 and CFCs was filtered by a gas purifier column packed with Molecular Sieve 13X (MS-13X) before the gas was introduced to the system. The mass flow rates of CFCs/SF_6-free N_2 for the carrier and detector make-up gases were 10 ml min^{-1} and 27 ml min^{-1}, respectively.

(4) Performance of CFCs/SF_6 measurements

The analytical precisions were estimated from over 200 duplicate samples. The estimated preliminary precisions were ± 0.015 pmol/kg, ± 0.009 pmol/kg, ± 0.004 pmol/kg, and ± 0.014 fmol/kg for CFC-11, CFC-12, CFC-113, and SF6, respectively.

(5) Data archives

These data obtained in this cruise will be submitted to the Data Management Group of JAMSTEC, and will be open to the public via "Data Research System for Whole Cruise Information in JAMSTEC (DARWIN)" in the JAMSTEC web site.

4.9 Carbon properties

(1) Personnel

Akihiko Murata (JAMSTEC)
Nagisa Fujiki (MWJ)
Atsushi Ono (MWJ)
Masanori Enoki (MWJ)
Yuta Oda (MWJ)
Daiki Kawata (MWJ)

(2) Objectives

Concentrations of CO_2 in the atmosphere are now increasing at a rate of about 2.0 ppmv y^{-1} owing to human activities such as burning of fossil fuels, deforestation, and cement production. It is an urgent task to estimate as accurately as possible the absorption capacity of the oceans against the increased atmospheric CO_2, and to clarify the mechanism of the CO_2 absorption, because the magnitude of the anticipated global warming depends on the levels of CO_2 in the atmosphere, and because the ocean currently absorbs 1/3 of the 6 Gt of carbon emitted into the atmosphere each year by human activities.

The Indian Ocean is one of the regions where uncertainty of uptake of anthropogenic CO_2 is large, because opportunities of high-quality ship-based observations are limited. On the other hand, the Southern Ocean is known to be a region where ~40% of anthropogenic CO_2 absorbed by the ocean is undertaken. In this cruise (MR19-04 legs 2 and 3), therefore, we intended to quantify how much anthropogenic CO_2 was absorbed in the ocean interior of the Indian Ocean and the Southern Ocean. For the purpose, we measured CO_2-system properties such as dissolved inorganic carbon (C_T), and total alkalinity (A_T) in the oceans.

(3) Apparatus

i. C_T

Measurement of C_T was made with automated TCO_2 analyzer (Nippon ANS, Inc., Japan). The system comprises of a seawater dispensing system, a CO_2 extraction system and a coulometer (Model 3000, Nippon ANS, Inc., Japan). Specification of the system is as follows:

The seawater dispensing system has an auto-sampler (6 ports), which dispenses seawater from a 250 ml borosilicate glass bottle (DURAN® glass bottle, 250ml) into a pipette of about 15 ml volume by PC control. The pipette is kept at 20 °C by a water jacket, in which water from a water bath set at 20 °C is circulated. CO_2 dissolved in a seawater sample is extracted in a stripping chamber of the CO_2 extraction system by adding phosphoric acid (~ 10 % v/v) of about 2 ml. The stripping chamber is approx. 25 cm long and has a fine frit at the bottom. The acid is added to the stripping chamber from the bottom of the chamber by pressurizing an acid bottle for a given time to push out the right amount of acid. The pressurizing is made with nitrogen gas (99.9999 %). After the acid is transferred to the stripping chamber, a seawater sample kept in a pipette is introduced to the stripping chamber by the same method as in adding an acid. The seawater reacted with phosphoric acid is stripped of CO_2 by bubbling the nitrogen gas through a fine frit at the bottom of the stripping chamber. The CO_2 stripped in the chamber is carried by the nitrogen gas (flow rates is 140 ml min^{-1}) to the coulometer through a dehydrating module. The module consists of two electric dehumidifiers (kept at ~4 °C) and a chemical desiccant ($Mg(ClO_4)_2$).

The measurement sequence such as system blank (phosphoric acid blank), 1.5 % CO_2 gas (nitrogen-base) in a nitrogen base, sea water samples (6) is programmed to repeat. The measurement of 1.5 % CO_2 gas is made to monitor response of coulometer solutions purchased from UIC, Inc.

ii. A_T

Measurement of A_T was made based on spectrophotometry with a single acid addition procedure using a custom-made system (Nippon ANS, Inc., Japan). The system comprises of a water dispensing unit, an auto-syringe (Hamilton) for hydrochloric acid, a spectrophotometer (TM-UV/VIS C10082CAH, Hamamatsu Photonics, Japan), and a light source (Mikropack, Germany), which are automatically controlled by a PC. The water dispensing unit has a water-jacketed pipette (~40 mL at 25°C) and a titration cell, which is also controlled at 25°C.

A seawater of approx. 40 ml is transferred from a sample bottle (DURAN® glass bottle, 100 ml) into the pipette by pressurizing the sample bottle (nitrogen gas), and is introduced into the titration cell. The seawater is used to rinse the titration cell. Then, Milli-Q water is introduced into the titration cell, also for rinse. A seawater of approx. 40 ml is weighted again by the pipette, and is transferred into the titration cell.

Then, for seawater blank, absorbances are measured at three wavelengths (730, 616 and 444 nm). After the measurement, an acid titrant, which is a mixture of approx. 0.05 M HCl at 25°C in 0.65 M NaCl and ~40 μM bromocresol green (BCG) is added into the titration cell. The volume of the acid titrant is changed between ~1.9 mL and ~2.1 mL according to estimated values of A_T. The seawater + acid titrant solution is stirred for over 9 minutes with bubbling by nitrogen gas in the titration cell. Then, absorbances at the three wavelengths are measured.

Calculation of A_T is made by the following equation:

$$A_T = (-[H^+]_T V_{SA} + M_A V_A)/V_S,$$

where M_A is the molarity of the acid titrant added to the seawater sample, $[H^+]_T$ is the total excess hydrogen ion concentration in the seawater, and V_S, V_A and V_{SA} are the initial seawater volume, the added acid titrant volume, and the combined seawater plus acid titrant volume, respectively. $[H^+]_T$ is calculated from the measured absorbances based on the following equation (Yao and Byrne, 1998):

$$pH_T = -\log[H^+]_T = 4.2699 + 0.002578(35 - S) + \log((R - 0.00131)/(2.3148 - 0.1299R))$$
$$- \log(1 - 0.001005S),$$

where S is the sample salinity, and R is the absorbance ratio calculated as:

$$R = (A_{616} - A_{730})/(A_{444} - A_{730}),$$

where A_i is the absorbance at wavelength i nm.

(4) Results

Cross sections of C_T, and A_T (uncorrected data) during the cruise are illustrated in Figs. 4.9.1 – 4.9.4.
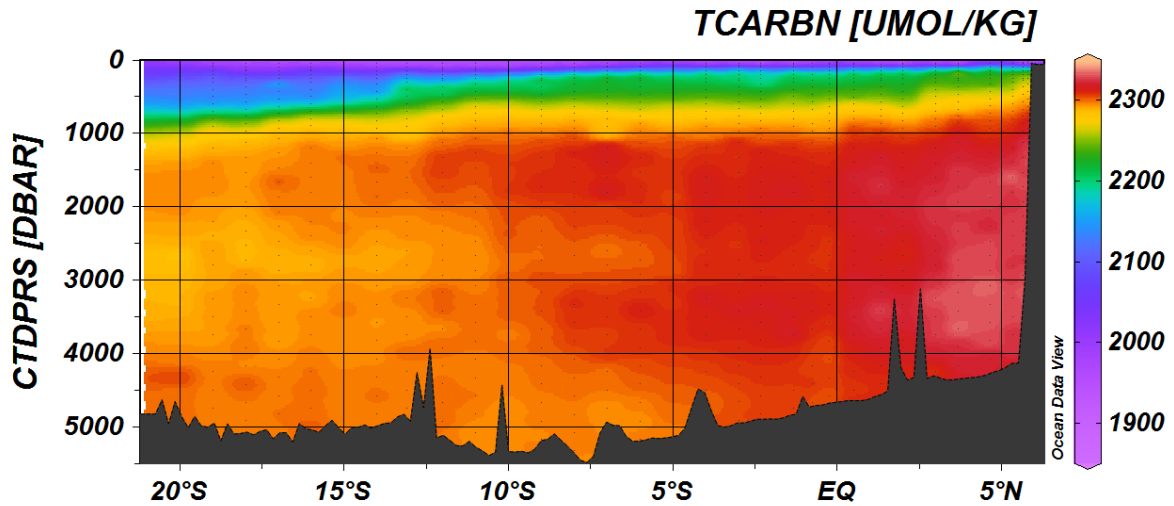
Fig. 4.9.1 Distributions of C_T along the section in MR19-04 leg 2.
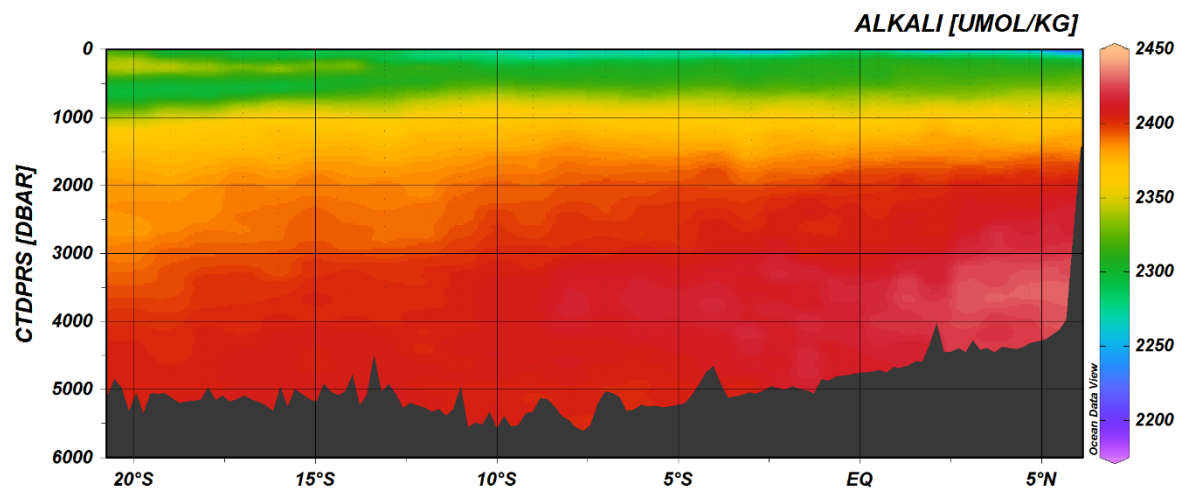
Fig. 4.9.2 Distributions of A$_T$ along the section in MR19-04 leg 2.
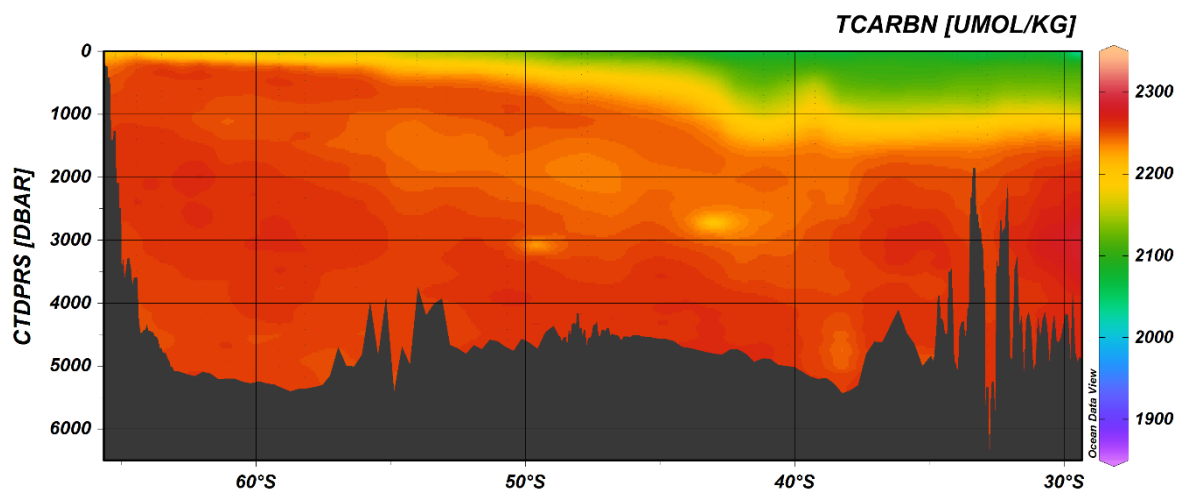
Fig. 4.9.3 Distributions of C$_T$ along the section in MR19-04 leg 3.
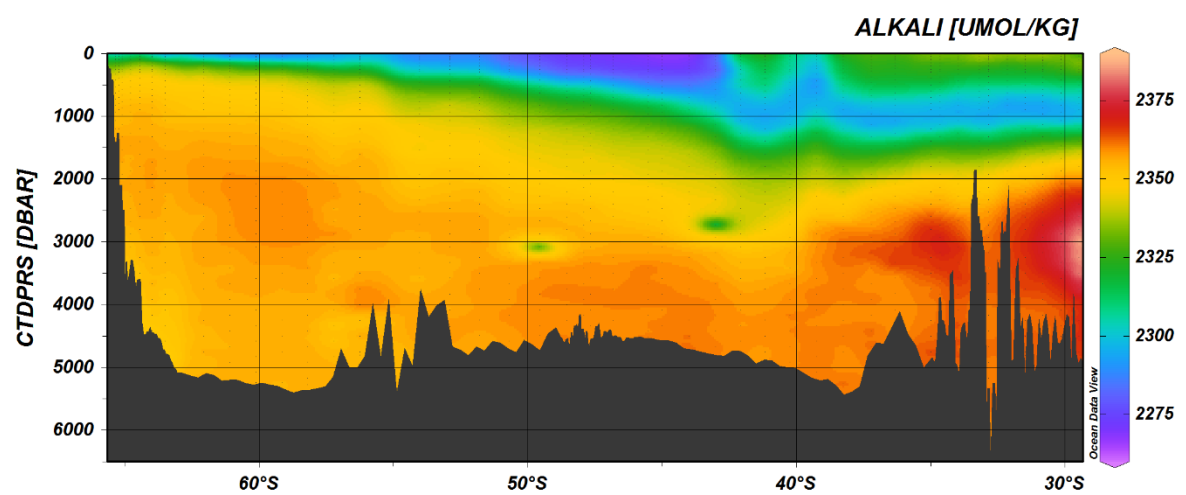
Fig. 4.9.4 Distributions of A$_T$ along the section in MR19-04 leg 3.

91

References

Yao W. and R. H. Byrne (1998), Simplified seawater alkalinity analysis: Use of linear array spectrophotometers. *Deep-sea Research Part I*, **45**, 1383-1392.

4.10 Chlorophyll *a*

(1) Personnel

       Kosei Sasaoka (JAMSTEC) (Leg.2, 3)
       Misato Kuwahara (MWJ) (Leg.2, 3)
       Erii Irie (MWJ) (Leg.2, 3)
       Yuko Miyoshi (MWJ) (Leg.2, 3)

(2) Objectives

    Chlorophyll *a* is one of the most convenient indicators of phytoplankton stock, and has been used extensively for the estimation of phytoplankton abundance in various aquatic environments. In this study, we investigated horizontal and vertical distribution of phytoplankton along the I08N section (Leg 2) in the Indian Ocean and I07S section (Leg 3) in the Southern Ocean. The chlorophyll *a* data is also utilized for calibration of fluorometers, which were installed in the surface water monitoring and CTD profiler system.

(3) Instrument and Method

    Seawater samples were collected in 500 mL (Leg 2: All stations, Leg 3: Station.70–97) and 250 mL (Leg 3: Station.99-153) brown Nalgene bottles without head-space. All samples were gently filtrated by low vacuum pressure (<0.02 MPa) through Whatman GF/F filter (diameter 25 mm) in the dark room. Whole volume of each sampling bottle was precisely measured in advance. After filtration, phytoplankton pigments were immediately extracted in 7 ml of N,N-dimethylformamide (DMF), and samples were stored at -20°C under the dark condition to extract chlorophyll *a* more than 24 hours. Chlorophyll *a* concentrations were measured by the Turner fluorometer (10-AU-005, TURNER DESIGNS), which was previously calibrated against a pure chlorophyll *a* (Sigma-Aldrich Co., LLC) (Figure 4.10.1). To estimate the chlorophyll *a* concentrations, we applied to the fluorometric "Non-acidification method" (Welschmeyer, 1994).

(4) Results

    Vertical distributions of chlorophyll *a* concentration at each stations along the I08N (Leg 2) and I07S (Leg 3) during the cruise are shown in Figure 4.10.2 and Figure 4.10.3, respectively. Cross section of chlorophyll *a* concentration along the I08N (Leg 2) and I07S (Leg 3) are shown in Figure 4.10.4 and 4.10.5, respectively. Sub-surface chlorophyll *a* maximum (SCM) was clearly seen in almost stations (Figure 4.10.2, 4.10.3). The SCM depths were deepened gradually from northern stations to around 12ºS along the I08N section (Figure 4.10.4). The chlorophyll *a* concentration was highest (about 1.6 mgm^{-3}) around 40ºS (the subarctic frontal zone) at the SCM depth (25m) along the I07S section (Figure 4.10.5). To examine the measurement precision, 29 (Leg 2) and 44 (Leg 3)-pairs of replicate samples were obtained from hydrographic casts at the chlorophyll *a* maximum depth. The absolute values of the difference between replicate samples were 0-0.12 mgm^{-3}, and those average relative errors were approximately 3% (Leg 2) and 4% (Leg 3).

(5) Reference
Welschmeyer, N. A. (1994): Fluorometric analysis of chlorophyll a in the presence of chlorophyll b and pheopigments. Limnor. Oceanogr., 39, 1985-1992.
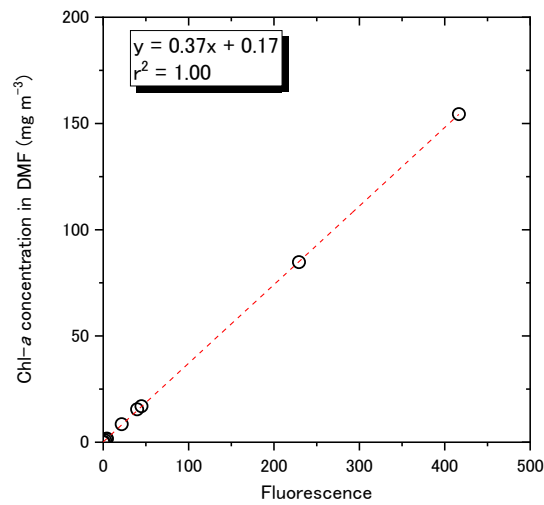
Figure 4.10.1 Relationships between pure chlorophyll *a* concentrations and fluorescence light intensity (n=10).
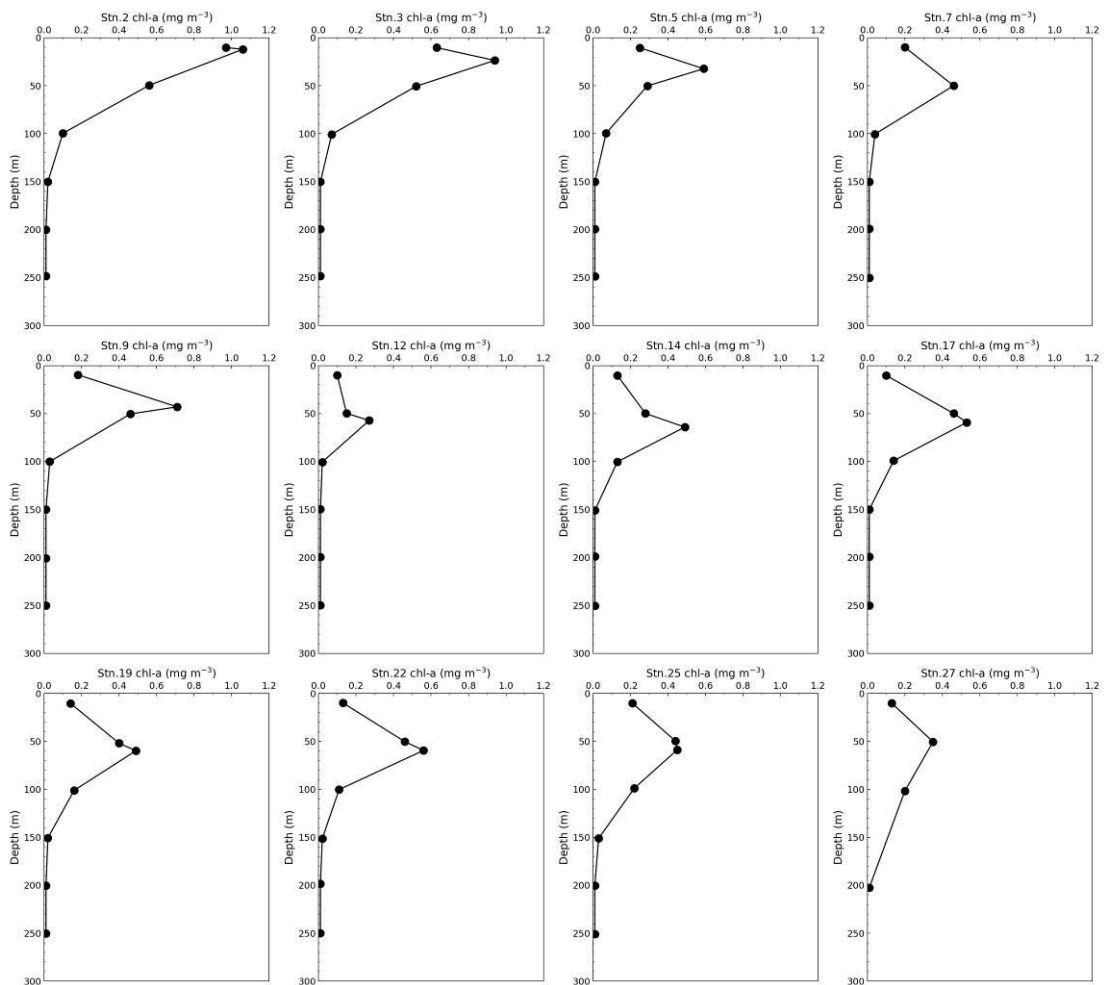

Figure 4.10.2 Vertical profiles of chlorophyll *a* concentrations (32-stations) along the I08N section (Leg 2) obtained from hydrographic casts.

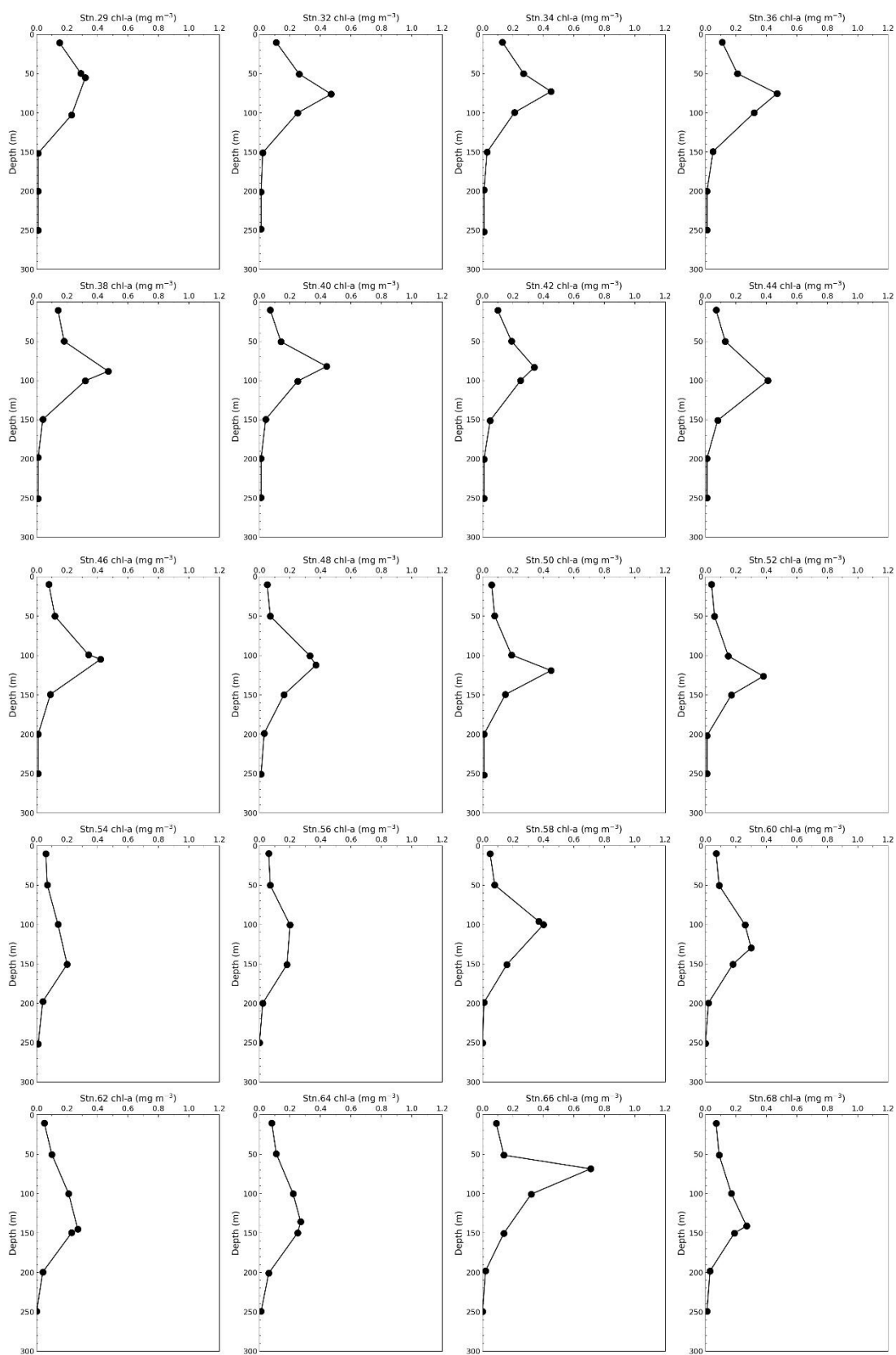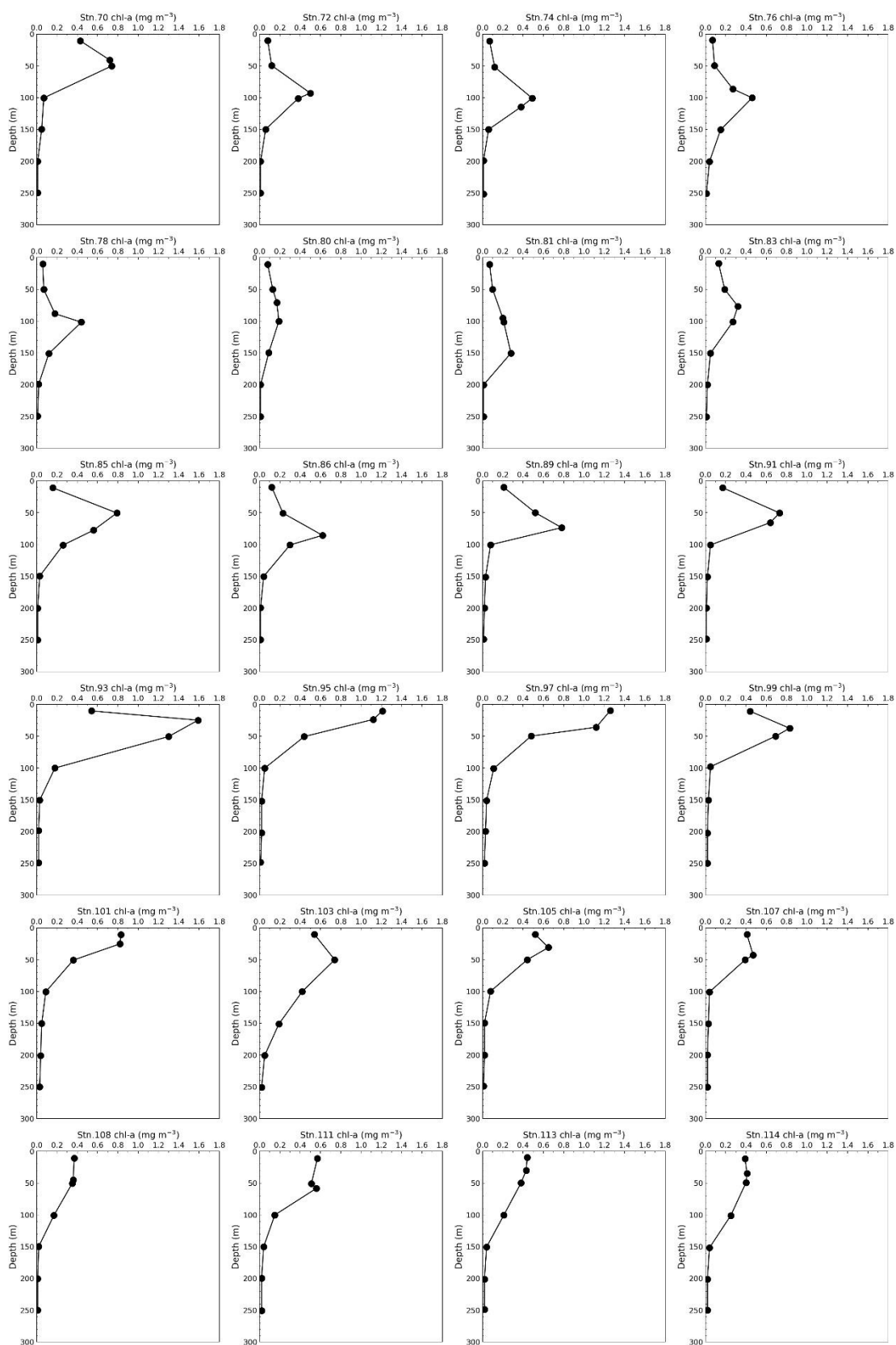Figure 4.10.2 (Continued)

95

Figure 4.10.3 Vertical profiles of chlorophyll *a* concentrations (44-stations) along the I07S section (Leg 3) obtained from hydrographic casts.
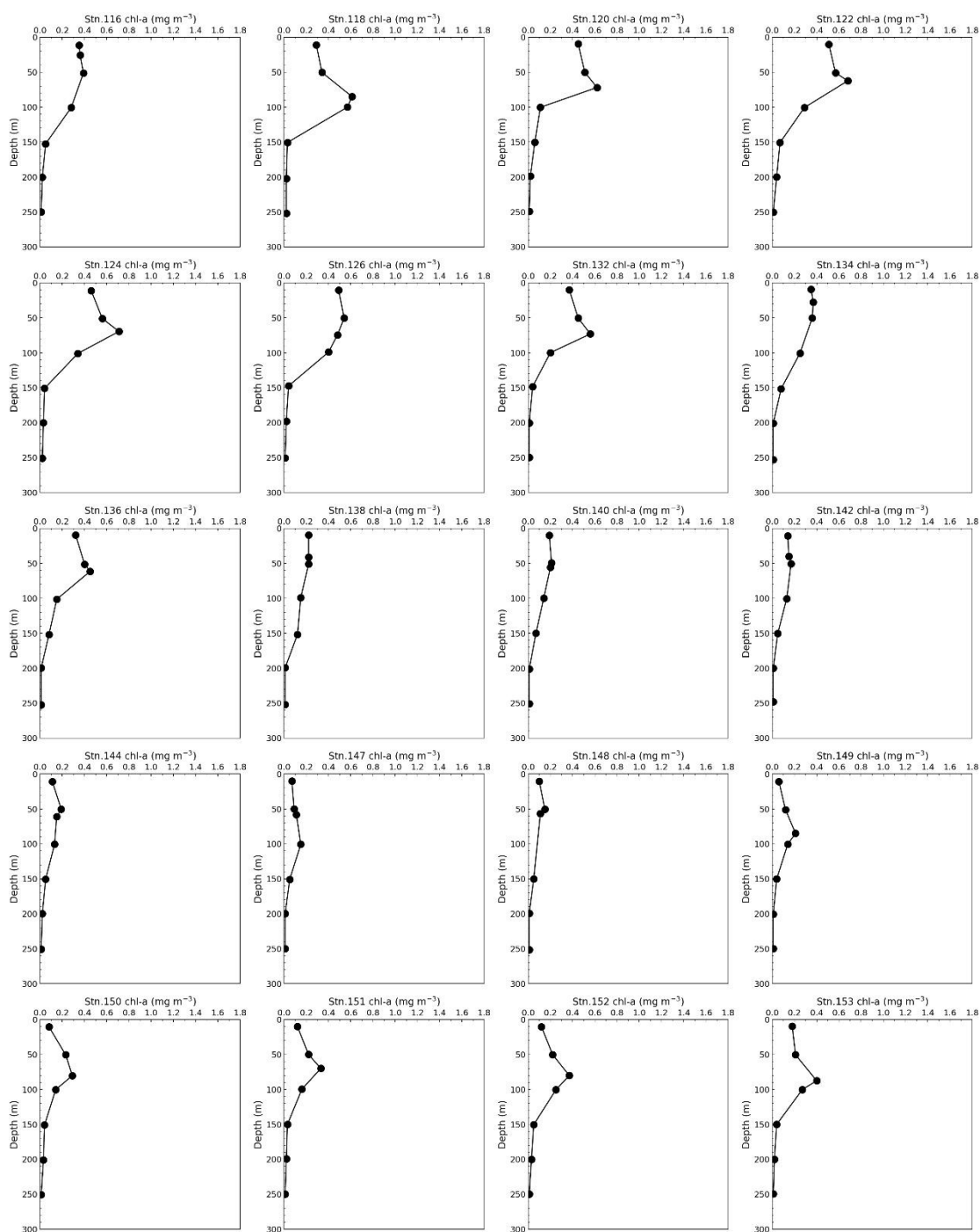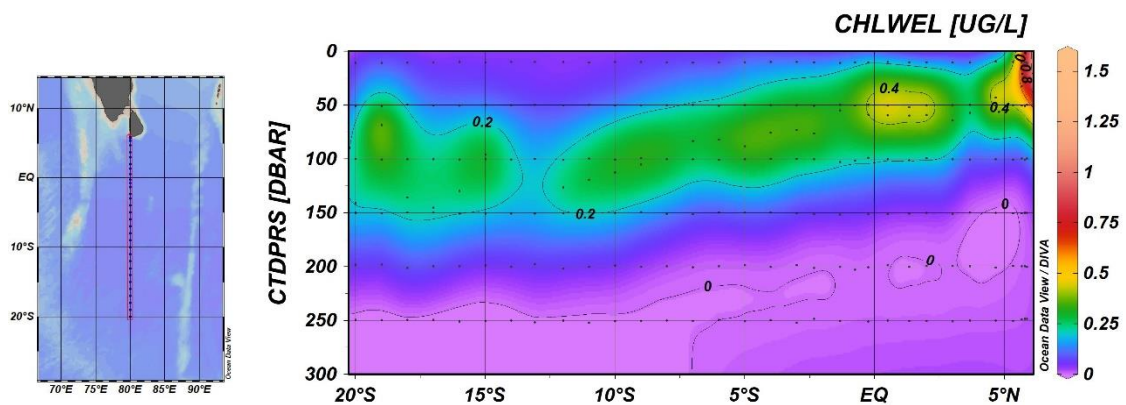
Figure 4.10.3 (Continued).

97

Figure 4.10.4 Cross section of chlorophyll *a* concentrations along the I08N (Leg 2) obtained from hydrographic casts.
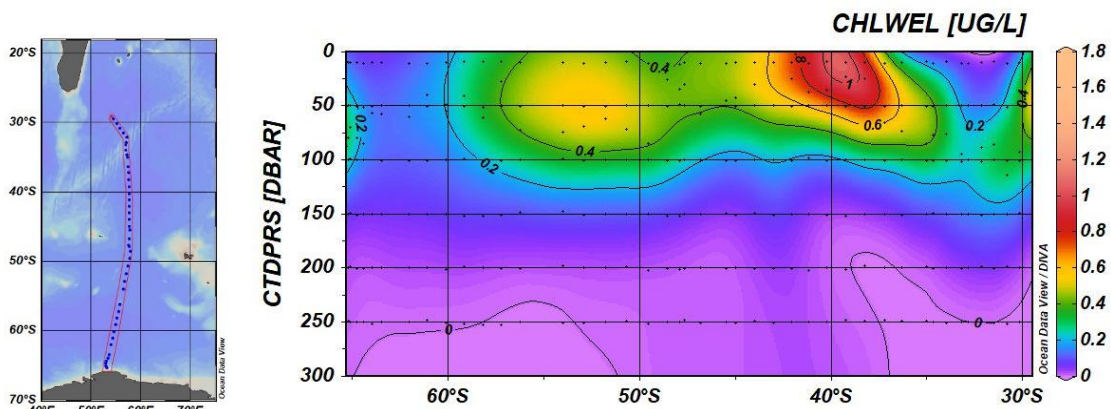
Figure 4.10.5 Cross section of chlorophyll *a* concentrations along the I07S (Leg 3) obtained from hydrographic casts.

4.11 Carbon isotopes

January 24, 2020

Yuichiro Kumamoto

Japan Agency for Marine-Earth Science and Technology (JAMSTEC)

(1) Personnel

Yuichiro Kumamoto

  Japan Agency for Marine-Earth Science and Technology

(2) Objective

  In order to investigate the water circulation and carbon cycle in the western Indian Ocean, seawaters for measurements of carbon-14 (radiocarbon) and carbon-13 (stable carbon) ratios of dissolved inorganic carbon were collected by the hydrocasts from surface to near bottom.

(3) Sample collection

  The sampling stations and number of samples are summarized in Table 4.11.1. All samples for carbon isotope ratios (total 199 samples) were collected at 6 stations using the 12-liter Niskin-X bottles. The seawater sample was siphoned into a 250 cm^3 glass bottle with enough seawater to fill the glass bottle 2 times. Immediately after sampling, 10 cm^3 of seawater was removed from the bottle and poisoned by 0.1 cm^3 μl of saturated $HgCl_2$ solution. Then the bottle was sealed by a glass stopper with Apiezon grease M and stored in a cool and dark space on board.

Table 4.11.1 Sampling stations and number of samples for carbon isotopic ratios.

Station	Lat. (N)	Long. (E)	Sampling Date (UTC)	Number of samples	Number of replicate samples	Max. Pressure (dbar)
019	1-20.05	80-00.00	2019/12/08	31	1	4625
050	-11-00.00	79-59.83	2019/12/17	34	1	5426
064	-17-59.93	80-00.48	2019/12/20	33	1	5186
074	-30-49.31	55-52.43	2020/01/01	31	1	4489
105	-43-59.99	57-45.52	2020/01/09	31	1	4712
142	-61-05.10	54-23.86	2020/01/19	33	1	5222
			Total	193	6	

(4) Sample preparation and measurements

  In our laboratory, dissolved inorganic carbon in the seawater samples will be stripped as CO_2 gas cryogenically and split into three aliquots: radiocarbon measurement (about 200 μmol), carbon-13

measurement (about 100 µmol), and archive (about 200 µmol). The extracted CO_2 gas for radiocarbon will be then converted to graphite catalytically on iron powder with pure hydrogen gas. The carbon-13 ratio ($^{13}C/^{12}C$) of the extracted CO_2 gas will be measured using a mass spectrometer (Finnigan MAT253). The carbon-14 ratio ($^{14}C/^{12}C$) in the graphite sample will be measured by Accelerator Mass Spectrometry.

(5) Data archives

The data obtained in this cruise will be submitted to the Data Management Group of JAMSTEC and will be opened to the public via "Data Research System for Whole Cruise Information in JAMSTEC (DARWIN)" in the JAMSTEC web site.

4.12 Dissolved organic carbon (DOC) and fluorescent dissolved organic matter (FDOM)

(1) Personnel
  Masahito Shigemitsu, Masahide Wakita and Akihiko Murata (JAMSTEC)

(2) Introduction
  Marine dissolved organic matter (DOM) is known to be the largest ocean reservoir of reduced carbon, and huge amounts of the carbon exist as refractory DOM (RDOM) (Hansell et al., 2009). RDOM is thought to be generated by microbial mineralization of organic matter produced in the sunlit surface ocean, and play an important role in the atmospheric CO_2 sequestration (Jiao et al., 2010). Some components of the RDOM can be detected as fluorescent DOM (FDOM).

  In this cruise, we try to gain insights into the interactions between DOM and microbial abundance, activity and diversity in the Indian Ocean. To this end, we measure dissolved organic carbon (DOC) and FDOM.

(3) Instruments and methods
Bottle sampling
  Discrete water samples for each station were collected using 12L Niskin bottles mounted on a CTD system. Each sample taken in the upper 250 m was filtered using a pre-combusted glass fiber filter (GF/F, Whatman). The filtration was carried out by connecting a spigot of Niskin bottle through silicone tube to an inline plastic filter holder.

  Filtrates were collected for DOC and FDOM measurements in acid-washed 60 mL High Density Polyethylene (HDPE) bottles and pre-combusted glass vials with acid-washed teflon-lined caps after triple rinsing, respectively. Other samples taken below 250 m were unfiltered. The samples for DOC and FDOM were collected at the stations 2, 5, 9, 12, 17, 25, 26, 36, 44, 45, 52, 60, 61, 68, 69, 70, 85, 93, 101, 114, 122, 138, 147, 151 and 153.

DOC measurement
  The samples for DOC were immediately stored frozen onboard until analysis on land. The samples will be thawed at room temperature and measured by a Shimadzu TOC-L system coupled with a Shimadzu Total N analyzer in JAMSTEC. The standardization will be achieved using glucose, and the analyses will be referenced against reference material provided by Hansell Laboratory, University of Miami.

FDOM measurement
  Fluorescence excitation-emission matrices (EEMs) were measured onboard using the Horiba Scientific Aqualog after the samples were allowed to stand until reaching near room temperature. Emission scans from 248 to 829 nm taken at 2.33-nm intervals were obtained for the excitation wavelengths between 240 and 560 nm at 5-nm intervals. The fluorescence spectra were scanned with a 12-s integration time and acquired in the high CCD gain mode. The following corrections of the fluorescence spectra were carried out: 1) the inner filter effect was corrected using the absorbance spectra measured simultaneously, and 2) fluorescence intensities were corrected for the area under the water Raman peak (excitation = 350nm), analyzed daily, and were converted to Raman Units (R.U.).

(4) Preliminary results of FDOM
  We measured all samples of FDOM onboard, but all data are still preliminary. Here, we show the results of FDOM (FDOM370) for the single pair of excitation and emission wavelengths (370/440 nm) which are considered to be humic-like FDOM (Coble, 2007) (Figures 4.12.1, and 4.12.2). The FDOM370 results are similar to the apparent oxygen utilization profiles detailed

elsewhere in this cruise report and indicate that this type of FDOM is produced in the ocean interior during mineralization of organic matter.
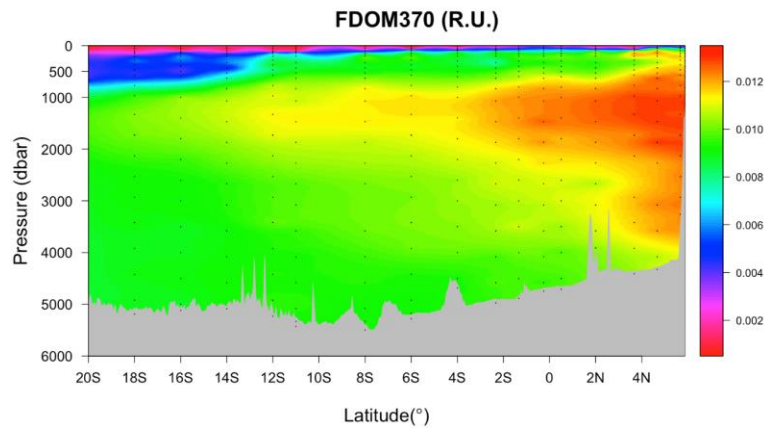
FDOM370 (R.U.)

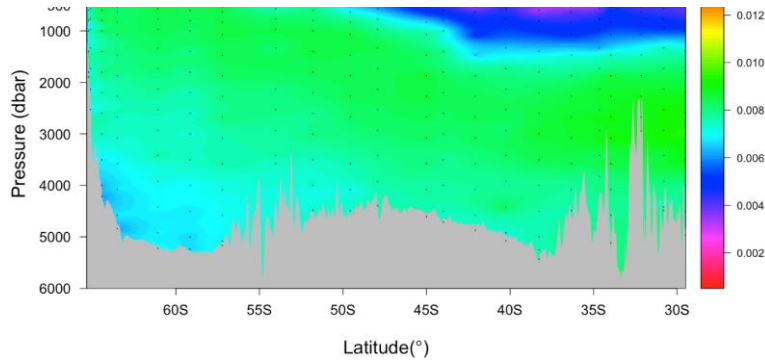*Figure 4.12.1 Contour map of FDOM370 during leg2.*

Figure 4.12.2 Contour map of FDOM370 during leg3.

4.13 $N_2/O_2/Ar$
(1) Personnel
      Bofeng Li, Chenye Wang, Yutaka Watanabe (Hokkaido University)

(2) Introduction
      The concept of excess nitrogen based on the dissolved N_2/Ar was proposed to quantify the nitrogen budget, since the dissolved N_2/Ar is sensitive to both biological and physical processes (*Devol et al*., 2006; *Hamme et al*., 2013). In the early stage, the N_2/Ar was only used in the three main oxygen deficient zones (ODZs) to estimate the water column denitrification in the intermediate layer. To make a better use of this and estimate the exceed N_2 in a broader field, *Shigemitsu et al*. (2013a) proposed a tracer N_2^* which can estimate biological and physical processes simultaneously as follows:

$$N_2^* = [N_2]_{meas} - ([N_2]_{sat}/[Ar]_{sat}) \times [Ar]_{meas} \qquad (1)$$

where $[N_2]_{meas}$ and $[Ar]_{meas}$ are the observed values of $[N_2]$ and $[Ar]$, respectively; and $[N_2]_{sat}$ and $[Ar]_{sat}$ are the saturated values of $[N_2]$ and $[Ar]$, respectively. To analyze the components that contribute to N_2^*, *Ito et al*. (2014) constructed the relationship between N_2^* and three processes: denitrification, air injection and rapid cooling based on a multiple linear regression analyze and got the following equation:

$$N_2^* = a_0 + a_1 \cdot J_{den} + a_2 \cdot J_{air} + a_3 \cdot J_{cool} \qquad (2)$$

where J_{den}, J_{air} and J_{cool} represented the impact of denitrification, bubble injection and rapid cooling, respectively. And they used observed N^* values ($N^* = ([NO_3^-] + [NO_2^-] + [NH_4^+] - 16[PO_4^{3-}] + 2.9) \cdot 0.87$) as the proxy for J_{den}, the product of the difference between observed and saturated Ar concentrations and the atmospheric mixing ratio of N_2/Ar for J_{air}, and the difference between the potential temperature (θ) and freezing temperature at the sea surface (T_{ref}) for J_{cool}, as the following equations:

$$J_{den} = N^* \qquad (3)$$

$$J_{air} = \Delta Ar \cdot \chi c \qquad (4)$$

$$J_{cool} = \theta - T_{ref} \qquad (5)$$

Using above method, the nitrogen budget will be clarified in the India Ocean.

(3) Sampling and measurement
      $N_2/O_2/Ar$ samples were collected at 16 CTD stations from all depths. The collected seawater for $N_2/O_2/Ar$ was directly transferred from the Niskin bottle to a 60-ml glass vial. After opening the vent of the Niskin bottle, the vessel was washed twice and overflowed with three times the volume of the vessel to avoid air contamination during the transfer procedure. For the final filling, we added 50 µl of saturated mercuric chloride solution to prevent biological activity, and covered the vial with a butyl rubber cap and aluminum seal (pay particular attention to assure that no air bubble contamination occurred). We preserved these vials in the dark and in a cool seawater bath (about 4ºC).
      The $N_2/O_2/Ar$ concentrations will be measured by a gas-chromatographic system with thermal conductivity detection (*Tanaka and Watanabe*, 2007) in Hokkaido University. The analytical precisions for replicate measurements of gas concentrations are within 0.03 % for N_2 and within 0.04 % for Ar.

References
Devol, A. H. *et al.* Denitrification rates and excess nitrogen gas concentrations in the Arabian Sea oxygen deficient zone. *Deep. Res. Part I Oceanogr. Res. Pap.* 53, 1533–1547 (2006).
Hamme, R. C. & Emerson, S. R. Deep-sea nutrient loss inferred from the marine dissolved N₂/Ar ratio.

Geophys. Res. Lett. 40, 1149–1153 (2013).

Shigemitsu, M., Gruber., Oka, A., Tanaka, S. S. & Yamanaka, Y. (2013). Potential use of N_2* as a constraint on the oceanic fixed nitrogen budget. In: The Oceanographic Society of Japan, Fall meeting in 2013, Sapporo.

Ito, M., Watanabe, Y. W., Shigemitsu, M., Tanaka, S. S. & Nishioka, J. Application of chemical tracers to an estimate of benthic denitrification in the Okhotsk Sea. *J. Oceano*gr. 70 (5), 415–424 (2014).

Tanaka, S. S. & Watanabe, Y. W. A high accuracy method for determining nitrogen, argon and oxygen in seawater. *Mar. Chem.* 106, 516–529 (2007).

4.14 Absorption coefficients of colored dissolved organic matter (CDOM)

(1) Personnel

Kosei Sasaoka (JAMSTEC) (Leg. 2,3)

(2) Objectives

Oceanic dissolved organic matter (DOM) is the largest pool of reduced carbon, and its inventory in the ocean is approximately 660 Pg C (Hansell et al., 2009). Thus, investigating the behavior of oceanic DOM is important to exactly evaluate the carbon cycle in the ocean. Colored (chromophoric) dissolved organic matter (CDOM) play an important role in determining the optical properties of seawater, and the global CDOM distribution appears regulated by a coupling of biological, photochemical, and physical oceanographic processes all acting on a local scale, and greater than 50% of blue light absorption is controlled by CDOM (Siegel et al., 2002). Additionally, some investigators have reported that CDOM emerges as a useful tracer for diagnosing changes in the overturning circulation and evaluating DOM compositions, similar to dissolved oxygen (e.g., Nelson et al., 2010; Catala et al., 2015). The objectives of this study are to clarify the north-south distribution of light absorption by CDOM along the I08N (Leg 2) in the Indian Ocean and I07S (Leg 3) section in the Southern Ocean.

(3) Methods

Seawater samples for absorption coefficient of CDOM ($a_y(\lambda)$) were collected in 250ml bottles using Niskin bottles from surface to bottom at 11-24 sampling layers including a chlorophyll a maximum depth. CDOM samples were filtered using 0.2 μm Nuclepore polycarbonate filters on board. After filtration, optical densities of the CDOM ($OD_y(\lambda)$) in this filtered seawater between 190 and 600 nm at a rate of 0.5 nm were immediately measured by an UV-VIS recording spectrophotometer (UV-2600, Shimadzu Co.), using 10-cm pathlength quartz cells. Milli-Q water was used as a base line. A blank (Milli-Q water versus Milli-Q water) was subtracted from each wavelength of the spectrum. The absorption coefficient of CDOM ($a_y(\lambda)$ (m^{-1})) was calculated from measured optical densities ($OD_y(\lambda)$) as follows:

$$a_y(\lambda) = 2.303 \times OD_y(\lambda) / L \ (L \text{ is the cuvette path-length } (L = 0.1m)).$$

(4) Preliminary results

Vertical profiles of CDOM (as absorption coefficient at 300 nm, unit = m^{-1}) at 18-stations along the I08N (Leg 2) section and at 23-stations along the I07S (Leg 3) section were shown in Fig. 4.14.1, and 4.14.2. Cross section of CDOM (as absorption coefficient at 300 nm, unit = m^{-1}) along the I08N (Leg 2) and I07S (Leg 3) were shown in Figure 4.14.3 and 4.14.4, respectively.

(5) References

Catala, T. S., et al., 2015, Turnover time of fluorescent dissolved organic matter in the dark global ocean, Nat. Com., 6, 1-8, doi:10.1038/ncomms6986.

Hansell, D. A., C. A. Carlson, D. J. Repeta, and R. Shlitzer, 2009, Dissolved organic matter in the ocean: A controversy stimulates new insight, Oceangr., 22, 202-211

Nelson, N. B., D. A. Siegel, C. A. Carlson, and C. M. Swan, 2010, Tracing global biogeochemical cycles and meridional overturning circulation using chromophoric dissolved organic matter, Geophys. Res. Lett., 37, L03610, doi:10.1029/2009GL042325.

Siegel, D.A., Maritorena, S., Nelson, N.B., Hansell, D.A., Lorenzi-Kayser, M., 2002, Global distribution

and dynamics of colored dissolved and detrital organic materials. J. Geophys. Res., 107, C12, 3228, doi:10.1029/2001JC000965.
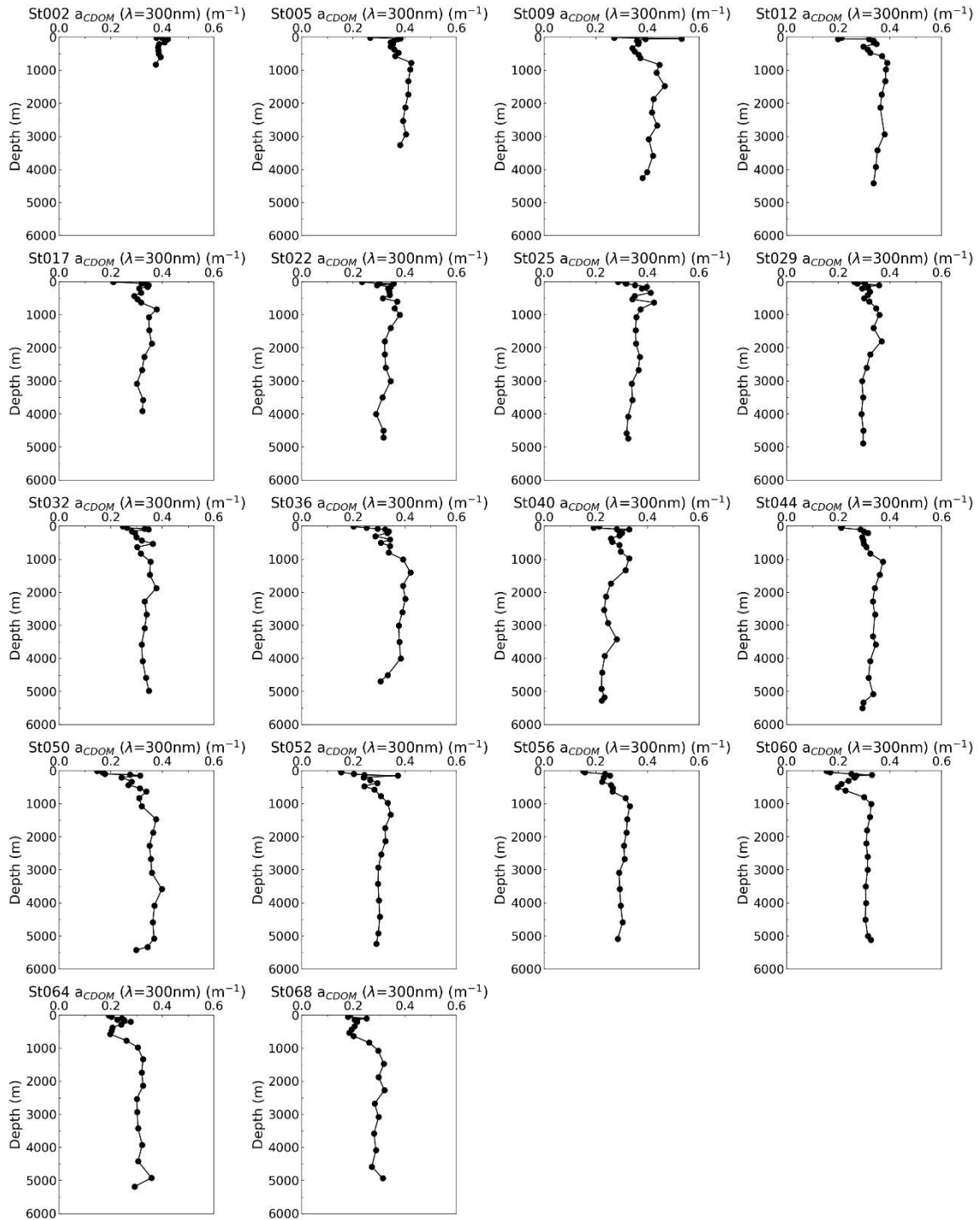
Fig.4.14.1 Vertical profiles of CDOM (as absorption coefficient at 300 nm, unit = m^{-1}) at 18-stations along the I08N section (Leg 2).
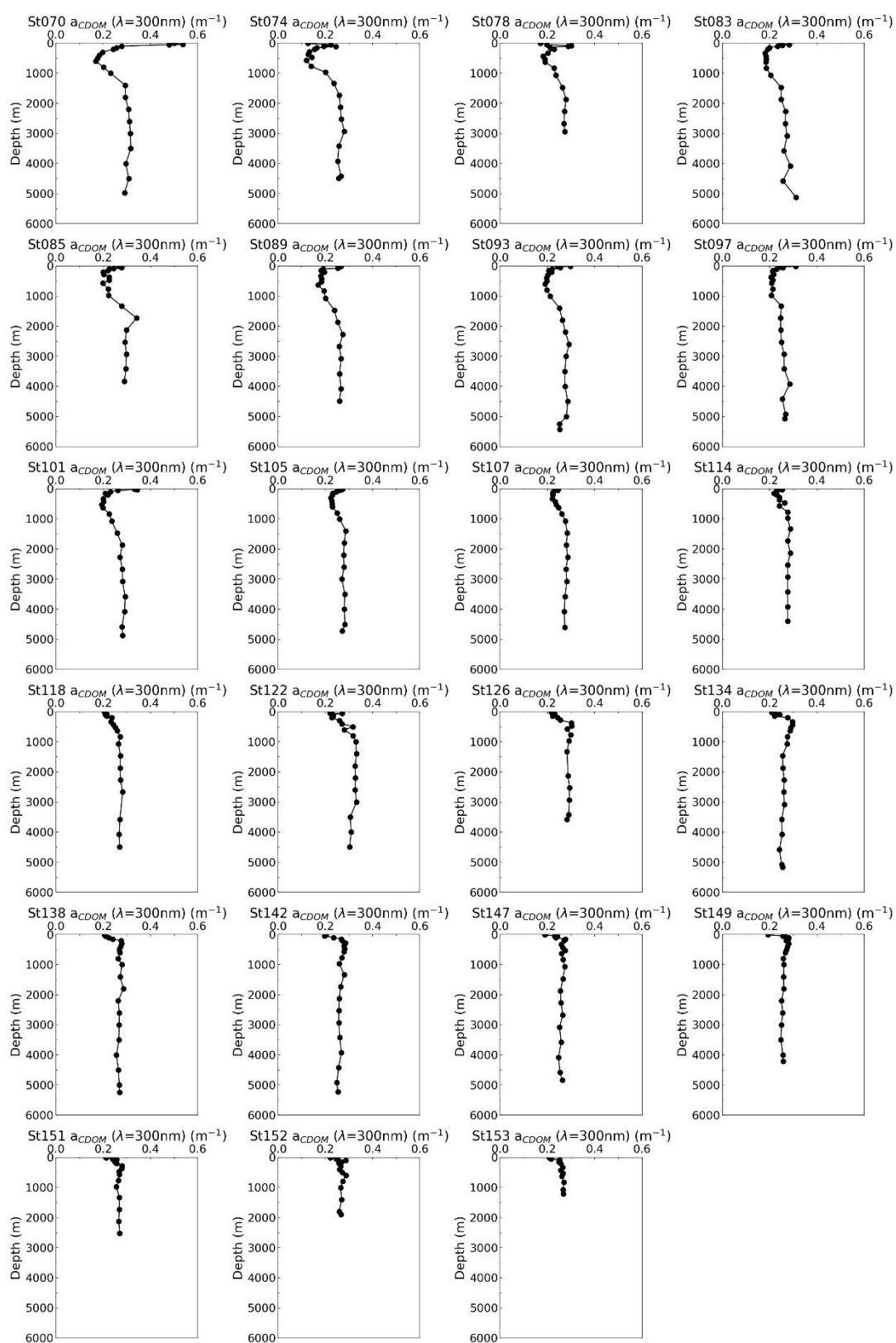
Fig.4.14.2 Vertical profiles of CDOM (as absorption coefficient at 300 nm, unit = m^{-1}) at 23-stations along the I07S section (Leg 3).
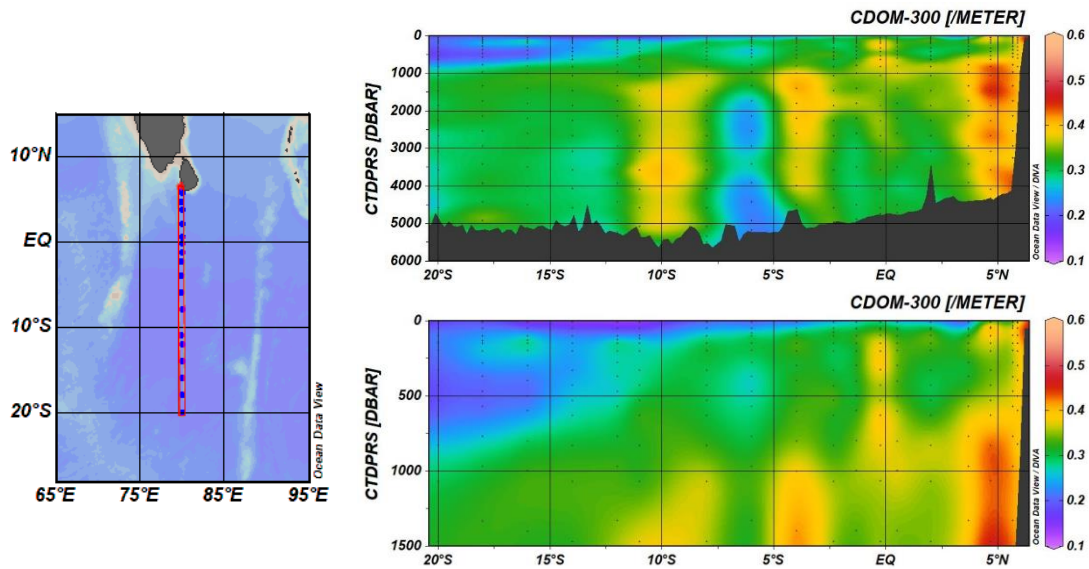
Fig.4.14.3 Sections of CDOM (as absorption coefficient at 300 nm, unit = m⁻¹) along the I08N section (Leg 2) obtained from hydrographic casts. The top section covers surface to the bottom and the lower section covers the upper 1,500 m.
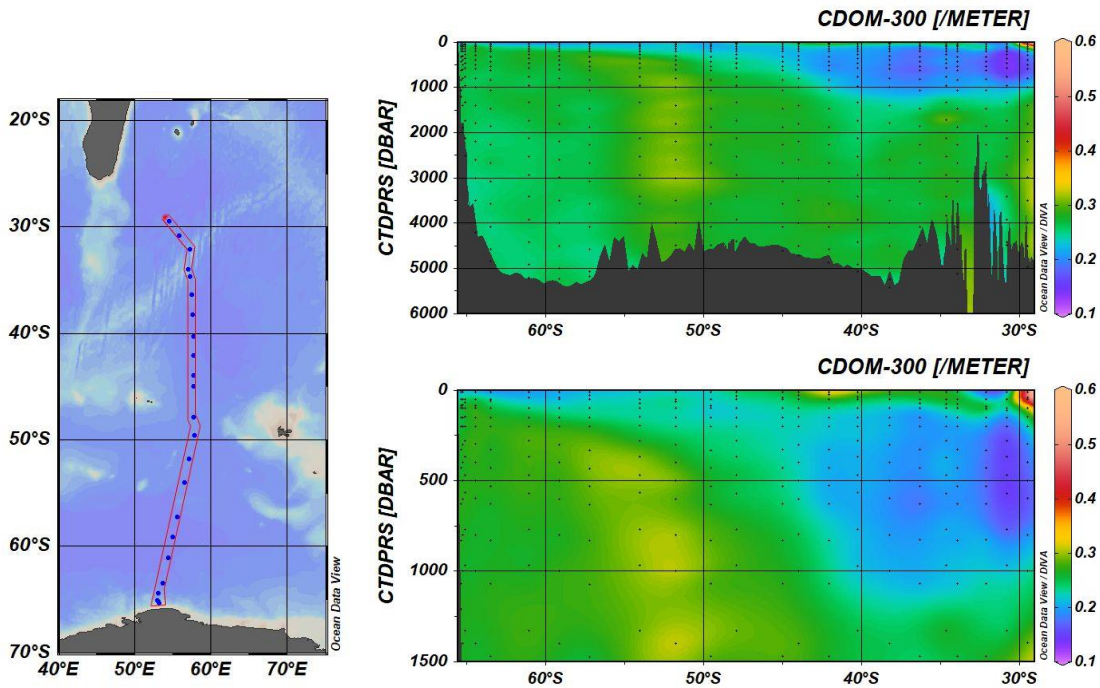
Fig.4.14.4 Contours showing distribution of CDOM (as absorption coefficient at 300 nm, unit = m⁻¹) along the I07S section (Leg 3) obtained from hydrographic casts. The top section covers surface to the bottom and the lower section covers the upper 1,500 m.

4.15 Radiocesium

January 24, 2020
Yuichiro Kumamoto
Japan Agency for Marine-Earth Science and Technology (JAMSTEC)

(1) Personnel

Yuichiro Kumamoto
   Japan Agency for Marine-Earth Science and Technology

(2) Objective

In order to investigate the water circulation and ventilation process in the western Indian Ocean, seawater samples were collected for measurements of radiocesium (^{137}Cs), which was mainly released from the global fallout in the 1950s and 1960s.

(3) Sample collection

The sampling stations and number of samples are summarized in Table 4.15.1. The total 45 seawater samples for radiocesium measurement were collected at 6 stations from surface (10 m) to 1000 m depth using 12-liter Niskin-X bottles. The seawater sample was collected into two 20-L plastic containers (40 L each) after two time washing. All the seawater samples were acidified by adding of 40-cm^3 of concentrated nitric acid on board.

Table 4.15.1 Sampling stations and number of samples for radiocesium.

Station	Lat. (N)	Long. (E)	Sampling Date (UTC)	Number of samples	Max. Pressure (dbar)
020	1-00.04	79-59.90	2019/12/09	8	970
051	-11-29.93	80-00.02	2019/12/17	8	1070
065	-18-29.85	79-59.98	2019/12/21	8	973
075	-31-09.22	56-13.08	2020/01/01	7	770
106	-44-29.99	57-46.38	2020/01/10	7	801
143	-61-34.10	54-15.22	2020/01/19	7	770
			Total	45	

(4) Sample preparation and measurements

In our laboratory on shore, radiocesium in the seawater samples will be concentrated using ammonium phosphomolybdate (AMP) that forms insoluble compound with cesium. The radiocesium in AMP will be measured using Ge γ-ray spectrometers.

(5) Data archives

The data obtained in this cruise will be submitted to the Data Management Group of JAMSTEC and will be opened to the public via "Data Research System for Whole Cruise Information in JAMSTEC (DARWIN)" in the JAMSTEC web site.

4.16 Radium isotopes

January 24, 2020

Yuichiro Kumamoto

Japan Agency for Marine-Earth Science and Technology (JAMSTEC)

(1) Personnel

Yuichiro Kumamoto
  Japan Agency for Marine-Earth Science and Technology

(2) Objective

In order to investigate the water circulation and ventilation process in the western Indian Ocean, seawater samples were collected for measurements of radium isotopes (^{226}Ra and ^{228}Ra).

(3) Sample collection

The sampling stations and number of samples are summarized in Table 4.16.1. The total 35 seawater samples for radiocesium measurement were collected at 5 stations from surface (10 m) to 800 m depth using 12-liter Niskin-X bottles. The seawater sample was collected into two 20-L plastic containers (40 L each) after two time washing.

Table 4.16.1 Sampling stations and number of samples for radium isotopes.

Station	Lat. (N)	Long. (E)	Sampling Date (UTC)	Number of samples	Max. Pressure (dbar)
018	1-40.00	80-00.01	2019/12/08	7	770
049	-10-40.00	80-00.01	2019/12/16	7	830
073	-31-09.22	55-31.54	2020/01/01	7	770
104	-43-29.93	57-44.97	2020/01/09	7	800
141	-60-36.17	54-32.66	2020/01/19	7	771
			Total	35	

(4) Sample preparation and measurements

In our laboratory on shore, Ra-free Barium carrier and SO_4^{2-} are added to the seawater sample to coprecipitate radium with $BaSO_4$. After evaporating to dryness, the $BaSO_4$ fractions are compressed to disc as a mixture of $Fe(OH)_3$ and NaCl for gamma-ray spectrometry using Ge-detectors.

(5) Data archives

The data obtained in this cruise will be submitted to the Data Management Group of JAMSTEC and will be opened to the public via "Data Research System for Whole Cruise Information in JAMSTEC (DARWIN)"

in the JAMSTEC web site.

4.17 Nitrogen cycles in the Indian Ocean and Southern Ocean

(1) Personnel

Akiko Makabe, Eiji Tasumi and Chisato Yoshikawa (JAMSTEC)

(2) Introduction

The marine nitrogen cycle in surface waters is known to control biological activity in the ocean, because inorganic forms of nitrogen such as nitrate are indispensable nutrients for phytoplankton. Following the primary production, organic nitrogen compounds are metabolized into ammonium and low molecular organic nitrogen compounds that are substrates for nitrification and/or nitrogen source of microbes. In low-nutrient region, nitrogen fixation is important source of nitrogen. Nitrous oxide (N_2O), known to be produced by microbial activity such as nitrification, is recognized as significant anthropogenic greenhouse gas and a stratospheric ozone destroyer.

To understand transformation of nitrogen compound by (microbial) organisms and production processes of greenhouse gasses (N_2O and CH_4), both natural abundance and tracer stable isotope technique are useful. We collected water samples to analyze natural abundance stable isotope ratio of dominant nitrogen species such as nitrate, nitrite, ammonium and nitrous oxide, which will have records of biological processes. On the other hand, tracer technique is relatively tough work but strongly useful tool to detect or determine rates of each process. We conducted on-board incubation experiments to analyze nitrification and nitrogen fixation activities. As alternative method, we measured dissolved H_2 concentration which is by-product in nitrogen fixation.

(3) Methods

Nitrate and nitrite isotope ratio

Samples for nitrate and nitrite stable isotope analysis were collected into a 50mL plastic syringe with a filter (pore size: 0.45μm) and filtered immediately after sampling in the Indian Ocean, while samples were collected into a 50mL PE bottle in the Southern Ocean and frozen until filtration at the laboratory in JAMSTEC. We will measure both nitrogen and oxygen stable isotope ratio of nitrate and nitrite using the bacterial method.

Samples for nitrate and nitrite stable isotope ratio were collected in Station#: 2, 5, 6, 9, 12, 17, 22, 25, 26, 29, 32, 36, 40, 44, 45, 50, 52, 56, 60, 61, 64, 68, 69, 70, 74, 78, 83, 85, 89, 93, 97, 101, 105, 107, 111, 116, 120, 124, 128, 132, 136, 140, 144, 149, 154.

Ammonium isotope ratio

Samples for ammonium stable isotope analysis were collected into a PE bottle and filtered with a syringe filter (pore size: 0.45μm) as soon as possible after sampling. A glass fiber filter (GF/D) with sulfuric acid solution and MgO were added to subsamples of 50 ml filtrate. The glass fiber filters trapped with ammonia after shaken for 5days were removed from the subsamples and collected into glass bottles with silica gel desiccant. Nitrogen stable isotope ratio of ammonium will be measured using the bacterial method followed by wet oxidation at JAMSTEC.

Samples for ammonium isotope ratio were collected in Station#: 6, 26, 45, 61.

N_2O and CH_4 isotope ratio

Samples for N_2O and CH_4 stable isotope analysis were collected into 100 mL glass vials and added with $HgCl_2$ solution immediately after sampling. Nitrogen and oxygen stable isotope ratio of N_2O and carbon stable isotope ratio of CH_4 will be measured by GC-IRMS in JAMSTEC.

Samples for N_2O and CH_4 stable isotope ratio were collected in Station#: 2, 5, 6, 25, 26, 44, 45, 60, 61, 68, 69.

Nitrification activity

Samples for nitrification activity measurement were collected into 100 mL amber glass vials without head space. Substrates of nitrification, ammonium or urea (^{15}N 99 atom %), were added to the vials and incubated in dark at near in situ temperature on board. At the end of incubation period, water samples were filtrated by a syringe filter (pore size: 0.45μm) and frozen until analysis. The transfer rate from substrates to nitrite and nitrate were determined by enrichment of ^{15}N in nitrite and nitrate.

Samples for nitrification activity measurement were collected in Station#: 5, 6, 25, 26, 44, 45, 60, 61, 68, 69.

Nitrogen fixation activity

Samples for N_2 fixation activity measurement were collected into 250 mL PC bottles without head space. Seawater with ^{15}N enrichment of dissolved N_2 gas was prepared by adding ^{15}N 99 atom % N_2 gas after filtration and degasification of seawater. Each 10 mL of sample was replaced to the ^{15}N enriched seawater by syringe injection. The PC bottles with/without ^{15}N enriched seawater were incubated in seawater baths for 24 hours under appropriate screen to simulate the in situ temperature and light intensity. Each incubated sample was filtered with 2μm polycarbonate filters and 0.3μm glass fiber filters after the incubation. The filters and filtrate were frozen until analysis of ^{15}N enrichment in each size fraction.

Samples for N_2 fixation activity measurement were collected in Station#: 6, 26, 45, 61, 69.

H₂ concentration

Samples for H_2 analysis were collected into 100 mL glass vials and added with $HgCl_2$ solution immediately after sampling. Each 20 mL of seawater was replaced to ultrapure N_2 gas to make head space in each vial. The vials were shaken until achievement of equilibrium between the dissolved and head-space gases. Concentration of dissolved H_2 was determined by measurement of the head-space gas using GC on board.

Samples for H_2 concentration measurement were collected in Station#: 6, 26, 45, 61, 69.

4.18 Spatial patterns of prokaryotic abundance, activity and community composition in relation to the water masses in Indian Ocean and Southern Ocean

(1) Personnel

Taichi Yokokawa and Masahito Shigemitsu (JAMSTEC)

(2) Introduction

Prokaryotes (Bacteria and Archaea) play a major role in marine biogeochemical fluxes. Biogeochemical transformation rates and functional diversity of microbes are representative major topics in marine microbial ecology. However, the link between prokaryotes properties and biogeochemistry in the meso- and bathypelagic layers has not been explained systematically despite of the recent studies that highlight the role of microbes in the cycling of organic and inorganic matter. Moreover, microbial community composition and biogeography in meso- and bathypelagic ocean and its relationship with upper layers and deep-water circulation have also not been well studied.

The objectives of this study, which analyze the water columns from sea surface to 10m above the bottom of Indian ocean and Southern Ocean, were 1) to determine the abundance of microbes; 2) to study the heterotrophic/autotrophic production of prokaryotes; 3) to assess the community composition of prokaryotes; 4) to know microbial diversity through water columns along the latitudinal transect.

(3) Methods

Microbial abundance

Samples for microbial abundances (prokaryotes, eukaryotes and viruses) were collected in Station#: 17, 25, 26, 36, 44, 45, 52, 60, 61, 68, 69, 70, 85, 93, 101, 114, 122, 138, 147, 151 and 153. Samples were fixed with glutaraldehyde (final concentration 1%) and frozen at -80°C. The abundance and relative size of microbes and viruses will be measured by a flow cytometry in JAMSTEC after nucleic acid staining with SYBR-Green I.

Microbial activity measurements

Heterotrophic microbial production was determined based on ^{3}H-leucine incorporation rate. ^{3}H-leucine incorporation rate was determined as a proxy for heterotrophic or mixotrophic prokaryotic production. Triplicate subsamples (1.5 mL) dispensed into screw-capped centrifuge tubes amended with 10 nmol L^{-1} (final concentration) of [^{3}H]-leucine (NET1166, PerkinElmer) and incubated at in situ temperature (± 2°C) in the dark. One trichloroacetic acid (TCA) killed blank was prepared for each sample. Incubation periods were 1 hour and 24 hours for the upper (0 – 250 m) and deeper (300 – bottom) water layers, respectively. After the incubation, proteins were TCA (final conc. 5%) extracted twice by centrifugation (15000 rpm, 10 min, Kubota 3615-sigma), followed by the extraction with ice-cold 80% ethanol.

The samples will be radioassayed with a liquid scintillation counter using Ultima-GOLD (Packard) as scintillation cocktail. Quenching is corrected by external standard channel ratio. The disintegrations per minute (DPM) of the TCA-killed blank is subtracted from the average DPM of the samples, and the resulting DPM is converted into leucine incorporation rates.

Samples for leucine incorporation activity measurements were taken at stations 25, 26, 44, 52, 60, 68, 70, 85, 93, 122, 138, 147 and 151 in the routine casts.

Autotrophic microbial production is determined based on ^{14}C-bicarbonate incorporation rate. ^{14}C-bicarbonate incorporation rate is determined as a proxy for autotrophic or mixotrophic prokaryotic production. Triplicate subsamples (30 mL) dispensed into screw-capped centrifuge tubes were inoculated with 1480 kBq (final concentration) of NaH^{14}CO$_3$ (NEC086H, PerkinElmer) and incubated at in situ temperature (± 2°C) in the dark for 3 days and 10-15 days. One glutaraldehyde-killed blank was prepared for each sample. Incubations were terminated by adding glutaraldehyde (2% final concentration) to the samples, and the samples were filtered onto 0.2-μm polycarbonate filters.

The samples will be radioassayed with a liquid scintillation counter using Filter-Count (PerkinElmer) as scintillation cocktail, after the filters are fumed with concentrated HCl for 12 hours. Quenching is corrected by external standard channel ratio. The DPM of the glutaraldehyde-killed blank is subtracted from the average DPM of the samples and the resulting DPM is converted into bicarbonate incorporation rates.

Samples for ^{14}C-bicarbonate incorporation activity measurements were taken at stations 52, 60, 68, 70, 85, 93, 122, 138, 147 and 151 in the routine casts.

Microbial diversity

       Microbial cells in water samples were filtrated on cellulose acetate filter (0.2µm) and stored at -80˚C. Environmental DNA or RNA will be extracted from the filtrated cells and used for 16S/18S rRNA gene tag sequencing using MiSeq, quantitative PCR for genes for 16S rRNA, and/or metatranscriptomics. Samples for microbial diversity were taken at stations 17, 25, 26, 36, 44, 45, 52, 60, 61, 68, 69, 70, 85, 93, 101, 114, 122, 138, 147, 151 and 153 in the routine casts.

4.19. Placeholder

This page is left blank, unintentionally.

4.20. Delta O18

(1) Personnel

Shigeru Aoki (Hokkaido University)

(2) Objectives

Salinity/freshwater budget in the high-latitude oceans is an essential factor in determining the stratification and hence global meridional overturning. Near-surface freshening is observed in the high-latitude Southern Ocean (eg. Boyer et al., 2005) and understanding the balance of freshwater input and its origins are of critical importance in climate change study related to global hydrological cycle.

In the freshwater input near surface, excess precipitation (over evaporation) is a dominant factor in relatively fresh nature of the Antarctic Surface Water. Near the Antarctic continent, net sea ice melt and iceberg melt can contribute to the freshwater input as well. However, relative contribution from each component is not sufficiently understood. Oxygen isotope is a good tracer in detecting the origin of freshwater since its value is significantly among the different freshwater sources such as local precipitation, ice shelf/iceberg melt water, and sea ice (Heywood et al., 1998). However, there is few observation of oxygen isotope in the Indian Ocean sector of the Southern Ocean until recently.

To obtain the oxygen isotope data for I07S line for the first time, we collected water samples for the oxygen isotope analysis. This will hence lead to set the baseline for the future climate change study.

It is a slight addtion of workload to sample the I08N section, which was hence performed at selected stations.

(3) Apparatus

The relative proportion of principal stable isotopes of oxygen in seawater is usually quoted as $\delta^{18}O$, defined as the ratio of ^{18}O to ^{16}O relative to Vienna Standard Mean Ocean Water.

$$\delta^{18}O = \frac{(^{18}O/^{16}O)_{sample} - (^{18}O/^{16}O)_{VSMOW}}{(^{18}O/^{16}O)_{VSMOW}} \times 1000$$

We collected water samples for the $\delta^{18}O$ analysis from all Niskin bottles with 30ml glass vials at all stations. The vials are stored in the refrigerator. The vials were sealed with Parafilms.

The samples are to be shipped to ILTS, Sapporo, and the analysis will be conducted with an IRMS mass spectrometer and CRDS isotope analyzer. The samples that well represent the watermass core property will be analyzed first and by Finnigan Delta Plus spectrometer. Water samples will be set in equilibrium with CO_2 gas within the 18 degree Celcius water bath. The rest of the samples will be analyzed with a CRDS spectrum analyzer.

References

Boyer, T.P., S.Levitus, J.I.Antonov, R.A.Locarnini, and H.E.Garcia (2005) Linear trends in salinity for the World Ocean, 1955-1998, Geophys. Res. Lett., 32, L01604, doi:10.1029/2004GL021791.

Heywood, K., R.A. Locarnini, R.D. Frew, P.F. Dennis and B.A. King (1998), Ocean, Ice and Atmosphere: Interactions at Antarctic continental margin, Antarc. Res. Ser., Vol.75, 203-213.

4.21 Urea and Iodate

(1) Personnel

Peter Croot (NUI Galway):	Principal investigator (onboard Leg 2)
Maija Heller (PUCV):	Co-investigator (onboard Leg 3)

(2) Objective

The key objectives of this work were to obtain data on two less well studied chemical species, iodate (IO_3^-) and urea ($CO(NH_2)_2$), for which there are little or no data from the Indian Ocean nor any basin scale overview for any of the ocean basins currently available. The rationale for measuring these two species together on a GO-SHIP basin scale expedition, is that they conceptually represent different aspects (and related hypotheses), concerning nutrient regeneration in the ocean (L'Helguen et al., 2005; Tian et al., 1996) and the depths at which it is occurring. These datasets will also provide baselines for ongoing ocean and atmospheric modelling efforts into the nitrogen and iodine cycles. Importantly, both analytes can be measured at sea relatively quickly and cheaply, using spectrophotometric techniques, and this then provides a good test case for involving scientists from countries making their first steps in GO-SHIP related activities that can likely be replicated in the future with other groups.

Urea is a small nitrogen containing organic molecule, for which recent studies have shown plays an important role in the marine nitrogen cycle, as it is rapidly turned over in the environment and acts as a nitrogen shuttle within the microbial loop. Urea is mostly produced in the ocean via excretion from heterotrophic organisms of all size classes from bacteria upwards, this urea provides a source of bioavailable nitrogen for heterotrophic bacteria, cyanobacteria and eukaryotic phytoplankton. There are only a few published reports for Urea in near surface waters from the oligotrophic Indian Ocean (Baer et al., 2019) and Indian sector of the Southern Ocean (Thomalla et al., 2011) with concentrations ranging from below detection (less than 10 nM) in the oligotrophic tropics up to 2.5 μM in the region between the subtropical front and the subantarctic front. While the turnover time for urea is on the order of days and it is thus a rather transient species, this GO-SHIP expedition provides a good opportunity to obtain basic scale data on urea across a wide range of marine ecosystems with differing nitrogen dynamics.

Iodate is the thermodynamically stable form of iodine in oxygenated seawater. It is however easily reduced to iodide by UV radiation, chemical reductants and bacterial/phytoplankton metabolism (Bluhm et al., 2010). The re-oxidation of iodide to iodate is facilitated by O_2 and H_2O_2 but is significantly slower than the reduction step with a half life of around 70 days in oligotrophic tropical regions (Campos et al., 1996). The redox cycling between iodate and iodide resulting in a small but significant release of volatile halogen species of intermediate redox state (e.g. I_2, HOI, CH_3I etc) from the surface ocean to the atmosphere. Interest in the marine cycling of iodine has grown over the last decade because of discovery of the role of marine sources of iodine to the atmosphere, where upon the iodine is a major sink for ozone and the resulting IO produced is a source of new particles that can act as cloud condensation nuclei (Saiz-Lopez et al., 2011). The development of satellite methods to measure IO in the atmosphere (Schönhardt et al., 2016; Schonhardt et al., 2008) have also highlighted the strong link between iodine speciation in seawater and atmospheric IO concentrations. Recently published overviews of iodine distributions in the ocean, show a distinct lack of data in the Indian ocean (Chance et al., 2014; Sherwen et al., 2019), while there is data for the Southern Ocean only from the Atlantic sector of the Southern Ocean (Bluhm et al., 2011; Campos et al., 1999). This lack of data is further highlighted by the publication of a recent shipboard study of IO in the Indian Ocean using a MAX-DOAS instrument (Mahajan et al., 2019) where the iodide concentrations were modelled according to algorithms based on existing datasets for other regions. Thus, the opportunity to obtain a basic scale distribution for iodate in the Indian Ocean is very timely.

As our analysis is based on spectrophotometry at trace levels through the use of Liquid Wave Capillary Cells (LWCC) with pathlengths from 50 to 250 cm, we also collected data during this expedition on the absorbance spectrum of Coloured Dissolved Organic Matter (CDOM) as it impacts our baseline measurements. For this expedition we have also employed a newer type of LWCC, which has a wider internal diameter and can be used with unfiltered water allowing the collection of data on the hyperspectral absorption of whole seawater and filtered seawater, with the particulate absorption being calculated by the difference between the two measurements. These measurements are then comparable to the Quantitative Filter Technique (QFT) often employed to measure the particulate absorption.

(3) Apparatus

Seawater samples were collected and analyzed from the upper 1700 m of the water column from 19 stations in (Table 4.21-1) during MR19-04 Leg 2 and 20 stations (Table 4.21-2) during MR19-04 Leg 3.

(i)   Inherent optical properties (IOPs)

The water absorbance and CDOM absorbance were measured using a LWCC-4100 (pathlength 102.9 cm) coupled with an Ocean Optics Maya2000Pro spectrophotometer and DH-Mini light source via 600 μm diameter solar resistant fibre optic cables. Data was converted to units of m^{-1} by the formula a_λ=2.303 x A$_\lambda$/1.029, where A$_\lambda$ is the wavelength specific absorbance. Particulate absorption values were calculated as the difference between unfiltered and filtered samples.

(ii)   Iodate

Iodate was measured using a simple spectrophotometric method (Jickells et al., 1988) based on the earlier work of Truesdale (Truesdale, 1978; Truesdale and Smith, 1979; Truesdale and Spencer, 1974) which has been adapted by us for use with small volumes (2 mL or less). Briefly sulfamic acid is added to lower the pH and destroy any nitrite that may interfere in the analysis, and after a suitable period of time (150 seconds), a 10% solution of KI is added which results in the following reaction:

$$IO_3^- + 5\ I^- + 6H^+ \downarrow 3I_2 + 3H_2O$$
$$I_2 + I^- \prod I_3^-$$
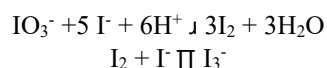
The resulting I$_3^-$ that is formed has two major absorption bands (288 and 350 nm) and we use these to quantify the iodate concentration in the sample. Previously for iodate, pathlengths of 5 or 10 cm have been used, for this work we employed an LWCC-3050 with a pathlength of 48.9 cm which allows then a higher precision analysis over the complete range of expected iodate concentrations but while still being in the linear range for the instrumental setup. The LWCC-3050 was setup with the same spectrophotometer and light source as described above for the IOP measurements, with the exception that 400 μm diameter solar resistant fibre optic cables were used instead.

(iii)   Urea

During MR19-04 we adapted existing methods using a single reagent (COLDER) (Alam et al., 2017) for dissolved urea with a low level approach using LWCC (Chen et al., 2015), applying it to small volume samples (2 mL or less) and removing the need for a 70° or 85° water bath by utilizing a thermostated dry bath (Fisher Scientific) instead. Both an LWCC-3050 and LWCC-3250 (pathlength 252 cm) were used for this work with the same optical setup as described above for the Iodate analysis. The use of a dry bath and small volume samples significantly reduces the risks in this analysis but does not completely eliminate them as sulfuric acid is still required in this procedure. Care was taken at all times to minimize contamination in the laboratory, particularly during filtration of the samples.

(4) Preliminary Results

All samples were analyzed onboard the ship during MR19-04 Leg 2 and 3, however all data should be considered preliminary as there are still post-processing corrections to be applied before the data sets are finalized.

(i)   Inherent Optical Properties

During Leg 2&3 of MR19-04 we measured 615 for Water absorbance and 688 samples for CDOM from 39 stations (Table 4.21-1 & 4.21-2). This data is complementary to the CDOM and FDOM data detailed elsewhere in this cruise report. CDOM data was collected over the wavelength range 250 to 800 nm and the full water column profile is shown for a_{325} in figure 4.21.1a, where there is a clear decreasing trend from north to south and from surface to deep during Leg 2. During Leg 3 the absorbance increased again slightly towards the south, with higher values in deeper waters (Figure 4.21.1b).
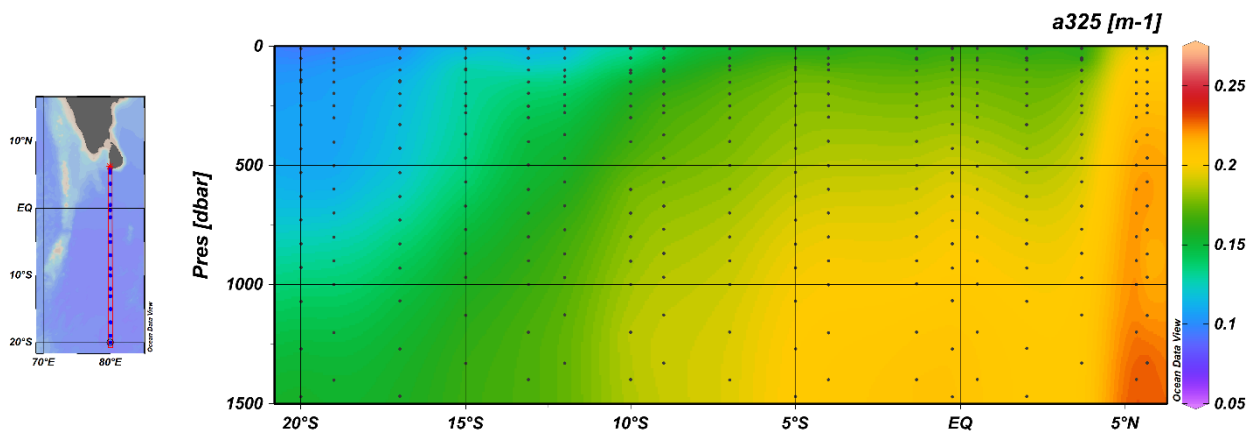
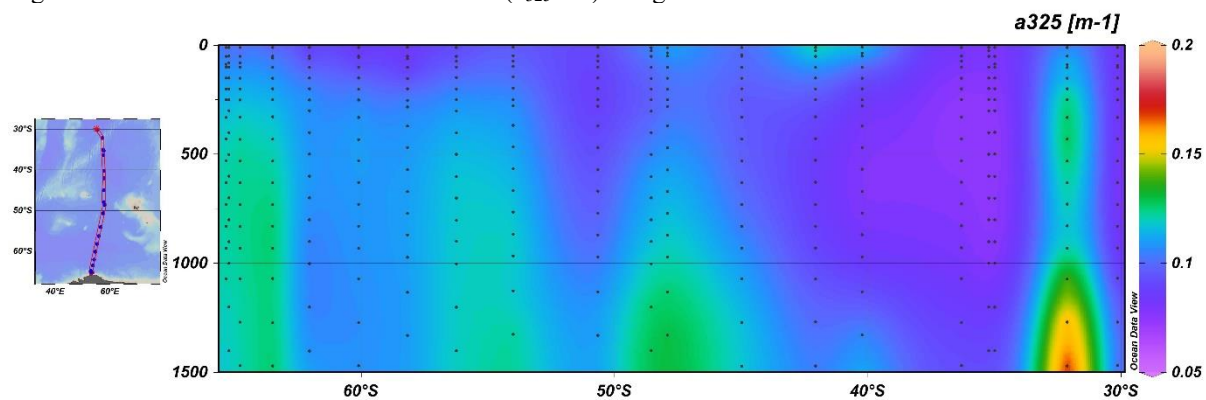Figure 4.21.1a: CDOM absorbance at 325 nm (a_{325} m^{-1}) along the I08N transect.

Figure 4.21.1b: CDOM absorbance at 325 nm (a_{325} m^{-1}) during Leg3

More informative however are values of the spectral slope (Helms et al., 2008) between 275 and 295 nm, $S_{275-295}$, (Figure 4.21.2) which indicate strong photo bleaching of equatorial surface waters and also the likely influence of subantarctic mode water (SAMW) and Antarctic intermediate water (AAIW) at the southern end of the I08N transect. As expected, there was no photo bleaching during the transect of Leg 3, as can be seen in Figure 4.21.2b. Higher values continue in saltier and warmer waters in the upper water column until 42° south, afterwards concentrations show low values throughout the water column. The particulate absorption data (not shown) requires further processing on land, including salinity corrections, as the particulate signal was very small with low signal to noise (small difference between two large values), as to be expected in a relatively oligotrophic environment. However, it was possible to discern the chlorophyll maximum at most stations from the chlorophyll absorption line height at 676 nm (data not shown) and this will be a focus of future work.
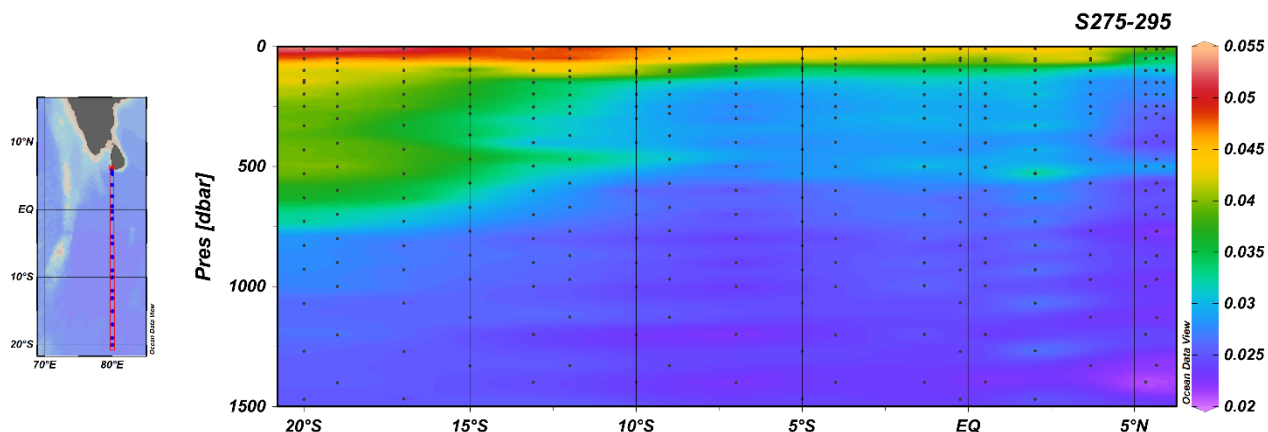
Figure 4.21.2a: CDOM Spectral Slope S$_{275-295}$ (nm^{-1}) along 80° E
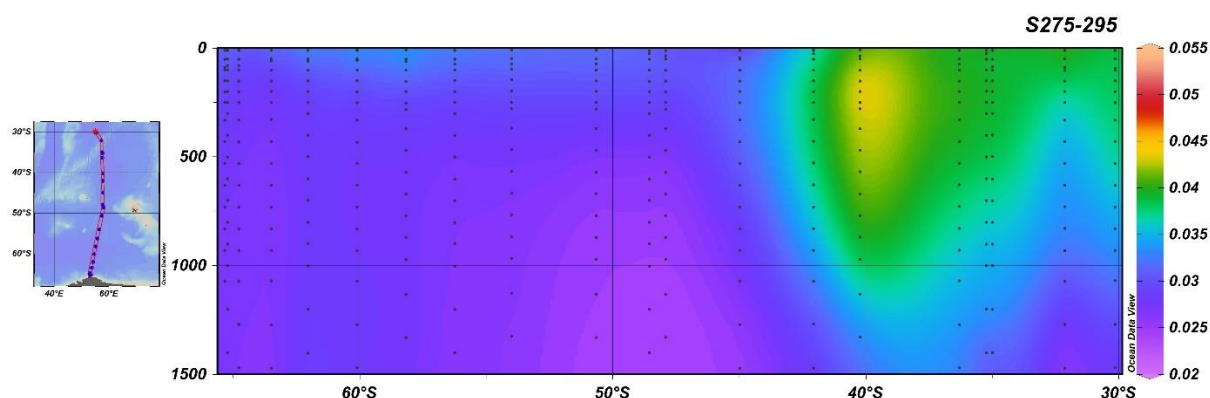

Figure 4.21.2b: CDOM Spectral Slope S$_{275-295}$ (nm^{-1}) along Leg3 of MR19-04

(ii)   Iodate

Iodate concentrations were measured in the top 1600 metres of the water column at 19 stations (Table 4.21-1) along the transect of Leg 2. As expected, iodate varied little in the deeper waters, at around 450 nM, with most of the variation seen in the upper 250 m (Figure 4.21.3b) where iodate is reduced to iodide via photochemical and biological processes. Lowest concentrations of iodate were found in the surface water at the northern end of the transect in the coastal waters of Sri Lanka. There is a possible indication of excess iodine (> 450 nM) in the water column along the Sri Lankan shelf zone, presumably input from bottom sediments underlying the low oxygen waters there. At many stations the iodate minimum was found at the surface (10 m depth) in line with the strong solar irradiation in this region but at some stations it was located at the deep chlorophyll maximum indicating biological reduction was also an important process.

During Leg 3 the concentrations increased in surface waters and were similar throughout the water column towards the end of the southward transect (Figure 4.21.3b).
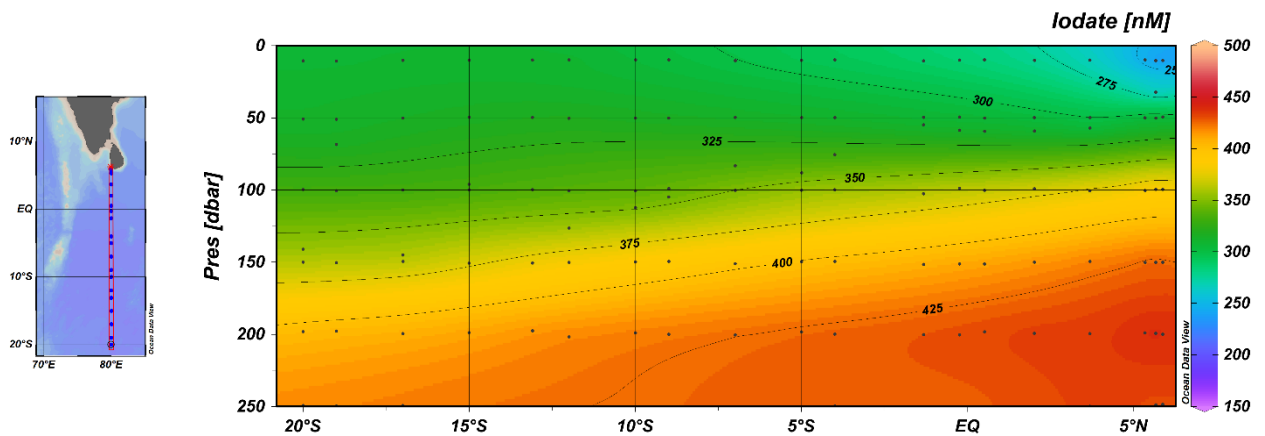
Figure 4.21.3a: Iodate (preliminary data) in the upper 250 m along the I08N transect.
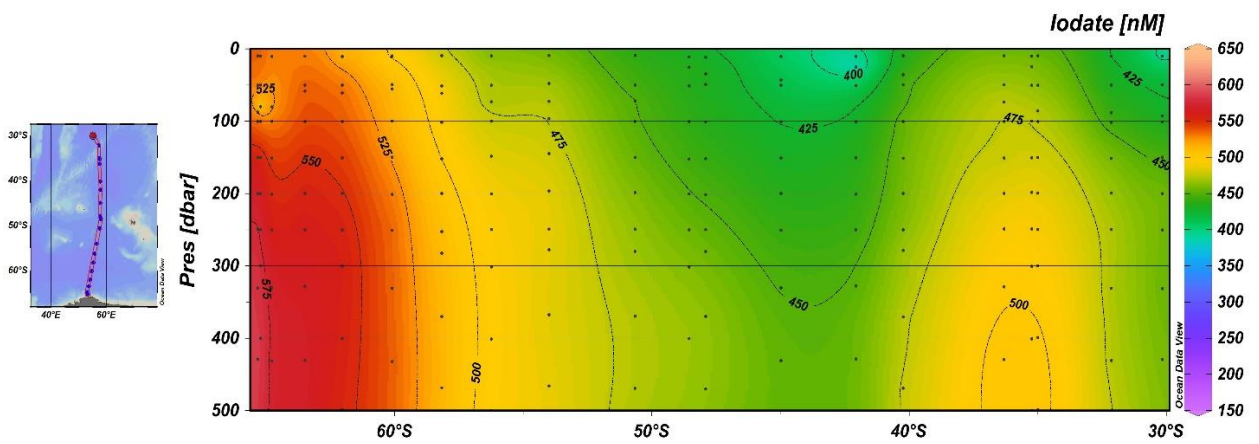

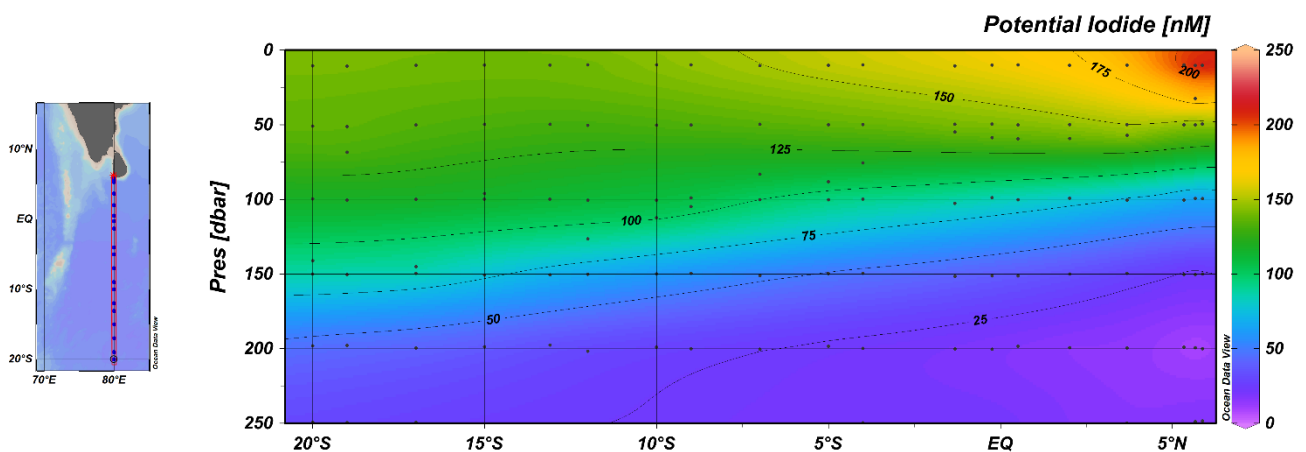Figure 4.21.3b: Iodate (preliminary data) in the upper 500 m along Leg3.

Figure 4.21.4: Potential Iodide (preliminary data) in the upper 250 m along the I08N transect.

As Iodine is quasi-conservative in seawater at approximately 450 nM for salinity 35, the difference from the total iodine due to iodate can be calculated and used as an estimate for the potential iodide concentration (Figure 4.21.4). It is assumed here that there is little dissolved organic iodine (DOI) present. As expected

the iodide concentrations are highest in the most productive waters at the Northern end of the transect and in the equatorial region but interestingly they do not decline through the oligotrophic region where the chlorophyll maximum was down to 140 m, this illustrates the photochemical conversion of iodate to iodide in the clear blue waters of this region. There is a gradual deepening of the iodide-cline moving south indicating slower re-oxidation of iodide back to iodate.

(iii)   Urea

Urea in the upper 250 m of Leg 2 in the water column is shown in Figure 4.21.5a and indicates higher values in the northern part of the transect across the Sri Lankan shelf along with slightly elevated concentrations around the equatorial region, whilst in the Southern part of the transect concentrations were uniformly low but still significantly above the detection limit (1-2 nM). During Leg 3 (Figure 4.21.5b) higher concentrations were detected at station 70 and 78, before also here low levels continued towards the south. We expected higher values for urea close to the polar front, however concentrations increased around 60 degree south and here especially in surface waters.
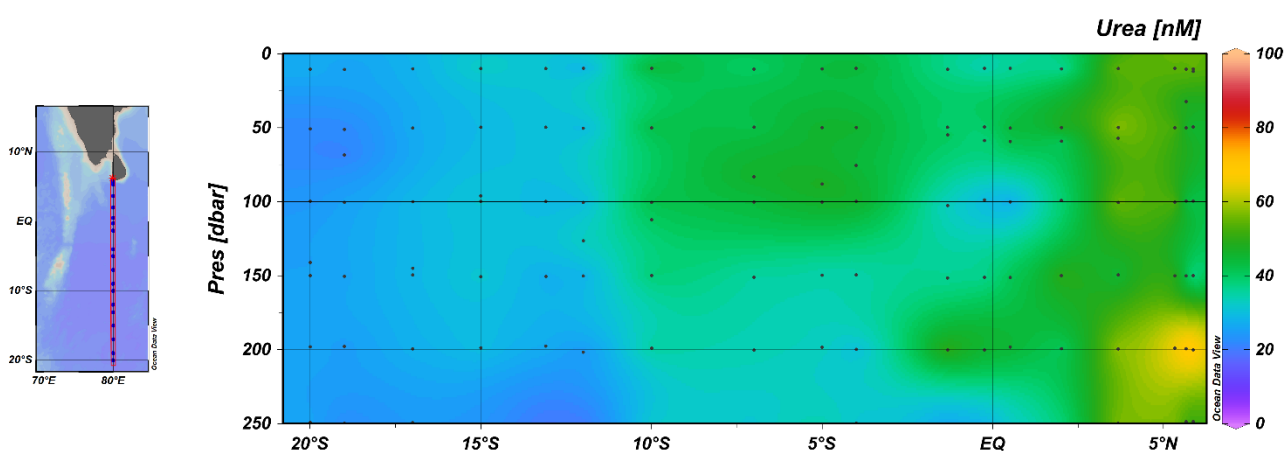

Figure 4.21.5a: Preliminary data for Urea (nM) in the upper 250 m along 80° E (preliminary data).
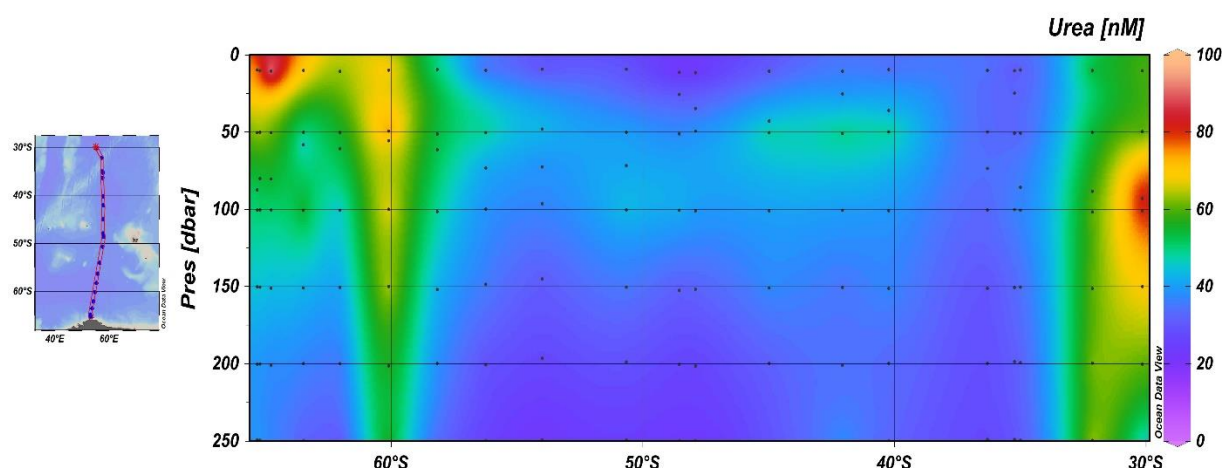

Figure 4.21.5b: Preliminary data for Urea (nM) in the upper 250 m along Leg3.

Please note that in out work we quantify urea in terms of moles of urea, as urea contains 2 nitrogen atoms it's nitrogen content is double that of the value we present, in the literature this sometimes causes confusion as it is not stated whether it is moles of urea or moles of N-urea. The monoxime reaction employed here will react with urea preferably but can also form a coloured complex with other molecules containing the ureido functional group ($R_1NH(CO)NHR_2$ - e.g. Citrulline, Allantoate and Allantoin) (Reay et al., 2019). Previous studies have shown that in the coastal ocean (Aminot and Kerouel, 1982), other ureido containing molecules are not likely to be present in significant amounts but this has not been verified

for low urea containing open ocean waters.

References

Alam, M.S., Casareto, B.E., Suzuki, Y., Sultana, R. and Suzuki, T., 2017. Optimization of dissolved urea measurements in coastal waters with the combination of a single reagent and high temperature. Journal of Oceanography, 73(2): 249-258.

Aminot, A. and Kerouel, R., 1982. Dosage automatique de l'urée dans l'eau de mer : une méthode très sensible à la diacétylmonoxime. Canadian journal of fisheries and aquatic sciences, 39: 174-183.

Baer, S.E. et al., 2019. Carbon and nitrogen productivity during spring in the oligotrophic Indian Ocean along the GO-SHIP IO9N transect. Deep Sea Research Part II: Topical Studies in Oceanography, 161: 81-91.

Bluhm, K., Croot, P., Wuttig, K. and Lochte, K., 2010. Transformation of iodate to iodide in marine phytoplankton driven by cell senescence. Aquatic Biology, 11(1): 1-15.

Bluhm, K., Croot, P.L., Huhn, O., Rohardt, G. and Lochte, K., 2011. Distribution of iodide and iodate in the Atlantic sector of the southern ocean during austral summer. Deep Sea Research Part II: Topical Studies in Oceanography, 58(25-26): 2733-2748.

Campos, M., Farrenkopf, A.M., Jickells, T.D. and Luther, G.W., 1996. A comparison of dissolved iodine cycling at the Bermuda Atlantic Time-Series station and Hawaii Ocean Time-Series Station. Deep-Sea Research Part Ii-Topical Studies In Oceanography, 43(2-3): 455-466.

Campos, M., Sanders, R. and Jickells, T., 1999. The dissolved iodate and iodide distribution in the South Atlantic from the Weddell Sea to Brazil. Marine Chemistry, 65(3-4): 167-175.

Chance, R., Baker, A.R., Carpenter, L. and Jickells, T.D., 2014. The distribution of iodide at the sea surface. Environmental Science: Processes & Impacts, 16(8): 1841-1859.

Chen, L., Ma, J., Huang, Y., Dai, M. and Li, X., 2015. Optimization of a colorimetric method to determine trace urea in seawater. Limnology and Oceanography: Methods, 13(6): 303-311.

Helms, J.R. et al., 2008. Absorption spectral slopes and slope ratios as indicators of molecular weight, source, and photobleaching of chromophoric dissolved organic matter. Limnology and Oceanography, 53: 955-969.

Jickells, T.D., Boyd, S.S. and Knap, A.H., 1988. Iodine Cycling in the Sargasso Sea and the Bermuda Inshore Waters. Marine Chemistry, 24: 61-82.

L'Helguen, S., Slawyk, G. and Le Corre, P., 2005. Seasonal patterns of urea regeneration by size-fractionated microheterotrophs in well-mixed temperate coastal waters. Journal of Plankton Research, 27(3): 263-270.

Mahajan, A.S. et al., 2019. Observations of iodine oxide in the Indian Ocean marine boundary

layer: A transect from the tropics to the high latitudes. Atmospheric Environment: X, 1: 100016.

Reay, M.K. et al., 2019. High resolution HPLC-MS confirms overestimation of urea in soil by the diacetyl monoxime (DAM) colorimetric method. Soil Biology and Biochemistry, 135: 127-133.

Saiz-Lopez, A. et al., 2011. Atmospheric Chemistry of Iodine. Chemical Reviews, 112(3): 1773-1804.

Schönhardt, A., Richter, A. and Burrows, J.P., 2016. TIBAGS: Tropospheric Iodine Monoxide and Its Coupling to Biospheric and Atmospheric Variables—a Global Satellite Study. In: D. Fernández-Prieto and R. Sabia (Editors), Remote Sensing Advances for Earth System Science: The ESA Changing Earth Science Network: Projects 2011-2013. Springer International Publishing, Cham, pp. 15-34.

Schonhardt, A. et al., 2008. Observations of iodine monoxide columns from satellite. Atmospheric Chemistry And Physics, 8(3): 637-653.

Sherwen, T. et al., 2019. A machine learning based global sea-surface iodide distribution. Earth Syst. Sci. Data Discuss., 2019: 1-40.

Thomalla, S.J. et al., 2011. Phytoplankton distribution and nitrogen dynamics in the southwest indian subtropical gyre and Southern Ocean waters. Ocean Sci., 7(1): 113-127.

Tian, R.C. et al., 1996. Iodine speciation: A potential indicator to evaluate new production versus regenerated production. Deep-Sea Research Part I-Oceanographic Research Papers, 43(5): 723-738.

Truesdale, V.W., 1978. The Automatic Determination of Iodate and Total-Iodine in Seawater. Marine Chemistry, 6: 253-273.

Truesdale, V.W. and Smith, C.J., 1979. A Comparative Study of Three Methods for the Determination of Iodate in Seawater. Marine Chemistry, 7: 133-139.

Truesdale, V.W. and Spencer, C.P., 1974. Studies on the determination of inorganic iodine in seawater. Marine Chemistry, 2(1): 33-47.

Table 4.21-1 Samples analyzed during MR19-04 Leg 2

Station	IOP Unfiltered	IOP Filtered	Urea	Iodate
2	6	11	13	12
5	6	17	18	17
7	4	18	18	18
12	8	18	18	18
17	9	18	18	18
22	8	18	18	18
25	8	18	18	18
29	13	18	18	18
36	18	18	18	18
38	18	18	18	18
42	18	18	18	18
46	17	17	18	18
48	18	17	18	18
52	18	18	18	18
54	17	17	17	17
58	18	18	18	18
62	18	18	18	18
66	18	18	18	18
68	18	18	18	18
Σ 19	Σ 258	Σ 331	Σ 336	Σ 334

Table 4.21-2 Samples analyzed during MR19-04 Leg 3

Station	IOP Unfiltered	IOP Filtered	Urea	Iodate
70	18	18	18	18
78	18	18	18	18
86	18	18	18	18
89	18	18	18	18
93	18	18	18	18
97	18	18	18	18
101	18	18	18	18
107	18	18	18	18
114	18	18	18	18
116	18	18	18	18
120	18	18	18	18
126	18	18	18	18
132	18	18	18	18

136	18	18	18	18
140	18	18	18	18
144	18	18	18	18
147	18	18	18	18
150	18	18	18	18
152	18	18	18	18
153	15	15	15	15
Σ 20	**Σ 357**	**Σ 357**	**Σ 357**	**Σ 357**

4.22 Radon (gamma-ray) sensor

(1) Personnel

Kiminori Shitashima (TUMSAT): Principal investigator

(2) Objective

Underwater in-situ gamma-ray measurement is important scientific priority for oceanography, especially for survey and monitoring of the concentration distributions of natural and anthropogenic gamma-ray. The sensor was applied to observe and monitor natural gamma-ray in the deep open ocean.

(3) Apparatus

A plastic scintillator is made from polystyrene that doped NaI(Tl) and it absorbs gamma-ray like as liquid or crystal scintillator. The plastic scintillator was coated by light-resistant paint and used as a part of pressure housing. Therefore, the sensor can expect high sensitivity in comparison with NaI(Tl) crystal sealed in a container because the plastic scintillator contacts seawater directly. This sensor consists of plastic scintillator, photomultiplier tube, preamplifier unit, high-voltage power supply, data logger and lithium-ion battery, and all parts are stored in a pressure housing. The sensor was installed to the CTD-CMS frame and in-situ data of radon was measured every 1 second during descent and ascent of the CTD-CMS system.

(4) Results

The vertical distributions of gamma-ray at the Indian Ocean were obtained by the sensor attached to CTD-CMS system. The sensor provided high intensity until 1000m depth, and the intensity gradually decreased till 2000m depth. Below 2000m depth, the sensor showed very low intensity.

4.23 pH/pCO₂ sensor

(1) Personnel

   Kiminori Shitashima (TUMSAT): Principal investigator

(2) Objective

   The measurement of pH in the marine system is important because the pH of seawater reflects the oceanic carbon cycles and the exchange of CO_2 between the atmosphere and the ocean. Furthermore, pH relates to and the biological and chemical processes occurring in the ocean. Concerning the global warming, change of pH and pCO_2 in seawater should preferably be observed continually in a long term and a wide area (vertically and horizontally) to monitor air-sea CO_2 exchange and oceanic carbon cycle. In-situ measurement with a sensor is the most suitable for such observations.

   The objective of this study is to develop high performance pH/pCO_2 sensor for in situ measurement in the deep sea and apply it for chemical oceanography

(3) Apparatus

   The in-situ pH sensor employs an Ion Sensitive Field Effect Transistor (ISFET) as a pH electrode, and the Chloride ion selective electrode (Cl-ISE) as a reference electrode. The ISFET is a semiconductor made of p-type Si coated with SiO_2 and Si_3N_4 that can measure H^+ ion concentration in aqueous phase. New ISFET-pH electrode specialized for oceanographic use was developed. The Cl-ISE is a pellet made of several chlorides having a response to the chloride ion, a major element in seawater. The electric potential of the Cl-ISE is stable in the seawater, since it has no inner electrolyte solution. The in-situ pH sensor has a quick response (less than a second), high accuracy ($\pm$0.003pH) and pressure-resistant performance. The pCO_2 sensor was devised to incorporate the above-mentioned newly developed in-situ pH sensor to measure the in-situ pCO_2 in seawater. The principle of pCO_2 measurement by the pCO_2 sensor is as follows. Both the ISFET-pH electrode and the Cl-ISE of the pH sensor are sealed in a unit with a gas permeable membrane whose inside is filled with inner electrolyte solution with 1.5 % of NaCl. The pH sensor can detect pCO_2 change as pH change of inner solution caused by permeation of carbon dioxide gas species through the membrane. An amorphous Teflon membrane (Teflon AF™) manufactured by DuPont was used as the gas permeable membrane. The in-situ (3,000m, 1.8ºC) response time of the pCO_2 sensor was less than 60 seconds. The diode on ISFET can measure the temperature of seawater simultaneously. ISFET and Cl-ISE are connected to pH converter circuit in the pressure housing through the underwater cable connector. The pressure housing includes pH converter circuit, A/D converter, data logger RS-232C interface and Li ion battery.

   Two pH/pCO_2 sensors were installed to the CTD-CMS, and in-situ data of pH and pCO_2 ware measured every 1 second during descent and ascent of the CTD-CMS. Before and after the observation, the pH sensor was calibrated using two different standard buffer solutions, 2-aminopyridine (AMP; pH 6.7866) and 2-amino-2-hydroxymethil-1,3-propanediol (TRIS; pH 8.0893) described by Dickson and Goyet, for the correction of electrical drift of pH data. In this cruise, the calibration of the pCO_2 sensor was conducted using two different seawaters, surface and deep seawaters which measured pCO_2 concentration, before and after the observation. The recorded data (pH, pCO_2, temperature) is stored in the data logger. After recovery of the sensor, the data is transferred from the data logger into a personal computer (PC) connected with RS-232C cable, and the in-situ pH and pCO_2 are calculated using calibration data of each standards in a PC.

(4) Results

   The vertical distributions of pH and pCO_2 measured by sensor showed general profiles of them, but temperature correction of the electrode was necessary. After finishing temperature correction of each electrodes on land laboratory, all data will be re-calculated.

4.24 Determination of iodine concentration and ^{129}I/I

Leg-2

December 27, 2019

Satoko Owari

Tokyo University of Marine Science and Technology (TUMSAT)

(1) Personnel
Satoko Owari (TUMSAT):　　　Principal investigator

(2) Objective
Iodine in natural environment has one stable isotope (^{127}I) and one long-lived radioisotope (^{129}I) with the half-life of 15.7 Myr. Huge amount of ^{129}I were released into the atmosphere and the ocean after accidents of nuclear power plant in Fukushima and Chernobyl, ^{129}I/I in the ocean environment is increasing in last few decades. However, the iodine concentration and isotopic ratio especially in deep sea (over 4000 m below the sea level) are not well researched.

(3) Apparatus
Seawater samples were collected from station 7, 27, 38, 48, 58, 66 with 0, 10, 50, 100, 300, 500, 1000, 2000, 3000, 4000, 5000 meters below the sea level respectively.

Iodine in seawater is incorporated and concentrated by algae because of iodine strong biophilic character. Collected seawater samples were filtered by 0.22 μm mesh of Millipore filter immediately to avoid increase of iodine concentration released from algae after dying. The total iodine concentration of filters will be also measured.

Iodine is a redox sensitive element forming a wide variety of inorganic compounds and the most common inorganic forms of iodine are iodide (I^-) and iodate (IO_{3-}) in seawater. The concentration and isotopic ratio for iodide and iodate will be determined separately.

(4) Results
The determination of iodide and iodate concentration will be conducted by Inductively Coupled Plasma Mass Spectrometry and Ion Chromatography and the determination of isotopic ratio of iodide and iodate will be conducted by Accelerator Mass Spectrometry.

Leg-3

January 24, 2020

Yuichiro Kumamoto

Japan Agency for Marine-Earth Science and Technology (JAMSTEC)

(1) Personnel
Yuichiro Kumamoto

Japan Agency for Marine-Earth Science and Technology

(2) Objective
Determination of concentration of ^{129}I dissolved in seawater in the western Indian Ocean.

(3) Sample collection
The sampling stations and number of samples are summarized in Table 4.24.1. All samples for ^{129}I (total 182 samples) were collected at 6 stations using the 12-liter Niskin-X bottles. The seawater sample was siphoned into a 1-L plastic bottle after two-time rinsing.

Table 4.24.1 Sampling stations and number of samples for carbon isotopic ratios.

Station	Lat. (S)	Long. (E)	Sampling Date (UTC)	Number of samples	Max. Pressure (dbar)
074	30-49.31	55-52.43	2020/01/01	31	4489
095	39-14.74	57-41.49	2020/01/07	33	5229
105	43-59.99	57-45.52	2020/01/09	31	4712
124	52-54.29	56-50.00	2020/01/15	28	4346
142	61-05.10	54-23.86	2020/01/19	33	5222
150	64-46.99	52-59.27	2020/01/21	26	3480
			Total	182	

(4) Sample preparation and measurements

Iodine in the seawater samples is extracted by the solvent extraction technique. Extracted iodine is then precipitated as silver iodide by the addition of the silver nitrate. Iodine isotopic ratios (^{129}I/^{127}I) of the silver iodide are measured by the Accelerator Mass Spectrometry. To evaluate the ^{129}I concentration in the seawater samples, iodine concentration (^{127}I) will be measured by the inductively coupled plasma mass spectrometry and/or the voltammetry.

(5) Data archives

The data obtained in this cruise will be submitted to the Data Management Group of JAMSTEC and will be opened to the public via "Data Research System for Whole Cruise Information in JAMSTEC (DARWIN)" in the JAMSTEC web site.

4.25 Sound Velocity Sensor
January 31, 2020

(1) Personnel
        Hiroshi Uchida (JAMSTEC)

(2) Objective
    The objective of this study is to estimate absolute salinity profiles from sound velocity data with temperature and pressure data from CTD, and to evaluate the algorithm to estimate absolute salinity anomaly provided along with TEOS-10 (the International Thermodynamic Equation of Seawater 2010) (IOC et al., 2010).

(3) Instruments and method
    Sound velocity profiles were measured at the CTD casts by using a velocimeter (MiniSVP [serial no. 49618], Valeport Ltd., Devon, United Kingdom). The sound velocity sensing elements are a ceramic transducer (signal sound pulse of 2.5 MHz frequency), a signal reflector, and spacer rods to control the sound path length (10 cm), providing a measurement at depths up to 6,000 m. The velocimeter was attached to the CTD/water sampling frame and level of the sound path of the velocimeter was same as that of the CTD temperature sensors. Sound velocity data were stored in the velocimeter at a sampling rate of 8 Hz. Although temperature and pressure data were also measured by the velocimeter, only sound velocity data were combined with the CTD temperature and pressure data to estimate absolute salinity.
    Absolute salinity can be back calculated from measured sound velocity, temperature and pressure and will be calibrated in situ referred to the absolute salinity data measured by a density meter for water samples.
    Sound velocity data was not obtained at the station 016 due to misoperation. A part of the sound velocity data was lacking due to low voltage of the battery at the following stations: 029, 034, 037, 038, 043, 045-049, 094-101, 106-112, and therefore the data was not available for these stations. Data near the surface (~50 m) was lacking for the stations 103, 104 and 105.
    The sound velocity data were compared with sound velocity calculated from the CTD data (Fig. 4.25.1). Note that the velocimeter was not calibrated in situ.

(4) Reference
IOC, SCOR and IAPSO (2010): The international thermodynamic equation of seawater – 2010: Calculation and use of thermodynamic properties. Intergovernmental Oceanographic Commission, Manuals and Guides No. 56, UNESCO (English), 196 pp.

(5) Data archive
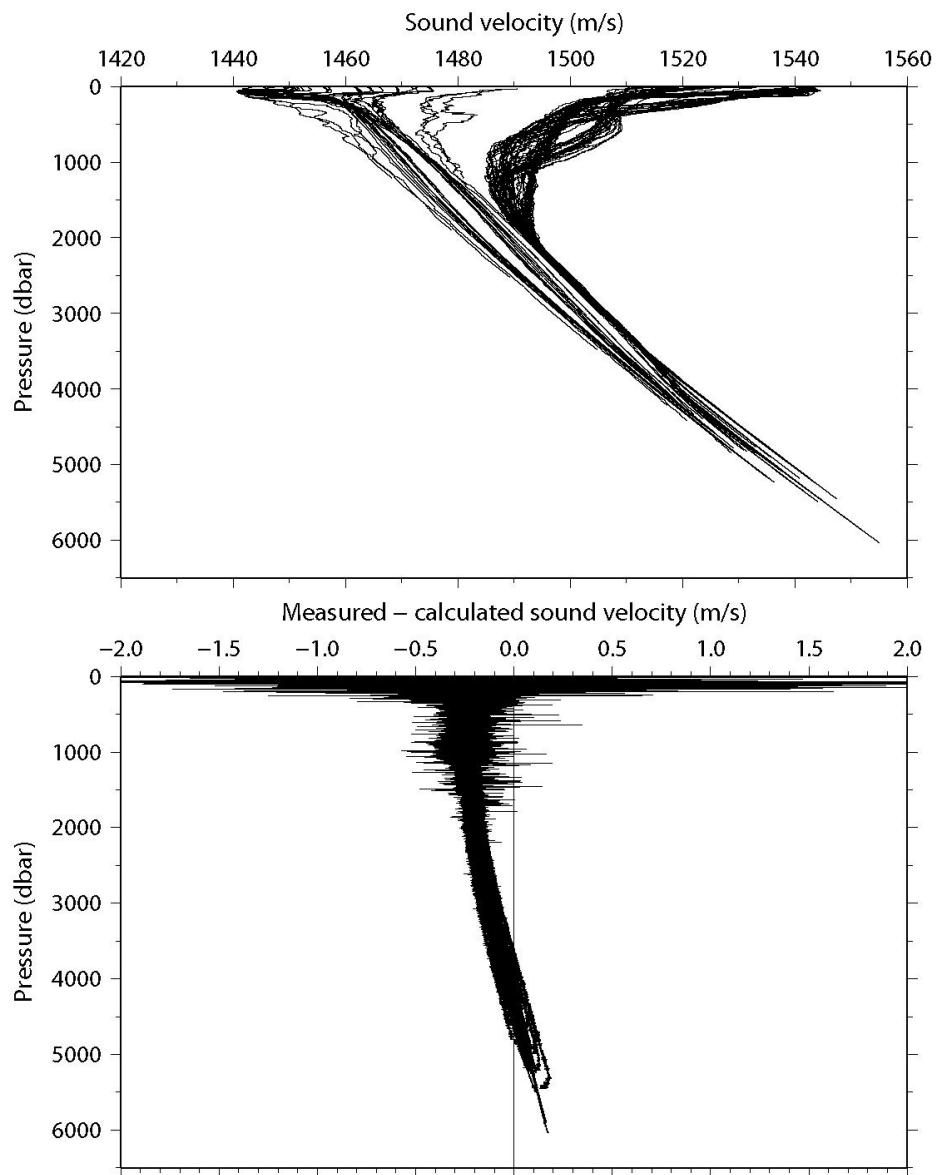   These obtained data will be submitted to JAMSTEC Data Management Group (DMG).

Figure 4.25.1. Vertical profiles of measured sound velocity (upper panel) and sound velocity differences between measured and calculated from the CTD data (lower panel).

4.26 Refractive Index Density Sensor
February 6, 2020

(1) Personnel
   Hiroshi Uchida (JAMSTEC)
   Yosaku Maeda (JAMSTEC)

(2) Objective
   The objective of this study is to estimate density (or absolute salinity) profiles from refractive index data with temperature and pressure data from CTD, and to evaluate the algorithm to estimate absolute salinity provided along with TEOS-10 (the International Thermodynamic Equation of Seawater 2010) (IOC et al., 2010).

(3) Instruments and method
   The interference method is one of the most sensitive methods for measuring the refractive index of seawater. A state-of-the-art density sensor was developed for seawater measurements based on measuring the refractive index by the interference method (Uchida et al., 2019). The temperature in the pressure-tight housing was measured by a temperature logger (model Duet T.D. deep [serial no. 095974], RBR Ltd., Ottawa, Canada) at an interval of 1 s to correct for the temperature dependency of the spectroscopic unit (model SI-F80, Keyence Co., Osaka, Japan). The density measuring cell was the prototype number 2.
   The density sensor output was low-pass-filtered with a half power gain at 1 s, and was stored at an interval of 0.0217 s through the Serial Data Uplink of the CTD system. An external power source (56 D size alkaline battery pack) was used to turn the density sensor on. The density sensor was used at all CTD casts in the legs 2 and 3. The temperature data in the pressure-tight housing was not obtained at the stations 070 and 071 because the leg 3 started one day earlier than the initial schedule.
   Intensity of the interference light (usually around 170) was greatly reduced lower than 100 at a part of stations 075, 076, and 077. Therefore, the measuring cell and the pressure-tight glass window were cleaned after the station 077.
   The density sensor data were compared with the density data measured by the vibrating-tube density meter (Fig. 4.26.1). The density data was calculated from TEOS-10 by using the measured density salinity, CTD temperature and CTD pressure.

(4) References
IOC, SCOR and IAPSO (2010): The international thermodynamic equation of seawater – 2010: Calculation and use of thermodynamic properties. Intergovernmental Oceanographic Commission, Manuals and Guides No. 56, UNESCO (English), 196 pp.
Uchida, H., Y. Kayukawa and Y. Maeda (2019): Ultra high-resolution seawater density sensor based on a refractive index measurement using the spectroscopic interference method. Sci. Rep., doi:10.1038/s41598-019-52020-z.

(5) Data archive
   These obtained data will be submitted to JAMSTEC Data Management Group (DMG).
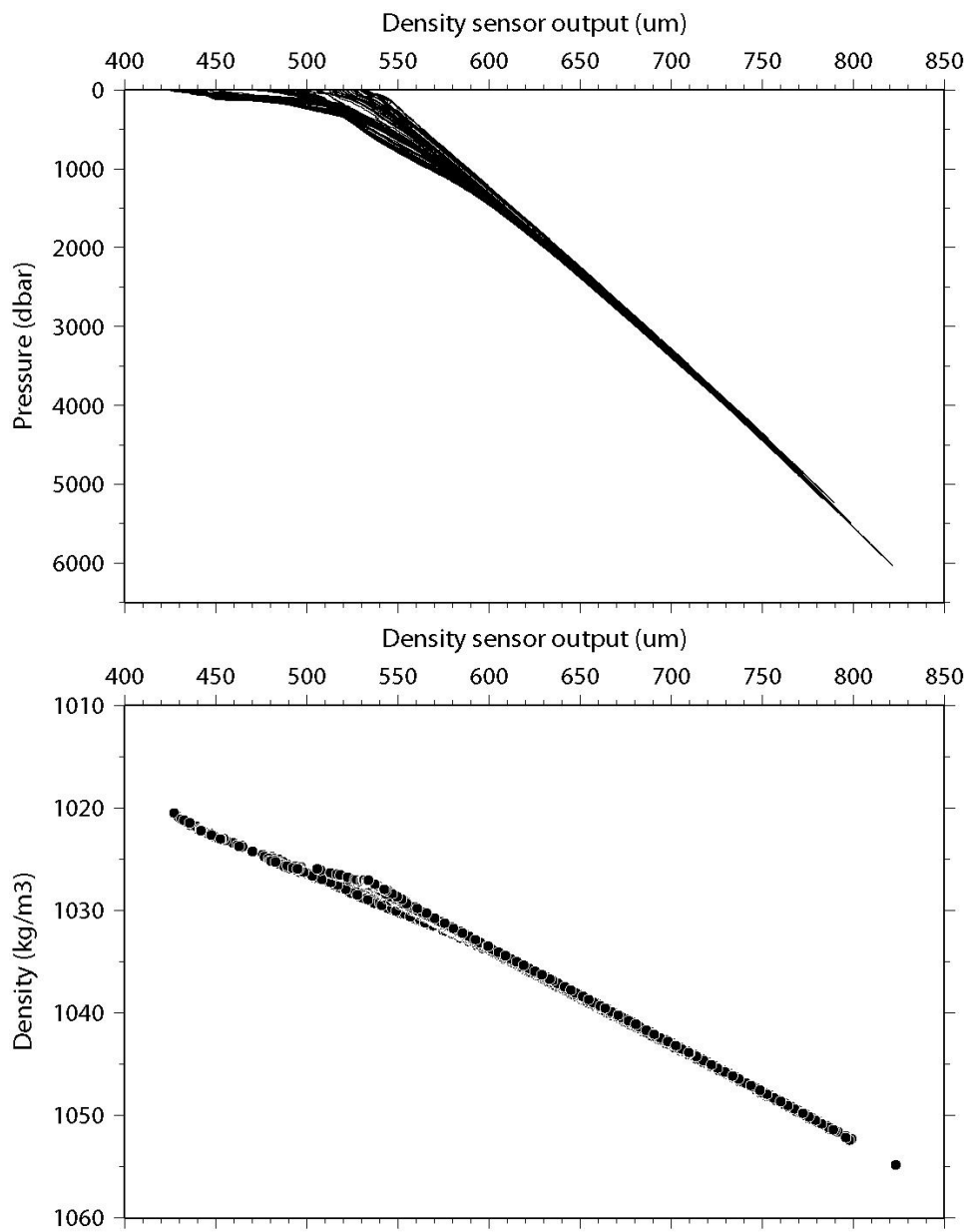
Figure 4.26.1. Vertical profiles of the density sensor output (upper panel) and comparison with the density data measured by the vibrating-tube density meter (lower panel).

4.27 Expendable Conductivity Temperature Depth profiler (XCTD)

(1) Personnel

        Katsuro Katsumata (JAMSTEC)
        Kazuho Yoshida (NME)
        Wataru Tokunaga (NME)
        Satomi Ogawa (NME)

(2) Objective

    With such restrictions as weather and shiptime, CTD/sampling observation were not performed at some stations and substituted with XCTD observations. At some CTD stations, XCTD-CTD side-by-side deployments were performed in order to calibrated the XCTD data in nearby and other stations following the method of Uchida *et al.* (2011).

(3) Insturumentation

    The XCTDs used in this expedition were XCTD-4 and the deck unit was MK-150N, both from Tsurumi-Seiki Co., Ltd., Yokohama Japan.The manufacturer's specification of the accuracy is ± 0.03 mS/cm, $\pm 0.02°C$ for conductivity and temperature, respectively. Depth is estimated by the elapsed time (seconds) from entry in to water as $Z(m) = at - bt^2$ with a=3.68081 (m/s) and b=4.7$\times$10^{-4}(m/s^2). The manufacturer's speciication of the accuracy for depth is the greater of 5 m or 2%.

(4) Deployments

    Station numbers in the 400's are XCTD only stations. Otherwise, the XCTD were deployed side-by-side to the CTD casts which the station numbers designate. In a side-by-side deployment, an XCTD was deployed as the CTD passed approximately 250 dbar downcast. XCTD deployments were mostly performed from Auto Launcher. Due to the unfavourable wind direction, we used a hand launcher at some side-by-side stations. The Station name in the table below followed by 'H' designates those deployments with hand launcher.

    The XCTD cast at Station 132 was misoperated and data from the upper 10 m were lost. The data were not used in the analysis.

Station	Date (UTC)	Time (UTC)	Latitude (deg-min)	Longitude (deg-min)	Depth [m]	SST [deg-C]	SSS [PSU]	Probe S/N
401	7/01/2020	8:36	-39:30.1462	57:42.8	5089	16.595	34.864	18117711
96	7/01/2020	10:17	-39:44.9476	57:43.5	5039	17.263	35.307	18117712
402	7/01/2020	14:18	-40:00.0431	57:44.3	4997	17.729	35.47	18117709
403	7/01/2020	21:01	-40:28.7446	57:44.9	4897	15.955	35.185	18117710
404	8/01/2020	2:47	-40:55.4518	57:44.7	4873	17.008	35.4	18117713
99H	8/01/2020	4:30	-41:09.6601	57:44.6	4889	17.06	35.472	18117714
405	9/01/2020	2:51	-42:46.2453	57:44.5	4760	15.244	35.058	18117715
103H	9/01/2020	4:42	-42:59.8214	57:43.9	4748	10.908	33.818	18117720
406	9/01/2020	9:25	-43:14.9899	57:44.4	4735	10.435	33.827	18117719
407	9/01/2020	15:15	-43:44.9967	57:45.2	4674	10.974	33.811	18117716
408	9/01/2020	21:47	-44:14.9936	57:46.0	4600	11.552	34.013	18117717
106	9/01/2020	23:29	-44:29.9881	57:46.4	4590	11.159	34.074	18117718
409	10/01/2020	3:26	-44:45.0021	57:46.8	4553	9.643	33.848	18117724
410	10/01/2020	10:05	-45:15.0196	57:47.6	4492	7.891	33.695	18117727
411	10/01/2020	16:24	-45:43.0525	57:46.7	4444	8.141	33.817	18117730
126	16/01/2020	5:40	-54:01.2103	56:30.0	3514	3.27	33.857	18117721
412	16/01/2020	10:50	-54:34.6886	56:20.1	4373	3.136	33.873	18117722
413	16/01/2020	14:17	-55:07.9922	56:10.2	3401	3.266	33.849	18117723

414	16/01/2020	17:32	-55:41.6559	56:02.3	3231	2.183	33.917	18117725
132H	17/01/2020	0:42	-56:15.0812	55:50.1	4765	1.926	33.893	18117728
137H	18/01/2020	8:31	-58:40.0252	55:07.1	5172	1.124	33.653	18117726
151	21/01/2020	18:43	-65:06.2154	53:01.0	2504	-0.195	33.727	18117729
415	22/01/2020	5:44	-65:21.9704	53:14.1	1318	-0.211	33.548	18117731
416	22/01/2020	6:05	-65:21.0914	53:14.8	1450	-0.363	33.533	18117732

(5) Calibration

The method employed here is that described in Uchida *et al*. (2011). We expect the biases in temperature and fallrate are common to all probes used in this cruise.

After smoothing and correcting the conductivity temporal delay, the comparison of fall rate from 7 side-by-side CTD casts suggests an fall rate error of -0.02 ms^{-1} in the terminal velocity, although there are some scatter amongst stations in the fall rate correction which maximised the correlation between the band-passs-filtered CTD and XCTD temperature profiles (Fig.4.27.1). The scatter gives an impression that our expectation of uniform fallrate bias was optimistic. In fact, the grounding depths at stations 415 and 416 were respectively 1318 and 1450 m, estimated from the density corrected multibeam echo sounder. The XCTD's recorded 1319.67 and 1474.64 m, respectively, as the deepest valid measurement, were corrected to 1312 and 1465 m, respectively.

When the depth bias is corrected, the temperature difference between side-by-side CTDs and XCTDs are approximately 0.02 $\pm$ 0.005°C for deep layers (z > 1800 m). See Fig.4.27.2.This positive bias is subtracted from all measurements.

For salinity, it is likely that the bias is different from probe to probe. If a tight TS relationship common to a side-by-side station and surrounding XCTD only stations exists within the depth of XCTD reach, it is possible to determine the probe-dependent bias, but such relationship could not be found. We therefore use the TS diagram below 1000 m from the side-by-side casts to estimate the salinity bias common to all probles used in thie cruise. We identify a part of the TS curve which is smooth and shows one-to-one relationship between T and S. Namely, between 2.6 and 3.0°C (station 96); 4.5 and 6.5°C (station 99); 2.4 and 2.7°C (station 103); 2.4 and 2.7°C (station 126); 1.4 and 2.2°C (station 126); 0.8 and 1.6°C (station 137); and 0.12 and 0.22°C   (station 151). Depth corretion and temperature bias correction have been applied to the XCTD data. The resultant salinity bias is +0.0150 $\pm$ 0.006. This positive bias is subtracted from the XCTD salinity.

 (4) Data archive

These obtained data will be submitted to JAMSTEC Data Management Group (DMG).

References:

Uchada, H., K. Shimada, T. Kawano, 2011, A method for data processing to obtain high-quality XCTD data, *Journal of Atmospheric and Oceanic Technology,* **28,** 816−826, doi:10.1175/2011JTECHO795.1
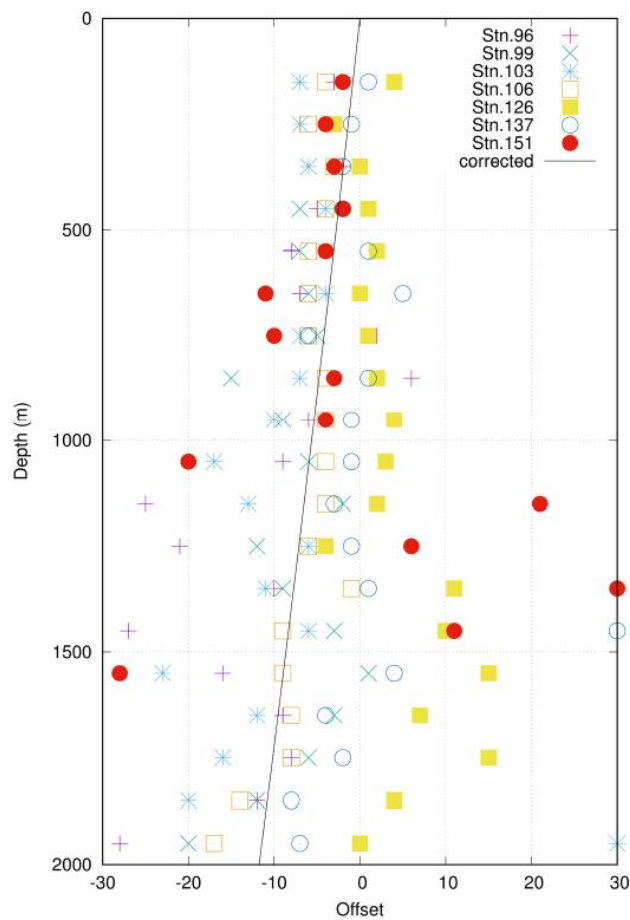
Fig.4.27.1: Offset in meters needed to maximize correlation between the band-pass-filtered XCTD and CTD temperature in side-by-side observations.
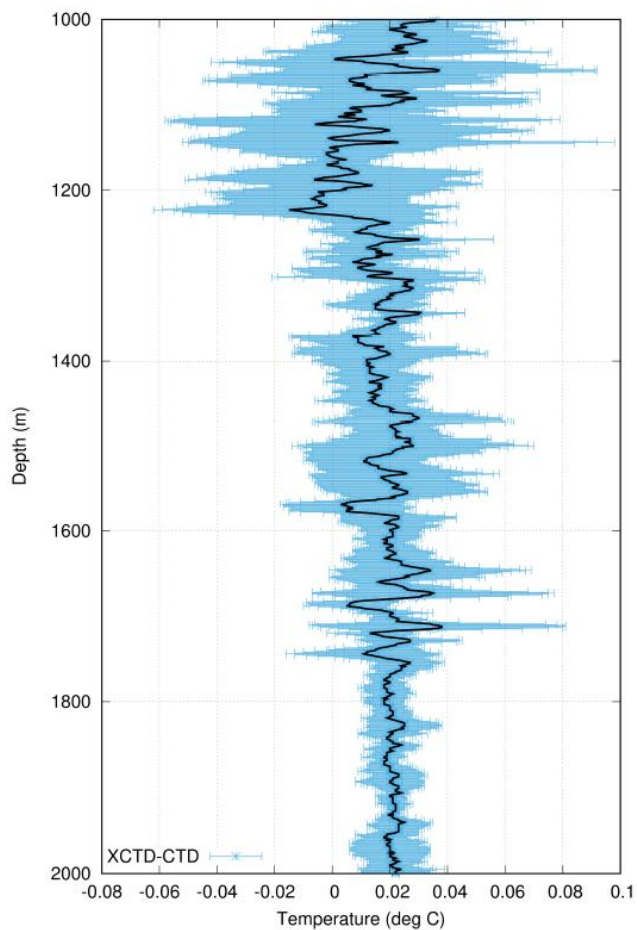

Fig.4.27.2: After depth correction, mean (black) and standard deviation (blue) of difference between XCTD and CTD in temperature for 7 side-by-side observations.

4.28 RBR Optode Testing
January 31, 2020

(1) Personnel
        Hiroshi Uchida (JAMSTEC)
        Mark Halverson (RBR LTD)
        Jon Taylor (RBR LTD)

(2) Objective
    The objective of this study is to evaluate the RBR optodes by comparing with the CTD/water sampling data.

(3) Instruments and method
    RBR Ltd. (Ottawa, Canada) designs and manufacturers self-contained CTDs and OEM sensors, and over the last few years has been developing instruments for deep applications (e.g. Argo and Deep Argo floats). In this study, three RBR TDs (RBR Concerto) with optodes (RBR Coda ODO fast) (Table 4.32.1) were tested in legs 2 and 3 by attaching the instruments to the CTD/water sampling frame (pressure and oxygen sensor downward). Height of these sensing elements from the CTD sensor is about 30 cm. These sensor data were obtained at a sampling rate of 16 Hz for pressure and temperature and 1 Hz for oxygen. In leg 2, the data were obtained at all CTD stations except for the stations in the EEZ of Sri Lanka (station 001 to 015). In leg 3, the data were obtained only at the water sampling stations to save the internal batteries. Data for station 103 for serial no. 060661 and for stations 99, 101, and 103 for serial no. 060663 were not obtained due to the battery's dead.
    The ODO oxygen data were compared with the bottle-sampled oxygen data at the bottle firing stops (Fig. 4.28.1). Note that the time-dependent pressure-induced hysteresis of the ODO sensors was not corrected in this comparison.

Table 4.28.1. List of serial number of the RBR TD/ODOs used in this cruise.

Serial no. of TD	Serial no. of ODO	Depth rating
060661	202900	6,000 m
060663	202901	6,000 m
060664	93146	6,000 m

(4) Data archive
    These obtained data will be submitted to JAMSTEC Data Management Group (DMG).
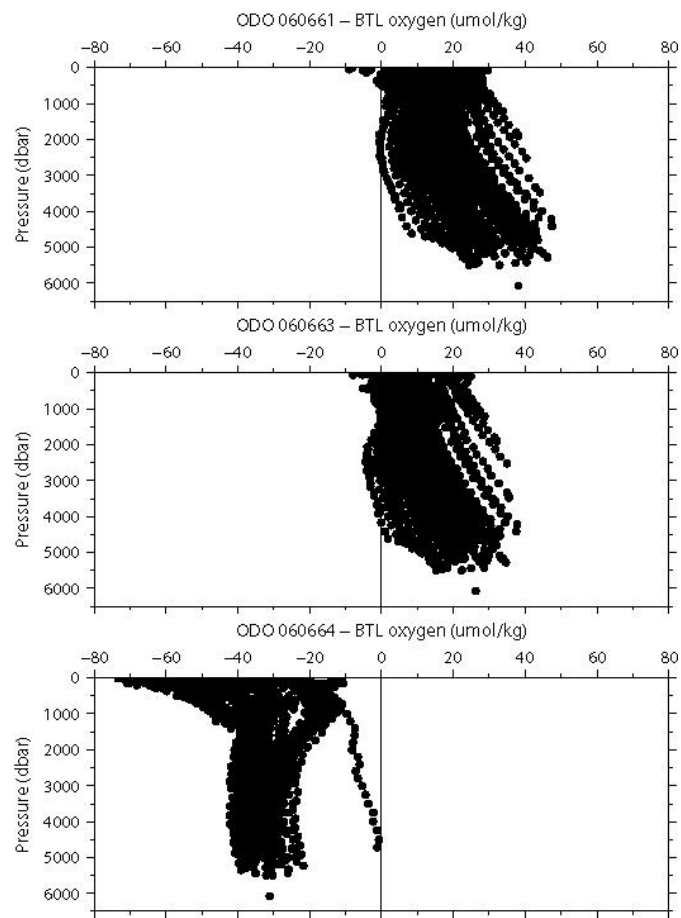
Figure 4.28.1. Oxygen difference between the ODO optodes and bottle-sampled oxygen.

141

4.29 Carbon sampling and HPLC/POC for SOCCOM project

(1) Personnel:

Melissa Miller (Scripps Institution of Oceanography)	onboard, leg 3
Andrew Meyer (University of Washington)	setup in Port Louis
Lynne Talley (Scripps Institution of Oceanography)	Principal Investigator
Steven Riser (University of Washington)	Principal Investigator
Ken Johnson (Monterey Bay Aquarium Research Institute)	Principal Investigator

(2) Objective:

The SOCCOM (Southern Ocean Carbon and Climate Observations and Modeling) project, a U.S. project sponsored by NSF, deploys autonomous biogeochemical floats to study the Southern Ocean and its impact on the climate. Eight SOCCOM floats were deployed during leg 3. SOCCOM floats include sensors measuring nitrate, pH, fluorescence, backscatter, oxygen, salinity, temperature, and pressure. Deployments corresponded with CTD casts sampled for the usual GO-SHIP suite of hydrographic parameter in order to calibrate each float's sensors. Niskin bottle samples were taken at various depths between the surface and 2000 meters, with samples sent back to the United States for analysis on shore. The floats were adopted by different schools around the world as part of the outreach program "Adopt-a-float". Each class named the float and received the details and pictures of their deployment from Melissa Miller, via SOCCOM personnel onshore George Matsumoto (MBARI). Together with their teachers, the students will follow the data of the float, which can be easily downloaded and plotted at the website www.mbari.org/science/upper-ocean-systems/chemical-sensor-group/soccomviz

As part of this outreach program, blog post were written by Melissa Miller and posted by George Matsumoto.

https://soccomatsea.blogspot.com/2020/01/rv-mirai-expedition-dec-30-2019-feb-10.html

(3) Apparatus:

All eight were UW-modified Teledyne Webb Apex floats with CTDs and added sensors for nitrate, pH, and oxygen. Six also had FLBB bio-optical sensors (fluorescence and backscatter). Those six were ballasted for subtropical waters, with the additional two deployed in sub-polar regions including ice-avoidance software. Andrew Meyer checked the floats in Port Louis, Mauritius before the cruise and all were deemed in good working order.

The floats have a 10 day cycle. After an initial test dive, the floats descend to a parking depth of 1000m, and then drift for 10 days with the ocean currents; after the 10 day drift, the floats dive to 2000m and then ascend to the surface, during which data are measured and saved. The 2000m-surface data profiles are then sent to shore via Iridium Satellite communication, using an antenna located at the top of the float. The floats that end up under ice will store the collected measurements until they can get free from the ice and send all data via satellite.

Each of these floats was self-activating, so no initial operations where required before their deployment to activate them. The windows of the nitrate sensor and FLBB (if applicable) were cleaned by Melissa Miller just before deployment using lens wipes, DI water, and lens paper.

After recovering the CTD, the ship moved off station at a speed of 1-2 knots. Float deployments were undertaken from the lower back deck using an arm to kept the float away from the side of the ship. Ship's crew connected a cable with a spring hook to the hole in the ring of the float and lowered via a line on a pulley connected to the arm. A second line was used to guide the bottom of the float, and removed when the float was about halfway to the water. The hook and line were disconnected once the float was on the ocean surface. Melissa Miller was present for every deployment.

Optical (HPLC/POC) samples were taken from Niskin bottles on CTD casts performed just before each deployment. Depths always included a surface bottle (~5m) and one at the chlorophyll maximum. When extra Niskins were possible, a third depth near the bottom of the mixed layer was added. All HPLC and POC samples were taken by Melissa Miller. The samples were filtered immediately (or after a short delay, in which case they were refrigerated) in the wet lab by Melissa Miller. Filters were flash-frozen in a dewar of liquid nitrogen and then stored in the -80C freezer. They will be shipped in a liquid-nitrogen charged dry shipper from Singapore. POC samples are analyzed in Dr. Lihini Aluwihare's lab at SIO and HPLC samples are analyzed at NASA's Goddard Space Flight Center.

pH/alkalinity samples were taken from Niskin bottles between the surface and 2000m on the eight stations immediately preceding the float deployments. Water was collected into 500ml glass bottles by the

JAMSTEC/MWJ team and poisoned with mercuric chloride by Melissa Miller before being sealed. The samples will be shipped from Singapore to the US for analysis by Dr. Andrew Dickson's lab at SIO. The SOCCOM team will use data from the other samples taken and analyzed onboard as part of the GO-SHIP program to validate the floats' sensors, including salts, alkalinity, dissolved inorganic carbon, nitrate, and oxygen. Data from the JAMSTEC fluorometer and turbidity sensors mounted on the CTD rosette will also be used for the validation of the FLBB sensors on the float. A dark value was obtained for the turbidity sensor by applying black electrical tape and putting the sensor in a bucket of water after the completion of science stations.

(4) Performance:
All eight floats were deployed successfully. Operations were done in sea states ranging from calm to stormy, and all were performed safely. Many thanks to the captain, chief officer, and the deck team for the smooth operations.
Only one deployment gave a cause for concern, though it turned out not to damage the float or sensors. The launch itself went fine, with the float released on the surface. At that moment, the ship rode a swell in such a way that the float was pulled under the ship and out of sight for 2-3 seconds. The float then rocketed out on the next wave and behaved normally, drifting on its side for a time and then rotating to be straight up and down. The concern from the chief scientist, captain, and chief officer after this event was appreciated and it was a relief to receive word 24 hours later that the float and all sensors were fine.
Niskins were tripped on the fly on station 126 (float 18013) due to worsening weather. All others included 30 second stops at each depth before Niskins were fired.
The ship itself is a great platform for science. There is sufficient lab space and facilities such as refrigerators, freezers, water, and power. The sampling team is efficient and the onboard analysis first rate.
Comforts such as a well-maintained gym and excellent food were much appreciated.
From start to finish, SIO's participation in this cruise was well accommodated by Chief Scientist Katsuro Katsumata He answered endless questions before, during, and after sailing, and helped with language translations onboard.
Yuichiro Kumamoto and Yasuhiro Arii facilitated procurement of mercuric chloride.

(5) Results:
Data from the CTD and other sensors mounted to the rosette was collected from the data server, along with preliminary bottle data. The final data set as submitted to CCHDO will be used to validate the sensors on the floats during their initial cast, and will contribute to the global carbon data set that is used for ongoing calibration of biogeochemical Argo floats over their full lifetimes.

Data sets were returned from each float within 24 hours of deployment (plots below), and every 10 days thereafter. Data will be posted online as it is collected.
http://soccom.princeton.edu/content/float-data

Known issues: On floats 17898, 18821, and 18994, pH data shows an offset at 1000m as the pump switches to continuous mode. This begins to even out from second profile on. Possible contamination in the pH cell that gets washed out when the pump runs more.
18082: no oxygen data, sensor not working for unknown reasons. Unlikely to have been caused by handling or deployment.
18864: nitrate sensor inadvertently turned off. Turned on after 2nd profile. Will be present from 3rd profile onwards.
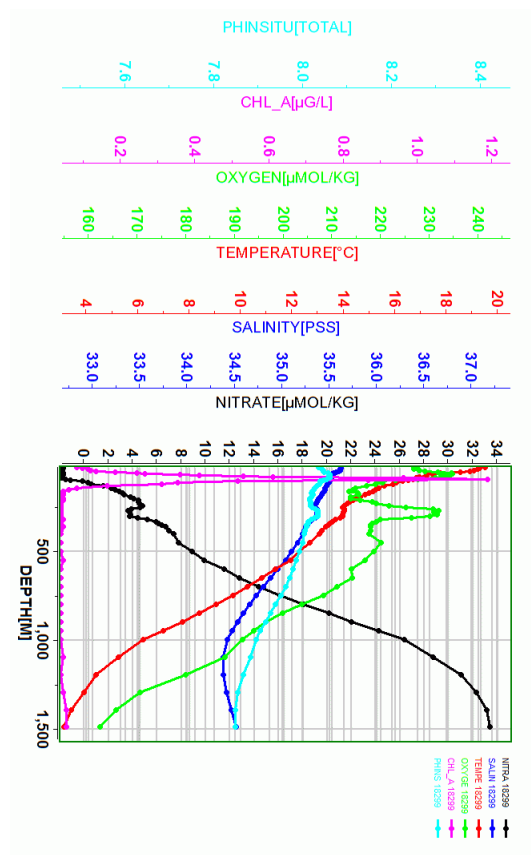
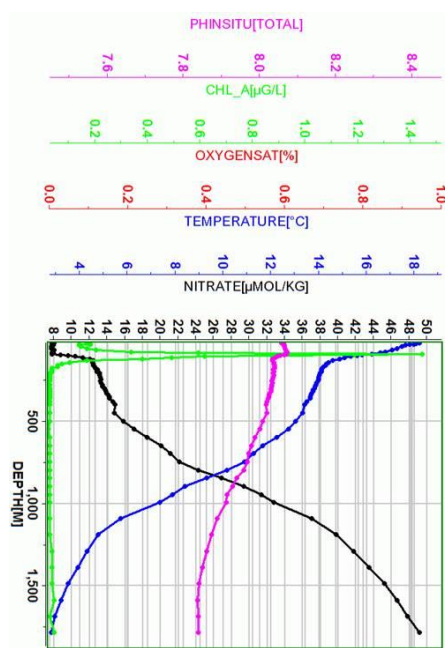Figure 4.29.1 First profile from float 18299. No issues.

Figure 4.29.2 First profile from float 18082. No oxygen data. Unknown cause, not likely to be due to handling or deployment.
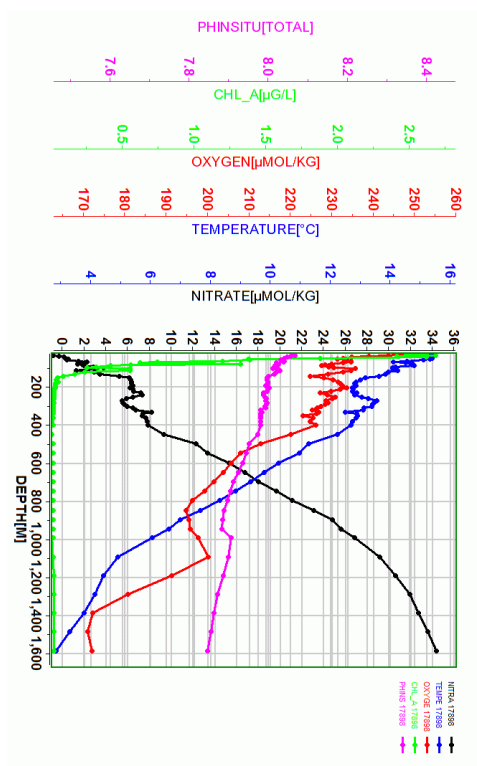
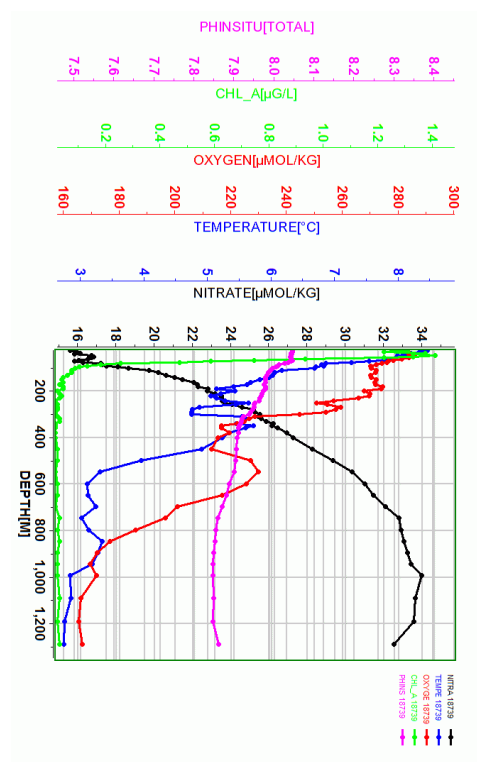Figure 4.29.3 First profile from float 17898. pH offset at 1000m.

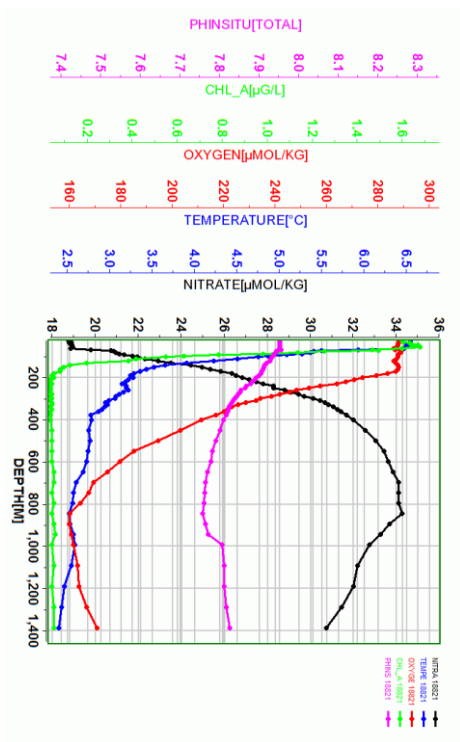Figure 4.29.4 First profile from float 18739. No issues.

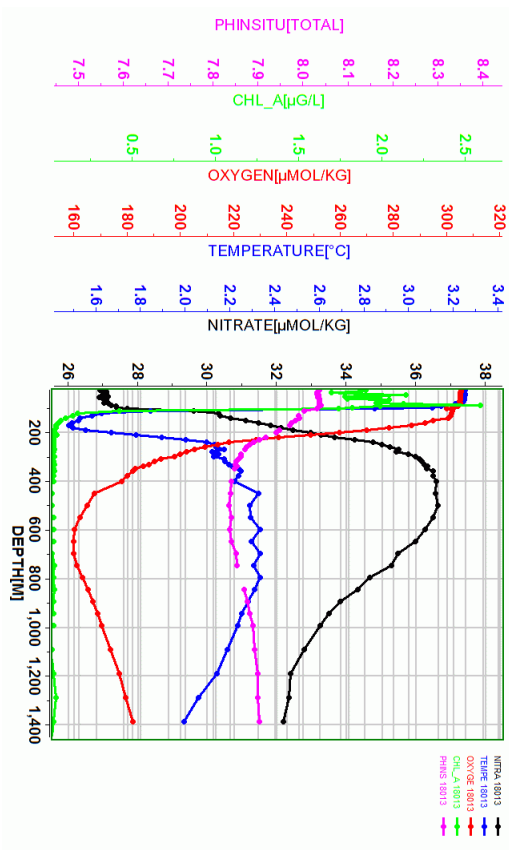Figure 4.29.5 First profile from float 18821. pH offset at 1000m.

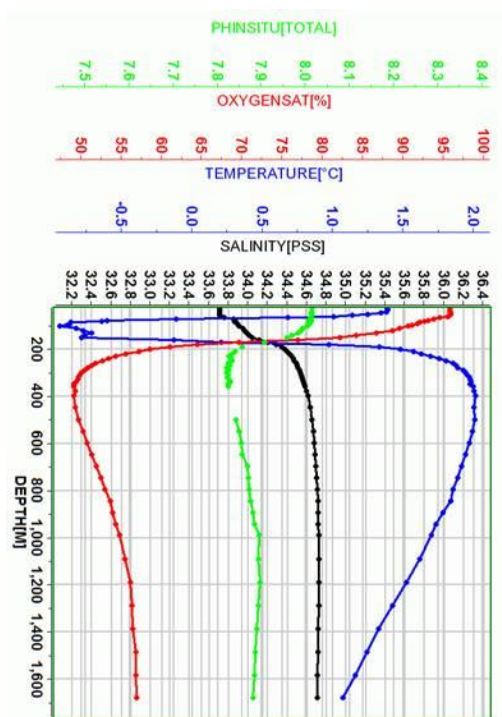Figure 4.29.6 First profile from float 18013. No issues.

Figure 4.29.7 First profile from float 18864. Nitrate sensor inadvertently off. Will be present from 3rd profile onwards.
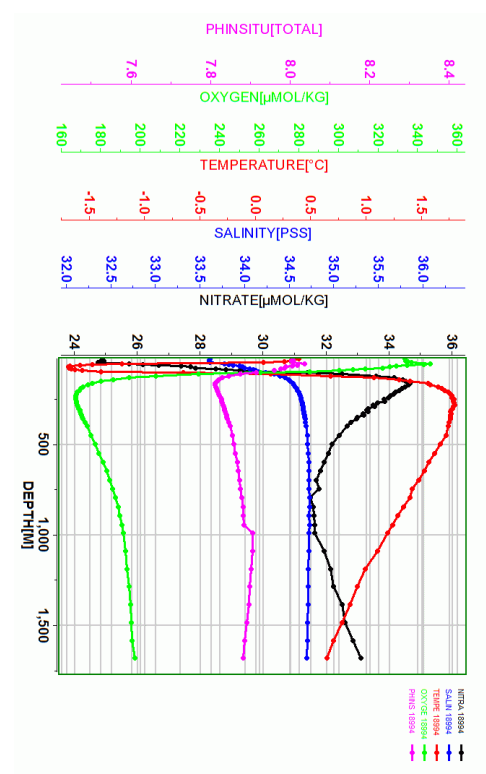
Figure 4.29.8 First profile from float 18994. pH offset at 1000m

147

5. Floats

5.1 Argo Floats by JAMSTEC
(1) Personnel
        Shigeki Hosoda (JAMSTEC)   Principal Investigator (not on board)
        Akihiko Murata (JAMSTEC)   on board
        Katsuro Katsumata (JAMSTEC)   on board
        Mizue Hirano (JAMSTEC)   not on board
        Keisuke Takeda (MWJ)   Technical Staff
        Shinsuke Toyoda (MWJ)   Technical Staff
        Hiroyuki Hayashi (MWJ)   Technical Staff

(2) Objective
        The research objective is to clarify the mechanisms of climate and oceanic environment variability, and to understand changes of earth system through estimations of heat and material transports, improving the Argo observing system in the global ocean. To achieve the objective, three core Argo floats are deployed to carry out automatically measurements of long-term temperature and salinity variations in the Indian ocean where the spatial density of the core Argo floats is constantly sparse due to a lack of float deployment opportunities. Data accumulated from core Argo floats also contribute to improve long-term forecasts of climate changes through data assimilation systems.
        Biogeochemical (BGC) Argo floats, that measure vertical profiles of biogeochemical parameters with temperature and salinity, are deployed to clarify changes of phytoplankton and dissolved oxygen concentrations related to physical and biological processes. As amount of BGC float data is still small due to a lack of measurement opportunities, the deployment of floats contributes to the BGC Argo program, the purpose of which is monitoring ocean acidification, biogeochemical process and exchange of carbon dioxide.
        Also, the aim of deep Argo float deployment (Deep Argo) is to clarify changes of deep ocean environment below 6000 m depth, contributing to the deep Argo observing system which started to construct since 2015. Recent climate change reports on IPCC AR5 documented that the deep ocean plays an important role of the global warming to accumulate huge heat from atmosphere, however, detailed mechanisms are still unknown because of less amount of observation. Since deep Argo float can obtain frequent temperature and salinity profiles with fine vertical resolution, accurate climate variability in the deeper ocean associated with circulation and water mass will be captured in collaboration with other measurements in the framework of the deep Argo observing system. Since some technical issues on deep Argo floats are investigated at this time, the deployed deep Argo floats will certainly contribute to improve the issues with accurate ship observation.
        The deep, BGC and Argo float data will also apply to the ESTOC, which is 4D-VAR data assimilation system to estimate state of global ocean for climate changes, to investigate whole mechanism of long-term changes in the ocean.

(3) Parameters
        ・Core Argo: Water temperature, salinity and pressure.
        ・Deep Argo :Water temperature, salinity and pressure.
        ・BGC Argo :Water temperature, salinity pressure, Oxygen, pH, Chlorophyll a,
        Backscattering, FDOM and Nitrate

(4) Method
i. Core Argo (APEX)

   We launched APEX float manufactured by Teledyne Webb Research. This float equips SBE41 CTD sensor manufactured by Sea-Bird Electronics Inc. The float drifts at a depth of 1000 dbar (called the parking depth) during waiting measurement, then goes upward from a depth of 2000 dbar to the sea surface every 10 days. During the ascent, physical values are measured every 2 dbar in advance following depth table. During surfacing for approximately half an hour, the float sends all measured data to the land

via the Iridium RUDICS telecommunication system. The lifetime of floats is expected to be about four-eight years. The status of float and its launching information is shown in Table 5. 1.

Table 5. 1 Specifications of floats and their launching positions

Float Type	APEX float manufactured by Teledyne Webb Research.
CTD sensor	SBE41 manufactured by Sea-Bird Electronics Inc.
Cycle	every 10 day (approximately 30minutes at the sea surface)
Iridium transmit type	Router-Based Unrestricted Digital Internetworking Connectivity Solutions (RUDICS)
Target Parking Pressure	1000 dbar
Sampling layers	2dbar interval from 2000 dbar to surface (approximately 1000 levels)

Launching position

Float S/N	WMOID	Date and Time of Launch (UTC)	Location of Launch		Cruise Leg.	Station
8609	1902337	2020/1/26 6:51	36°19.998S	57°32.532E	Leg.3	St.89
8608	1902336	2020/1/21 5:05	33°12.168S	57°2.616E	Leg.3	St.81

ii. Core Argo (Navis EBR)

We launched Navis float manufactured by Sea-Bird Scientific. This float equips SBE41 CTD sensor manufactured by Sea-Bird Scientific. The other specifications and observation method are the same as (i) Core Argo (APEX) The specifications and its launching information are shown in Table 5. 2.

Table 5. 2 Specifications of floats and their launching positions

Float Type	Navis float manufactured by Sea-Bird Scientific.
CTD sensor	SBE41 manufactured by Sea-Bird Scientific.
Cycle	every 10 day (approximately 30minutes at the sea surface)
Iridium transmit type	Router-Based Unrestricted Digital Internetworking Connectivity Solutions (RUDICS)
Target Parking Pressure	1000 dbar
Sampling layers	2dbar interval from 2000 dbar to surface (approximately 1000 levels)

Launching position

Float S/N	WMOID	Date and Time of Launch (UTC)	Location of Launch		Cruise Leg.	Station
F0587	1902334	2020/1/24 7:12:30	20°15.432S	67°59.940E	Leg.2	St.68'

iii. BGC Argo (Navis BGCi)

We launched one BGC Argo float manufactured by Sea-Bird Scientific. This float equips SBE41 CTD manufactured by Sea-Bird Scientific and some biogeochemical sensors. The float drifts at a depth of 1000 dbar (called the parking depth) during waiting measurement, then measures variable parameters from a depth of 2000 dbar to the sea surface every 10 days. During the ascent, physical values and biogeochemical parameters are measured following a measurement depth table. During surfacing for a few ten minutes, the float sends the all measured data to the land via the Iridium RUDICS telecommunication service. The lifetime of floats is expected to be about three to four years. The specifications and its launching information are shown in Table 5. 3.

Table 5. 3 Specifications and their launching positions for Navis BGCi

Float Type	Navis BGCi float manufactured by Sea-Bird Scientific.
CTD sensor	SBE41 manufactured by Sea-Bird Scientific.
Biogeochemical parameter	
Optical dissolved oxygen	SBE63 manufactured by Sea-Bird Scientific.
Chlorophyll a, FDOM, Backscattering	MCOMS manufactured by Sea-Bird Scientific.
pH	Float pH manufactured by Sea-Bird Scientific.

Nitrate	Deep SUNA manufactured by Sea-Bird Scientific.
Cycle	every 10 day (approximately 30minutes at the sea surface)
Iridium transmit type	Router-Based Unrestricted Digital Internetworking Connectivity Solutions (RUDICS)
Target Parking Pressure	1000 dbar
Sampling layers	Axis 1: CTD, Oxygen Chlorophyll a, FDOM and Backscattering 2000-1000dbar 8dbar interval 996-500dbar 4dbar interval 498-Surface 2dbar interval approximately 500 layers
	Axis2: Nitrate and CTD 2000-450dbar 50dbar interval 420-120dbar 30dbar interval 116-Surface 4dbar interval approximately 72 layers

Launching position

Float S/N	WMOID	Date and Time of Launch (UTC)	Location of Launch		Cruise Leg.	Station
F0884	1902332	2019/12/17 16:54	12° 0.018S	80° 0.018E	Leg.2	St.52

iv. Deep Argo (Deep APEX)

In this cruise, we launched four deep floats (Deep APEX) manufactured by Teledyne Webb Research. This float equips SBE61 CTD for deep observation manufactured by Sea-BirdScientific. The float basically drifts at a depth of 2000 dbar (called the parking depth), then goes down to a depth of 6000 dbar (or near sea bottom) and ascends to the sea surface every 10 days, measuring physical values at fixed depths following a depth table. During surfacing for a few ten minutes, the float sends the all measured data to the land via the Iridium RUDICS telecommunication service. The lifetime of Deep APEXs will be about four years. The status of float and its launching information is shown in Table 5.4.
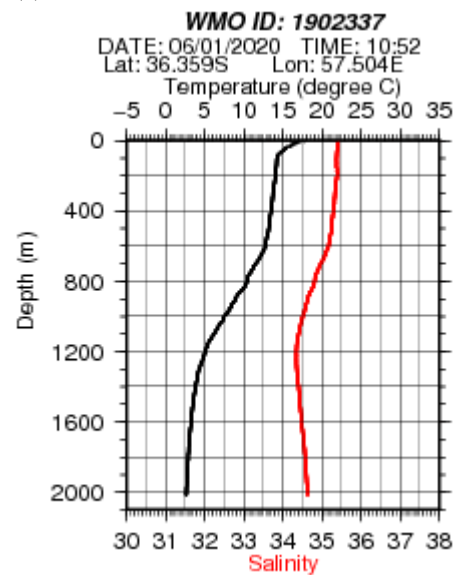
Table 5. 4 Specifications and their launching positions for Deep Argo (Deep APEX)

Float Type	Deep APEX float manufactured by Teledyne Webb Research.
CTD sensor	SBE61 manufactured by Sea-Bird Scientific.
Cycle	every 10 day (approximately 30minutes at the sea surface)
Iridium transmit type	Router-Based Unrestricted Digital Internetworking Connectivity Solutions (RUDICS)
Target Parking Pressure	2000 dbar
Sampling layers	2dbar interval from 6000 dbar to surface. (approximately 3000 levels in maximum)

Launching position

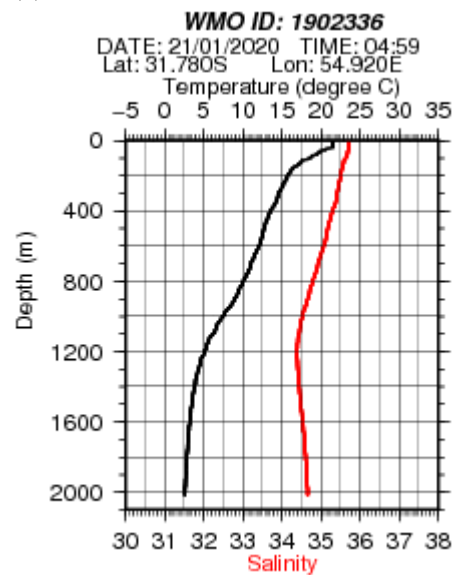| Float S/N	WMOID	Date and Time of Launch (UTC)	Location of Launch		Cruise Leg.	Station
00043	2903390	2019/12/13 03:30	4° 59.550S	79° 59.982E	Leg.2	St.38
00044	2903391	2019/12/16 15:23	9° 59.988S	79° 59.982E	Leg.2	St.48
00045	1902333	2020/1/21 22:09	20°0.012S	80°0.024E	Leg.2	St.68
00046	1902335	2020/1/1 7:44	30°9.390S	55°11.628E	Leg.3	St.72

(5) Data archive

The Argo float data will be provided conducting the real-time quality control within 24 hours following the procedure decided by Argo data management team. Then the delayed mode quality control will be conducted within 6 months ~ 1 year, to satisfy their data accuracy for climate research use. Those quality-controlled data of Argo and deep Argo floats are freely available via internet and utilized for not only research use but also weather forecasts and any other variable uses through internet from Global Data Assembly Center (GDAC: http://www.usgodae.org/argo/argo.html, http://www.coriolis.eu.org/) and Global Telecommunication System (GTS).

(a) S/N 8609 APEX

WMO ID: 1902337
DATE: 06/01/2020   TIME: 10:52
Lat: 36.359S   Lon: 57.504E
Temperature (degree C)

(b) S/N 8608 APEX

WMO ID: 1902336
DATE: 21/01/2020   TIME: 04:59
Lat: 31.780S   Lon: 54.920E
Temperature (degree C)

(c) S/N F0587 Navis

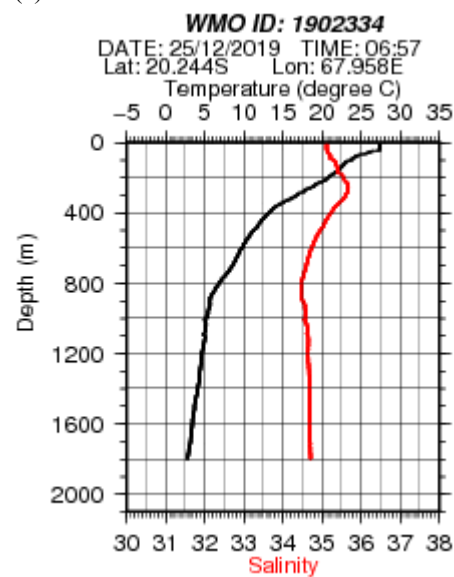**WMO ID: 1902334**
DATE: 25/12/2019   TIME: 06:57
Lat: 20.244S   Lon: 67.958E
Temperature (degree C)

Fig. 5.1 (a-c). Vertical temperature and salinity profiles of their first measurements for Core Argo floats (i) and (ii). Black and red lines show temperature and salinity profiles.
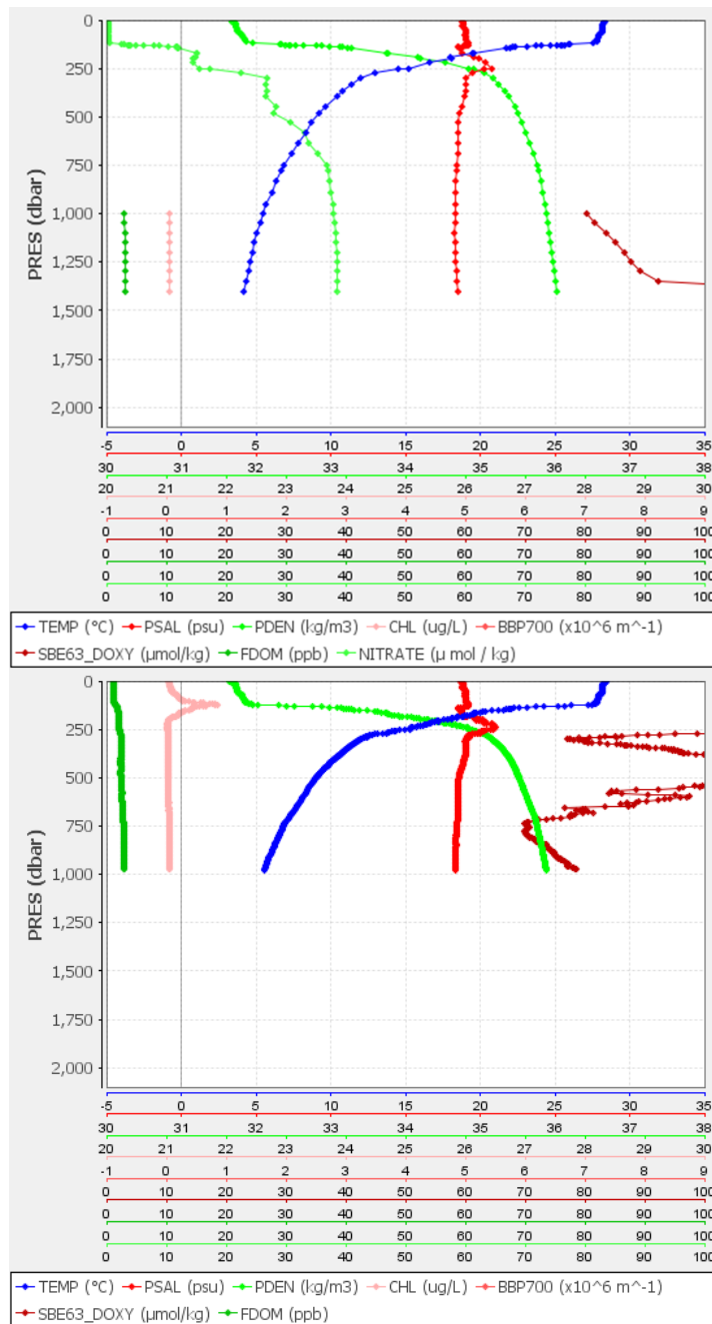
Fig. 5.2. Vertical profiles of temperature, salinity and biogeochemical parameters at its first measurements for BGC Argo float (iii) (WMO ID1902332, S/N F0884). (Upper) profiles with spot samplings. (Lower) profiles with continuously sampling modes. Blue, red, light green, pink, brown, dark green indicate temperature, salinity, potential density, chlorophyll-a, dissolved oxygen and FDOM, respectively.
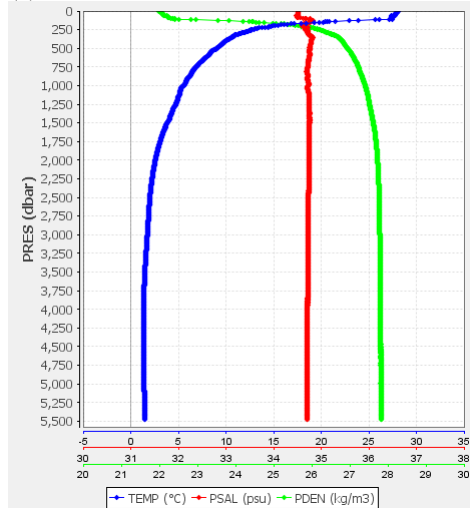.

(a) WMO ID 1902335 S/N0046
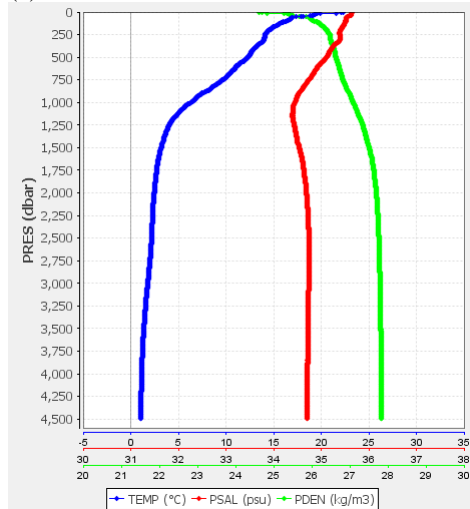
(b) WMO ID 1902333 S/N0045
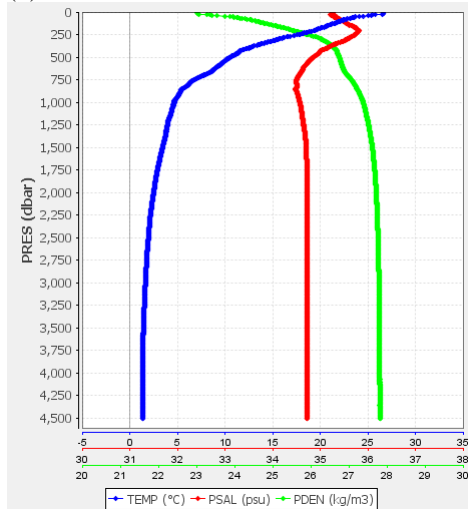
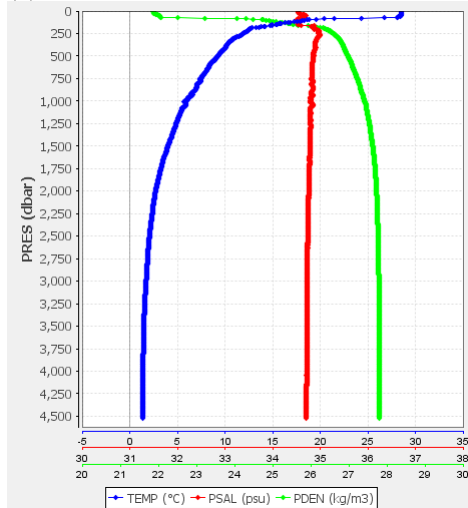(c) WMO ID 2903391 S/N00044

(d) WMO ID 2903390 S/N00043

Fig. 5.3 (a-d). Vertical profiles of temperature, salinity and potential density at their first measurements for four deep Argo floats (iv). Blue, red, light green indicate temperature, salinity, potential density, respectively

153

5.2 Argo Floats from CSIRO

Deployments of 15 floats were requested from CSIRO, Oceans and Atmosphere, Australia. The floats were loaded in Port Louis. On Leg 3, seven floats were deployed at CTD stations, one at an XCTD station. Seven floats were deplyed en route to Singapore after the last CTD station. All floats measure pressure, temperature, and salinity. Detail of floats deployments were recorded in SUM file included in the CTD output package (K. Katsumata).

5.3 Argo Floats for SOCCOM project

See Section 4.29 for detail. The table below show the summary of biogeochemical floats deployed as part of SOCCOM project.

UW serial #	Apex serial #	Adopt a float name	CTD sta #	lat	long	Depth	UTC date	UTC time	Notes
18299	8694	Toggweiler	72	-30 9.51	55 11.74	4764	2020 0101	0751	
18082	8697	Saguaro of the Sea	86	-35 0.62	57 25.05	4882	2020 0105	0413	oxygen sensor not working
17898	8696	Kekaihālana	97	-40 14.7 3	57 44.76	5076	2020 0107	1938	pH offset at 1000m
18739	8693	The Grouse	107	-44 59.8 7	57 47.10	4607	2020 0110	0826	
18821	8691	Lautan	114	-47 55.4 4	57 40.87	4395	2020 0112	0557	pH offset at 1000m
18013	8698	Lobo de Mar	126	-54 01.9 6	56 28.78	3580	2020 0116	0745	rough deployment but working fine
18864	8727	SaberScience	136	-58 11.66	55 16.03	5281	2020 0118	0524	nitrate sensor turned off, will report beginning with 3rd profile
18994	8688	Winston's Journey	147	-63 30.3 4	53 40.55	4841	2020 0120	2117	pH offset at 1000m

6. Notice on Using